

This item was submitted to Loughborough University as a PhD thesis by the author and is made available in the Institutional Repository (<https://dspace.lboro.ac.uk/>) under the following Creative Commons Licence conditions.



For the full text of this licence, please go to:  
<http://creativecommons.org/licenses/by-nc-nd/2.5/>

BLDSC no:- DX229904



**Pilkington Library**

Author/Filing Title ..... AL-MALIKY, N.S.J.

Accession/Copy No.

040152596

Vol. No. ....	Class Mark .....
---------------	------------------

LOAN COPY

26 JUN 1998

25 JUN 1999

~~14 JAN 2000~~

0401525961



# **STRAIN RATE BEHAVIOUR OF THERMOPLASTIC POLYMERS**

by

**NOORI SABIH JARRIH AL-MALIKY**

(MPhil, Loughborough Univ., UK)


(B.Sc., Basrah Univ., Iraq)

A Doctoral Thesis  
submitted in partial fulfilment of the requirements  
for the award of the degree  
Doctor of Philosophy  
of  
Loughborough University  
United Kingdom

Supervisor: Dr. D J Parry

June 1997

© by Noori Sabih Jarrih Al-Maliky (1997)

 <b>Loughborough University</b> Physical Library
Date <u>Jan 98</u>
Class
Acc No. <u>040152596</u>

919099431

## **ACKNOWLEDGEMENT**

I sincerely would like to thank all those individuals who have helped me during this work, particularly my supervisor Dr. David Parry for all his guidance, consistent encouragement, advice and support.

Also my thanks to Professor K.R.A Zeibeck for his provision of laboratory facilities and his kindness and help. Special thanks are due to Dr. G Swallowe for his assistance. Thanks are also due to Mr. Mark Ashton, Faraj Al-Hazmi, and Sinin Hamdan for their friendship and company. Thanks to Mr. John Oakley who machined most of the samples. I would also like to thank other members of the Department of Physics including Debby, Maureen, Linda, Karen, Frank Hatley and others who have helped me in any way.

My sincere thanks and love go to my parents, brothers and sisters for the encouragement and moral support. Finally I also would like to thank my wife Susan and my daughter Jinan for their love, encouragement and support during the final stages of my study.

## ABSTRACT

Polymers are increasingly used in structures that have to withstand impact conditions. This thesis describes an investigation of strain rate properties at room temperature of four engineering polymers; polyethylene (high density, HDPE and ultra high molecular weight, UHMWPE), nylatron and polyetheretherketone (PEEK 150g).

A split Hopkinson pressure bar (SHPB) system was used to study the response of these polymers in compression tests at high strain rates up to  $10^4 \text{ s}^{-1}$ . Stress equilibrium in SHPB samples was studied theoretically by examining multiple reflection effects during the initial elastic loading of the polymers; this study proved very useful in the analysis of SHPB tests. To cover a wide range of strain rate, compression studies were also made at low strain rates ( $10^{-3} - 10^{-2} \text{ s}^{-1}$ ) using a Hounsfield screw machine. Viscoelastic models have been applied to these results. These models fit quite well with the experimental results of HDPE, UHMWPE, and nylatron, but not to the PEEK due to the yield drop in the stress - strain curves, especially at high strain rates.

An exploding wire technique was used as an axial impulsive loading system for hollow cylindrical samples. An image converter camera at framing intervals of  $2 \mu\text{s}$  or  $10 \mu\text{s}$  recorded the radial expansion of the cylinder. The expanding cylinder was used as a driving system for a new technique called the freely expanding ring method, which was used to obtain the stress - strain behaviour of polymeric thin rings placed as a sliding fit on the cylinder. This method produced very high tensile strain rates up to fracture ( $>10^4 \text{ s}^{-1}$ ).

Comparisons have been made between results obtained from the quasi-static, SHPB, and expanding ring tests. The freely expanding ring and SHPB results were in good agreement indicating similar tensile and compressive high strain rate behaviour.

The mechanical properties of the above polymers are strongly dependent on strain rate. The Young's modulus and the flow stress increase with increasing strain rate. Nylatron showed high strain rate strain softening at high strain, this was due to the high temperature rise during loading, when the transition temperature ( $T_g$ ) of the material ( $50 \text{ }^\circ\text{C}$ ) was exceeded. However, the other materials showed continuous hardening behaviour. Plots of the flow stress at 5% and 10% strain vs log strain rate showed a linear increase up to a strain rate of about  $10^3 \text{ s}^{-1}$ . Above  $10^3 \text{ s}^{-1}$ , the stress rose more rapidly, but then showed significant drops for nylatron and PEEK. These drops in stress are probably due to both micro crack initiation in the sample and also high temperatures around the crack tips.

## CONTENTS

<b>CHAPTER 1 General introduction and literature survey</b>	
1.1 Background on some the mechanical properties of polymers	1
1.1.1 Elastic behaviour	2
1.1.2 Plastic behaviour	3
1.1.3 Yield point	4
1.1.4 Viscoelastic behaviour	7
1.1.5 Fracture	10
1.1.6 Strain rate dependency	12
1.1.7 Thermal effect	13
1.2 Literature survey	14
1.2.1 Strain rate and temperature properties	15
1.2.2 Yield behaviour	25
1.2.3 Elastic and plastic properties	29
1.2.4 Viscoelastic properties	30
1.2.5 Fracture of polymers	32
1.3 Work described in this thesis	33
<b>CHAPTER 2 Low strain rate tests</b>	
2.1 Introduction	35
2.2 Experimental background	36
2.3 Low strain rate results	42
2.4 Discussion	46
<b>CHAPTER 3 Split Hopkinson Pressure bar</b>	
3.1 Introduction	47
3.2 Hopkinson pressure bar theory	52
3.3 Problems in the SHPB analysis	59
3.3.1 Friction effects	59
3.3.2 Polymer/steel interfacing area variation	64
3.3.3 Inertia effect of the sample	64
3.3.4 Mechanical noise interference within the bars	65
3.3.5 Axial alignment	67
3.3.6 Temperature rise in the sample	67
3.3.7 Other problems can be met with analysis	69
3.4 Apparatus description and sample preparation	71
3.4.1 SHPB system	71
3.4.2 The gas gun	72
3.4.3 The projectile	72
3.4.4 The split bars	73
3.4.5 Recording system	75
3.4.6 Sample preparation and lubricant	78
3.5 Data acquisition and computation	79
3.5.1 Capturing and translating data	79
3.5.2 Description of SHPB program and data analysis	80
3.5.3 Temperature rise calculation	91
3.6 Summary	94

<b>CHAPTER 4 Split Hopkinson pressure bar results</b>	
4.0 Introduction	95
4.1 HDPE results	95
4.2 UHMWPE results	103
4.3 Nylatron results	110
4.4 PEEK results	118
4.5 Conclusions	125
<b>CHAPTER 5 The viscoelastic behaviour of polymers</b>	
5.1 Introduction	127
5.1.1 Basic elements	127
5.1.2 Kelvin-Voigt solid	128
5.1.3 Maxwell solid	131
5.2 Standard linear solid model	135
5.3 Bi-linear elasto-plastic model	138
5.4 Four element model	141
5.5 Examination of three models	143
5.5.1 Standard linear solid	143
5.5.2 Bi-linear model	149
5.5.3 Four element model	153
5.6 Discussion	157
<b>CHAPTER 6 Multiple reflections effect analysis in SHPB system within the elastic limit</b>	
6.1 Introduction	159
6.2 Theory	160
6.3 Analysis and computation	165
6.4 Computer simulation of SHPB multiple reflections	169
6.5 The pulse parameter and the plot resolution	171
6.6 Results and discussions	174
6.7 Comparison with experimental results	181
6.8 Conclusions	185
<b>CHAPTER 7 Exploding wire technique</b>	
7.1 Introduction	187
7.1.1 Exploding wires	187
7.1.2 Expanding cylinders	188
7.1.3 Expanding rings	189
7.2 Loughborough system:	
7.2.1 The exploding wire set-up	191
7.2.2 The recording equipment	193
7.3 Expanding cylinder	195
7.4 Freely expanding rings	195
7.5 Results and discussions	196
7.5.1 Exploding wire results	196
7.5.2 Expanding cylinder results	200
7.5.3 Expanding ring results	205
7.6 Conclusions	221



<b>CHAPTER 8 Discussion of results, conclusions and recommendations</b>	
8.1 Discussion of results	223
8.2 Conclusions	235
8.3 Recommendations for future work.	
<b>REFERENCES</b>	238
<b>APPENDIX</b>	
HOPK-BAR program list	

## **CHAPTER 1 GENERAL INTRODUCTION AND LITERATURE SURVEY**

### **1.0 Introduction**

Engineers are increasingly using polymers in structures that have to withstand impact conditions. However, the depth of study of the mechanical properties of polymers at high strain rates is small compared to the high strain rate testing of metals. In general, researchers of polymeric materials have to consider many factors influencing the polymers mechanical properties. These include the variation between commercial grades bearing the same name, the storage time of the polymers (because polymers are much more susceptible to change during storage, such as absorption of water from the air or exposure to ultra-violet). Also, a knowledge of strain rate dependency and thermal properties are important when considering high speed deformation (and hence adiabatic testing).

### **1.1 Background on some of the mechanical properties of polymers.**

Two interrelated objectives must be considered in discussing the mechanical properties of polymers. The first of these is to obtain an adequate macroscopic description of the particular facet of polymer behaviour under test. The second objective is to seek an explanation of this behaviour in molecular terms (microscopic description) (Dawson (1991)). For engineering applications of polymers a description of the mechanical behaviour under conditions that simulate their end use is often all that is required, together with empirical information concerning their method of manufacture.

The mechanical properties of polymers are dependent on the rate of loading, temperature and the amount of strain, hence it is difficult to classify polymers as a particular type of material such as a glassy solid or a viscous liquid. A polymer can also show all the features of a glassy, brittle solid or an elastic rubber or a viscous liquid depending on the temperature and the time scale of the measurement. But, in general, polymers are usually described as viscoelastic materials to emphasise their intermediate position between viscous liquids and elastic solids.

At low temperatures or high strain rates, a polymer may be glass - like and break or flow at small strains, but at high temperatures or low strain rates the same polymer may be rubber - like withstanding large strains without permanent deformation. At even higher temperatures, permanent deformation occurs and the polymer behaves like a viscous liquid. Figure (1.1) shows a typical stress - strain curve illustrating the elastic and plastic deformation of a polymeric material.

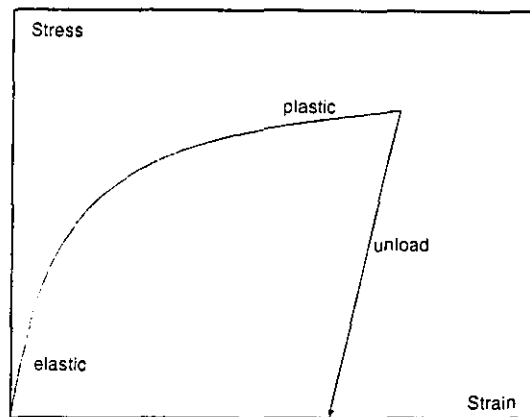


Figure (1.1) Elastic followed by plastic region.

### 1.1.1 Elastic behaviour

Material can be described as elastic if it springs back instantaneously to its initial shape after deformation when the load is removed, e.g. steel at small strains, and rubber. All engineering materials, including polymers are linearly elastic below the yield point, after which the material no longer obeys Hooke's Law (where the strain is proportional to the stress).

In elastic deformation, the material returns to its original shape and size after the load is removed (Megson (1987)). The ratio of axial stress to strain is called Young's modulus or elastic modulus and is approximately constant for most metals (Ritchie (1965)); however it is not constant for polymers but depends on strain rate and temperature. This instantaneous behaviour is called Hookean elasticity. The elastic behaviour described by Hooke's Law in its general form states that the stress components are linear functions of the strain components in the deformed body. The stress-strain relation describing the response of the material is termed the constitutive equation of the material. Some materials, such as soft polymers and rubbers, exhibit a non-linear stress-strain curve, but the deformation is sometimes considered elastic in the sense that the material

returns to its original shape on release of the load. All other types of deformation, in which the removal of the applied stress does not result in almost instantaneous corresponding decreases of strain, are called inelastic deformation. Under a cyclic strain the inelastic strain leads to a hysteresis loop on the stress-strain plot, which indicates the energy dissipation of damping as illustrated in Figure (1.2).

If a wave propagates through a material without causing any permanent deformation it is called an elastic wave. The elastic wave theory depends on the material obeying Hooke's Law. An elastic wave can propagate in different modes, such as a longitudinal wave in a rod with a speed of  $c = (E/\rho)^{1/2}$ , where  $E$  and  $\rho$  are the Young's modulus and density of the medium respectively. Also, it can propagate in an unbound solid, as a dilatational or irrotational wave with a speed of  $c = [(k + 4\mu/3)/\rho]^{1/2}$ , or as a distortional (equivoluminal) wave travelling with a speed of  $c = (\mu/\rho)^{1/2}$ , where  $k$  and  $\mu$  are bulk and rigidity moduli. So, the elastic wave speed depends only on the density of the material and the elastic constants (Kolsky (1963)). The wave propagation takes place by transmitting the energy between the molecules within the solid structure without disturbing its atoms mean locations.

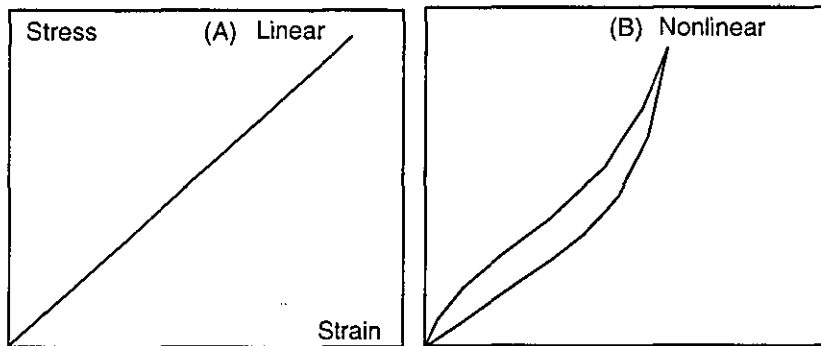


Figure (1.2) Stress-strain relation.

### 1.1.2 Plastic behaviour

Three different types of mechanism which are responsible for the deformation of a polymer are termed the elastic, anelastic and plastic mechanisms. The first of these types gives rise to a deformation which is instantaneously recovered on removal of the applied stress. The second gives rise to a deformation which eventually recovers, and the third gives rise to an irrecoverable deformation. The deformation process in the crystalline region of oriented high density

polyethylene accounts for the permanent deformation, while interlamellar slip contributes largely to the recoverable deformation.

When the applied stress exceeds the elastic limit or the yield point of a ductile material (such as polymer), plastic deformation occurs and the linear stress-strain relationship is no longer applies, the sample no longer returns to its shape as shown in Figure (1.1). The ratio of the stress/strain is smaller in plastic deformation than in elastic deformation, hence the stress wave travels slower in the plastic material, with speed of  $c = (\frac{\partial \sigma}{\partial \epsilon} / \rho)^{1/2}$ . Polymers have time dependent behaviour at the plastic stage due to viscosity.

### 1.1.3 Yield point

The yield stress is a stress required to cause an irreversible (plastic) deformation in a material, or in another words it is the minimum stress at which permanent strain is produced when the stress is subsequently removed (Ward (1979)). After reaching the elastic strain limit, materials either fracture or, in the case of soft metals such as copper and all polymers, undergo a continuing plastic deformation called the yield process (Matsuoka (1992)). This process of yielding is accompanied by slipping or twinning in metals, which can occur most easily in the plane of maximum shear stress.

The yield and flow are regarded by Bauwens-Crowet et al (1974) as activation processes with associated energies and volumes. Bauwens-Crowet and co-workers described the behaviour of polycarbonate (PC) (as an amorphous polymer) by an Eyring - type equation for strain rates of  $10^{-8}$  to  $10^2 \text{ s}^{-1}$  from room temperature to  $80 \text{ }^\circ\text{C}$ . The Eyring theory has been developed assuming no stresses acting, a dynamic equilibrium exists and chain segments move with a frequency ( $\nu$ ) over a potential barrier in each direction where

$$\nu = \nu_0 e^{-\Delta H/RT}$$

where  $\Delta H$  is the activation energy,  $\nu_0$  involves the fundamental vibration frequency and the entropy contribution to the free energy,  $R$  is the gas constant and  $T$  is the temperature (Ward (1979)). The yield stress denotes the point at which the internal viscosity falls to a value such that the applied strain rate is identical to the plastic strain rate ( $\dot{\epsilon}$ ) predicted by the Eyring equation (Dawson (1993)). The measurement of the yield stress in a constant strain rate

test is analogous to the measurement of the creep rate at constant applied stress ( $\sigma$ ) and the following Eyring equation applies

$$\dot{\epsilon} = \dot{\epsilon}_0 e^{-\Delta H/RT} \sinh(v\sigma / RT)$$

and for high values of stress,  $\sinh(x) = \frac{1}{2}e^x$ , then this gives yield stress in terms of strain rate as

$$\sigma = \frac{RT}{v} \left[ \frac{\Delta H}{RT} + \ln \frac{2\dot{\epsilon}}{\dot{\epsilon}_0} \right]$$

where ( $v$ ) is the activation volume, ( $\dot{\epsilon}_0$ ) is a constant pre-exponential factor.

The yield point defined by Brinson and DasGupta (1975) in their study on polycarbonate and PMMA is the tensile instability point at which localised yield began rather than the point after which the stress exceeds the limit of linear stress / strain proportionality.

Below  $T_g$  polymers (especially glassy) are generally thought of as being rather brittle materials, but they are in fact capable of displaying a considerable amount of ductility below  $T_g$  especially when deformed under the influence of an overall hydrostatic compressive stress (Young and Lovell (1991)). An important aspect of the deformation is that glassy polymers tend to show strain softening. The true stress drops after yield not because of necking, which cannot occur in compressive tests, but because there is an inherent softening of the materials. It is found that the process of shear yielding in epoxy resins is homogeneous and samples undergo a uniform deformation with no evidence of any localisation. The situation is similar in other glassy polymers but in certain cases strongly localised deformation is obtained. Young and Lovell (1991) found that when Polystyrene was deformed in a plane strain compression system, fine deformation bands occurred in which the shear was highly localised.

It is thought that the formation of shear bands may be associated with the strain softening in the material. Once a small region starts to undergo shear yielding it will continue to do so because it has a lower flow stress than the surrounding relatively undeformed regions. One of the explanations for the yield process which is related to the molecular structure of the material, is the stress-induced increase in free volume. It has been suggested that the one effect of an applied stress upon a polymer is to increase the free volume and hence increase the mobility of the molecular segments, and that may also have the effect of reducing  $T_g$ . Developments of this theory predict that during tensile deformation,

the hydrostatic tension should cause an increase in free volume and so aid plastic deformation. However, there are problems in the interpretation of compression tests where plastic deformation can still take place even though the hydrostatic stress is compressive. It has been reported by some researchers that in some measurements, there is a slight reduction in the sample volume during plastic deformation in both tension and compression. Therefore the concept of free volume is not very useful in the explanation of plastic deformation of polymers.

Another theory for explaining the yielding behaviour is by applying the Eyring theory to yield in polymers (Bauwens-Crowet et al (1974)). The yield and plastic deformation in polymers can be considered as a type of viscous flow, especially since glassy polymers are basically frozen liquids that have failed to crystallise. Eyring developed a theory to describe the behaviour of glassy polymers. The segments of the polymer chain can be thought of as being in a pseudo lattice and for flow to occur a segment must move to an adjacent site. The volume of the polymer segment which moves to cause plastic deformation is called the activation volume or Eyring volume. Eyring theory takes in account the strain rate dependence of the yield stress of polymers.

Specific kinds of molecular motion could be involved in the interpretation of the yield behaviour and plastic deformation of glassy polymers especially when planar zigzag molecular chains are present in polymer structures as in the simple vinylpolymer shown in Figure (1.3).

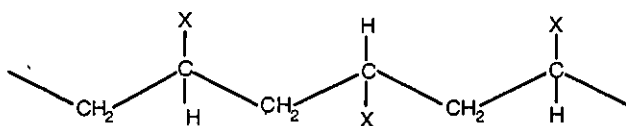


Figure (1.3) Simple vinylpolymer with a planar zigzag chain.

In some materials, regions where a yield drop may be observed are bounded by a brittle-ductile transition at low temperature, and in amorphous polymers by the glass transition at high temperatures (Ward (1979)).

By increasing the strain rate the yield stress increases without effecting the brittle stress limit of the material very much, and hence increases the temperature of the brittle-ductile transition which determines the lower boundary of the yield behaviour.

It has been seen that upper and lower yield points are often associated with a load drop on the load-extension curve, and always involves a change in slope on the true stress-strain curve. This load drop has sometimes been attributed to adiabatic heating of the sample or to the geometrical reduction in the cross-sectional area of a neck formed during tensile deformation. The local temperature rise causes strain softening and consequently a fall in the stiffness occurs (Ward 1979). The geometrical effect on the load drop is due to the fact that the fall in cross - sectional area during stretching is not compensated by an adequate degree of strain hardening. This effect called strain softening causes the reduction in the slope of the stress-strain curve with increasing strain in the tensile test.

Brown and Ward (1968) concluded that in most cases there is clear evidence for the existence of an intrinsic yield drop, i.e. that a fall in true stress can occur in polymers as in metals which have an upper yield point caused by a sudden increase in the amount of plastic strain which relaxes the stress. So, the yield combines the effect of the geometrical changes and an intrinsic load drop and cannot be attributed to the geometrical changes alone.

Brown and Ward show that the load drop takes place even in compression, although in the compressive test there is a geometrical hardening rather than a softening effect due to the increase in cross-section after yield. This is confirmation of their proposal that the load drop must be attributed to intrinsic yielding. The intrinsic yield is caused by the propagation of the yielding through the sample. The yield could occur due to the increase of a free volume under stress, and this free volume (volume of holes or voids between the molecules) growing until it reaches its maximum value at the glass transition temperature, where at this point flow can occur and the polymer can deform like a rubber. Also it has been noticed that the intrinsic yield drop in polymers depends on the dynamic relationship between the molecular processes and the applied strain rate. Thus it might be expected that whether an intrinsic yield drop is observed or not will depend upon the conditions of testing and the polymer structure.

#### **1.1.4 Viscoelastic behaviour**

Viscoelastic materials are materials, such as polymers, which when loaded exhibit aspects of both elastic recovery and viscous flow (i.e. creep). Other



manifestations of viscoelastic behaviour are time, rate or frequency dependent mechanical properties and the dissipation of energy under dynamic loads.

Under certain conditions of stress and temperature, all materials when subjected to a constant stress will exhibit an increase of strain with time. This phenomenon is called creep and materials such as polymers creep to a certain extent at all temperatures, although the engineering metals such as steel, aluminium, and copper creep very little at room temperature. High temperature leads to rapid creep, which is often accompanied by microstructural changes such as micro-cracks caused by the grain boundary sliding especially at high creep rate (Anderson et al (1974)). At temperatures and stress levels at which creep occurs, if a deformation is applied and held constant, stress will decrease with increasing time. This decrease of stress is known as stress relaxation (Ahmad (1988)).

Viscoelastic materials like polymers can undergo a yield process if deformed sufficiently. The criterion for the yield can be set by the total shear energy. This is a form of energy that causes a shape change. The stress components for shape change are called deviatoric, as opposed to the normal stress components, which are for volume change. The yield condition is given by the equation

$$\left\{ \frac{1}{2} [(\sigma_y - \sigma_z)^2 + (\sigma_z - \sigma_x)^2 + (\sigma_x - \sigma_y)^2] \right\}^{1/2} = \sigma$$

where  $\sigma_x, \sigma_y,$  and  $\sigma_z$  are the orthogonal principal stresses and  $\sigma$  is the uniaxial yield stress. This equation is often referred to as the von Mises relation.

The von Mises yield criterion can also be expressed in the following ways;

1) In terms of the principal components of the deviatoric stress tensor

$$\frac{1}{2} \{ (\sigma_x - p)^2 + (\sigma_y - p)^2 + (\sigma_z - p)^2 \} = k^2$$

where  $k$  is a constant, and

$$p = \frac{1}{3} (\sigma_x + \sigma_y + \sigma_z) \text{ is hydrostatic pressure (Ward (1979)).}$$

2) An equally well known representation of this criterion is

$$(\sigma_x - \sigma_y)^2 + (\sigma_y - \sigma_z)^2 + (\sigma_z - \sigma_x)^2 = 6k^2$$

which is readily obtained by algebraic manipulation. The shear stress  $\tau$ , can then be represented by

$$\tau = \frac{1}{3} \left\{ (\sigma_x - \sigma_y)^2 + (\sigma_y - \sigma_z)^2 + (\sigma_z - \sigma_x)^2 \right\}^{1/2}$$

giving the von Mises yield criterion as  $\tau^2 = \frac{2}{3} k^2 = \frac{2}{9} \sigma^2$ .

The critical strain rate  $\dot{\epsilon}$  at which the critical yield stress could take place is

$$\dot{\epsilon} = \frac{\sigma}{G\lambda}$$

where  $G$  and  $\lambda$  are the elastic shear modulus and relaxation time for the stress decay process.

For amorphous polymers large changes in viscoelastic behaviour may be brought about by the presence or absence of chemical cross-links or by changing the molecular weight which controls the degree of molecular entanglement or physical cross-linking.

The influence of chemical or physical cross-links is twofold. First, chemical cross-links prevent irreversible molecular flow at low frequencies (or high temperature) and thereby produce the rubbery plateau region of modulus or compliance. Physical cross-links due to entanglements will restrict molecular flow by causing the formation of temporary networks. Over long time periods such physical entanglements are usually labile and lead to some irreversible flow. Secondly, the value of the modulus in the plateau region is directly related to the number of effective cross-links per unit volume; this follows from the molecular theory of rubber elasticity (Ward (1979)).

The importance of time and temperature in the mechanical behaviour of polymers lies in the molecular mechanisms that are called into play when these materials are deformed (Ahmad (1988)). The polymer solid consists of a mass of macro-molecules which may be in the form of unconnected chains, cross-linked chains or networks. The chain molecules may have large or small side groups and in some instances will form side branches of the main chain. In addition, polar groups are sometimes present, either within the chains or in side groups. On top of this complicated structural picture is superimposed the continuous disorganisation caused by thermal energy. Individual atoms, molecular segments, or side groups and even whole molecules, are in constant motion. When a polymer is deformed there is always a certain amount of perfectly elastic strain, which consists of lengthening and shortening of interatomic and intermolecular bonds and changing of their angles along the chain. A whole series of configuration changes is caused by rotation and

translation of the molecular segments. These motions are hindered to varying degrees by the presence of atoms in the same chain and by neighbouring molecules. They are aided periodically by thermal motions, with the consequence that these molecular motions require varying amounts of time depending on the temperature, and continue to take place at an ever decreasing rate even when the deformation is held constant (relaxation). During any deformation, rearrangements of the molecules on a local scale are relatively rapid, but very slow on a long-range scale where long sections of macromolecules have to find new continuous time scales matching the response of such material to external deformation.

The inelastic deformation of a polymer is associated with the displacement of whole molecules relative to each other. In thermoplastics this type of motion is hindered by the weak Van der Waals intermolecular bonds and by other forms of interactions, such as entanglements and the formation of crystallites. In cross-linked polymers it is hindered by chemical bonds which must be broken to permit large molecular motions. Thermal energy helps by activating certain processes in various temperature ranges and these deformations are therefore highly time and temperature dependent.

### **1.1.5 Fracture**

Fracture is of great importance to scientists and engineers who work in the design of objects that are exposed to severe conditions like explosive, shock wave, or impact loading. Materials fail in a different manner according to their structure, the deformation speed, and also the level of temperature.

Ward (1979) quoted that the molecular weight does not appear to have a direct effect on the yield strength, but it is known to reduce the brittle strength. It has also been reported by Flory in 1945 that the fracture stress of a polymer was related to the average number of molecular weight  $\bar{M}_n$  by a relationship in a form of

$$\text{fracture stress} = A - \frac{B}{\bar{M}_n}$$

where A and B are constants which depend on temperature.

The yield stress could differ with the degree of branching (which affects the crystallinity) so that the temperature of the brittle-ductile transition would be a

complex function of at least molecular weight and branch content. The temperature of the brittle-ductile transition is the temperature at which the stress for brittle fracture is the same as the stress for yield (see Figure (1.4)).

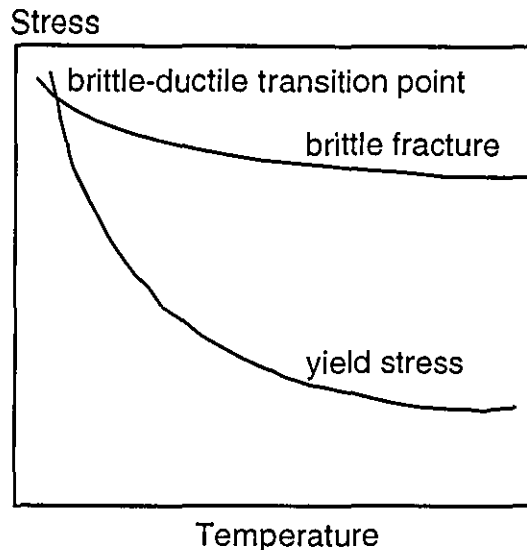


Figure (1.4) Diagram illustrating the brittle-ductile transition.

Also, Vincent (1960) suggested that rigid side groups increase both the yield strength and the brittle strength, whereas flexible side groups reduce the yield and the brittle strengths, but there is no general rule for the effect of side groups on brittle-ductile transition.

There is little effect of cross-linking on the brittle strength as quoted by Ward (1979). However, cross-linking increases the yield strength, therefore the brittle - ductile transition temperature is raised.

Other parameters can have an effect on the fracture of polymers; plasticizers can increase the chance of brittle failure because they usually reduce the yield stress more than they reduce the brittle strength. The orientation of molecules also has an effect on the polymer properties, especially fracture. Generally, it is considered that the brittle strength is more anisotropic than the yield. Hence a uniaxially oriented polymer is more likely to fracture when stress is applied perpendicularly to the symmetry axis than an unoriented polymer at the same temperature and strain rate.

### **1.1.6 Strain rate dependency**

Yielding in polymers is strongly strain rate dependent. From published experimental work, it has been seen that the yield stress of a polymer increases with the increase of strain rate and decreases with temperature increase, but not much effect has been noticed on the brittle failure stress. However the temperature of the brittle-ductile transition increases when the strain rate increases (Ward (1979)).

Polymers studied in this project are HDPE, UHMWPE, nylatron and PEEK. The flow stress of the first two polymers increases linearly with the logarithm of strain rate up to a certain level of strain rate, then above that level of strain rate the flow stress increases rapidly with the increase of the logarithm of strain rate. The last two polymers show a decrease in the flow stress after a certain level of strain rate (as will be shown in more detail in this thesis). The drop of flow stress at very high strain rates, with no proven explanation, has been reported by other researchers such as Walley et al(1991).

The shape of the stress-strain curves of polymers depends on the speed of deformation of the sample under test as shown in work done by Hamdan (1994) and Al-Maliky and Parry (1994). Some other researchers like Truss et al (1984), Fleck et al (1990), Arruda et al (1991) and Walley et al (1991), have investigated the effects of strain rate and temperature on amorphous polymers. It was seen that strain softening and strain hardening are normal phenomena which both occur during polymer deformation, but with different degrees depending on the rate of strain at which the polymers are being tested. The yield stress as well as the flow stress of polymers generally decrease with the increase of temperature due to the greater molecular motion causing weakening and/or breaking of Van der Waals bonds between the polymer molecules.

At high rates of strain there is not enough time for stress relaxation to occur to prevent brittle fracture in some cases, or prevent strain softening in others by relieving some of the stress at points of stress concentration.

PC, PVC, and PMMA have been studied over a number of years by Bowden (1973) and Bauwens-Crowet et al (1969) and they have examined the linear dependence of the yield stress on the logarithm of strain rate for a range of

temperature. Also they explained the relationship between the strain rate and temperature by Eyring viscosity theory which leads to the equation

$$\frac{\partial \tau}{\partial (\ln \dot{\epsilon})} = \frac{2kT}{v}$$

where  $\tau$ ,  $k$ ,  $T$ , and  $v$  are the applied shear stress, Boltzmann constant, temperature and activation volume respectively. This model has been modified and generalised by Bauwens in 1973 and again in 1980 by suggesting the formation of a free volume, the molecular motions giving rise to plastic deformation of activated segments rather than a constant value of free volume (Ahmad (1988)).

### **1.1.7 Thermal effects**

According to the theory of linear elasticity, the strain is linearly proportional to the applied stress, and a reversible process between external work and strain energy is accepted as a basic concept in solid mechanics (Hamdan 1994). However, this is not strictly true when considering the thermomechanical effect of a material where the temperature of the material changes during the deformation.

The terms thermoelasticity and thermoplasticity arise in the thermomechanical behaviour of materials due to the effects of the thermal and mechanical behaviour during the deformation process. During the deformation, the internal friction between the molecules of the material causes a temperature rise (Kolsky (1949)). This temperature rise has an effect on the properties of the material, by softening the overall structure. At low temperatures the Young's modulus of polymers are of order of 1 GPa - 10 GPa, and they fracture at strains of about 5 %, while at high temperatures the Young's modulus values are of the order 0.001 GPa - 0.01 GPa, and the polymer can be strained to a level of about 150 % before fracture. Therefore, a knowledge of thermal properties of the polymers is important especially when considering high strain rates and hence adiabatic deformation. At low strain rates the heat generated during the deformation is dissipated to the surrounding atmosphere and isothermal deformation can be achieved. When there is not enough time for the heat to be lost at high rates of strain, the deformation will take place adiabatically.

High levels of temperature rise occur for stiff polymers such as PEEK, PC, and nylon that have a large value for the product  $\sigma \epsilon$ ; hence a large amount of energy is dissipated during the flow. The stress - strain properties of polymers are sensitive to the temperature at which they are determined. The modulus, yield strength, and ultimate strength generally decrease as the temperature increases. Attwood et al (1981) showed that PEEK (semicrystalline) has a higher modulus at temperatures below the glass transition temperature ( $T_g = 144 \text{ }^\circ\text{C}$ ), and also showed the rapid loss of rigidity on passing through  $T_g$ .

Some other researchers have investigated the effects of temperature on polymer properties. Hall (1968) concluded that the transition from isothermal to adiabatic processes in oriented polymers occurs over two decades of strain rate from  $0.04 - 4 \text{ s}^{-1}$ , and the temperature rise during the adiabatic process will have a marked effect on the stress-strain properties. Also Hamdan (1994) has investigated the effect of temperature on the yield strength of polymers. In some cases it is seen that the polymer starts to soften at temperatures near the glass transition temperature when an adiabatic deformation occurs for some glassy polymers.

## **1.2 Literature survey**

Relatively few studies have been carried out on polymers at high rates of deformation compared to metals (Dawson (1993)).

The stress-strain behaviour of polymers is more complicated, and hence less understood than that of most other structural materials. The main difference between polymers and conventional materials is that the stress-strain behaviour shows a very marked dependence on rate and temperature. In order to help the designers to develop constitutive equations to predict how materials will behave under specified conditions, it is necessary to measure the properties of materials as a function of strain rate and temperature. The structure of the molecular chains also needs to be characterised. One of the difficulties in studying polymers is separating the intrinsic stress - strain properties from the geometry and mechanical / thermal history of the samples under test. Hence the crystallinity and molecular orientation of samples should be known when comparing data on the mechanical properties of different polymers.

## **1.2.1 Strain rate and temperature properties**

Due to the nature of the information in this section, it can be divided under two subheadings; macroscopic and microscopic analysis.

### **1.2.1.1) Macroscopic analysis**

Several studies have been carried out by Walley and co-workers (1991a, b, 1989, and 1994) on the rapid deformation of a range of polymers at strain rates from  $10^{-2} \text{ s}^{-1}$  to  $10^4 \text{ s}^{-1}$  using an Instron, drop - weight machine, and direct impact Hopkinson pressure bar. The main source of error in their results is the friction at the sample faces, which they minimise by using petroleum jelly as a lubricant. Also they used Avitzur theory to calculate the friction and hence friction corrections were made for stress-strain curves. Another source of error is oscillation on their curves due to the ringing in the instruments. This oscillation is removed by FFT filtering and consequently it may not give very accurate results especially for stiff materials. Walley and co-workers found that in general all polymers exhibited higher yield stresses at higher strain rates. Also, they found that polymers fractured at smaller strains at 100 K than at 300 K. They used high speed photography to visualise the failure mechanisms and the heat evolution and to capture the fracture initiation. Useful mechanical properties are also examined for a range of temperature between the glass-transition temperature and the melting point.

Walley mentioned that in some cases it seems that some mechanism, possibly thermal in origin, gave a drop in yield stress at the highest rates of strain studied. However, the thermal conditions are already adiabatic at strain rates of  $10^3 \text{ s}^{-1}$ , so it is unlikely that the temperature rise for a given strain will be even greater at a strain rate of  $10^4 \text{ s}^{-1}$ . Another possible cause that has been suggested is softening due to diffusion of the lubricant into the very small samples used at the highest strain rates. Walley and co-workers do not think this a very likely explanation since they calculated the distance that the lubricant should diffuse as being only about 10 - 25  $\mu\text{m}$  in PE.

Strain rate effects on the ratio of recoverable to non-recoverable strain in linear polyethylene were studied by Fotheringham and Cherry (1978a, b). The effect of strain rate on the amount of unrecovered strain is determined by long term and fast recovery tests. This investigation has led to the fact that the



extrapolated yield point cannot be associated with the onset of permanent flow. Also it has revealed that the dependency of strain rate on the yield point is controlled by recoverable rather than irrecoverable processes.

Foot et al (1987) observed that the strain rate behaviour of PET and polyethylene were related to mechanical relaxation transitions observed in the linear viscoelastic behaviour of the material. Also Steer and co-workers (1985) pointed out a transition at a critical strain rate which they related to a relaxation transition in PC.

Haward et al (1971) has discussed strain hardening in detail, associating it with uncoiling polymer chains or sections of chains in the stretch direction. The chain orientation process is reversible, leading to recovery of macroscopic sample shape when the plastically deformed glass is heated above  $T_g$ . Haward (1994) derived the strain hardening modulus from true stress-strain curves for thermoplastics such as PVC, PEEK and PMMA. Difficulties in measuring the true stress-strain arise when the variation of temperature makes the polymer deform at lower stress, necking makes the tested part of the sample not parallel, and strain rate affects the value of the yield stress.

The split Hopkinson pressure bar has been used by Briscoe and Nosker (1984, 1985) to measure the flow stress of a high density polyethylene at room temperature and a strain rate of  $5 \times 10^3 \text{ s}^{-1}$ . They found that when thin samples are used to obtain a large strain, the friction constraint between the polymer and the bars can be the dominant experimental problem and it becomes important whenever the inequality  $\mu d / \ell_0 \ll 1$  is not satisfied, where the sample has diameter  $d$ , length  $\ell_0$  and interface friction coefficient  $\mu$ . The interface introduces an effective hydrostatic term that makes the apparent flow stress of the polymer greater than the true flow stress. However they suggested that a  $10 \mu\text{m}$  thick film of petroleum jelly is an ideal lubricant for impact testing. In their experimental study Briscoe and Nosker showed that interface friction was influencing the yield behaviour of HDPE when compressed to a large strain (25 %) at a rate of strain as high as  $5 \times 10^3 \text{ s}^{-1}$ . The diameter / length ratio of the sample also has a significant effect on the friction and hence on the results of compressive testing using SHPB. Diah et al (1993) reported results of MDPE, HDPE, PC and PEEK for high compressive strain rates using the SHPB technique.

Dioh and co-workers demonstrated in the results the effect of the sample thickness on the flow stress at high strain rates. The results showed that at high strain rates the flow stress for thinner samples are lower than for the thicker samples of all materials tested.

A sudden increase in the strain rate sensitivity (see Figure (1.5)) of a range of polymers at rates above  $10^3 \text{ s}^{-1}$ , has been observed by several authors like Chou et al (1973), Walley et al (1991), Rietsch and Bouette (1990), and Briscoe and Nosker (1985). This behaviour was interpreted as a transition from one or more of a series of thermally activated flow mechanisms (Dioh et al (1993)) at low strain rates to a flow process dominated by viscous drag at high rates, while Follansbee et al (1988) suggested that this behaviour can be interpreted as a change in the way the structure evolves with strain.

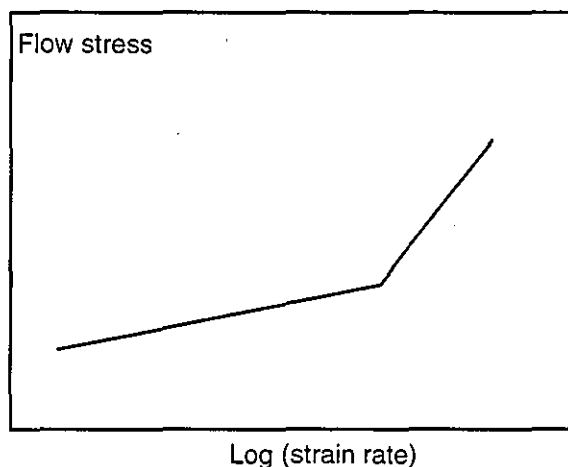


Figure (1.5) Identical diagram for flow stress / log (strain rate).

The deformation velocity, friction and inertia at high strain rates may be responsible for the sudden increase in strain rate sensitivity (Gorham (1991)). Gorham argues that the sharp increase in high strain rate sensitivity is influenced by the geometry of the sample.

Cansfield et al (1983) studied the dependency of the stress-strain behaviour on strain rate for ultra high modulus linear polyethylene (UHMLP). They demonstrated high sensitivity of the UHMLP to the testing conditions. The tensile strength of UHMLP is highly temperature and strain rate dependent.

Fleck et al (1990) measured the high strain rate response of polycarbonate (PC) and polymethylmethacrylate (PMMA) using the split Hopkinson torsion bar for shear strain rates  $\dot{\gamma}$  from  $500 \text{ s}^{-1}$  to  $2200 \text{ s}^{-1}$ , and temperatures in the range

-100 °C to 200 °C. The measured shear yield stress was compared with results in accordance with the Eyring theory of viscous flow. At low temperature the backbone chain becomes frozen and the shear yield stress is greater than the Eyring prediction.

Kukureka and Hutchings (1984) measured the mechanical properties of the polymers HDPE, PC, and PES in compression at strain rates in the range of 300–500 s<sup>-1</sup>. Their tests employed a gravity driven pendulum to load a sample on the end of an instrumented Hopkinson output bar. They presented stress-strain curves over a range of temperatures. They found the yield stress for these polymers to vary linearly with log(strain rates) at strain rates up to 500 s<sup>-1</sup>. The true stress in the sample was computed by the equation:

$$\sigma_s(t) = \frac{EA_0}{V} \varepsilon_b(t) \left\{ \ell_0 - \int_0^t \left[ v_0 - \frac{1}{M} \int_0^t EA_0 \varepsilon_b(t) dt \right] dt + \int_0^t c \varepsilon_b(t) dt \right\}$$

where  $\ell_0$ , and  $V$  are the initial length and volume of the sample,  $E$  and  $A_0$  are the Young's modulus and the cross-sectional area of the bar,  $c$  is the elastic wave velocity in bar,  $M$  and  $v_0$  are mass and the velocity at  $t=0$  of the block pendulum and  $\varepsilon_b$  is the instantaneous strain in the bar.

Nazarenko et al (1994) studied the effect of temperature and hydrostatic pressure on necking behaviour of polycarbonate (PC), following the concepts that neck geometry and neck propagation were related to the material parameters: strain rate sensitivity and strain hardening parameter. They established the relationship between the neck profile and the true stress-strain curve. This is made by combining an analytical expression for the macroscale mechanics of the flow process with a constitutive equation involving the true stress, strain and strain rate dependence of the material. They found that the strain hardening was insensitive to changes in pressure and temperature in the range they studied, whereas the strain rate sensitivity parameter increased with pressure and decreasing temperature. In their study, the constant strain hardening coefficient confirmed the insensitivity of the molecular network to pressure and temperature, while the strain rate sensitivity, reflecting the thermally activated shear process, was affected by changes in pressure and temperature.

An exploding wire method is used by Parry et al (1988, 1990) to produce high pressure blast-wave loading of thick polymeric cylinders. They measured outer

surface hoop strain at strain rates of about  $10^3 \text{ s}^{-1}$ . From their results the measured hoop strain profiles agree best with predictions for values of Young's modulus which are much higher than those measured under quasistatic conditions. Their computer prediction is based on a discontinuous step numerical method developed by Mehta and Davids (1966). Parry and co-workers found that LDPE shows a six-fold increase of modulus, HDPE more than 100%, nylon 66 about 75%, and nylatron a 25% increase compared with the static results.

Rosenberg and Partom (1983) used a longitudinal strain gauge technique to measure the residual strains and uniaxial tension states of shock loaded PMMA. They showed that the residual strains are related to residual temperatures which prevail in the sample after completion of the loading-unloading cycle, through the thermal expansion coefficient. After shock loading, and subsequent release from a free surface, the sample reaches a residual temperature  $T_R$  which is higher than the room temperature  $T_0$ . This residual temperature causes a residual uniaxial strain  $\epsilon_R$  in the sample which is connected to  $T_R$  through the thermal expansion coefficient  $\alpha$  as in the formula

$$\alpha(T_R - T_0) = \epsilon_R$$

This formula is implied for materials where one can attribute the whole residual strain to the residual temperature.

An experimental and analytical investigation of the large strain compressive and tensile response of a glassy polymer is reported by Boyce and Arruda in 1990. They examined the plastic flow of PC by obtaining true stress - strain data over a range of strain rates at room temperature through homogeneous, uniaxial, constant strain rate compression testing to strains up to 125 %. Under the uniaxial compression loading conditions, the underlying polymeric network chain structure is undergoing a planar orientation process which gives rise to the corresponding observed strain hardening behaviour in compression. The necked region of the tensile sample is being cold drawn resulting in a uniaxial state of orientation. Therefore the observed macroscopic strain hardening in uniaxial tension distinctly differs from that obtained in uniaxial compression, giving different stress-strain curves. During the tensile testing a neck develops creating a very inhomogeneous deformation field and thus making it difficult to accurately monitor the strain and obtain conditions of constant strain rate. One

of the techniques used to compensate for the occurrence of necking is principally monitoring the local stress and strain fields in the necking area. It is relatively easier to achieve a controlled homogeneous deformation in compression than in tension or torsion despite the barrelling which may occur in the compression test. The barrelling can be reduced by using lubricant and also by keeping length / diameter ratio small. In general, the strain hardening in tension is a result of a uniaxial orientation process, whereas in compression planar orientation is achieved.

The temperature effect on tensile yield of polyethylene has been studied by Hartmann and co-workers (1986). Their uniaxial tension tests to yield were performed as a function of temperature from 21 – 117 °C at a strain rate of 0.03 s<sup>-1</sup>. They found that yield energy is a linear function of temperature, extrapolating to zero at melting point (140 °C). The ratio of yield to (initial) Young's modulus is found to increase with increase of temperature, and to decrease with log strain rate.

Hasan et al (1993) have undertaken an experimental investigation to assess the effect of thermomechanical treatment on the inelastic deformation behaviour and corresponding 'structural' state of glassy polymers. They conducted uniaxial, constant strain rate and isothermal compression tests over a range of strain rates and temperature. They concluded that the compressive yield stress of an aged polymer can be substantially greater than that of an identical, but unaged polymer. After sufficient inelastic deformation, the initial thermomechanical history of glassy polymer samples is completely erased as evidenced by identical values of flow stress following strain softening for both annealed and quenched polymer samples. The amount of strain softening which occurs during isothermal deformation was found to be independent of strain rate. The obtained stress-strain results provide experimental evidence that an increase in free volume with inelastic straining accompanies the macroscopic response of strain softening and that strain softening is a deaging effect.

Johnson and Goldsmith (1969) studied polyethylene, nylon and polyester to ascertain the existence of a simple relationship between stress history, temperature, strain rate, and birefringence. The amorphous nylon was found to be very birefringent in the plastic region, but it displayed plastic instability. The polyethylene tested was found to be very tough and had a large plastic

deformation. It had a good strain-optic coefficient and yielded to a uniform plastic section with large deformations. Johnson and Goldsmith found that the materials they tested exhibit a linear strain-birefringence relation up to a strain of about 20 %, but no significant strain rate dependence. However, they found that when strain up to 100 % is induced, the strain-birefringence results can no longer be expressed as a straight line. The materials were tested at a strain rate of about  $10^{-2} \text{ s}^{-1}$ .

Four hard plastics were tested at various strain rates and the temperature rises measured during the sample deformation by Chou et al (1973). Chou and co-workers showed the significant effects of strain rate and temperature rise on the stress-strain relationships for these polymers. The temperature rise was linearly related to the strain after the yield point of the sample. The reason for not measuring the temperature before the yield point, is that the temperature rise is small due to the viscous behaviour of polymers. The measurements were made by a thermocouple embedded in the sample tested by a SHPB system.

#### 1.2.1.2) Microscopic analysis

The large deformation of polymers is based on the behaviour of the molecules during yielding (Ward (1979)). This yield is temperature and strain rate dependent and molecular re-orientation can occur with plastic deformation (Dawson (1993)). During the deformation, the molecular chains are aligned by orientation leading to crystallisation of the polymers and this may cause strain hardening.

Beguenlin and Kausch (1994) studied the effect of the loading rate on the fracture toughness of PMMA, PEEK and modified PVC at room temperature and testing speeds from  $10^{-4}$  to  $10 \text{ ms}^{-1}$ . Their results are correlated with fractographic studies using scanning electron microscopy (SEM). The results show that for some materials the high values of critical fracture toughness ( $K_{Ic}$ ) at low testing rates are associated with deformation detectable by SEM.

Weiss and co-workers (1970) in their investigation on polyester-styrene copolymer found that the optical behaviour is linear with strain and independent of strain rate while the elastic-plastic mechanical behaviour was only slightly dependent on strain rate. Comparison with the results of similar experiments at lower strain rates obtained by means of Instron tests reveals that both

mechanical and optical properties vary significantly with strain rate and these variations of flow stress with strain rate obey a power law.

Blundell et al (1994) studied the changes in orientation and crystallinity during annealing of cold drawn samples of PEEK. This study was made using two-dimensional wide- and small-angle x-ray scattering. It is important to study the effect of physical properties and annealing on the microstructure and morphology of polymers. The principal reason for this is that the production of fibres and films from a thermoplastic polymer commonly involves drawing at a variety of temperatures. Also their study contributes to fundamental polymer science through an understanding of molecular mechanisms which determine the response of a polymer to thermal and mechanical stress. Blundell and co-workers observed in their study at temperatures around  $T_g$  that the molecular orientation present as a result of cold drawing is apparently lost and subsequently recovered during a heating programme.

Deopura et al (1983) studied the variation of physical properties with increasing moisture content in nylon. Their study led to an explanation based on the difference in mobility and free volume of the nylon structure due to the different methods of bonding of water molecules within the polyamide chains at different regions. The change in glass transition temperature and mechanical properties are a function of moisture level, in both oriented and unoriented nylons. The  $T_g$  and mechanical properties decrease with increasing moisture content.

Dawson, Swallowe and Xinwu (1991) have carried out experiments to measure stress-strain and bulk and localised temperature rises in a wide range of polymers during the high strain rate deformation. Their results suggest that a significant thermal decomposition may occur ahead of running cracks in some materials and in all cases heating leads to deviations from a true isothermal stress-strain curve. Dawson and co-workers in their work raised two points. First, that temperature rises in polymers with a high yield stress are sufficiently high, even at relatively low strains, to considerably change the experimentally determined stress-strain curve from its isothermal value. Secondly, that temperature rises ahead of cracks in materials such as PC, PEK, and PEEK are likely to be sufficiently high to form craze like regions and voids which may act as craze initiators. For materials which did not exhibit cracking the temperatures achieved were not sufficient to cause appreciable decomposition despite the much larger duration of these bulk temperature rises.

Gilbert and co-workers (1986) studied the modulus maps for amorphous polymers: PMMA and PS. They identified four regimes of deformation dependent on time scale and temperature. These regimes are:

a) the glassy regime, with a modulus of between 1 and 10 GPa, associated with stretching and bending of intermolecular bonds, and showing only a slight time-dependence associated with a number of secondary relaxations. In this regime, bond stretching and bending control the modulus which directly reflects the stiffness of the Van der Waals bonds which bind one chain to another. The covalent C-C bonds which form the chain backbone are about 100 times stiffer than the Van der Waals bonds and their stretching and bending contribute nothing of significance to the elastic deformation.

b) the glass-transition regime, in which the modulus drops steeply from around 1 GPa to near 1 MPa with increasing temperature or time of loading.

c) the rubbery regime, with a modulus around 1 MPa, associated with the rubber-like sliding of the long-chain network of molecules, constrained by entanglements which behave physically like cross-links.

d) the viscous regime, at temperature above the glass transition temperature, in which the polymer can be thought of as a viscous liquid, whose molecules move relatively to each in a snake-like manner which, biased by stress, leads to viscous flow. After this region the chemical breakdown begins and the mechanical properties change in an uncontrolled way. The viscosity regime depends on molecular weight (i.e. reducing the molecular weight will increase the polymer viscosity).

Imai and Brown (1976) investigated the effect of strain rate on craze yielding, shear yielding and brittle fracture of PMMA, PC, PTFE, and PS in liquid nitrogen (at 77 K) over the strain rate range of  $2 \times 10^{-4} \text{ min}^{-1}$  to  $660 \text{ min}^{-1}$ . These polymers deformed by crazing which was induced by liquid nitrogen. They found the stress versus log strain rate curve was sigmoidal in that its slope increased and then decreased with strain rate. They suggested that the non-linear behaviour of stress versus log strain rate at low strain rates was associated with a decrease in activation volume with increasing strain rate whereas the non-linear behaviour at high strain rates was associated with an increase in density



and decrease in length of the crazes with strain rate. However they concluded that the effect of strain rate on the tensile stress was sigmoidal in the case of crazing and linear for shear deformation. The activation volume for crazing decreased from about 350 to  $100\text{\AA}^3$  as the stress increased. The activation volume for shear deformation in PC was  $360\text{\AA}^3$  for compression and larger for tension. There is a critical strain rate above which the crazes become too short to be seen. Above that strain rate, tensile strength becomes almost constant. The diffusion coefficient of the liquid nitrogen into the polymer, which governs the crazing, can be estimated from the stress-strain experiments and from the density and length of the crazes.

Klein et al (1986) studied the effect of electron irradiation of the structure and mechanical properties of oriented monofilaments produced by drawing of an isotropic polyethylene. The study was made by elasticity measurements, x-ray diffraction, differential scanning calorimetry and tensile creep behaviour of the oriented (draw ratio 12:1) polyethylene filaments produced by drawing electron-irradiated isotropic monofilament. For irradiation of up to a gel dose of 2.4 Mrad, the degree of crystallinity (DC) of drawn filaments remains, but the melting temperature decreases slightly owing to network junctions at the fold surfaces. Above the gel dose, DC drops significantly and melting temperature falls more sharply, as a result of crystallite distortion. Irradiation dramatically affects the creep behaviour, increasing the activation volume of the process occurring in the crystal, and is ascribed to an increase in crystallite imperfections and hence the mechanical behaviour is affected. The electron irradiation of polyethylene below its melting temperature produces extensive branching, and at doses above about 2.4 Mrad, the formation of a permanent network.

Swallowe, Field and Horn (1986) used a heat sensitive film to measure the transient high temperatures during the deformation of polymers under impact using a drop weight machine. In their measurements they found very high temperatures up to  $700^\circ\text{C}$  can be generated in materials which undergo catastrophic failure, and that the temperatures obtained are related to the material's thermal and mechanical properties. The mechanical energy is converted into heat during deformation at high strain rates. This heat depends on the mode of deformation and may be localised at crack tips on the shear planes or may produce a more uniform bulk temperature rise. The measurements were taken for polymers HDPE, PP, PVC, PC, PMMA, PS and PTFE.

## 1.2.2 Yield behaviour

The earliest ideas of yielding mechanisms were based on mechanical work raising the sample temperature to  $T_g$ , or on free volume from a dilatometric strain bringing  $T_g$  down to the test temperature. In either case, chain stretching would occur quickly in a stressed glassy polymer. These ideas do not seem to be the fundamental reasons for polymer yielding because the work done on a glassy polymer is not always sufficient to raise the sample temperature to  $T_g$  even in the adiabatic limit. Furthermore, the yielding occurs at a low strain rate or with the sample under conditions which are isothermal ( $T < T_g$ ) to a high degree of certainty.

Young and Lovell (1991) studied the mechanism of deformation of semi-crystalline polymers, two phase materials where properties such as the modulus depend not only on the proportion of crystalline material present, but also on the size, shape and distribution of the crystals within the polymer sample. It has been thought that amorphous polymers are brittle materials, but they can display a considerable amount of ductility before the glassy rubber transition, especially when deformed in compression. The glassy polymers tend to show strain softening when the true stress drops after yield.

Seguela and Rietsch (1990) showed two mechanisms of plastic deformation in polyethylene during tensile tests. These mechanisms were governed by two structural processes: slip of crystal blocks past one another in the mosaic crystalline structure and a homogeneous shear of crystal blocks.

In 1976 Briscoe and Hutchings used the Taylor impact method to study the impact yielding of HDPE at high strain rates of about  $3 \times 10^3 \text{ s}^{-1}$ . The technique involves impacting a cylindrical sample against a massive steel anvil, and photographing the deformation of the sample during the impact, using high speed photography. The yield stress  $\sigma$  was estimated from the geometry of the impacted sample using the following formula:

$$\sigma = \frac{\rho V^2 (L_0 - X)}{2(L_0 - L) \ln(L_0 / X)}$$

and the mean rate of strain  $\dot{\epsilon}$  during the impact:

$$\dot{\epsilon} = \frac{V}{2(L_0 - X)}$$

where  $\rho$  and  $V$  are respectively the density of the sample and impact velocity.  $L_0$  is the original length of the cylinder and  $L$  is the final length including the

undeformed length  $X$  of the cylinder. Briscoe and Hutchings compared their results with ones they obtained using instrumented drop-weight apparatus used for high strain rates tests, though the cylindrical samples used here are smaller than those used in the impact tests (diameter 6 mm, length 6 mm) and a certain amount of barrelling was detected in the deformed samples.

Channel, Clutton and Capaccio (1994) studied the impact behaviour of a linear low density polyethylene LLDPE using the energy partitioning methodology. The aim of their study was to investigate the origin of the high toughness of the polymer and to establish whether a rubber toughening mechanism is involved. They found that LLDPEs have a high intrinsic toughness and that there is a significant ductile contribution to the total fracture energy from shear lip energy absorption. They also found no evidence of a rubber toughening mechanism. They concluded their investigation by identifying two distinct factors that were responsible for the high fracture toughness of LLDPE. First, the apparently high value of the intrinsic toughness, which is related to the energy required to create two new surfaces, is a fundamental material parameter which is likely to be sensitive to the structure of the polymer, e.g. to the presence or absence of short chain branching. Second, there is a ductile failure phenomenon which involves extensive regions near the surface of the sample (shear lips). The presence of a segregated rubbery phase has no effect on the intrinsic toughness, but it affects the extent of shear lips formation. Hence the higher the concentration of segregated phase, the larger the shear lips area and hence the specific component of the absorbed energy.

G'Sell and Jonas (1979) performed a tensile test at constant cross-head speed to investigate the mechanical properties of solid polymers i.e. yield stress and maximum draw ratio, which are needed when these materials are employed in structural applications. The early occurrence of necking in their tests was one of the difficulties in the physical interpretation of the quantities usually derived from the experimental data. G'Sell and Jonas found that a large variation in local strain rate occurs while necking and cold-drawing take place. Hence, they used a new method in which the samples are tested at constant local true strain rate. This method is based on using a diameter measuring transducer, an exponential voltage generator and a closed-loop testing machine. The tests were made to study the plastic behaviour of polymers, HDPE and PVC at constant true strain rate. G'Sell and Jonas concluded that the nominal stress-strain curve obtained from the conventional tensile test does not reflect the local flow behaviour of

polymers. This is because during a test at constant cross-head speed, the local true strain rate exhibits very large variations. In general the internal stress acts as a backward driving force which tends to return the material to its undeformed state.

Gent (1986) measured draw ratios for samples of polyethylene and trans-polyisoprene, crystallised at various temperatures and at various degrees of orientation. The most remarkable feature of partially crystalline polymers is their ability to undergo large plastic deformations (drawing) without rupture. This phenomenon is readily distinguished from plastic yielding in ductile metals, which is considerably smaller in extent, or in glassy polymers, where yielding is localised within narrow shear bands. Gent found the yield stress to be virtually unchanged by prior orientation but the natural draw ratio decreased in inverse proportion to the amount of reorientation.

Bauwens-Crowet (1973) has observed a beta relaxation at  $T \approx 20^\circ\text{C}$  in the yielding of PMMA, associated with side chain motions of ester groups. This relaxation appears to have little influence on the fracture behaviour of PMMA: a single-stage Eyring equation suffices. The shear activation volume  $v_f = 0.46 \text{ nm}^3$  for fracture of PMMA is an order of magnitude less than the values  $v = 4 - 6 \text{ nm}^3$  observed in the tensile and compressive yield of PMMA, by Haward and Thackray (1968) and by Bauwens-Crowet (1973). This suggests much less co-operative motion of chain segments required for nucleating crazing (and thereby causing fracture) than for nucleating yield.

Wiebusch and Richter (1986) used a modified Charpy test with double -V notches to determine the impact strength of nylon. Their tests were adjusted to obtain a sensitive, accurate and reproducible method for the determination of impact strength in the dry and moist states. They found that the dry state is unstable and that the impact strength decreases exponentially with storage. Therefore comparison tests are not valid unless the measurements are performed within a restricted period of time after the samples had been remoulded.

Brooks et al (1992) found double yield points in the stress-strain curve of polyethylene using three samples with different degrees of short-chain branching. They showed stress-strain curves with clear double yield points at tests made over a range of temperature. Measurement of residual strains of the

samples as a function of the level of maximum strain applied under constant strain rate test show that the first yield point marks the onset of "plastic strain" which is slowly recoverable at least in part. Deformation beyond the second yield point is effectively irrecoverable and is associated with a sharp necking of the sample. For samples which initially deform homogeneously the maximum point (yield point) occurs due to the internal plastic strain rate of the material increasing to a point where it becomes equal to the applied strain rate. For the polyethylene, the yield point becomes less defined as the testing temperature is increased or the strain rate is decreased. The temperature at which the local yield disappears is lowest for the most branched material and highest for the unbranched, high density material.

Thermal history imparted during processing has a large effect on the mechanical properties even at temperatures far below  $T_g$ . As Cebé and co-workers (1987) reported, drawing PEEK at a temperature near  $T_g$ , produced an increased degree of crystallinity and thus increased yield stress and stress for neck deformation in tension. The slowly cooled film of PEEK broke at comparatively low strain, while the air cooled film was drawn to a much greater extension. The double yield behaviour is attributed to an inhomogeneous deformation process, possibly the result of voids remaining in the sample after compression moulding. Voids would act as stress concentrators and the material surrounding a void could yield by a slip - and stick mechanism, and this would account for the highly irregular stress-strain behaviour between the two yield points. Cebé and co-workers mentioned that during fracture the cross-sectional area decreases as the crack propagated, and local regions can experience much larger stresses.

Hope, Ward and Gibson (1980) tested different grades of PMMA and found that the higher molecular weight grade exhibits substantial strain softening whereas the lower molecular weight grade shows very little.

Kamei and Brown (1984) studied the crazing behaviour of polyethylene at low temperature. It was found that in general polyethylene crazes in gases such as nitrogen at low temperature. The decrease in the tensile strength of polyethylene in an environmental gas is greater with crystallinity. The differences in the intrinsic low temperature brittle fracture stress are attributed to differences in the density of the molecules. The intrinsic yield point at room temperature showed the usual increase with increasing crystallinity, but all polyethylenes have the same yield point below transition temperature. The gas

when absorbed by the polyethylene acts as a plasticizer by crazing the intermolecular bonds. So, in order to produce crazing, the gas need only dissolve in the surface layer and then enter the interior through the pores of the craze.

### **1.2.3 Elastic and plastic properties**

In their study of linear polyethylene Fotheringham and Cherry (1978a, b) showed that the difference between the applied force and the recovery force represents the effective force which acts on the anelastic processes and a consideration of the kinetics of deformation suggests that the anelastic process consists of the co-operative movement of a number of molecular segments. They found that up to the elastic limit the recovery stress is a linear function of strain at a given cross-head speed of the testing machine. They did not find a consistent trend in results above a strain of 0.3 and some of the permanent plastic strain in linear polyethylene is a continuous function of the applied strain, showing no discontinuity at the extrapolated yield point. They noted that the yield stress (which is defined by the appearance of slip bands) of amorphous polymers falls to zero as the temperature rises to the glass transition.

Plane simple shear tests were performed by G'Sell et al (1983) using a simple shear apparatus to determine the plastic behaviour of various amorphous and semicrystalline polymers at large shear strains. They showed that a nearly homogeneous plastic shear strain could be achieved without buckling, provided the thickness, width and length of the sample's calibrated part are proportional to 3, 4 and 60 respectively. Due to the absence of crazing, large shear strains could be reached before rupture even for polymers which exhibit a very brittle behaviour in tension.

Hillier (1949) measured some dynamic elastic constants of polythene by taking measurements of velocity of propagation and attenuation of longitudinal sound oscillations in the high polymer filaments at a range of temperature between 0 °C and 50 °C and a frequency range of 500 Hz to 30kHz. His aim was to study the mechanical behaviour of some long chain polymers when subjected to small, rapidly changing forces, in order to separate the elastic and plastic components of strain. This method involved sending a sonic or ultrasonic wave along a filament of the material, and measuring the velocity of propagation and attenuation per unit length.

Hillier and Kolsky (1949) used frequencies between 1 kHz and 6 kHz in their investigation of the transmission of sound along filaments of polythene, neoprene and nylon. The measurements were made for unstrained samples and samples during testing at a constant strain rate. The stress-strain curve in such measurements is complicated by orientation produced by the applied stresses. In general the elastic moduli are found to be much greater for highly oriented materials than for such materials in the isotropic state.

Morris and Riley (1972) developed a method for elastoplastic stress analysis using optical effects of transparent materials. They found that unload birefringence (fringe order immediately upon removal of load) could be used to determine strain for a uniaxial stress field, and provide a means for evaluating stress and strain concentration factors.

Saimoto and Thomas (1986) published a paper describing a method to measure the elastic modulus of semicrystalline polyethylene as a function of tensile deformation during an instantaneous strain rate change. The elimination of machine transients during the strain rate change permits the observation of the stress reduction which must occur to maintain the steep change in non-elastic strain rate. This change can be fast enough to determine the incremental changes in stress and strain before relaxation processes take place. Their results show that at 23.1 °C the unrelaxed modulus decreases with strain whereas at 51 °C it is constant. It seems that at room temperature the strain dependence of modulus change decreases with decrease in the degree of crystallinity.

#### **1.2.4 Viscoelastic properties**

A number of commercial polymers were tested by G'Sell and Jonas (1981) in tension at 22 °C at constant true strain rates of  $10^{-4}$  to  $10^{-1} \text{ s}^{-1}$ . They observed the true yield drops in rigid glassy polymers, whereas yielding was more gradual in the semi-crystalline or plasticized polymers. They performed strain rate change tests, during which one order of magnitude increases and decreases were imposed on the samples. G'Sell and Jonas have set a model of the deformation behaviour of the polymers based on composing the total strain into three components

$$\varepsilon = \varepsilon_{el} + \varepsilon_{visc} + \varepsilon_{pl}$$

where elastic strain  $\varepsilon_{el}$  is due to the deformation of intermolecular bonds, is immediately recoverable and is characterised by high modulus  $E$ , so that it can be expressed to a first approximation as  $\varepsilon_{el} = \sigma / E$ .

The viscoelastic strain  $\varepsilon_{visc}$ , associated with the limited retarded movement of amorphous chains, is largely recoverable within a short time scale and is homogeneously distributed within the amorphous parts of the sample. It is responsible for generating the internal or back stress in the regions in which it has effect. The viscoelastic response can be large only in polymers whose  $T_g$  is lower than the testing temperature. The  $\varepsilon_{visc}$  can be obtained from the classical Voigt-Kelvin viscoelastic equation

$$\dot{\varepsilon}_{visc} = \frac{\frac{\sigma}{E_v} - \varepsilon_{visc}}{\tau_R}$$

where  $\tau_R$  is the mean retardation time and  $E_v$  the relaxed modulus.

The plastic strain  $\varepsilon_{pl}$  has been shown in amorphous as well as in semicrystalline polymers to have a fundamentally inhomogeneous nature. It proceeds by local shearing within deformation bands, which can be narrow or more diffuse according to the material. The constitutive equation for the plastically deformed regions is

$$\dot{\varepsilon}_{pl} = \dot{\varepsilon}_0(T) e^{(v_a \sigma^* / kT)}$$

where  $\dot{\varepsilon}_0(T)$  is a pre - exponential factor which incorporates both the probability of thermally aided deformation (i.e. the activation energy term) and the dependence of the microstructure on temperature ( $T$ ),  $k$  is the Boltzmann constant and  $v_a$  is the apparent activation volume which characterises the strain rate sensitivity of the material, and  $\sigma^*$  is the effective stress. One of the aims of the study of G'Sell and Jonas is to determine the intrinsic material behaviour under constant strain rate conditions.

A constitutive equation is derived by G'Sell and Jonas relating stress to strain and strain rate, by suggesting that experimental data could be fitted with an additive equation of the type

$$\sigma(\varepsilon, \dot{\varepsilon}) = \sigma_i(\varepsilon) + \sigma^*(\dot{\varepsilon})$$

where  $\sigma$  = stress

$\varepsilon$  = strain

and  $\dot{\varepsilon}$  = strain rate

The first term  $\sigma_i(\varepsilon)$  represents the internal stress and measures the effect of true plastic strain accumulated in the material during the previous mechanical



history of the sample. Also it is stated by Fotheringham and Cherry (1978a, b) that this internal stress acts as a backwards driving force which tends to return the material to its undeformed state. The internal stress can be considered to be caused by the rubber-like entropic forces which make the chains retract when they are unloaded after an extension. The second term  $\sigma'(\dot{\epsilon})$  of the G'Sell and Jonas equation, reflects the strain rate sensitivity of the material.

The strain rate sensitivity can be determined from a plot of  $\sigma$  against  $\log(\dot{\epsilon})$ . The effective stress  $\sigma'$  increases with  $\log(\text{strain rate})$  as

$$\sigma' = \frac{kT}{v_a} \ln\left(\frac{\dot{\epsilon}}{\dot{\epsilon}_0}\right)$$

where T is the temperature.

The exact microstructural origin of the internal stress is difficult to specify with certainty, especially in the semi-crystalline polymers when the contribution of the crystalline lamellae and amorphous regions cannot be easily understood.

### **1.2.5 Fracture of polymers**

Egorov et al (1990) used broad-line proton NMR and scanning electron microscopy to study the cessation of drawing and the local fracture processes that are occurring in linear polyethylene near ultimate draw ratios. They noticed that when the ultimate draw ratio is reached during drawing, the sample whitened and kink bands similar to those observed in the deformation of low molecular weight solids were formed. They were convinced by NMR that the segmental mobility of chains in the amorphous regions is almost completely suppressed because of a sharp increase of the orientation stress near the ultimate draw ratio (though the temperature of drawing is close to the melting temperature). This phenomenon of mechanical vitrification is regarded as a fundamental reason for cessation of drawing and for transition to the "solid state" fracture mechanism. The main interest was to achieve the highest possible draw ratios for flexible-chain polymers, and this is important for producing ultra - high strength and ultra high modulus film and fibres since the tensile strength and the elastic modulus grow with increasing draw ratio.

Field et al (1984) studied the mechanical and ignition behaviour of explosives including some polymer bonded explosives (PBX's) at high strain rates using drop-weight apparatus with high speed photographic recording of the impact and ignition processes.

Frounchi et al (1994), conducted mechanical properties and fracture tests on the thermoset diethylene glycol bis (allyl carbonate) (ADC) resins. He found that both  $\sigma_y$  and  $E$  increase as testing rate increases. Linear elastic fracture mechanics concepts were employed to analyse the stress intensity factors versus the yield stress. It is suggested that the stick-slip behaviour is due to blunting of the crack, which is controlled by the yield behaviour of the resin. The fracture surfaces were analysed using SEM and optical microscopy. An Instron 1122 machine was used for compressive tests for yield measurement of cylindrical samples 10 mm long and 5 mm in diameter using various crosshead speeds at room temperature. The samples for Young's flexure modulus determination were rectangular plates (14 × 80 mm). The crack propagation was studied using the double torsion (DT) testing geometry, where the samples were cut in the form of 3.7 × 30 × 6 mm rectangular plates from cast sheets of ADC. The samples were notched at one end and a sharp blade was run along the sample from the notch tip. The DT samples were also tested in the Instron machine under compressive loading at different crosshead speeds. The Young's modulus and yield stress were noted to increase with the increase of crosshead speed.

### **1.3 Work described in this thesis**

The present work is involved in studying polymer behaviour from low to very high strain rates in uniaxial compression and tension.

This thesis describes an investigation of high strain rate behaviour of four engineering polymers: HDPE, UHMWPE, nylatron and PEEK 150g (g stands for granule). Extensive work has been done using the Split Hopkinson Pressure Bar (SHPB) system to study the response of polymers to high strain rates in compression. Studies were also made at low strain rates using a Hounsfield testing machine to enable a wide range of strain rate properties of the polymers to be studied.

Parallel studies have been carried out using an exploding wire technique (impulsive loading of the inside of a hollow cylindrical sample), in conjunction with high speed photography to study the behaviour of the polymers under very high tensile strain rates and fracture conditions. This system is also used in conjunction with a freely expanding ring technique in which a thin ring of material to be tested is placed on the outside of a hollow cylinder.

A theoretical study has been made to examine the stress equilibrium in the SHPB sample using multiple reflections theory in the sample. This study simulates the elastic behaviour of the polymers, and hence helps in the interpretation of the SHPB analysis.

Another theoretical study also has been made to study the viscoelastic behaviour of the materials by applying viscoelastic models to the stress-strain curves of the results at different strain rates. Different combinations of spring, dashpot, and yield parameters were used in the theoretical model to fit the experimental data.

## **CHAPTER 2**

### **LOW STRAIN RATE TESTS**

#### **2.1 Introduction**

The main aim of this project is to investigate the response of some engineering polymers to uniaxial compressive loading at high strain rates at room temperature. However, to cover a wide range of strain-rates to large strain, quasi-static tests were also performed using an electronically controlled 5000 kg capacity Hounsfield testing machine.

The Hounsfield H50KM series of tensile testing machines has been designed to cover a wide range of materials being tested in tension or compression up to a maximum loading capacity of 50 kN (5000 kg). Table (2.1) shows the maximum applied force for each of the five force recorder ranges. The force display LED indicates kilo unit and the force display decimal point is changed automatically when the force recorder range is altered. There is a 1 volt output for each range.

Table (2.1) Force ranges of Hounsfield machine.

Force rec. range (%)	Force display (kN)	Applied force (N)
100	50.00	50000
50	25.00	25000
20	10.00	10000
10	5.000	5000
5	2.500	2500

The force recorder electronics has incorporated a force alarm activated when the force recorder output voltage exceeds 1.05 volts (i.e. 105% of the maximum permissible force for those recorder ranges). When this alarm is activated it sets the machine to a stop condition and the appropriate direction switch indicator and the force indicator start flashing.

The extension recorder range can be set to 5 sensitivities. Table (2.2) shows the maximum cross-head movement allowable for each range with respect to zero position (i.e. extension display reset to zero) for 1 volt on the extension recorder output.

Table (2.2) Extension ranges

Ext. Rec. Range (mm)	Extension display (mm)	Cross-head movement (mm)
1000	1000.0	1000
500	500.00	500
100	100.00	100
50	50.000	50
10	10.000	10

If the range has been exceeded the extension alarm which is incorporated with the extension recorder range electronics will be activated. This indicates that the extension recorder output exceeds 1 volt. If the indicator starts flashing you can set the extension range to a higher range, return the display to zero and continue the test. The total extension is now the first range plus the current display value.

The cross head speed of the machine can be controlled and set between 0.1 and 500 mm/min.

## 2.2 Experimental background

Figure (2.1) shows the block diagram of the set-up for the compressive static tests. The testing machine consists of lower and upper platens of hardened steel.

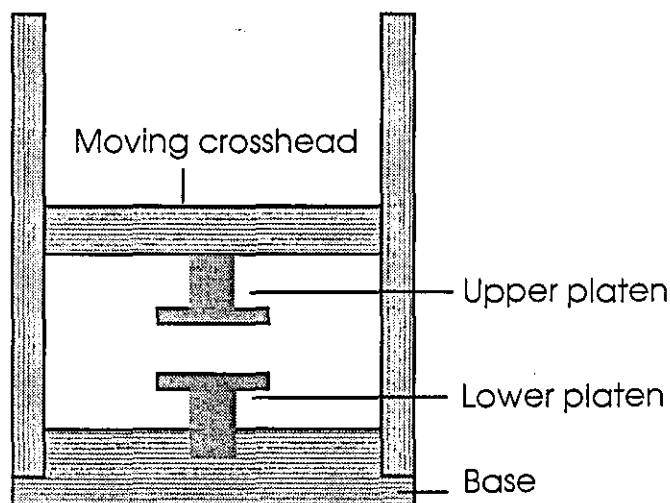


Figure (2.1) Block diagram for the testing machine.

There are several ways to acquire force and displacement data from the machine for compressive tests.

1) The machine is provided with digital indicators on the control panel to display the force and the cross-head displacement which can be read directly while the machine is running.

2) The machine can be controlled by a PC-computer via an RS232 interface built into the machine, and by this way digital data can be transferred to the computer and displayed as a graph of load against displacement. This method is not recommended at this time because the software provided with the machine cannot save the data in a file to be retrieved and used in future work. Also this software does not take the machine compliance into account which could have a significant effect on the results especially when hard materials are tested.

3) The conventional method can be used in which the analogue outputs for the load and displacement provide 1 volt maximum output. By feeding the load output into an XY plotter and running the machine without the sample a compliance plot of load against time including the steel platens can be made. Then running the machine with the sample placed between the platens, the load against time can be plotted for the sample deformation and the machine compliance. The time axis can be converted to displacement using the XY plotter and the cross-head speeds.

$$\Delta x(\text{mm}) = \frac{X\text{speed}(\text{mm}/\text{min})}{XY\text{speed}(\text{mm}/\text{min})} \times t.\text{diff}(\text{mm})$$

where  $\Delta x$  is the displacement, Xspeed and XYspeed are respectively the crosshead and the chart recorder speeds, and t.diff is the time deflection on the chart recorder. The difference in deflection between the two plots represent the sample deformation as shown in Figure (2.2). The load can be calculated by multiplying the vertical deflection in volts by the full load for a particular force range per volt. The real sample displacement versus load is determined by subtracting the compliance curve at given loads from the sample + compliance curve.

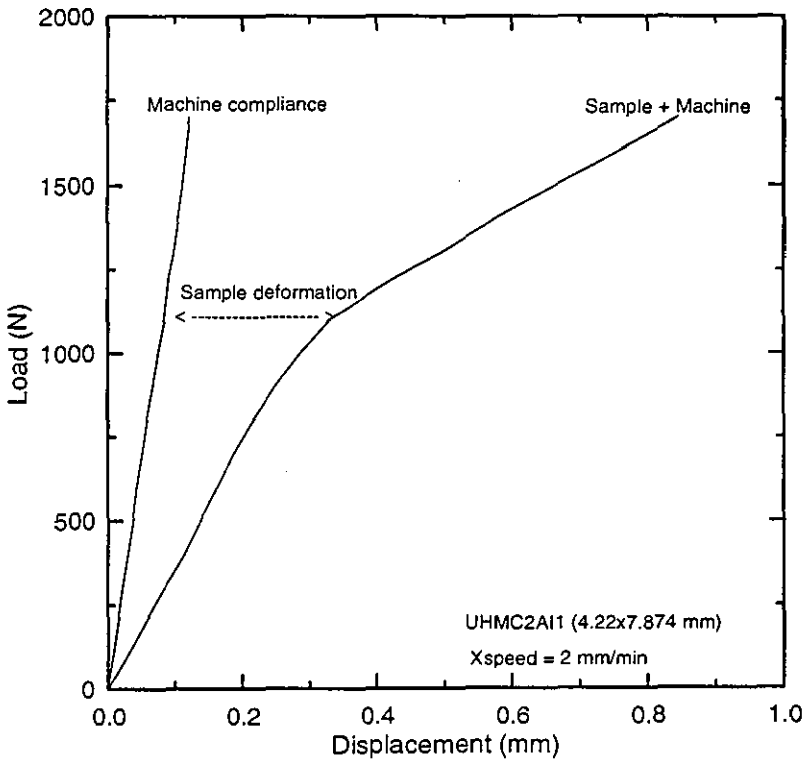
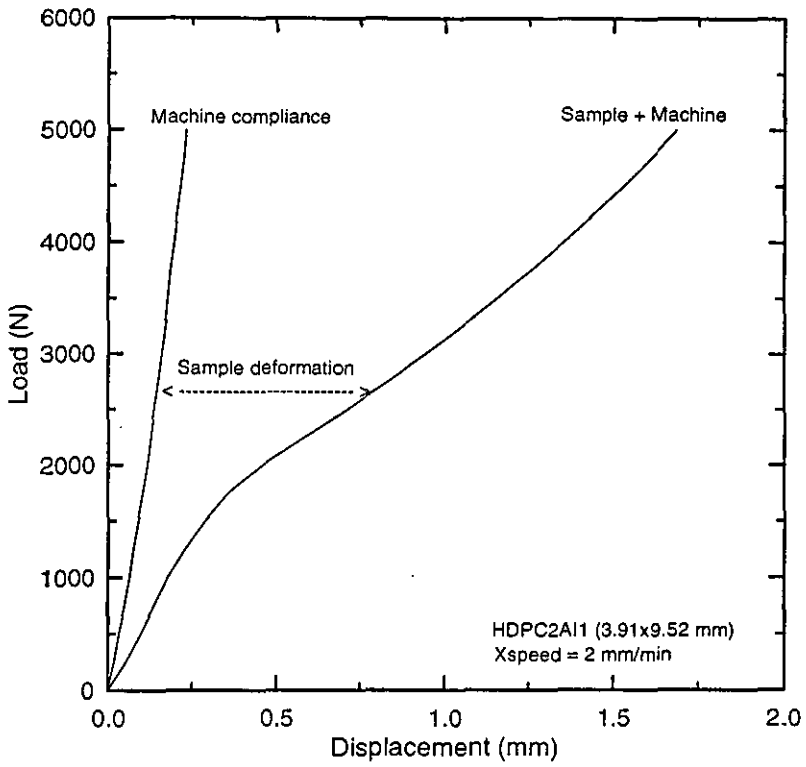


Figure (2.2[A]) Graphs of compressive tests of HDPE, UHMWPE using the Hounsfield machine.

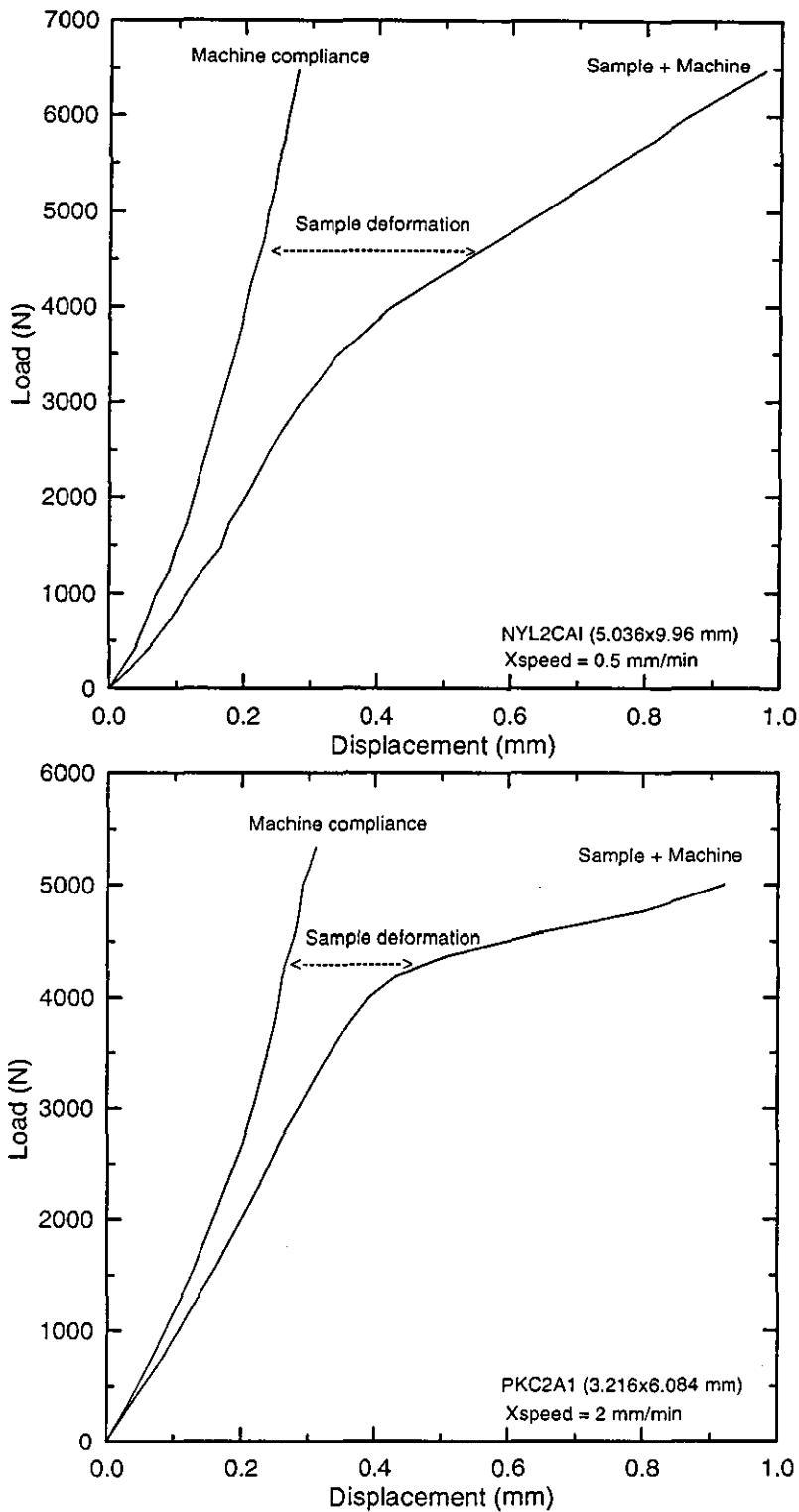


Figure (2.2 [B]) Graphs of compressive tests of nylatron and PEEK using the Hounsfield machine.

4) The analogue outputs can be captured by using a DSO (digital storage oscilloscope) and then transferred into a computer to be analysed. This method is similar to the conventional method.



5) There are a few other methods available which can be used such as using a transducer to measure the displacement directly, an optical method using a laser beam or a travelling microscope to monitor the cross head movement. Also strain gauges can be attached to the sample to read strain directly from the sample.

Some tensile tests have been achieved for UHMWPE and nylatron using a special workshop made adapter (see Figure (2.3)) with the Hounsfield machine. The tensile samples have been cut from a commercial rod to a shape as shown in Figure (2.3). The compliance data for tensile tests is obtained using a steel rod instead of the sample.

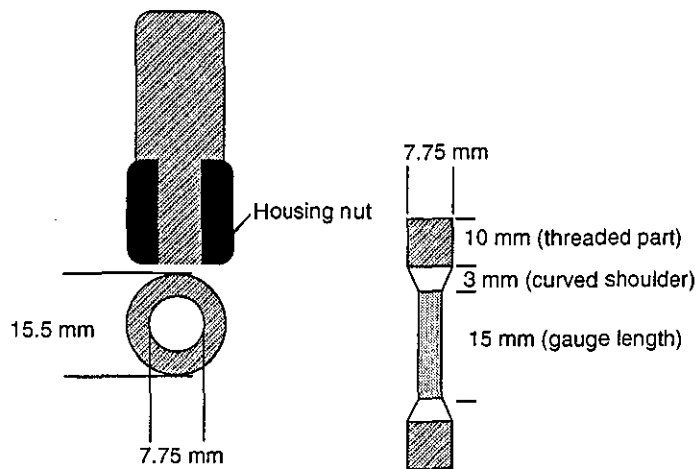


Figure (2.3) Diagram for tensile sample and a tensile adapter.

The shoulder between the threaded part and gauge length part is rounded to reduce any stress concentrations when the sample is stretched. The sample is held by a steel housing nut to support the threads on the end part in order to withstand the loading. Figures ((2.4) and (2.5) ) show load-extension curves of tensile tests of UHMWPE and nylatron samples respectively.

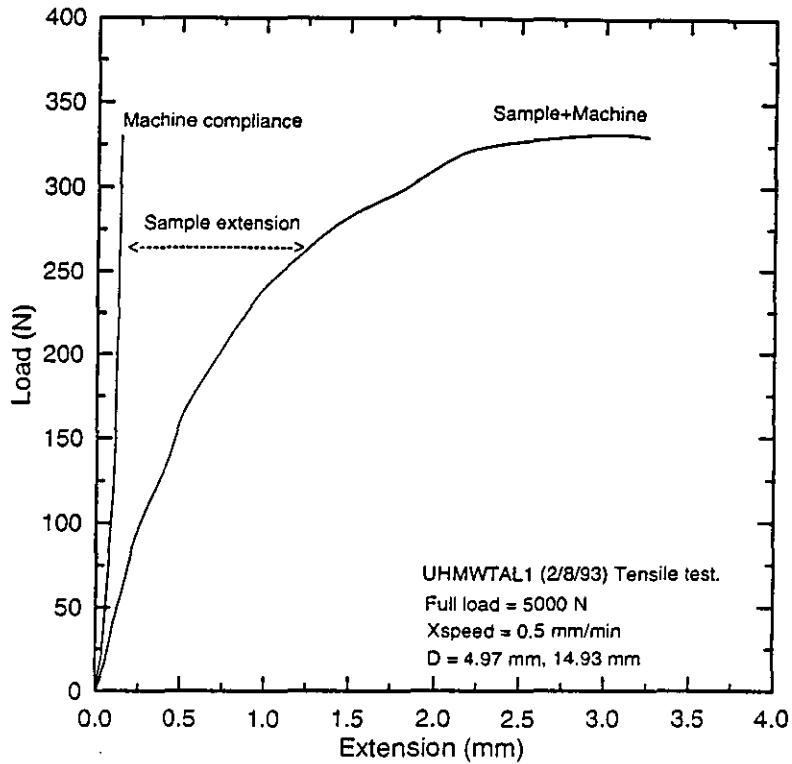


Figure (2.4) Load-extension graph of UHMWPE tested in tension by the Hounsfield machine.

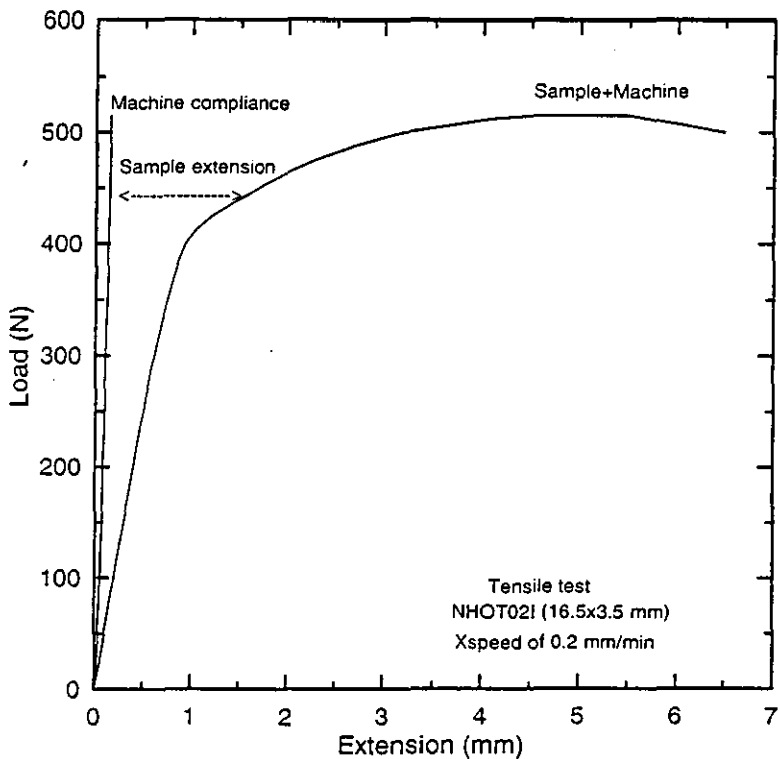


Figure (2.5) Load-extension plot for nylatron tested in tension by the Hounsfield machine.

Having measured the original sample dimensions it is an easy matter to calculate the engineering strain ( $e$ ) and stress ( $\sigma_e$ ) from the load-displacement graph. These are converted in turn to true strain ( $\epsilon$ ) and stress ( $\sigma$ ) as

$$\epsilon = \pm \ln(1 \pm e)$$

$$\sigma = \sigma_e(1 \pm \epsilon)$$

The ' $\pm$ ' sign is '+' for tensile tests and '-' for compressive tests.

### **2.3 Low strain-rate results**

A parallel study of the low strain-rate deformation of polymeric samples similar to those used in the high strain-rate testing has been performed. The quasi-static tests were carried out on the Hounsfield machine with different cross-head speeds to obtain strain rates approximately between  $10^{-4}$  and  $10^{-2} \text{ s}^{-1}$ .

The compression samples used are all of the same dimensions as on the high strain-rate tests using the split-Hopkinson pressure bar (SHPB). The sample faces are lubricated with silicone grease to minimise the friction effects.

HDPE, UHMWPE, nylatron and PEEK have been tested in compression at room temperature, while UHMWPE and nylatron have also been tested in tension. Figures (2.6), (2.7), (2.8) and (2.9) show the stress-strain curves for HDPE, UHMWPE, nylatron and PEEK respectively. Some selected results from these plots are tabulated in Tables 2.3, 2.4, 2.5 and 2.6.

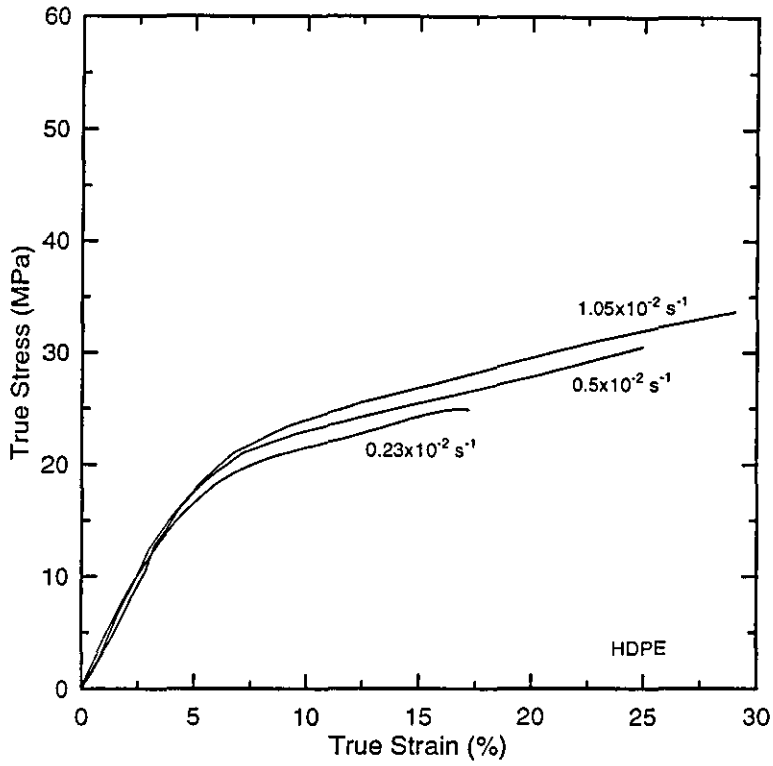


Figure (2.6) Stress-Strain curves of HDPE tested at various quasi-static strain rates.

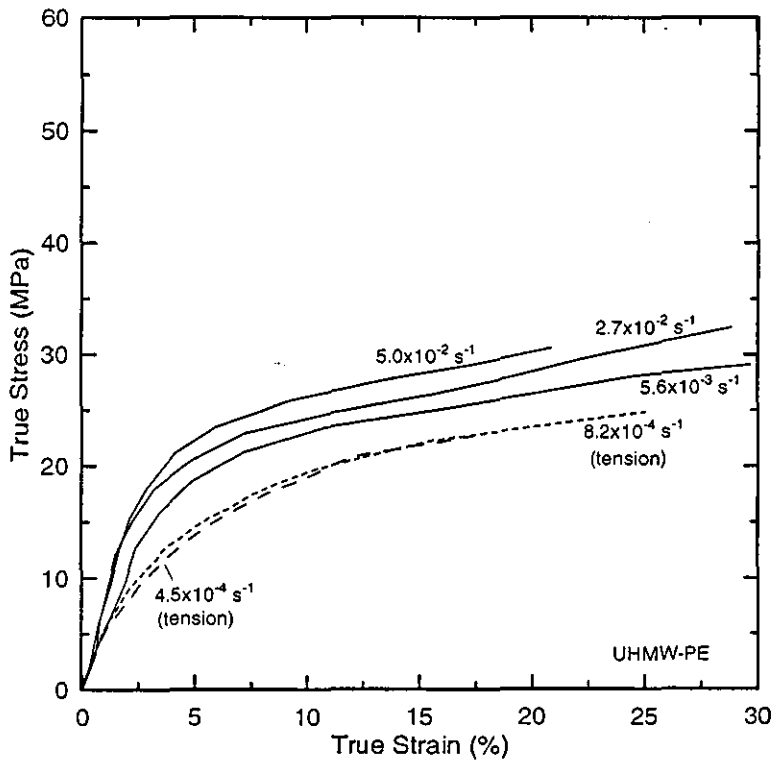


Figure (2.7) Stress-strain curves for UHMWPE at various strain rates.

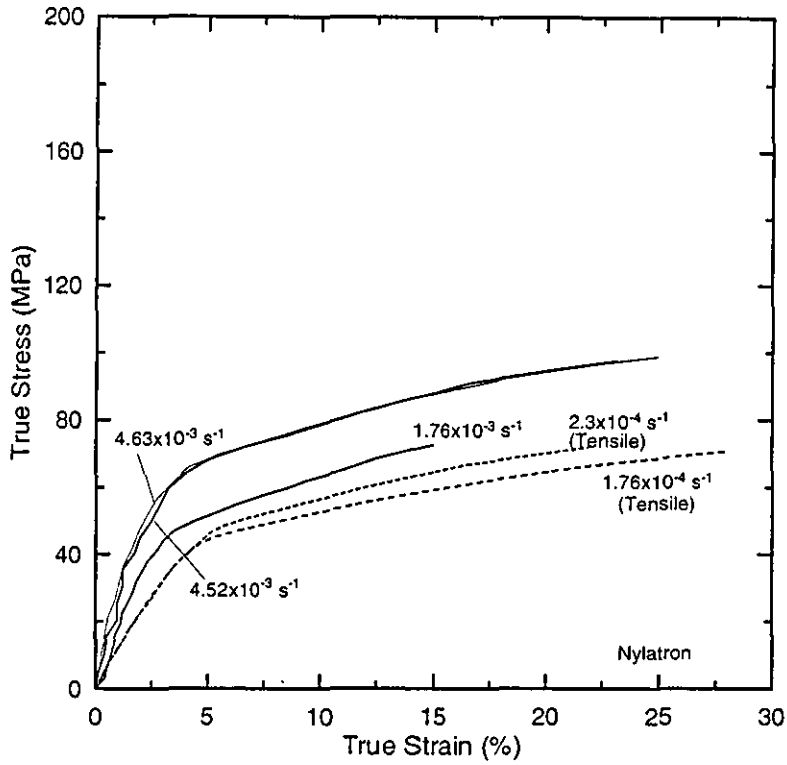


Figure (2.8) Stress-strain curves for nylatron at various strain rates.

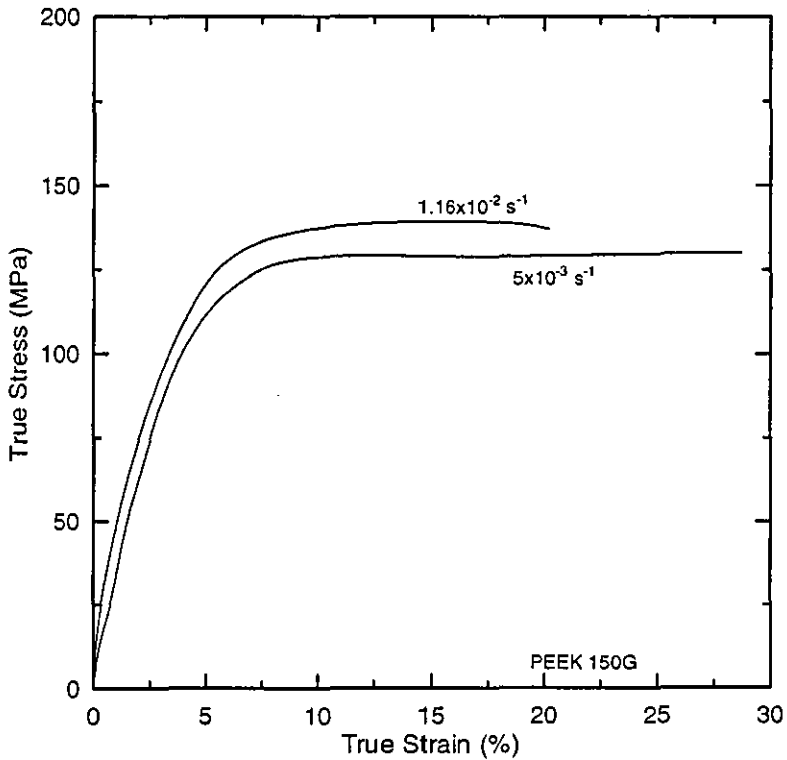


Figure (2.9) Stress-strain curves for PEEK 150G at various strain rates.

Table 2.3 HDPE results

Test type	Strain rate (s <sup>-1</sup> )	E GPa	σ <sub>5%</sub> MPa	σ <sub>10%</sub> MPa
Compression	0.23x10 <sup>-2</sup>	0.40	16.50	21.32
"	0.50x10 <sup>-2</sup>	0.41	17.50	22.96
"	1.05x10 <sup>-2</sup>	0.43	17.50	20.14

Table 2.4 UHMWPE results

Test type	Strain rate (s <sup>-1</sup> )	E GPa	σ <sub>5%</sub> MPa	σ <sub>10%</sub> MPa
Tension	0.45x10 <sup>-3</sup>	0.69	14.00	19.10
"	0.82x10 <sup>-3</sup>	0.80	14.52	19.60
Compression	0.56x10 <sup>-2</sup>	0.63	18.70	22.93
"	2.70x10 <sup>-2</sup>	0.81	20.55	24.80
"	5.00x10 <sup>-2</sup>	0.80	22.35	26.13

Table 2.5 Nylatron results

Test type	Strain rate (s <sup>-1</sup> )	E GPa	σ <sub>5%</sub> MPa	σ <sub>10%</sub> MPa
Tension	1.70x10 <sup>-4</sup>	1.20	44.30	52.60
"	2.30x10 <sup>-4</sup>	1.20	45.85	56.61
"	3.10x10 <sup>-4</sup>	1.40	58.30	75.05
Compression	1.70x10 <sup>-3</sup>	2.08	53.00	63.84
"	4.52x10 <sup>-3</sup>	2.31	67.17	78.47
"	4.60x10 <sup>-3</sup>	2.41	68.20	78.62
"	7.02x10 <sup>-3</sup>	2.12	55.60	66.01

Table 2.6 PEEK results

Test type	Strain rate (s <sup>-1</sup> )	E GPa	σ <sub>5%</sub> MPa	σ <sub>10%</sub> MPa
Compression	0.27x10 <sup>-2</sup>	3.19	124.00	131.00
"	0.30x10 <sup>-2</sup>	3.29	110.90	126.90
"	0.35x10 <sup>-2</sup>	3.10	111.63	130.50
"	0.48x10 <sup>-2</sup>	3.47	115.67	130.12
"	0.50x10 <sup>-2</sup>	3.30	110.30	126.96
"	1.16x10 <sup>-2</sup>	3.90	131.30	136.80

## **2.4 Discussion**

In general the yield stress of each of the polymers tested is not well defined. Bowden (1973) suggested in his work on PMMA, that the intrinsic yield point is the strain at the point where maximum stress first occurs in the stress-strain curves. However, this method cannot be used for the polymers studied above (with the possible exception of PEEK) since the stress increases steadily with the strain. Instead, the flow stress has been noted at 5% and 10% strain from the results shown in Figures (2.5)-(2.9). The flow stresses as well as the moduli have been used to compare the material properties. Often the fracture strength or the yield strength are used to compare the materials, but in this work fracture does not occur in the compression tests. In addition to flow stress values Young's moduli have been obtained by taking the slopes of stress-strain curves at strains <2%, with errors of approximately 5% due to the uncertainty of determining the exact slope of the elastic region. Tensile tests have been made for UHMWPE and nylatron using the Hounsfield machine. The samples were cut from rods of the same materials used in the compressive tests, in the shape of a dog bone. The results presented in this chapter show that there is a good agreement between the results from compressive and tensile tests.

Only nylatron and UHMWPE have been tested in tension, because the HDPE was too soft to make tensile samples, and the PEEK material was in the form of a thin plate which could not be used to make cylindrical tensile samples.

In order to cover a wide range of strain-rate, the split Hopkinson pressure bar (SHPB) technique was also used to study the four polymers, as will be described in detail in this thesis.

## **CHAPTER 3**

### **SPLIT HOPKINSON PRESSURE BAR TECHNIQUE**

#### **3.1 Introduction**

A large number of techniques have been developed to test materials at high strain rate and some comprehensive review papers have been written on the subject.

In the strain rate range of  $10^2$  to  $10^4$  s<sup>-1</sup> the Kolsky apparatus or split Hopkinson pressure bar (SHPB) introduced by Kolsky in 1949, is widely used, and is the dominant technique for testing and determining material properties. This system has been modified many times since it has been invented to meet the appropriate demands. Basically, the SHPB system consists of a gas gun which launches a projectile that acts as a striker bar impacting axially with the incident bar. The incident bar transmits the loading pulse to the sample sandwiched between the incident bar and the transmitter bar (Malvern et al (1986)). This system is attached to strain gauge circuits to detect the stress pulses, and an oscilloscope to capture the pulses.

Several researchers have been involved in the historical developments or modifications of the SHPB technique to test materials at high strain rates [e.g. Lindholm (1964), Ellwood (1983), Follansbee (1983, 1986), and Walker (1987)]. The SHPB technique takes its name from Bertram Hopkinson who was the first to investigate the propagation of stress waves in a long elastic bar in 1914. The stress waves were initially generated by the detonation of explosives or impact of bullets at one end of the bar. A short bar was loosely fixed at the end of the long bar, which could fly free once the initial stress wave had passed through it. By using a series of short bars of different lengths and measuring their final momenta the details of the original stress disturbance in the bar could be reconstructed assuming the wave had propagated with no attenuation.

A theoretical and experimental study of the SHPB has been made by Davies in 1948. Davies replaced the short bars with a condenser to monitor the displacement in the bar.

In 1949 Kolsky introduced a split in the bar in which a small cylindrical sample could be sandwiched. This modification of the Hopkinson pressure bar allows



the stress and strain within the deforming sample to be related to the displacements in the split bars (incident and transmitter bars). The stress pulse generated in the incident bar by impact of a projectile or detonation of an explosive charge will propagate along the incident bar. When the pulse reaches the sample, part of it will be reflected and the other part will be transmitted through the sample into the transmitter bar. Kolsky used capacitive displacement transducers to measure these reflected and transmitted components, while nowadays most of the SHPB users use strain-gauges attached to the bars at equidistant points from the sample.

In some cases the researchers use the projectile itself as an incident bar [Dharan and Hauser (1970), Wulf (1974), and Gorham et al (1984)]. This technique is called the direct impact Hopkinson bar (DIHB). The SHPB is often referred to as the Kolsky bar, due to the major contribution from Kolsky to the technique.

Hauser et al (1960) reported on the first attempts of using strain gauges to detect the stress pulses in the incident and transmitter bars. The strain gauge can detect the deformation directly from the sample by attaching it to the sample under test (Watson 1970). Watson also used piezoelectric disks beside the strain gauges in his study of pure iron.

Malatynski et al (1980) also used the SHPB technique to investigate the plastic properties of lead at high strain rates.

Chiem and Liu (1986) used a torsional version of SHPB to obtain shear stress-strain curves for carbon fibre composite at shear strain rates ranging from  $10^3$  to  $10^4$  s<sup>-1</sup>.

Optical methods have been used to measure sample deformation throughout the test. Sharpe and Hoge (1972) used interferometry to obtain strain in a sample whose cylindrical surface was marked with a set of closely spaced grooves. In 1979 Griffiths et al used an optical method in which shutters were connected to the bars adjacent to the sample. Knowing the variations of the amount of light incident on a photodetector, the sample displacement is determined.

High speed photography has been used by Albertini and Montagnani (1974) and Gorham (1979) to observe sample displacement during the SHPB test.

From the review it seems that the SHPB is the most popular high strain rate compression technique. However, SHPB systems have been developed to produce other modes of deformation. These include shear (Campbell and Dowling (1970)), torsion (Duffy (1974), and Gilat and Pao (1988)), pure uniaxial strain in which radial displacement is constrained (Bhusham and Jahsmann (1978)).

The SHPB system in the Physics Department at Loughborough University has been used to study the dynamic mechanics of a variety of materials. In the original system, the incident bar was loaded by impact from a standard 0.22" calibre bullet by Griffiths and Martin (1974) who used an optical shutter method to record the sample strains. Parry and Griffiths (1979) modified the SHPB loading system by developing a compact gas gun to fire a short steel projectile at the free end of the incident bar. The gas gun uses atmospheric pressure to drive the projectile, producing a uniform stress pulse, which could be repeated more consistently than the 0.22" bullet system. A longer and larger bore gas gun has been used by Ellwood (1983) to fire large projectiles which then produce large amplitude stress pulses.

Ellwood, Griffiths and Parry (1982) modified the SHPB system apparatus to a three bars system in which a dummy sample was placed in the split between the first two bars, while the actual sample under test was placed between the second and third bars. The result of this modification was to shape the incident pulse in such a way in order to produce a constant strain-rate during the test.

Walker (1987) devised an optical fibre based system to measure the impact velocity of the projectile. This device replaced the mechanical triggering system used by Ellwood. Walker also improved and expanded the software for the Commodore Pet computer, first introduced by Ellwood, to analyse the SHPB data (Parry and Walker (1988)). Dixon (1990) designed an infra-red projectile velocity measuring device. Since then many advancements have been made in the Loughborough materials testing facility. The current project involves developing the three bar SHPB recording system (by using a more advanced digital recorder\oscilloscope), which is connected to an IBM PC to store data to a floppy drive. This technique gives more accuracy, takes less time in capturing

the stress pulses, and plots the signals with a greater quality. The software has been re-written by the present author on an IBM PC computer to obtain better analysis, higher performance and accuracy, and to have more options like smoothing and averaging of the results (Al-Maliky 1992).

The Loughborough SHPB system has two principal components as shown in Figure (3.1): a gas gun and a 3 m length of pressure bars. The gas gun accelerates a projectile until it impacts with the free end of the incident bar thereby creating a stress pulse in the bar of duration:

$$\tau = \frac{2\ell_0}{c_0} \quad (3.1)$$

where  $\ell_0$  is the projectile length and  $c_0$  is the velocity of longitudinal waves in the projectile bar. The amplitude of the incident wave  $\varepsilon_1$  is expressed by:

$$\varepsilon_1 = \frac{v}{2c_0} \quad (3.2)$$

where  $v$  is the projectile velocity upon impact, assuming that the projectile and the pressure bars are made of the same material.

The incident pulse propagates along the incident bar and reflected and transmitted pulses are created at the sample (Figure 3.1). All these waves are detected by pairs of strain gauges mounted at equidistant points 40 cm either side from the sample. The momentum bar at the end of the line flies away from the rest of the bars after the transmitted pulse has been reflected back as a tensile wave. The momentum bar is trapped in a Plasticine filled box thereby dissipating the energy released by the system without causing damage to the apparatus. To avoid a pulse coming back from the momentum bar towards the transmitter strain gauge, the momentum bar length should be greater than half the length of the projectile, but the disadvantage of having a short momentum bar is that it moves at very high speed and may damage the system. So, the momentum bar is usually longer than the projectile but shorter than the transmitter bar.

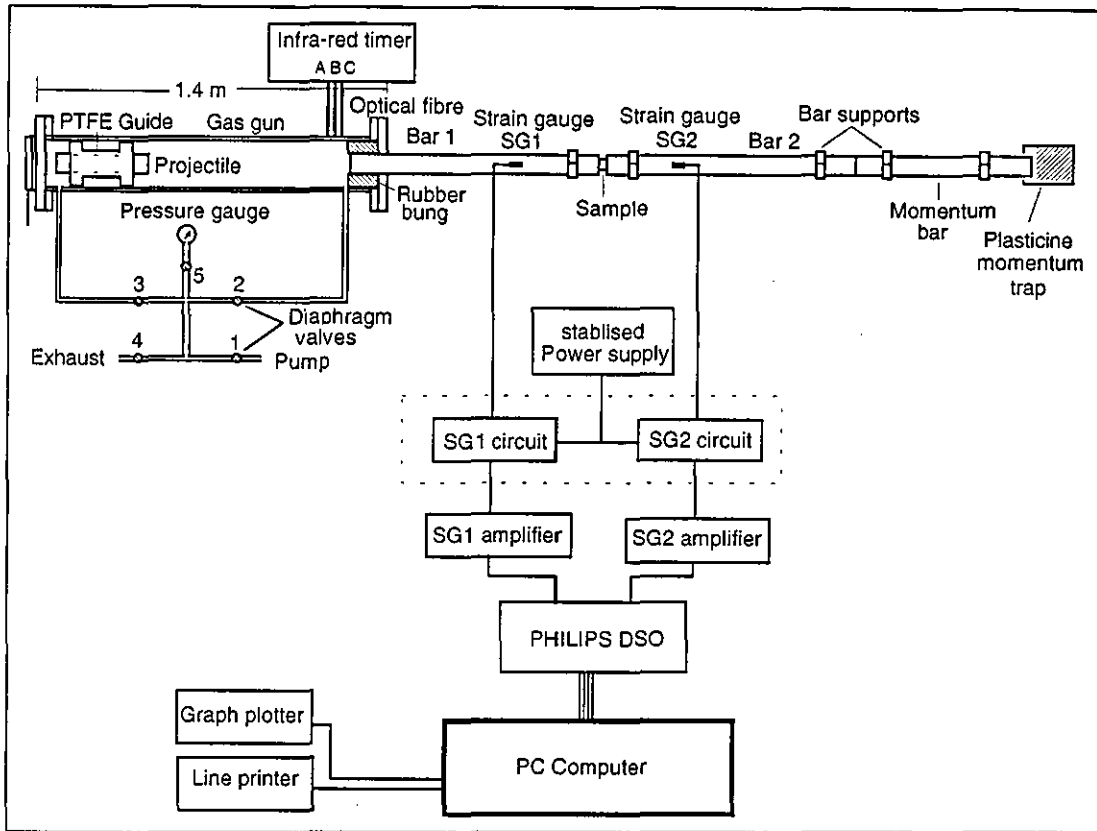


Figure (3.1) Block diagram of the split Hopkinson pressure bar system.

The SHPB is used for dynamic testing of a wide range of materials from soft materials like plastics to hard materials like steel and composites.

Several problems can be met in using the SHPB technique for high strain rate testing which arise from the increasing influence of dynamic effects associated with inertial forces. In the intermediate strain rate range to approximately  $50\text{ s}^{-1}$ , the mechanical response within the sample and testing machine must be considered. Measurements are made during the passage and reflection of shock waves in a plane strain type experiment. At high strain rates, another effect of the time scale involved is that the deformation becomes essentially adiabatic rather than isothermal. The internal heat generated during the inelastic deformation process does not have time to dissipate, and so the mean temperature of the sample is increased. This temperature rise can affect the stress in the material and this has to be taken into account when comparison is made with isothermal data. However, in many cases the temperature rise is small, except for very large strains. More details are provided in this chapter about these effects beside the description of the system.

### 3.2 Hopkinson pressure bar theory

Having recorded the incident, reflected and transmitted strain pulses (denoted  $\epsilon_i$ ,  $\epsilon_R$ , and  $\epsilon_T$  respectively) the following theory can be applied, in which it is assumed that a plane stress wave is being propagated (Walker (1987)).

Axial force = Axial stress  $\times$  Area

$$\begin{aligned} F &= \text{Young's modulus} \times \text{Axial strain} \times \text{Area} \\ &= \sigma \times A = E_b \times \epsilon \times A \end{aligned}$$

where  $E_b$  is the elastic modulus of the bar and  $A$  is the cross-sectional area of the bar.

From one-dimensional theory of elastic wave propagation

$\sigma = \rho c_0 \dot{u}$  is the axial stress, then

$$\dot{u} = \frac{\sigma}{\rho c_0} \text{ is the particle velocity}$$

Now  $c_0 = \sqrt{E_b / \rho}$  is the elastic wave velocity in the bar, and so

$$\dot{u} = \frac{E_b \epsilon}{\rho \sqrt{E_b / \rho}} = c_0 \epsilon$$

$$\therefore u = c_0 \int \epsilon \, dt \quad (3.3)$$

where  $u$  is displacement at time  $t$ , and  $\epsilon$  is strain. The displacement  $u_1$  of the face of bar 1 (Figure (3.2)) results from both the incident pulse  $\epsilon_i$  travelling in the positive  $x$ -direction and the reflected pulse  $\epsilon_R$  travelling in the negative  $x$ -direction.

Hence:

$$\begin{aligned} u_1 &= c_0 \int \epsilon_i \, dt + (-c_0) \int \epsilon_R \, dt \\ &= c_0 \int_0^t (\epsilon_i - \epsilon_R) dt \end{aligned} \quad (3.4)$$

Similarly, the displacement  $u_2$  of bar 2 is obtained from the transmitted pulse  $\epsilon_T$  as

$$u_2 = c_0 \int_0^t \epsilon_T \, dt \quad (3.5)$$

The engineering strain in the sample  $\epsilon_s$  is then

$$\epsilon_s = \frac{u_1 - u_2}{l_0} = \frac{c_0}{l_0} \int_0^t (\epsilon_I - \epsilon_R - \epsilon_T) dt \quad (3.6)$$

where  $l_0$  is the initial length of the sample.

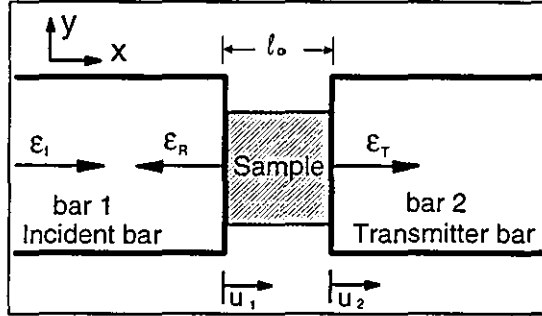


Figure (3.2) Enlarged view of sample between incident and transmitter pressure bars, showing strain pulses and displacements of ends of the bars.

Assuming the stress across the compressed sample is constant, an assumption which becomes more exact as  $l_0$  approaches zero, then

$$E_b (\epsilon_I + \epsilon_R) = E_b \epsilon_T, \text{ giving} \\ \epsilon_R = \epsilon_T - \epsilon_I \quad (3.7)$$

Substituting Equation (3.7) into Equation (3.6) gives

$$\epsilon_s = \frac{-2c_0}{l_0} \int_0^t \epsilon_R dt \quad (3.8)$$

and the engineering strain rate,

$$\dot{\epsilon} = \frac{-2c_0}{l_0} \epsilon_R \quad (3.9)$$

The applied loads  $F_1$  and  $F_2$  on each face of the sample are:

$$F_1 = EA(\epsilon_I + \epsilon_R) \quad (3.10)$$

and  $F_2 = EA\epsilon_T \quad (3.11)$

where  $E$  is the modulus of elasticity of the pressure bars (i.e. Young modulus) and  $A$  is the cross-sectional area of the pressure bars.

Hence the average stress in the sample,  $\sigma_s$ , is given by

$$\sigma_s = \frac{F_1 + F_2}{2A_s} = \frac{1}{2} E \cdot \frac{A}{A_s} \cdot (\varepsilon_l + \varepsilon_R + \varepsilon_T) \quad (3.12)$$

where  $A_s$  is the cross-sectional area of the sample.

From Equation (3.7), Equation (3.12) becomes

$$\sigma_s = \frac{EA}{A_s} \varepsilon_T \quad (3.13)$$

This equation shows that the engineering stress is directly proportional to the transmitted pulse, while the engineering strain rate is directly proportional to the reflected pulse.

By digitising the values of  $\varepsilon_R$  and  $\varepsilon_T$  at set time intervals then the complete stress versus strain rate relation can be derived for the compressive test sample.

The SHPB can be used to determine the mechanical properties of materials at high strain rates providing that the following assumptions are maintained by the conditions of the experiment :

- a) the sample is in a state of one-dimensional stress,
- b) the stress and strain are uniform throughout the sample.

These assumptions are invalidated by radial and axial inertia effects and by friction between the sample and the pressure bars.

Kolsky (1949, 1963) introduced a correction for radial inertia. Assuming small strains, he obtained

$$\sigma_s = \sigma_b - \frac{1}{8} v_s^2 d^2 \rho_s \ddot{\varepsilon} \quad (3.14)$$

where  $\sigma_b$  is the axial stress determined by the average of the stresses measured in the two bars,  $\sigma_s$  is the axial stress required to deform the sample in a one-dimensional stress state, and  $v_s$ ,  $\rho_s$ ,  $d$ , and  $\varepsilon$  are the Poisson's ratio, density, diameter and axial strain of the sample, respectively.

In order to minimise friction effects, samples with a length-diameter ratio of about 0.5 should be made (Davies and Hunter (1963)). Also Kolsky attempted to achieve early stress equilibrium in the axial direction, and used a small length-diameter ratio. The dimensions which were used by Davies and Hunter (1963) were as a result of an analysis by Siebel (1923) which had  $(\mu d/3\ell) \ll 1$  as a correction for neglecting friction effects, where  $\mu$  is the coulomb friction coefficient and  $\ell$  is the sample length. They added an axial correction to Kolsky's Equation (3.14)

$$\text{i.e.} \quad \sigma_s = \sigma_b + \rho_s \left( \frac{\ell^2}{6} - \frac{v_s^2 d^2}{8} \right) \dot{\epsilon} \quad (3.15)$$

Other correction factors arising from friction and radial and axial inertia, have been introduced by Rand (1967) and Samanta (1971). Hauser et. al. (1960), Conn (1965), Chiu and Neubert (1967) and Jahsman (1971) and others have made their analysis of the split Hopkinson pressure bar including the one dimensional corrections.

The two-dimensional computer analysis by Bertholf and Karnes (1975) showed that by lubricating the sample and using a length to diameter ratio of  $v_s \sqrt{(3/4)} \approx 0.5$  as proposed by Davies and Hunter then the corrections for friction can be ignored. Assuming that the material is ductile, which is generally true for plastically deforming materials, then Poisson's ratio is 0.5. Hence a length to diameter ratio of at least 0.5 satisfies this correction. Full details of friction and other limiting parameters will be treated in this chapter.

Equations (3.8), (3.9), and (3.13) are valid in these circumstances except in the very early period of loading the sample before stress equilibrium has been attained.

In equations (3.8) and (3.9) the elastic wave velocity ( $c_0$ ) and the sample length are constants, therefore as the strain rate ( $\dot{\epsilon}$ ) increases, so does the amplitude of the reflected pulse ( $\epsilon_R$ ) and hence the plastic strain ( $\epsilon_s$ ), experienced by the sample after a given time  $t$ , increases as  $\dot{\epsilon}$  increases. If a time  $t_E$  elapses before stress equilibrium is reached, then a greater sample strain  $\epsilon_s$  occurs before the SHPB equations are valid at high strain rate than at a lower strain rate. Therefore when comparing curves of stress versus strain for a given low plastic strain it is essential to realise that the data becomes less accurate as the



strain rate increases. For experiments of this type to yield definitive measurements, that is "absolute" stress-strain curves characteristic of the mechanical response of the materials, account must be taken of the principal features of the experiment which can be summarised as follows (and fully described in the next section):

1) Friction restraints on the loaded surfaces of the sample:

The frictional restraint has been reduced to a minimum by applying a thin layer of lubricant to the pressure bar/sample interfaces, giving deformed samples which exhibit negligible barrelling.

2) Inertial restraints imposed by both radial and longitudinal particle acceleration in the sample (which is studied by Davies-Hunter (1963), (see above)).

3) Distinguish between nominal stress and true stress:

Uniform true stress can be obtained by using samples having an initial diameter smaller than that of the pressure bars and selecting an impact velocity  $V_1$  to yield a deformed sample whose final diameter  $d_w$  is less than that of the pressure bars  $d_b$ . Allowing for the area mismatch at the pressure bar sample interfaces, true stress can be derived as follow

The true axial strain  $\epsilon = \int_{L_0}^L \frac{dL}{L} = \ln\left(\frac{L}{L_0}\right) = \ln(1 - \epsilon_s)$ , where  $\epsilon_s$  is the engineering strain.

The true radial strain  $\epsilon_r = -\nu \times$  the true axial strain

or 
$$\epsilon_r = \ln\left(\frac{d}{d_0}\right) = -\nu \ln\left(\frac{L}{L_0}\right) = -\nu \epsilon$$

Since true stress  $\sigma = \frac{F}{A}$  and engineering stress  $\sigma_s = \frac{F}{A_0}$ , then

$$\begin{aligned} \frac{\sigma}{\sigma_s} &= \frac{A_0}{A} = \left(\frac{d_0}{d}\right)^2 \\ \ln\left(\frac{\sigma}{\sigma_s}\right) &= 2\ln\left(\frac{d_0}{d}\right) = -2\ln\left(\frac{d}{d_0}\right) \\ &= -2\epsilon_r = 2\nu\epsilon \end{aligned}$$

$\therefore \sigma = \sigma_s e^{2\nu\epsilon}$  (3.16)

The sign of the exponent is +ve for tensile or -ve for compression test, so Equation (3.16) can be rewritten as,

$$\sigma(t) = \sigma_s(t)e^{\pm 2\nu\varepsilon(t)}$$

where  $\sigma(t)$  is the true stress at time  $t$ ,  $\sigma_s$  is the engineering stress required to deform the sample,  $\nu$  is the Poisson's ratio, and  $\varepsilon(t)$  the true strain in the deformed sample at time  $t$ . Also the true stress can be written as

$$\sigma(t) = \sigma_s(t)[1 \pm \varepsilon(t)] = \frac{A}{A_s} \cdot E\varepsilon_T(t) \cdot [1 \pm \varepsilon(t)] \quad (3.17)$$

where  $A$  and  $A_s$  are the cross-sectional area of the pressure bars and the undeformed sample, respectively, and  $\varepsilon_T(t)$  is the bar strain at time  $t$ , where true sample strain  $\varepsilon(t)$  is

$$\varepsilon(t) = \pm \ln[1 \pm \varepsilon_s(t)] \quad (3.18)$$

where  $\varepsilon_s(t)$  is the engineering strain.

4) Verification, or otherwise, of internal stress equilibrium within the sample:

Internal stress equilibrium within the sample is verified by comparing the bar strain-time curves. Figure (3.3) shows typical examples of strain-time curves. The Pochhammer-Chree oscillations following the initial rise of the incident pulse can be seen.

To simplify the analysis the curves are smoothed. To obtain a dynamic stress-strain curve it is necessary to relate the three strain-time histories accurately in terms of the deformation time  $t$ . To check the equation  $[\varepsilon_I(t) + \varepsilon_R(t) \approx \varepsilon_T(t)]$ , three characteristic times exist that should be noted (Billington and Brissenden (1971)). These are indicated in Figure (3.3) as the points  $t_1$ ,  $t_2$ , and  $t_3$ . For every recording that was made using them, the terminal point in time of the incident pulse  $t_1$  was always located without difficulty. It is evident from Figure (3.3) that the maximum positive value of the reflected pulse must coincide in time with the point  $t_1$ . Having located the reflected pulse relative to the incident pulse in time, the transmitted pulse can now be displaced in time to satisfy two conditions. These are that the trailing edge of the transmitted pulse must coincide with the trailing edge of the reflected pulse for times in excess of  $t_1$ , and that the time  $t_2$  at which the incident pulse has the same instantaneous value as the transmitted pulse must coincide in time with the

condition that the reflected pulse is instantaneously zero at  $t_2$ . The negative amplitude of the reflected pulse must coincide in time with the point  $t_3$  at which the incident pulse first attains its maximum value  $\epsilon_{lmax}$ . In general a final test is to note that application of equation

$$\epsilon_s(t) = \frac{-2c_0}{l_0} \int \epsilon_R dt \quad (3.19)$$

should yield the independently measured value of the final strain, irrespective of whether this be zero or finite.

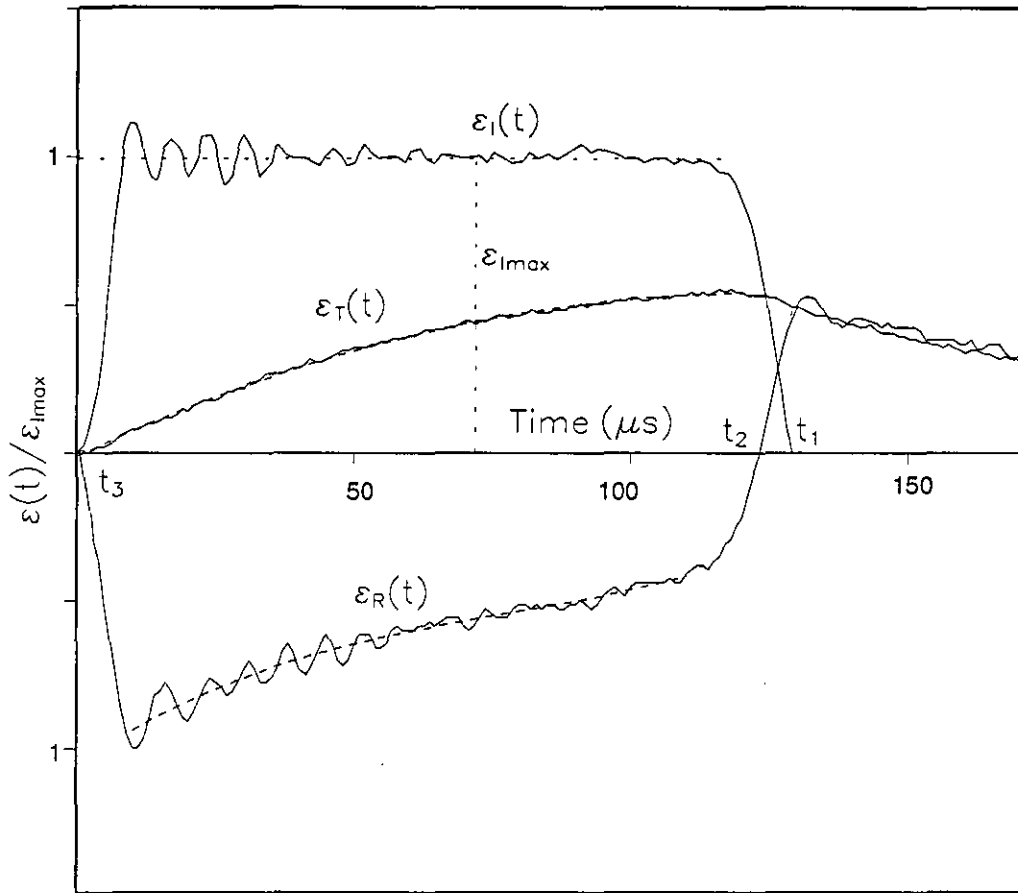


Figure (3.3) Comparison of measured strain pulse amplitudes to confirm the approximate equivalence of the forces on both faces of the sample. Dashed line on the reflected pulse denotes  $\epsilon_l(t) - \epsilon_T(t)$ . The data are for an HDPE sample tested at an impact velocity of 10 m/s.

The comparison of the measured pulse amplitudes confirms the approximate equivalence of forces on both sides of the sample as in Figure (3.3). The dashed curve represents the difference between the full line curves labelled by

$\varepsilon_i(t)$  and  $\varepsilon_T(t)$ . For a good comparison the equation  $\varepsilon_i(t) + \varepsilon_R(t) \approx \varepsilon_T(t)$  should be verified for any impact velocity and for all materials.

The average strain  $\varepsilon(t)$  of the sample can be calculated by integrating the  $\varepsilon_R(t)$  curve ( $\varepsilon_s(t) \approx \frac{-2c_0}{\ell_0} \int \varepsilon_R dt$ ), and the average stress  $\sigma_s$  can be evaluated by using equation  $\sigma_s \approx \frac{A}{A_s} \rho_b c_0^2 \varepsilon_T(t)$  for various values of deformation time  $t$ . The characteristic stress/strain curves for the test materials can be obtained. The strain rate increases with increasing impact velocity, so the stress/strain curves vary corresponding to the impact variation.

### 3.3 Problems in the SHPB analysis

The SHPB analysis has some factors which lead to inaccuracy in finding the stress/strain results for the materials, so these factors should be treated to minimise their effects. These factors are discussed in detail as follows;

#### 3.3.1 Friction effects

These effects are caused by interfacial friction at the sample-steel bar interfaces, and effectively stiffen the sample - especially in the compressive tests. With a thin sample the friction is particularly important and a potentially serious complication, especially when the sample is subjected to high strains. The following theoretical approximation treatment has been used by Briscoe and Nosker (1984).

For no body forces and no internal stresses, the equilibrium equation in cylindrical co-ordinates is reduced to;

$$\frac{\partial \sigma_r}{\partial r} + \frac{\partial \tau_{rz}}{\partial z} + \frac{\sigma_r - \sigma_\theta}{r} = 0 \quad (3.20)$$

where the  $z$ -direction is along the cylinder.

The Von Mises yield criterion is

$$(\sigma_z - \sigma_r)^2 + (\sigma_r - \sigma_\theta)^2 + (\sigma_\theta - \sigma_z)^2 = 2\sigma_y^2 \quad (3.21)$$

where  $\sigma_z$ ,  $\sigma_r$ , and  $\sigma_\theta$  are the principal stresses of the  $z$ -direction stress, radial stress and hoop stress, and  $\sigma_y$  is the yield stress in simple compression.

Assuming the frictional coefficient  $\mu$  is constant, then

$$\frac{\partial \tau_{rz}}{\partial z} = \frac{2\mu\sigma_z}{\ell_0} \quad (3.22)$$

To make the problem mathematically tractable, the following assumption has been used.

$$\begin{aligned} \sigma_z &\text{ is constant in the } z\text{-direction, and} \\ \sigma_r &= \sigma_\theta \end{aligned} \quad (3.23)$$

From Equation (3.23) and Equation (3.21), then

$$\sigma_z - \sigma_r = \sigma_y \quad (3.24)$$

and from Equation (3.22) and Equation (3.24), and Equation (3.20),

$$\frac{\partial \sigma_z}{\partial r} = \frac{-2\mu\sigma_z}{\ell_0} \quad (3.25)$$

which integrates to

$$\therefore \sigma_z = -\sigma_y e^{\left\{\frac{2\mu}{\ell_0}(a-r)\right\}} \quad (3.26)$$

By putting the boundary condition of  $\sigma_z = \sigma_y$  at  $r = a$ , then the mean pressure over the entire contact is:

$$\therefore P = \int_0^a \frac{2\pi r \sigma_z}{\pi a^2} dr = \frac{\sigma_y \ell_0^2}{2\mu^2 a^2} \left\{ e^{\left(\frac{2\mu a}{\ell_0}\right)} - \frac{2\mu a}{\ell_0} - 1 \right\} \quad (3.27)$$

$$\text{or } \frac{P}{\sigma_y} = \frac{\ell_0^2}{2\mu^2 a^2} \left\{ e^{\left(\frac{2\mu a}{\ell_0}\right)} - \frac{2\mu a}{\ell_0} - 1 \right\} \quad (3.28)$$

where  $P$  is the mean applied stress at yield,  $\sigma_y$  is the true uniaxial yield stress, and  $\mu$  is the frictional coefficient. The ratio  $P / \sigma_y$  increases strongly with  $\mu a / \ell_0$ .

Therefore friction is a particularly important and potentially serious complication, especially when thin samples are used to give a high strain. If  $\mu \approx 0$ , then  $P \approx \sigma_y$ . When the frictional coefficient becomes quite substantial, the assumption that  $\sigma_z$  is constant will not be valid and then neither is Equation (3.28). A plot of Equation (3.28) is shown in Figure (3.4).

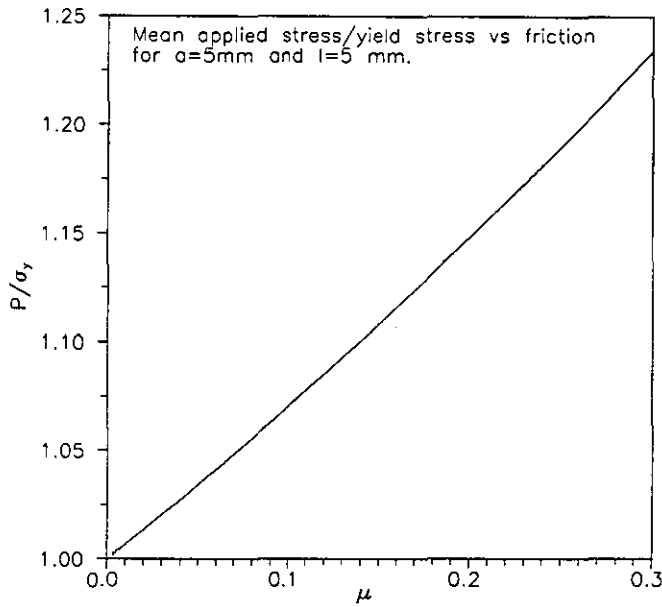


Figure (3.4)

Another method has been used for correcting the friction error, by using a liquid lubricant (silicone grease) at the polymer/steel interfaces instead of assuming a constant coefficient of friction. This assumption of Equation (3.23) is represented by a shear stress  $\tau_{rz}$  generated at the polymer surface by the lubricant with viscosity  $\eta$

where,

$$\tau_{rz} = \frac{\eta V_r}{h} \quad (3.29)$$

where  $V_r$ , is the radial velocity and  $h$  the thickness of the lubricant.

During the compressive test, the lubricant flows outwards, and the sample diameter increases. These two velocities have to be considered. Considering the lubricant or the sample as an incompressible disk with volume of  $\pi r^2 b$ , the radial velocity is

$$V_r = \frac{r}{2} \frac{db}{dt} \quad (3.30)$$

For the lubricant of thickness  $b = h$ , the maximum radial velocity occurs when the two rigid platens come together. This occurs in the SHPB test.

Assuming the lubricant is isoviscous and isothermal, the Stefan equation [Booth and Hirst (1970)] applies.

$$\frac{dh/dt}{h} = \frac{2h^2f}{3\pi\eta a^4} \quad (3.31)$$

where  $f$  is the compressive force between the two polymer and steel faces.

Letting  $\sigma_y \approx f / \pi a^2$ , and setting values for  $h(10 \mu\text{m})$ ,  $\eta(0.125 \text{ Pa}\cdot\text{s})$ ,  $\ell_0(5 \text{ mm})$ ,  $a(5 \text{ mm})$ , and  $\sigma_y \approx 50 \text{ MPa}$  (for HDPE),  $(dh/dt)/h$  will be  $1.067 \times 10^3 \text{ s}^{-1}$ . For the polymer of thickness  $b = h = \ell_0$ , the SHPB configuration gives  $(d\ell_0 / dt) / \ell_0 = \dot{\epsilon}$  (where  $\eta = 0.0097 \text{ MPa}\cdot\text{s}$ ). Using  $\dot{\epsilon}$  instead of  $\frac{db/dt}{b}$ , Equation (3.30) becomes

$$V_r = \frac{r}{2} \dot{\epsilon} \quad (3.32)$$

where  $\dot{\epsilon}$  is axial strain rate.

From Equation (3.29)

$$\therefore \tau_{rz} = \frac{\eta r \dot{\epsilon}}{2h} \quad (3.33)$$

Substitute for Equation (3.23) is

$$\frac{\partial \tau_{rz}}{\partial z} = \frac{\eta r \dot{\epsilon}}{h \ell_0} \quad (3.34)$$

Then, following the same approach as for a constant coefficient of friction, stress and pressure are obtained

$$\sigma_z = \sigma_y + \frac{\eta \dot{\epsilon}}{2h \ell_0} (a^2 - r^2) \quad (3.35)$$

$$P = \sigma_y + \frac{\eta \dot{\epsilon}}{4h \ell_0} a^2 \quad (3.36)$$

Using the values above gives  $P = 1.002 \sigma_y$  for a strain rate of  $6.7 \times 10^3 \text{ s}^{-1}$ , and  $P = \sigma_y$  for a strain rate of  $10^{-2} \text{ s}^{-1}$ , then the liquid lubricant is very effective for the SHPB, even with the thin polymer samples employed in the experiment.

For low strain rates ( $\approx 10^{-2} \text{ s}^{-1}$ ) in the low speed experiment (Hounsfield), Equation (3.31) is not valid. The polymer is not a rigid platen; instead, the sample will deform and trap the lubricant in a cavity. Equation (3.37) can be used with strain rates ( $\approx 10^{-2} \text{ s}^{-1}$ ) and an average  $h$  somewhat smaller than  $10 \mu\text{m}$ . For the smooth steel counter faces (centre-line-average (c.l.a.)

roughness, about  $0.2\mu\text{m}$ ) a good approximation for  $P$  gives  $P = \sigma_y$ ; for the high counter faces, (c.l.a. roughness, about  $6\mu\text{m}$ ), there is some direct polymer-steel contact even before pressure is applied (Briscoe and Nosker (1984)).

Briscoe and Nosker (1984) examined the lubricant effect on SHPB strain readings. They assumed that the lubricant displacement during elastic shear equals displacement as viscous flow for a given time interval

$$\Delta t = \frac{\eta}{G} \quad (3.37)$$

after the onset of compression, where  $\eta$  is the viscosity and  $G$  is the shear modulus of the lubricant. At longer time intervals, the viscous displacement predominates. The viscosity of petroleum jelly for example is  $0.125 \text{ Pa}\cdot\text{s}$  after initial thinning. The material will shear thin in this case; as the polyethylene sample compresses by 20%, its average radius increases by nearly 10%, which puts an average 6000% strain into the lubricant. The shear modulus is  $1 \text{ GPa}$ , so  $\Delta t = 1.25 \times 10^{-4} \mu\text{s}$ . The elastic shear is therefore not of consequence in the SHPB experiment.

Another assumption has been made by Briscoe and Nosker (1984), which is that the lubricant displacement due to the elastic compression is equal to displacement during viscous flow over the time interval

$$\Delta t = \frac{3a^2\eta}{2h^2k} \quad (3.38)$$

For  $h(10\mu\text{m})$ ,  $a(12.7 \text{ mm})$ ,  $\eta(0.125 \text{ Pa}\cdot\text{s})$ , and  $k$  the bulk modulus ( $2 \text{ GPa}$ ),  $\Delta t = 151\mu\text{s}$ .

During the stress pulse in the SHPB, most of the lubricant thinning takes place by bulk compression and not by viscous flow out of the contact, and so the force distribution is uniform across the face of the sample. The elastic compression of the lubricant is about  $\sigma_y h / k \approx 0.25 \mu\text{m}$  for  $\sigma_y = 50 \text{ MPa}$ , so the total apparent strain due to two lubricant thicknesses in a sample  $5 \text{ mm}$  thick is about 0.01% which is reasonably small. Therefore the lubricant does not significantly affect the strain readings in the SHPB, and it remains the same thickness during the experiment.

The apparent stiffening of the polymer is primarily the result of liquid shear against outward radial movement of the sample, as illustrated by results in



Equation (3.36) for the mean pressure. The lubricant is therefore very effective for the SHPB, even with the thin polymer sample employed.

### **3.3.2 Polymer / steel interface area variation**

The cross sectional area of a deformed sample increases with increasing compressive strain. This means that the contact area between the polymer and the steel bars increases. This increase causes an increase in the transmitted energy as the strain increases, and this is paralleled by a reduction in the free surface of reflection of the bars. Obtaining true stress and strain from Equations (3.16) and (3.18) in the SHPB analysis section requires some correction for these area effects. Also if the sample extends beyond the diameter of the bars, this introduces a further complication which is caused by the overhang of the sample. The hoop stress created by this overhang generates a substantial stiffening of the polymer during compression. To avoid this overhang effect, samples with an initial diameter less than that of the bars should be used, and with a maximum compressive strain which is just sufficient to fill the measuring cavity during the experiment (Briscoe and Nosker (1984)).

### **3.3.3 Inertia effects of the sample**

These effects are caused by both radial and longitudinal particle acceleration in the sample (Lindholm (1964)), and raise the magnitude of the measured stress over the effective stress on the sample (the stress that truly represents the material's elastic-plastic and viscous response).

Axial inertia effects can be neglected for samples with large diameter to length ratios. This technique has been used by Kolsky (1949). In addition he made corrections for the radial inertia effects as in Equation (3.14).

To avoid the effect of the hoop stress which is caused by the overhang of the sample, the sample diameter should be less than the diameter of the bars. The sample diameter is then limited by the bars diameter, so the only parameter that can be varied to change the length/diameter ratio is the length. So, to make the ratio large, thin samples should be used. This, on the other hand, increases the friction effects.

The Kolsky technique has been criticised by Davies and Hunter (1963), because in this technique the sample proportions would lead to large frictional errors, for which it would be difficult to calculate a correction factor. They used an approximation to the stress correction for radial and longitudinal inertia. This approximation appears in the following equation (Lindholm (1964))

$$\sigma_s = \sigma_b - \rho_s \left( \frac{\ell^2}{12} + \frac{1}{8} v_s^2 d^2 \right) \dot{\epsilon} \quad (3.39)$$

with reference to the centre of the sample, or

$$\sigma_s = \sigma_b + \rho_s \left( \frac{\ell^2}{6} - \frac{1}{8} v_s^2 d^2 \right) \dot{\epsilon} \quad (3.40)$$

if the stress is measured at the back surface of the sample as in the present system. This inertia correction vanishes if

$$\frac{\ell^2}{6} = \frac{1}{8} v_s^2 d^2$$

then  $\frac{\ell}{d} = \sqrt{\frac{6 v_s^2}{8}} = 0.866 v_s \quad (3.41)$

For plastic flow, with  $v_s \approx 0.5$ , then  $\ell/d = 0.433$ . It also vanishes when the strain rate can be held constant (Lindholm (1964)). Thus Davies and Hunter showed that a sample of the proportions given above will not need correction for inertia effects. Bertholf and Karnes (1975) showed that by the lubrication of the sample and using a length/diameter ratio of  $v_s \sqrt{(3/4)} \approx 0.5$  as proposed by Davies and Hunter, then the correction for friction and inertia can be ignored.

### **3.3.4 Mechanical noise interference within the bars**

The mechanical noise occurs in several forms as:

a) simple plane wave interference (Ahmad (1988)), which normally limits the duration of the experiment.

b) longitudinal waves dispersion, which appears as higher frequency components of the wave form travelling more slowly than the lower frequency groups. These components change the shape of the transmitted and the reflected pulses causing difficulties in interpretation of the signals. The simple one-dimensional equation of motion for the particles of the bar leads to a wave

equation  $c_0 = \sqrt{E/\rho}$ , where  $c_0$  is the longitudinal wave velocity,  $E$  is the Young's modulus, and  $\rho$  is the density of the bar. This equation is accurate for  $\lambda/a > 10$ , where  $a$  is the bar radius.

Love and Rayleigh derived an approximation for  $\lambda/a$  to allow for transverse radial motion of the particles. This solution leads to a phase velocity,  $c_p$ ;

$$c_p = c_0 \left[ 1 - v^2 \pi^2 \left( \frac{a}{\lambda} \right)^2 \right] \quad (3.42)$$

This solution is reasonable for  $\lambda/a > 1.4$ , but can give large errors for short wavelengths.

c) flexural or bending waves, which can also be propagated along the bars. The extended length of the steel bars, coupled with the difficulty of precise axial alignment, readily facilitates the generation of undesirable flexural or bending waves within both metal bars. The waves' magnitude can be significant but their primary contribution to the monitored strain at the sensing gauges can be completely suppressed by mounting in series two gauges in diametrically opposite positions at each recording location on the bars. The flexural modes suffer dispersion and undergo reflection and create signal distortions of a type similar to these generated by longitudinal waves.

Rayleigh derived a phase velocity for flexural waves as:

$$c_f = \frac{c_0}{\lambda / \pi a} = \frac{c_0 \pi a}{\lambda} \quad (3.43)$$

for bars of circular cross-section. This implies that infinitely short waves travel at infinite speed. However, this simple expression only fits experimental results for long wavelengths,  $\lambda/a > 10$  (Ellwood (1983)).

Simple analysis of torsional forces on a bar element leads to a velocity for torsional waves of

$$c_T = \sqrt{\frac{G}{\rho_0}} \quad (3.44)$$

where  $G$  is the shear modulus. This velocity is exactly correct for the principal energy mode even when inertial effects have not been neglected, unlike in the cases of longitudinal and flexural waves.

Data distortion arising from flexural wave dispersion cannot readily be distinguished from the distortions formed by plane waves. Torsional waves, as might be anticipated, are not generated at a significant level (Briscoe and Nosker (1984)) in compression SHPB tests.

Pochhammer and Chree independently derived exact equations to describe infinite wave trains in circular cross-section bars by applying equations of motion using cylindrical co-ordinates. These equations are useful when short wavelength, longitudinal, torsional or flexural waves are considered and can be used to study the distortion of a pulse due to the differing velocities of its Fourier components. This dispersion produces an increase in the rise time of a pulse and a tail due to a delay in the recovery of strain after a pulse.

Griffiths, Parry and Worthington (1979) showed that the unwanted flexural waves generated by the impact, travel more slowly than the required axial waves and can therefore be made to arrive at the sample after the axial stressing is complete. There is then no effect on sample loading. This may be achieved by the choice of an approximate ratio of incident pulse length to bar length.

### **3.3.5 Axial alignment**

One of the difficulties of using an SHPB to achieve reasonable results is the axial alignment of the bars of the system. Misalignment between bars can cause localised high stresses in the sample, especially in the initial loading stages. This important point must be considered before doing an experiment. In the present work, an optical method is used to check the bars alignment, and to close the gaps at bar-bar, and sample-bar interfaces as much as possible to give a good axial alignment for the system before the experiment.

### **3.3.6 Temperature rise in the sample**

Polymers are sensitive to temperature as well as strain rate. When a sample is compressed beyond its yield point, virtually all the work of plastic deformation is converted into heat. The resultant temperature rise is generally neglected in the analysis of data obtained for other less temperature dependent materials like metals. However, since polymers are sensitive to the temperature changes, the heat developed during deformation will affect the stress-strain curve especially

at high strain rates. This applies to the bulk temperature rise only, which is due to the adiabatic nature of the deformation process at high strain rates.

If the deformation of a sample takes place at a low strain rate, heat generated in the sample will be lost at the same rate to the surroundings by natural cooling and hence there will be a slight change in the temperature of the sample (Dawson (1993)). A compression test under such conditions can be considered as an isothermal test. However, if the deformation takes place at a high strain rate, then there will not be enough time for the heat to escape and the sample temperature will rise according to the level of the plastic strain. Such a test can be called adiabatic if the strain rate is high enough that no heat is lost during the test.

It is important to consider the adiabatic heating in the compression testing at high strain rates, because in some polymeric materials, especially the stiff polymers, the temperature rise could be large enough to cause a significant reduction in the flow stress. With this in mind, when comparing stress-strain curves at different strain rates, the difference between the isothermal and adiabatic conditions should be considered. The shape of the stress-strain curves in the plastic region may be affected by the thermal condition in the test. A change in the gradient of the work hardening curves could be observed at high strain rates due to the temperature effect.

Considering the volume of a plastically deforming sample as constant, and equating the mechanical to the thermal energy, the temperature rise is then :

$$\Delta T = \frac{1}{s\rho_s} \int \sigma d\varepsilon \quad (3.45)$$

where  $\sigma$  is the applied stress,  $s$  is the specific heat and  $\rho_s$  is the density of the sample ( $2.4\text{KJ Kg}^{-1} \text{ }^\circ\text{C}$  and  $955\text{Kg/m}^3$  respectively in case of high density polythene (HDPE)). For perfectly plastic behaviour at a maximum strain  $\varepsilon_{\max}$ ,  $\Delta T = \sigma\varepsilon_{\max} / s\rho_s$ . For typical values of  $\varepsilon_{\max} = 24\%$ , and  $\sigma = 48\text{MPa}$  for HDPE,  $\Delta T$  equals  $5 \text{ }^\circ\text{C}$ . The temperature rise is then not so important in such an experiment, but it can be for very stiff polymers that are taken to large strains, because it causes softening of the material.

### **3.3.7 Other problems can be met within the analysis**

1) The electrical response of the recording apparatus. The apparatus should have a response time comparable with the equilibration time of the elastic strain in the sample, e.g. for a polymer this is about  $3\mu\text{s}$  (Briscoe and Nosker 1984). The present system has a response time faster than that used by the above authors.

2) The sampling rate of the recording system should be comparable with the deformation speed and the rise time of the strain gauge signals. In the present work, a  $1\mu\text{s}$  sampling rate is usually used, which meets the required criterion.

3) The sample dimensions. If the sample faces are not smooth or not parallel, this can cause misalignment resulting in localised stresses in the initial part of the test. So, the sample should be well prepared to avoid localised stresses. The present preparation of the polymer samples is by machining (slow cutting and smoothing) out of a high density polyethylene rod. The sample faces are smoothed by 400 grit paper, with variations in length of  $\pm(5 - 20)\mu\text{m}$ .

4) The amplifiers response and stability. The bandwidth response of the amplifiers is limited for a certain frequencies, and this could cause a lost in the signals. Also these amplifiers may generate noise frequencies imposed on the real signals. Therefore strain gauge amplifiers should be designed for a signal frequency range corresponding to the measured strain levels and not generate a noise frequency with the signal. Also these amplifiers should be stable with temperature to avoid the drift in the baseline of the pulses.

5) The timing between the three pulses. These times are influenced by imperfect interfacing, the presence of lubricant, propagation time of the stress wave through the sample and the bars, and the distances between the strain gauges and the sample. The dispersion of the elastic wave will combine with the problems above, complicating the selection of the starting time of the signals. With small strain rates the effect of these problems is small, but they can have a large influence on the predicted stress strain curve as the strain rate is increased.

To minimise these errors the following calibration routines to the SHPB test procedure should be followed:

a) establish the actual timing between incident and the reflected pulses by firing the projectile at the incident bar which is separated from the transmitter bar (i.e. no sample).

b) establish the actual timing between the incident and the transmitted pulses by firing the projectile at the incident bar which is in contact with the transmitter bar without a sample. During this calibration run, verification of the gauge factors of both strain gauges can be done by accurately measuring the projectile velocity and converting it to bar strain.

c) using equations

$$\sigma_s(t) = \frac{E}{2} \frac{A}{A_s} [\varepsilon_I(t) + \varepsilon_R(t) + \varepsilon_T(t)] \quad (3.46)$$

and

$$\varepsilon_s(t) = \int \frac{c_0}{\ell_0} [\varepsilon_I(t) - \varepsilon_R(t) - \varepsilon_T(t)] \quad (3.47)$$

rather than the simplified equations;

$$\sigma_s(t) = E \frac{A}{A_s} \varepsilon_T(t) \quad (3.48)$$

and

$$\varepsilon_s(t) = \int \frac{-2c_0}{\ell_0} \varepsilon_R(t) dt \quad (3.49)$$

to calculate stress and strain in the deforming sample. The advantage of this is that it reduces the uncertainty in the timing, since the timing between the incident and the reflected pulses has been established. Also it allows the use of the incident pulse which is the most sharply rising wave, to establish the zero time. The disadvantage of this procedure is that it can introduce large Pochhammer-Chree oscillations into the stress/strain curve which do not truly represent the behaviour of the sample (Follansbee (1986)).

The traverse time which is the time required for the wave to pass through the sample, should be considered in the reflected and the transmitted wave times. The transmitted wave starts one traverse time after the reflected wave as will be discussed in Chapter 6.

### **3.4 Apparatus description and sample preparation**

#### **3.4.1 SHPB system**

The SHPB system as shown in Figure (3.1) consists of a 1.4 m long gas gun evacuated by a rotary vacuum pump, and a 1m long 431 steel bar called the incident bar 12.7 mm in diameter attached to the gas gun and sealed firmly by "O" rings. The "transmitter bar" with the same dimensions as the incident bar is attached to the incident bar. A short steel bar loosely fixed at the end of the transmitter bar is called momentum bar. This momentum bar can fly away from the rest of the bars after the compressive transmitted pulse has been reflected back as a tensile pulse, taking some of the energy away from the bars and dissipating this energy by being trapped in a plasticine filled box.

The incident bar is loaded by impacting it with a 25 cm long steel projectile accelerated by the gas gun. This impact generates a stress pulse in the incident bar with a duration of 100 $\mu$ s according to Equation (3.1), and amplitude can be calculated from Equations (3.2).

The incident pulse propagates along the incident bar, and a reflected and transmitted pulses are created at the sample. The three pulses are detected by pairs of strain gauges mounted at equidistant points 40 cm either side of the sample. If the momentum bar was not present, the stress pulses would travel forwards and backwards along the incident and transmitter bars. These multiple reflections can be detected by the strain gauges and can be plotted as time against distance on a "Lagrangian" graph as shown in Figure (3.5). These reflections cause multiple loading on the sample and could also cause damage to the system. To avoid this, the momentum bar is used to absorb and take away the unwanted stress energy from the system.



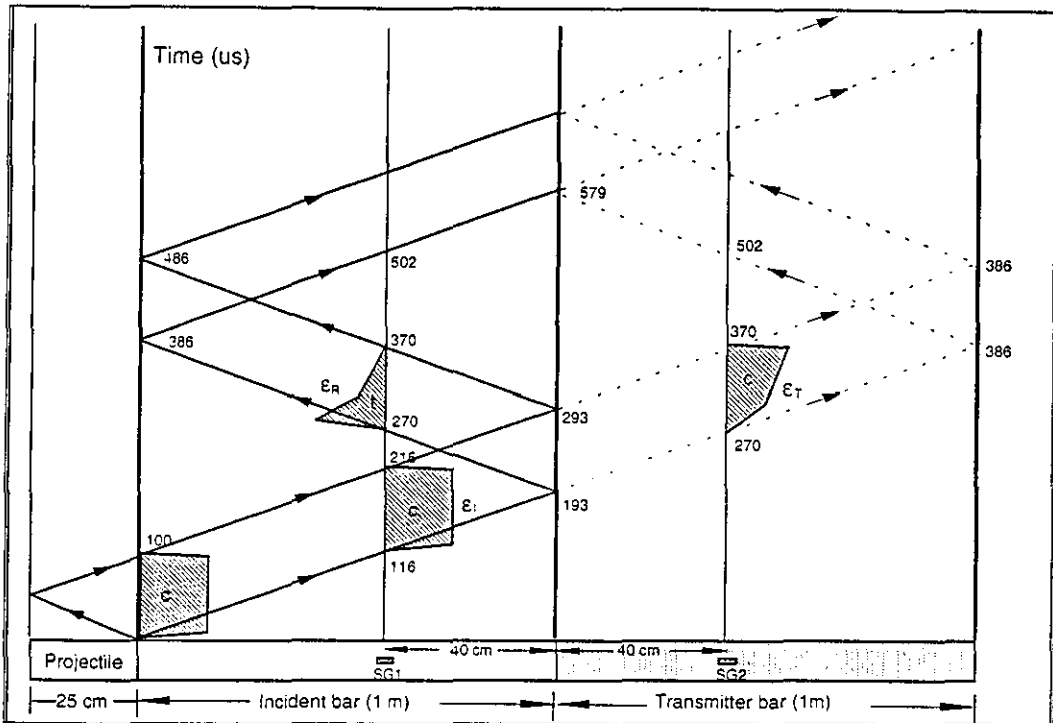


Figure (3.5) Lagrangian diagram for strain pulses in SHPB.

### 3.4.2 The gas gun

The gas gun is a 1.4 m long stainless steel tube having a polished bore of 51 mm diameter. The tube is joined to a rotary type vacuum pump at both its ends via a set of four diaphragm valves (see Figure (3.1)). The gas gun operates by loading the projectile at the furthest point from the split Hopkinson bar, evacuating the gas gun to a pressure of about 1 mbar, and then suddenly exposing the projectile to atmospheric pressure by releasing a lever which moves a flat end plate uncovering a hole in the aperture plate. Each aperture plate has a certain sized hole. The amount of air entering the tube is controlled by the size of the hole. Thus, the projectile velocity is controlled by these holes in the aperture plates.

### 3.4.3 The projectile

The projectile used in the SHPB system is a 25 cm long 431 stainless steel bar of 12.7 mm diameter -the same diameter as the split Hopkinson bars. The projectile bar is guided by a cotton reel-shape body made from PTFE (Figure (3.6)). 'O' rings and brass locating rings allow the bar to slip centrally through the PTFE guide upon impact with SHPB bar. The PTFE guide also

allows the bar to slide easily along the polished bore of the gas gun. The leading part of the PTFE guide has reflecting tape around the perimeter from which the projectile velocity measurement can be made. It is recommended that the projectile is cooled in a refrigerator, so that it can move freely along the interior of the gas gun without sticking or jamming especially on warm summer days. Leaving the projectile on the laboratory bench for a long time could cause an inconsistency in the projectile velocity, because the ambient temperature could cause swelling and sticking of the PTFE guide. The PTFE guide is protected from being smashed against the steel end plate as it slides along the projectile bar after impact by a rubber bung with its central core removed located at the end of the gas gun.

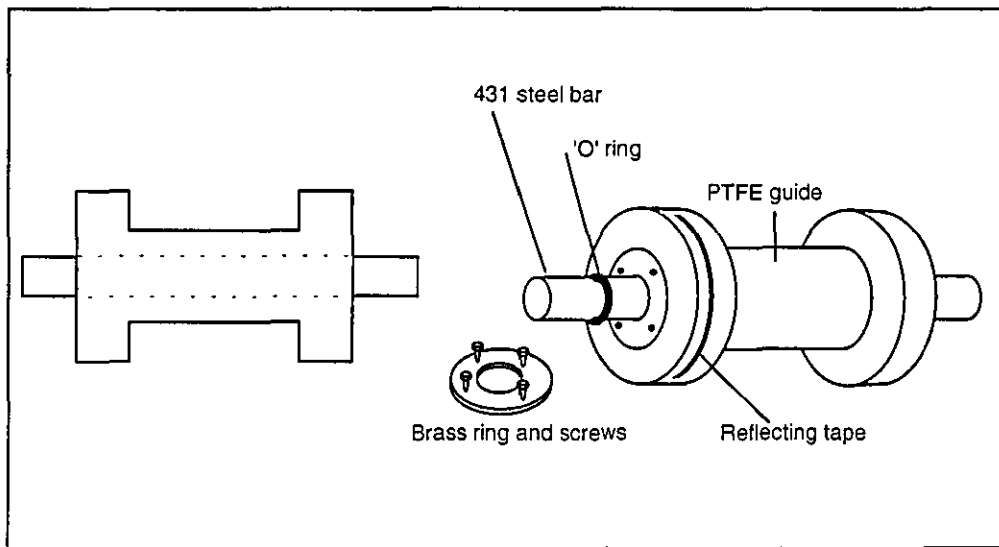


Figure (3.6) Diagram of the projectile.

### 3.4.4 The split bars

The incident and transmitter bars in the SHPB system are of 12.7 mm diameter and 1 m length. They are made of 431 stainless steel with a yield strength of 700 MPa (Dixon (1990)). The 431 bars can attenuate the high frequency components of the stress superimposed on the top of the loading stress pulses which are generated by the impact of the projectile. This feature of the 431 steel bar can provide good attenuation which is clearly observed at high impact velocity and thus provides a clearer and more uniform stress pulse. A 431 steel bar of identical length and diameter is used as a momentum bar, to absorb the released energy and trap it in a plasticine filled box located at the free end of the momentum bar.

The bars as well as the gas gun rest on two separate mild steel supports to reduce unwanted vibrations from the gas gun, as it is being fired, being transmitted to the strain gauges. Also, the incident bar is inserted into the gas gun through a pair of vacuum tight 'O' rings which permit a certain amount of movement of the bar through them after the impact. These 'O' rings reduce any vibration generated in the initial stages of the projectile launch from being transmitted to the bars.

The Hopkinson bars rest on V-shaped nylon clamps (Figure (3.7)) mounted on optical bench stands. The stands have a screw driven movement in two perpendicular directions allowing variation in height and transverse distance from the centre of the optical bench. This arrangement enables precise alignment of the bars which can be checked by shining a diffuse light from a small hand-held torch behind each bar/bar and bar/sample interface. The bars were able to slide freely through the nylon clamps, preventing spurious reflections to occur during the passage of the stress pulses. Strong elastic cords were used to pull together the bar/bar or the bar/sample interfaces to avoid small gaps that may occur.

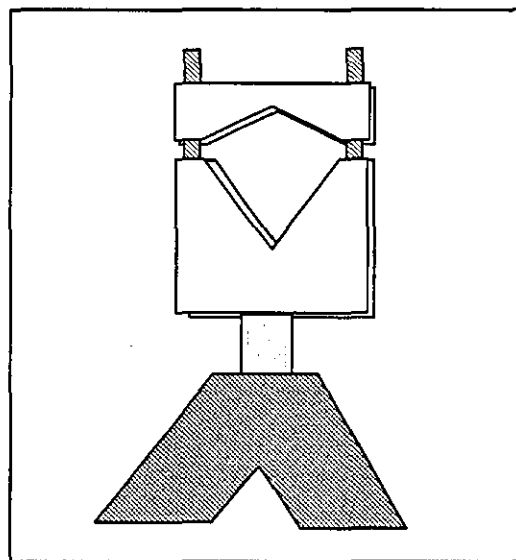


Figure (3.7) V-shaped nylon clamp.

The alignment of the bars is important to prevent any damage to the bars and to avoid any unwanted reflection from the bar interfaces caused by gaps.

### 3.4.5 Recording system

#### a) Velocity measurement

The impact velocity of the projectile is measured using an electronic system consisting of a transmitter circuit which has three infra-red emitter diodes, and a receiver consisting of three photo diode detectors. The received signals trigger timer counters via a 3 channel amplifier. Three twin core optical fibres are mounted through vacuum proof sealed holes on the gas gun near the Hopkinson bar, and situated (A, B and C) 10 cm apart. The timer counter counts the time required for the projectile to travel between the optical fibre probes which are located immediately before the impact.

The ends of each transmitter-receiver fibre pair are cut at an angle of about  $40^\circ$  to the fibre-axis to provide a good recapture of the transmitted infra-red beam reflected from the reflector tape mounted on one of the PTFE guide collars. By knowing the time that the projectile takes to travel the two 10 cm distances, the impact velocity can be determined.

#### b) Strain gauges

The incident and reflected stress pulses and the transmitted pulse are detected by two strain gauge pairs denoted by SG1 and SG2 respectively. The total resistance of each pair is  $240\Omega$ . The strain gauge pairs are wired in series and form part of a simple potential divider bridge circuit (Figure (3.8)) including a  $2.3k\Omega$  ballistic resistor, and a 90 V dc stabilised power supply. The power supply polarity is configured in a way that when a compressive strain pulse reduces  $R_s$ , a positive output voltage  $V_s$  is produced.

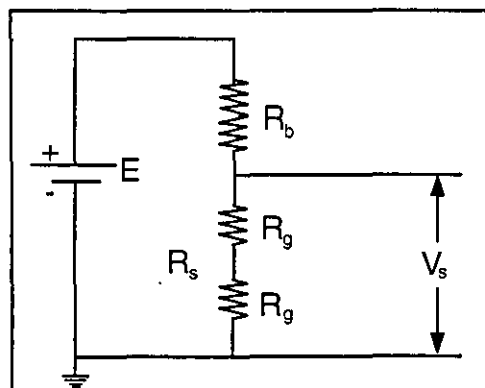


Figure (3.8) Strain gauge circuit.

The strain gauges of each pair oppose each other in location in order to eliminate the bending waves that may occur in the bars and to double the output from the stress pulses. The strain ( $\varepsilon$ ) recorded by the strain gauge is related to the change in its electrical resistance ( $dR_s$ ) as in the following equation

$$\varepsilon = \frac{dR_s}{FR_s} \quad (3.50)$$

where  $F$  is the strain gauge factor .

Simple analysis of the strain gauge potential divider circuit gives;

$$V_s = \frac{R_s}{R_b + R_s} E = \frac{1}{n+1} E \quad (3.51)$$

where  $E$  and  $V_s$  are the power supply and the voltage across the strain gauge pair respectively.

$$n = \frac{R_b}{R_s} \quad (3.52)$$

Differentiating Equation (3.51) with respect to  $n$  gives ;

$$\frac{dV_s}{dn} = -\frac{E}{(n+1)^2} \quad (3.53)$$

Differentiating Equation (3.52) with respect to  $R_s$  gives;

$$\frac{dn}{dR_s} = -\frac{R_b}{R_s^2}$$

or 
$$dn = -\frac{R_b}{R_s^2} dR_s \quad (3.54)$$

Substituting  $dn$  in Equation (3.53) gives;

$$\begin{aligned} \frac{dV_s}{dR_s} &= -\frac{R_b}{R_s^2} \left[ -\frac{E}{(n+1)^2} \right] \\ dR_s &= R_s^2 \frac{(n+1)^2}{R_b E} dV_s \end{aligned} \quad (3.55)$$

Substituting Equation (3.55) in Equation (3.50) gives;

$$\varepsilon = \frac{(n+1)^2}{nFE} dV_s \quad (3.56)$$

For convenience  $n$  can be expressed in terms of voltages as

$$n = \frac{R_b}{R_s} = \frac{I R_b}{I R_s} = \frac{(E - V_s)}{V_s} \quad (3.57)$$

Equation (3.56) gives a direct relation between the strain in the bars and the variation in the voltage across the strain gauges, considering  $(n+1)^2 / nFE$  is constant. This variation in the voltage can be recorded and digitised by a digital storage recorder and displayed by an oscilloscope. At the present time these pulses are recorded by a Philips PM3335 analogue digital oscilloscope of 4 kbyte storage capacity. The traces can be dumped directly from the oscilloscope to a GRAPHTEC HP compatible plotter, or transferred to a PC via an RS232 connection cable and stored using Phillips 'DSOCOM' software.

To obtain a reliable output from the strain gauge, it is important to ensure that the strain gauge is properly affixed to the bar. After the bar has been cleaned, slightly roughened using a silicon carbide paper of 120 or 240 grit, then cleaned again using a suitable solvent, the strain gauge can be attached to the bar using a super glue. Some pressure needs to be exerted on the strain gauge by hand for about two minutes to allow the glue to gain some initial strength. This pressure also helps the glue excess to be squeezed out on one side of the strain gauge.

Two sizes of FLA-6-17 and FLE-1-11 strain gauges of gauge factor of 2.14 have been used in the LUT SHPB system, 1 or 6 mm long mounted at a distance of 40 cm either side of the sample. The 1 mm long strain gauge gives better resolution than the 6 mm strain gauge and lasts longer when testing at high strain rates.

The resolution time of the SHPB obtained from these strain gauges is;

$$\Delta t = \frac{L_g}{c_0} \quad (3.58)$$

where  $L_g$  is the strain gauge length,  $c_0$  is the sound speed in the bar, hence  $\Delta t$  obtained from the strain gauge is

$$\frac{6\text{mm}}{4.8\text{mm}/\mu\text{s}} \approx 1\mu\text{s}$$

and for 1mm strain gauge is

$$\frac{1\text{mm}}{4.8\text{mm}/\mu\text{s}} \approx 0.2\mu\text{s}$$

If the stress pulses are small they can be amplified if required. The circuit diagram of the amplifier used in this project is shown in Figure (3.9). This amplifier is powered by a 9 V power supply, and has gains of 10, 20, 50, and 100 with frequency band width of about 100 Hz to 3 MHz. The output circuit of the amplifier consists of a 10  $\mu\text{F}$  capacitor in series to avoid the dc. and the low frequency interference. The high frequency is minimised by using a 2200 pF capacitor connected in parallel with the coaxial cable near the input of the oscilloscope.

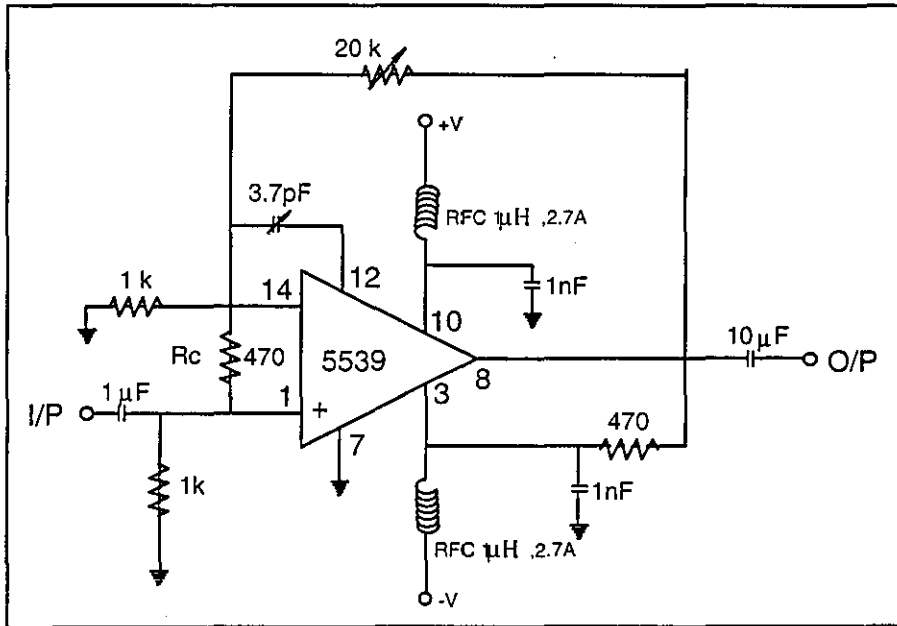


Figure (3.9) Circuit diagram of high speed operational amplifier.

### 3.4.6 Sample preparation and lubrication

Three sizes of solid cylindrical sample were used; 10 mm ( $\approx \pm 0.1$  mm) diameter  $\times$  5 mm ( $\approx \pm 50$   $\mu\text{m}$ ) length, 8 mm ( $\approx \pm 0.1$  mm) diameter  $\times$  4 mm ( $\approx \pm 50$   $\mu\text{m}$ ) length and 6 mm ( $\approx \pm 0.1$  mm) diameter  $\times$  3 mm ( $\approx \pm 50$   $\mu\text{m}$ ) length. The samples were machined from large rods supplied from Polypenco. The machining was performed on a lathe in the Physics Department's mechanical workshop, with a coolant to ensure that the temperature generated did not disturb the internal structure of the polymer. After the samples were cut, they were finely ground to produce smooth flat faces.

The lubrication in the SHPB test is very important as demonstrated by several workers e.g. Ellwood (1983), Follansbee et al (1984), Dixon (1990) and others, in order to avoid frictional constraint. Some workers such as Walley et al (1989) and Dawson (1993) used petroleum jelly for lubrication in their drop-weight impact techniques. Care must be taken not to use too much lubricant as it can cause some samples to slip sideways and hence deform unevenly.

As mentioned before, friction causes untrue results in the SHPB analyses and it may result in barrelling of the sample during deformation; also it makes the measured stress higher than the stress for the lubricated samples. Thus, all the compression tests have been carried out using silicone grease lubrication. A thin layer of the silicone grease is smeared on the sample/bar interfaces, to eliminate the friction effects on the analysis.

### **3.5 Data acquisition and computation**

#### **3.5.1 Capturing and translating data**

As outlined in the schematic form in Figure (3.1), the SHPB data acquisition system consists of strain gauges and their circuits, the amplifier, and the oscilloscope to capture the signals which can then be fed to a PC to store the data.

The low strain in the bar ( $<0.3\%$ ) causes a change in the voltage ( $dV_s$ ) across the strain gauges, which is linearly proportional to the strain ( $\epsilon$ ) in the gauges. The variations in the voltages across SG1 and SG2 are fed to linear high bandwidth amplifiers if required.

The amplified signals are fed to two channels of a Philips digital storage oscilloscope, which digitises and stores each strain gauge signal in a separate channel. To gain as good a resolution as possible, the signals should fill as much space as possible from the 255 voltage steps memory scale.

After capturing the signals by the digital oscilloscope, the data are transferred via RS232 interfaces to a PC to be saved in two separate files, one for each channel. Each file name ends with an extension **.ASC**, and contains 4096 pairs of data points. The first point of each pair of points is the time in seconds; and the second point is the voltage in volts -separated from the time by ','.



4096 points cover the full memory of each channel of the oscilloscope, which is equal to half of the points displayed on the oscilloscope screen. Knowing the sampling rate of the data or the digitising rate of the signals is important for the analysis. Thus setting the time base of the oscilloscope to give the right sampling interval value (e.g. 1  $\mu$ s) is an important requirement. The sampling rate is equal to the time base/200, hence to get 1  $\mu$ s sampling rate, the time base should be set to 200  $\mu$ s/div. The format in which the data have been stored in is not readable by the SHPB analysis program - also not all the stored data are required for the analysis. Thus, a simple QBASIC program has been written to translate and save the required and important part of the data in a proper format in a file with a name constructed from the material tested name, projectile velocity, identity letter and the channel number. The program saves the files with file name, date of test, and time of test on the first line, followed by the number of points on the second line. These two lines are followed by the time and voltage data, line by line in two columns.

In some experiments a Thurlby DSA524 'Digital Storage Adapter' with DC-PC link software is used to capture and store in ASCII code, the SHPB signals occupying 4 kbyte for each channel. It is difficult to analyse the ASCII code data directly, and usually only a small part of the data is required for the analysis. Thus the data need to be modified to real decimal values and the useful parts saved. Thus, a special program has also been written to read, visualise, translate and save the important part of the DSA data record.

### **3.5.2 Description of SHPB program and data analysis (Hopk-bar.bas)**

After saving the incident and the reflected pulses and the transmitted pulse data into two files, the SHPB equations can be applied to calculate the stress, strain and the strain-rate development of the materials tested. A QBASIC program (Appendix 1) has been written to do the Hopkinson bar analysis, calculate the material properties, save and also modify the results by smoothing and averaging the results data (as described later in this section).

This program runs quickly and has been revised a few times to ensure its accuracy in analysing the SHPB signals. Simple and clear functions have been chosen to make this program as simple as possible for the users to run. The functions performed by the Hopk-bar program are shown in Figure (3.10)

```
Transmitter      Sample      Incident      Projectile
-----
HOPK-BAR DIRECTORY      09-07-1994
-----
* 1. TRANSFER PARAMETERS TO DISK      *
* 2. HOPK BAR DATA ANALYSIS      *
* 3. LIST DATA      *
* 4. LIST RESULTS      *
* 5. PARAMETERS ENTERED FROM KEYBOARD      *
* 6. BAR STRAIN & IMPACT VELOCITY      *
* 7. AVERAGE OF RESULTS FILES      *
* 8. SMOOTH THE RESULTS      *
* 9. FINISH      *
* D. DOS SHELL      Noori 11/01/1994*
*****
SELECT NUMBER (1 TO 9 or D).
```

Figure (3.10) Main directory of Hopk.bar program.

The table in Figure (3.10) shows the main functions of the SHPB program directory as displayed on the computer screen after completing the program initialisation of all the variables. Initialisation is made by calling the subroutine *initil*, performing the procedures in lines 1-390, declaring the subroutines in the main program, giving simple user instructions and making the dimensions for the arrays used in the program. The variables and the initial headings are displayed on the screen. The Young's modulus values and longitudinal acoustic velocity and mechanical impedance are selected by the program according to the pressure bar material which is either maraging or 431 steel as in lines 400-440.

### 1. Transferring and listing the parameters

The function of this directory is to transfer the parameters of the sample and the apparatus to a file structured by the program according to some of the following parameters;

Example: if the test parameters are

Material tested HDPE

Projectile time (1 to 2) in msec: 5.00

Projectile time (2 to 3) in msec: 5.00

Identity letter (e.g A) : A

The name of the parameters file is HDPE20A3, where 20 is the projectile velocity in m/s corresponding to the projectile times of 5 msec between the optical probe positions 1 to 2 and 2 to 3. The file name for the channel 1 data should be called after the translation as HDPE20A1 and for channel 2 as HDPE20A2. The file name should not be longer than 8 characters including the

last sequential number. The velocity space is not more than two characters, so the other five characters will be combined from the tested material name and the identity letters. Entering and saving the parameters is controlled in lines 520-1320.

A list of all the parameters entered via the computer keyboard prior to an impact test can be obtained by selecting option 5 on the directory. The parameters listed by the subroutine in lines 5010-5400, are displayed as shown in Figure (3.11): a typical parameters list. This list can either be displayed on the screen or sent to a line printer according to whether the operator's reply to line 5020 is **S** or **P** to open a suitable file either for the screen or the printer in lines 5080-5100.

```
*****
* PARAMETERS ENTERED FROM KEYBOARD *
-----*
* Date of the experiment   = Mon. 14/3/94
* Time of the experiment  = 5:00 PM
* Date of analysis        = 03-15-1994
* Time of analysis        = 15:29:26
* Filename                 = peek26c
* Sampling rate           = 1 us
* Test type                = Compression
* Projectile material      = Steel
* Projectile length       = 25 cm
* Test temperature        = 20 C
* Annealing temperature   = 0 C
* Gain of SG1 amplifier   = 1
* Gain of SG2 amplifier   = 1
* Strain gauge factor (f1) = 2.14
* Strain gauge factor (f2) = 2.14
* Sample length           = 3.178 mm
* Sample diameter         = 6.972 mm
* Power supply voltage    = 90 volts
* Voltage across SG1      = 8.8 volts
* Voltage across SG2      = 8.75 volts
* Poisson's ratio         = 0.500
* Delay between pulses    = 0 us
* Velocity of impact      = 26.4973 m/s
*****
```

Figure (3.11) Table of a typical parameters list.

## **2 Hopkinson-bar data analysis (lines 1950-4310)**

After completing the parameters file (which will be the third file besides the other two data files for both oscilloscope channels), the analysis function can be used at any time.

In lines 1970-2120 the third file containing the parameters previously entered via the keyboard is read back into the memory by opening the file, and using the subroutine in lines 5080-5400 to display the parameters on the screen. Reading this file is useful for reminding the user of the parameters in the analysis. The calibration factors F1 and F2 are calculated in lines 2130-2190 for both channels by entering the strain gauge factors, or leaving the default values as they are to be used in the calculation.

The program reads data from the second file as transmitter pulse data if the test was in compression, but it reads from the first file as the transmitter pulse data for a tensile test, (this is done by lines 2200-2410). The data will first be analysed to find the start of the transmitter pulse. After removing any electrical spikes in the pulse and setting the baseline of the pulse, the data between the start and the end of the pulse are analysed to calculate the engineering stress (lines 2420-2750).

In lines 2770-2930 the program changes the file name by replacing the channel number (z\$) to load the incident and reflected pulses data. Finding the starting point of the incident pulse takes place after setting the conditions of the test whether the test is compressive or tensile. The start of the incident pulse is found by searching for the large rise of the pulse, 20 points from the beginning of the record. Using the same sub routine (lines 6290-6700), the program finds the reflected pulse start by skipping about 130  $\mu$ sec in time ahead of the incident pulse width which is dependent on the projectile length. The manual checking and modification of the pulses starting points can be done in this subroutine. The 20 points which are shown in line 2940 ( $b=b+pn+20$ ) are between the incident and the reflected pulses, where b is the beginning of the pulse and pn is its duration (here  $pn=130$ ). 20 points after the end of the reflected pulse are used for calculating the baseline for this channel by taking the average of the 20 points. This baseline can be altered manually. The delay time between the reflected and the transmitted pulses is calculated by subtracting the transmitted pulse start time from the reflected one. This delay depends on the distance of the gauges from the sample, and can be modified automatically to be set as in the parameters file. The delay time is usually initially set as zero for gauges which are equidistant from the sample. If the actual measured delay is then not zero this usually implies poor sample alignment or quality. It could also be an indication of the wave propagation time through the sample. Figure (3.12) shows this effect on the reflected pulse.

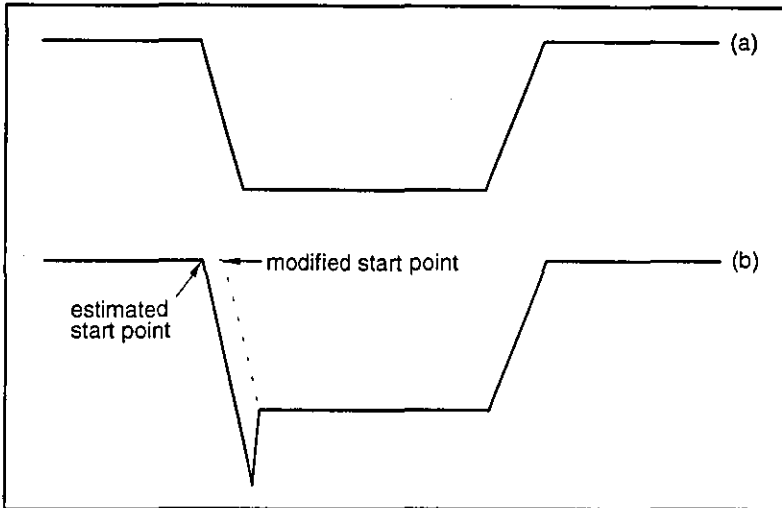


Figure (3.12) Reflected pulse from (a) perfectly aligned sample.  
(b) imperfectly aligned sample.

In lines 3360-3710 the program displays the modified timing of the reflected pulse if it is required. Also it displays the start (beginning of the pulse) and the end (end of the pulse) corrections of the reflected pulse. The program then calculates the area of the reflected pulse between these two points after correction of the reflected pulse baseline. The correction introduces a sloping baseline, so that the values of gauge strain at either end of the reflected pulse are set to zero. Figure (3.13) shows the sloping baseline correction where the dotted line indicates the previously estimated horizontal baseline, and the dashed line is the sloping baseline correction which is defined by the expression contained in line 3700.

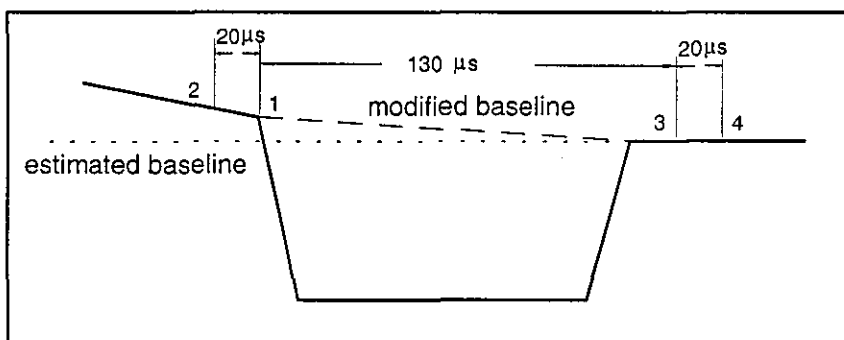


Figure (3.13) Reflected pulse sloping baseline correction.

The engineering strain variation in the specimen with time is evaluated in lines 3720-3900 by using Equation (3.19).

The engineering values of the mechanical parameters are converted into their true counterparts i.e. true stress, strain and the strain rate by using the Equations (3.16) and (3.18).

First derivative of Equation (3.18) gives the true strain rate as

$$\text{tr} = \frac{\partial(\text{es}) / \partial t}{1 + \text{es}} \quad (3.59)$$

The option to save the values of time, true stress, strain, and the strain rate, and engineering stress and strain onto a floppy disk is shown in lines 4030-4300.

In line 4100 the results file has the same name as the data file but with a sequential number of 4. The results file is opened and saved by lines 4110-4290. After finishing the analysis and saving the results, the program returns to the main directory to let the operator choose another option.

### **3. List data**

This function of the Hopkinson bar program is to read a disk file into memory after entering the name of the file holding the data (line 1340). The number of data points in this file are displayed on the screen by line 1470 after reading the heading of the translated data file. After selecting how much of these data are to be displayed (lines 1480-1510), four options appear for displaying the data, i.e. either the computer screen or the printer as in lines 1520-1580. The options are displayed in the following format:

Select code (1 - 4):

- 1- List data on Screen
- 2- List data on Line printer
- 3- Return to Hopk-bar directory
- 4- Return to change the selected data points.

If the operator chooses the first option, the program opens "SCRN" file for output to display the data (in mV) on the screen in ten columns beside the time column (in  $\mu\text{s}$ ). The second option is to open an "LPT1:" file for output to activate the line printer to print the data in ten columns (in mV) besides the time column (in  $\mu\text{s}$ ) with step 10 as shown in Figure (3.14). The third and fourth options are for returning to the main directory and returning to re-select the data points to be displayed respectively. The program determines in lines 1680-1690 whether the

data are from bar 1 , i.e. incident and reflected pulses data from a compressive test, or from bar 2, i.e. transmitted pulse data from compressive test. Incident/reflected and transmitted pulse data are derived from bar 2 and bar 1 respectively for tensile tests.

Incident bar data from 190 to 400 peek26c [Compression test]

Time (us)	Data values (mV)									
	0	1	2	3	4	5	6	7	8	9
190	-4.4	-4.4	-4.4	-4.4	-4.8	-4.8	-5.6	-5.6	-5.6	-4.8
200	-2.8	0.0	3.6	7.6	12.0	16.0	20.0	22.8	25.6	27.2
210	28.0	28.4	28.4	28.8	29.2	29.2	29.2	29.6	29.6	29.6
220	29.6	30.0	30.4	30.0	30.0	30.0	30.0	30.4	30.4	30.4
230	30.0	30.4	30.4	30.8	30.4	30.4	30.4	30.8	31.2	31.2
240	30.8	30.8	30.8	31.2	31.2	31.2	30.4	31.2	31.2	31.2
250	31.2	30.8	31.2	31.2	31.6	31.2	31.2	31.2	31.2	31.2
260	31.2	31.2	31.2	31.2	31.2	31.2	31.2	31.2	31.2	31.6
270	31.2	31.2	31.2	31.6	31.2	31.2	31.6	31.2	31.6	31.6
280	31.2	31.2	31.6	31.6	31.2	31.6	31.2	31.6	32.0	31.2
290	31.2	31.6	30.8	30.0	28.8	27.2	25.6	22.8	19.6	17.6
300	15.2	12.4	10.0	7.2	5.2	3.6	1.6	0.4	-0.8	-0.8
310	-1.2	-1.2	-1.2	-1.2	-1.6	-2.0	-2.0	-2.0	-2.0	-2.0
320	-2.0	-2.4	-2.4	-2.4	-2.4	-2.4	-2.4	-2.4	-2.4	-2.8
330	-2.4	-2.8	-2.8	-2.8	-2.8	-2.8	-3.2	-2.8	-3.2	-2.8
340	-2.8	-3.2	-3.2	-2.8	-3.2	-3.2	-3.2	-3.6	-3.6	-4.4
350	-4.8	-6.0	-6.8	-8.0	-10.4	-12.0	-14.8	-18.0	-20.4	-22.8
360	-24.4	-26.8	-28.0	-29.6	-30.8	-31.2	-32.0	-32.4	-32.8	-32.8
370	-32.8	-32.8	-33.6	-33.2	-33.6	-33.6	-34.4	-34.0	-34.0	-34.0
380	-34.0	-34.0	-34.0	-34.4	-34.4	-34.4	-34.4	-34.4	-34.4	-34.4
390	-34.4	-34.4	-34.4	-34.8	-34.8	-34.4	-34.4	-34.8	-34.8	-34.4
400	-34.4	-34.4	-34.4	-34.4	-34.8	-34.8	-34.4	-34.4	-34.4	-34.4

Dou want to list more data (Y or N)? █

Transmitter bar data from 340 to 500 peek26c [Compression test]

Please wait.....

Time (us)	Data values (mV)									
	0	1	2	3	4	5	6	7	8	9
340	-2.2	-2.4	-2.3	-2.3	-2.3	-2.2	-2.3	-2.2	-2.3	-2.2
350	-2.2	-2.2	-2.1	-2.1	-1.8	-1.8	-1.7	-1.4	-1.1	-0.6
360	-0.5	-0.2	0.2	0.5	0.9	1.1	1.4	1.6	1.8	1.8
370	2.0	2.1	2.1	2.3	2.2	2.3	2.4	2.3	2.4	2.5
380	2.5	2.5	2.5	2.5	2.6	2.5	2.6	2.6	2.6	2.6
390	2.6	2.6	2.6	2.7	2.6	2.8	2.7	2.8	2.8	2.8
400	2.8	3.0	3.0	3.0	3.1	3.0	3.1	3.2	3.2	3.3
410	3.5	3.4	3.4	3.4	3.4	3.6	3.6	3.7	3.8	3.8
420	3.8	3.9	4.0	4.2	4.2	4.3	4.3	4.6	4.5	4.6
430	4.6	4.9	4.9	4.9	5.1	5.0	5.3	5.4	5.5	5.4
440	5.7	5.7	5.9	5.9	6.0	6.2	6.2	6.2	6.4	6.4
450	6.2	6.3	6.2	6.1	6.1	5.9	5.6	5.6	5.4	5.1
460	4.9	4.8	4.5	4.2	4.0	3.8	3.7	3.4	3.3	3.2
470	3.0	2.9	2.7	2.6	2.5	2.5	2.3	2.2	2.0	1.9
480	1.9	1.8	1.7	1.6	1.7	1.4	1.4	1.4	1.1	1.1
490	1.1	1.0	0.8	0.9	0.8	0.8	0.7	0.7	0.7	0.6
500	0.6	0.5	0.6	0.5	0.4	0.3	0.2	0.2	0.3	0.2

Dou want to list more data (Y or N)? █

Figure (3.14) Typical incident and transmitter bars data.

#### 4. List results

This function of the Hopk - bar directory is for listing the calculated or the saved results. By running this function, a short menu is displayed of options of the form:

TRANSFER RESULTS TO:-

- 1- Screen
  - 2- Line printer
  - 3- Return to Hopk-bar menu
- Select code:

From one of the chosen codes 1 or 2 the results are listed. This is shown in lines 4320-4820. If this function is run immediately after the analysis the results can be read from the memory to be listed. The subroutine in lines 4840-4990 reads the results from a file on a floppy disk. The options of displaying the results on the screen or the printer are given in lines 4380-4420. The operator can choose the time interval (in  $\mu\text{s}$ ) between each line of results (line 4490).

Lines 4520-4580 print the results headings on the chosen medium and these are followed by the table of results (lines 4590-4750) as shown in Figure (3.15).

User name : Noori Al-Maliky    09-07-1994    00:22:45					
Stress/Strain results					
Filename holding results = peek26c    09-07-1994					
Time(us)	True stress(MPa)	True Strain(%)	Strain rate (/sec)	Engineering stress(MPa)	Engineering strain(%)
0	0.00	0.00	0.00E+00	0.00	0.00
2	1.04	0.03	1.46E+02	1.04	0.03
3	2.29	0.06	3.01E+02	2.29	0.06
4	5.76	0.11	4.79E+02	5.77	0.11
5	9.75	0.19	7.35E+02	9.78	0.19
6	13.69	0.29	1.02E+03	13.75	0.29
7	19.93	0.43	1.39E+03	20.04	0.43
8	27.63	0.62	1.84E+03	27.84	0.62
9	38.66	0.85	2.32E+03	39.06	0.84
10	49.34	1.13	2.81E+03	50.00	1.12
11	59.63	1.45	3.26E+03	60.63	1.44
12	71.22	1.83	3.71E+03	72.68	1.81
13	83.35	2.24	4.12E+03	85.41	2.21
14	96.45	2.69	4.50E+03	99.29	2.65
15	108.74	3.17	4.85E+03	112.48	3.12
16	119.96	3.68	5.13E+03	124.70	3.61

HIT <SPACE BAR> TO CONTINUE

Figure (3.15) Typical results for PEEK.



## 6. Bar strain and impact velocity

This option calculates and displays the strains recorded by the pairs of strain gauges mounted on bars 1 and 2 (lines 5440-5800). It also translates the strain produced by impact into the projectile velocity which can then be compared with that calculated from the projectile velocity measuring system. The results should agree within a reasonable error.

## 7. Average of results files

A subroutine has been written for averaging two results files and finding the mean of stress/strain curves. The average results file produced is automatically saved in a separate file with a sequential number of 6. The data to be averaged should be taken from tests at the same nominal strain rate. This option can also be used to enter the averaged results file via keyboard to be stored on a disk. The automatic averaging is done by the subroutine **average** (lines 7570-7630), by opening two files and reading the data from both of them to be added and then divided by 2. The results are stored on disk in a file ended by the number 6.

## 8. Smoothing the results

This option can be used at any time after the analysis to cut off the high frequencies in the results by using the following statement (lines 7080-7480)

**IF ABS(a(j))<>ABS((a(j+1)+a(j-1))/2) THEN a(j)=(a(j+1)+a(j-1))/2**

This means if the condition is not satisfied that any point should equal the average of the previous and the next points, then a new value should be given by the average value as in the following example.

Example;

Table (3.1) shows an example for the smoothing operation. For  $x_0=0$ ,  $x_1=1$ ,  $x_2=1.5$ ,  $x_3=2$ , and  $x_4=2.5$ , etc, the smoothing subroutine gives a new values of  $x_i$  as

$$x_0' = 0, x_1' = (x_0+x_2)/2 = (0+1.5)/2 = 0.75$$

$$x_2' = (x_1'+x_3)/2 = (0.75+2)/2 = 1.375$$

$$x3' = (x2'+x4)/2 = (1.375+2.5)/2 = 1.9375, \text{ and so on..}$$

Same way for y axis, when  $y_0 = 0$ ,  $y_1 = 7$ ,  $y_2 = 5$ ,  $y_3 = 6$ , and  $y_4 = 5$ , the program gives the values as;

$$y0' = 0, y1' = (y0'+y2)/2 = (0+5)/2 = 2.5,$$

$$y2' = (y1'+y3)/2 = (2.5+6)/2 = 4.25,$$

$$y3' = (y2'+y4)/2 = (4.25+5)/2 = 4.625, \text{ and so on ..}$$

This operation is applied for stress and strain data independently from each other corresponding to a fixed time interval of  $1 \mu\text{s}$ .

Table (3.1)  
Arbitrary values show the smoothing effects

T	X	Y	X'	Y'
0	0	0	0	0
1	1.0	7	0.7500	2.500
2	1.5	5	1.3750	4.250
3	2.0	6	1.9375	4.625
4	2.5	5	2.4687	5.181
5	3.0	7	3.2344	5.910

The smoothed results are saved in a file with a sequential number of 5 beside the original results file of sequential number 4 beside the file sequential number 4 for the unsmoothed results. A practical example of this operation are shown in Figures (3.16).

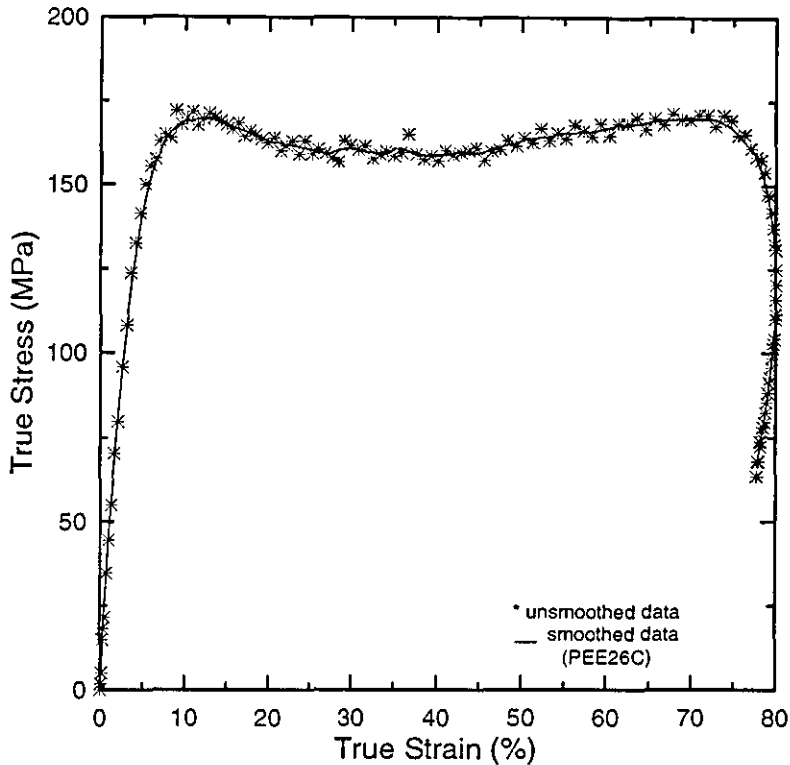


Figure (3.16) Stress/strain curves for PEEK.  
(\* unsmoothed and — smoothed data)

## 9. Finish

By selecting the finishing option the operator exits from the program. The program has been written in quick basic compiler version 4.5, and then compiled to be an executable file. The executable Hopk-bar program requires about 91 kbyte memory and about 10 kbyte for the data.

## D. DOS shell

If the computer is needed to perform other jobs, such as plotting data or copying, deleting, or renaming files without losing the data from the memory a DOS shell function can be used, which leaves the Hopk-bar program temporarily to do the job. Typing the word **EXIT** from the DOS prompt will bring the Hopk-bar program into action again with all the data restored in the memory.

A subroutine called (eer) in lines 7640-7700 is used for handling errors if they occur, and allows the user to return to the main program directory without losing the data from the memory. A help function was added lately to help the user how use the Hopk-bar program.

### 3.5.3 Temperature rise calculation

The deformation of materials such as polymers at high strain rates leads to the conversion of mechanical energy into heat. The heat may be localised at crack tips or on shear planes or the deformation may produce a uniform bulk temperature. The bulk temperature rise can be measured by a thermocouple or by using a heat sensitive film as in work done by Swallowe et al (1984). The temperature rises produced during the deformation processes can be very high. The time scale for the flow of the heat away from the sample becomes greater than the duration of the experiment, and so significant temperature rises can occur which will tend to produce strain softening.

The bulk temperature rise for the material was calculated by measuring the area under the stress-strain curve using a simple program with a flowchart as shown in Figure (3.17).

The equation of specific heat is

$$s_p = \frac{\text{thermal energy}}{\text{mass} \times \Delta T} \quad (3.60)$$

Therefore, the temperature rise  $\Delta T(K) = \frac{\text{energy}}{\text{mass} \times s_p}$

The area under stress-strain curve =  $\int \sigma d\epsilon = \frac{\text{energy}}{\text{volume}}$  (3.61)

The density  $\rho = \frac{\text{mass}}{\text{volume}}$  (3.62)

$$\Delta T = \frac{\text{energy}}{\text{volume} \times \rho \times s_p}$$

or  $\frac{\text{energy}}{\text{volume}} = \Delta T \times \rho \times s_p$  (3.63)

Equations (3.61) and (3.63) give

$$\int \sigma d\epsilon = \Delta T \times \rho \times s_p$$

$\therefore \Delta T = \frac{1}{\rho s_p} \int \sigma d\epsilon$  (3.64)

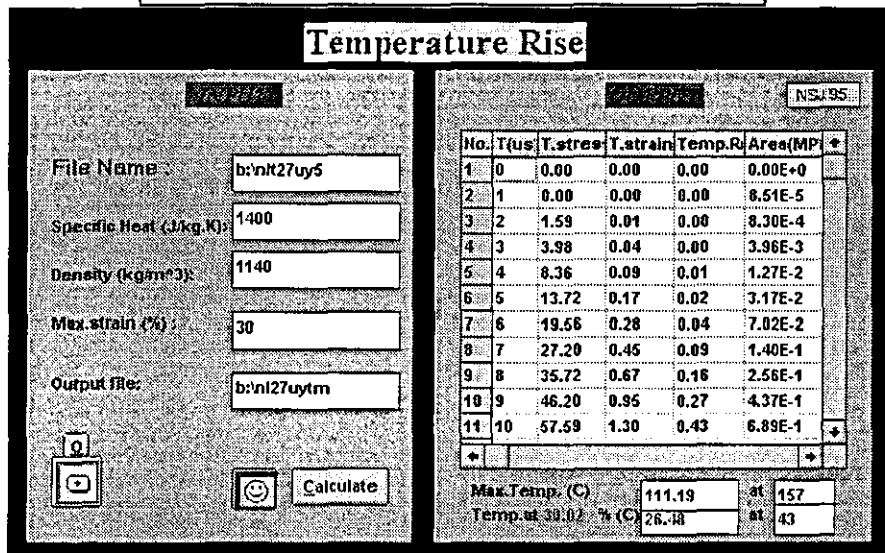
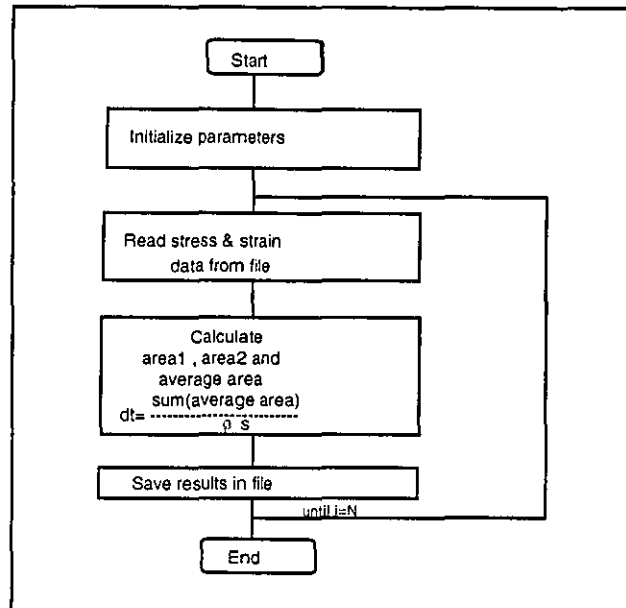


Figure (3.17) Flowchart and menu of temperature calculation program.

The computer program uses a digital integration method for Equation (3.64) to calculate the area under the stress-strain curve. The curve is divided into small segments or strips with a time scale duration of  $1\mu\text{s}$  according to the sampling rate. The area of each segment is the product of the width and the average of the height as shown in Figure (3.18).

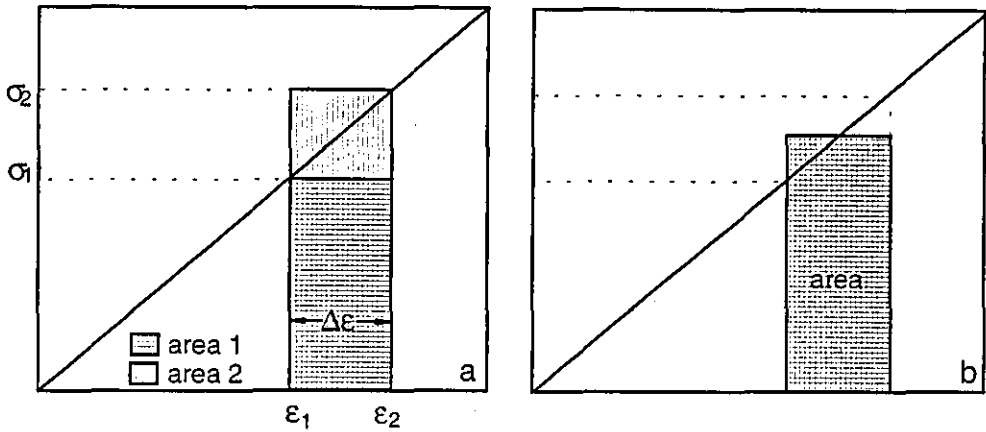


Figure (3.18)

$$\begin{aligned} \text{area1} &= \Delta\epsilon \times \sigma_1 \\ \text{area2} &= \Delta\epsilon \times \sigma_2 \end{aligned}$$

$$\text{Average area} = \frac{(\text{area1} + \text{area2})}{2}$$

$$\text{or average area} = \frac{(\sigma_1 + \sigma_2)}{2} \Delta\epsilon$$

where  $\Delta\epsilon$  is the strain change during  $1\mu\text{s}$  time.

The computer program uses the equations;

$$\text{area1}(i) = \sigma(i) \times [\epsilon(i) - \epsilon(i-1)]$$

$$\text{area2}(i) = \sigma(i+1) \times [\epsilon(i) - \epsilon(i-1)]$$

$$\text{average area}(i) = [\text{area1}(i) + \text{area2}(i)] / 2$$

The total area =  $\sum_{i=0}^{i=N}$  average area(i), where N is the number of data points.

The results obtained from this calculation have been examined and compared with experimental data for temperature rise history measured by using a K-type thermocouple inserted into the centre of the sample. The measured temperature has a final value that agrees very well with the value calculated by the program. This calibration has been made for metal as well as polymer samples, to confirm the accuracy of the prediction of the temperature from the program.

### **3.6 Summary**

The split Hopkinson pressure bar (SHPB) has evolved into a useful high strain rate testing apparatus because the stress pulse generated in a long cylindrical bar is relatively simple and is capable of precise analysis. In addition, sample dimensions have been chosen to minimise delays associated with stress pulse propagation.

The application of the SHPB method to the dynamic testing of materials gives records of the stress vs. time, strain vs. time, strain rate vs. time and stress vs. strain. The loading stress pulse in the SHPB system is initiated by an axial impact from a steel projectile, which is launched to an impact velocity by a gas gun using atmospheric air pressure.

The impact generates a pulse in the incident bar with a duration twice the length of the projectile. The amplitude of the stress pulse is directly proportional to the impact velocity which can be controlled by controlling the speed of the air entering the gas gun.

When the compressive pulse in the incident bar reaches the sample, part of the pulse is reflected from the interface, while part is transmitted through the sample to the transmitter bar. The magnitudes of the reflected and the transmitted pulses depend on the physical properties of the sample. Thus, from these pulses the properties of the sample can be calculated. These pulses were recorded by using resistance strain gauges mounted on the bars at equidistant points on either side of the sample.

Results for HDPE, UHMWPE, Nylatron, and PEEK polymers using the SHPB technique are reported in detail in the next chapter. The strain rate can be varied by varying the projectile speed or by varying the sample dimensions. A QBASIC computer program is used to capture, translate and analyse the useful part of the strain gauge records to get the mechanical properties of the material under test.

## **CHAPTER 4**

### **SPLIT HOPKINSON PRESSURE BAR RESULTS**

#### **4.0 Introduction**

High density polyethylene (HDPE), ultra high molecular weight polyethylene (UHMWPE), nylatron, and polyetheretherketone (PEEK) have been tested in compression for different strain rates at room temperature (24 °C). HDPE, UHMWPE and nylatron samples were machined out of rods obtained from Polypenco, while PEEK samples were made from plates obtained from Victrex (ICI). The Loughborough SHPB bars are 12.7 mm in diameter. A 25 cm steel projectile has been used for all tests except where otherwise mentioned. The initial diameter of the samples were made smaller than the bar diameter to ensure the sample did not extend outside the faces of the bars. To satisfy the criteria proposed in the previous chapter (the minimisation of friction, inertia and wave propagation effects), the length/diameter ratios that have been used are 5 mm/10 mm, 4 mm/8 mm, and 3 mm/6 mm. For any particular sample, the variation in length is 5–10 μm and in diameter 5–20 μm. Great care is taken during the machining to make the sample faces as parallel as possible. The sample faces are then smoothed by using fine wet and dry paper to improve the flatness.

All DSO records in this chapter are plotted as bar strain against time (μs). The bar strains can be calculated by multiplying the traces in these records by the corresponding multiplication factor indicated on the y-axis.

#### **4.1 HDPE results**

High density polyethylene samples have been tested using the SHPB system at different strain rates and different strain levels. Figures (4.1.1a,b and c) show typical DSO traces of the incident, reflected and transmitted pulses (25 cm steel projectile). A tufnol projectile has also been used to produce a longer loading pulse with a smaller amplitude; hence it produces lower strain rates for longer times. Figure (4.1.2) shows a DSO record for an 18 cm length tufnol projectile which produces an incident pulse of 120 μs duration. Figure (4.1.3) shows the true stress histories obtained from the digital data corresponding to Figures (4.1.1a, b, c) and (4.1.2). The corresponding strain and strain rate histories for these stresses are shown in Figures (4.1.4) and (4.1.5) respectively.



The engineering stress-time curves are proportional to corresponding transmitted traces, and the true strain rate curves are proportional to the corresponding reflected traces.

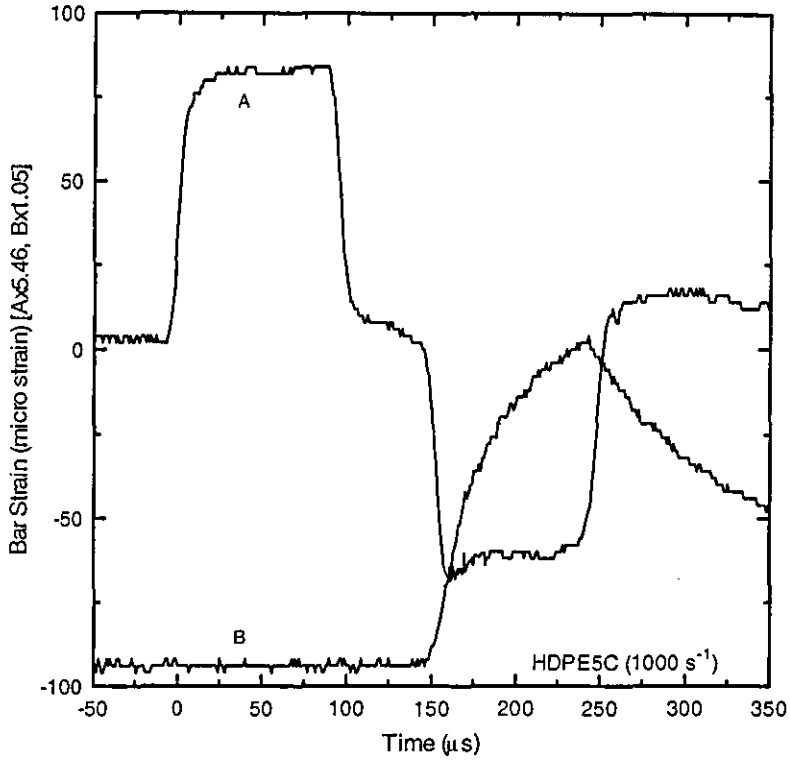


Figure (4.1.1a) DSO record for an HDPE tested at an impact speed of 5.3 m/s.

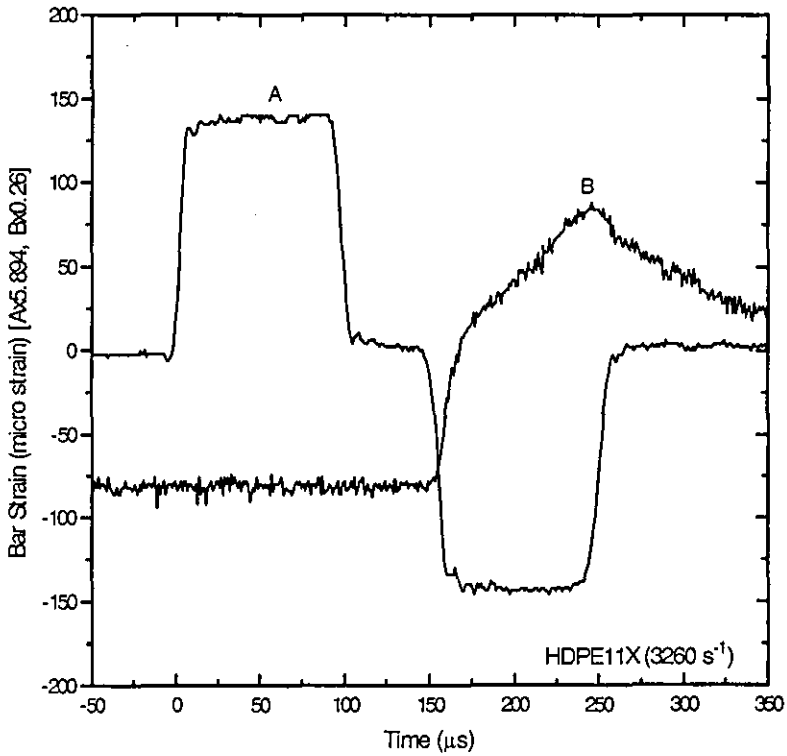


Figure (4.1.1b) DSO record for an HDPE tested at an impact speed of 10.7 m/s.

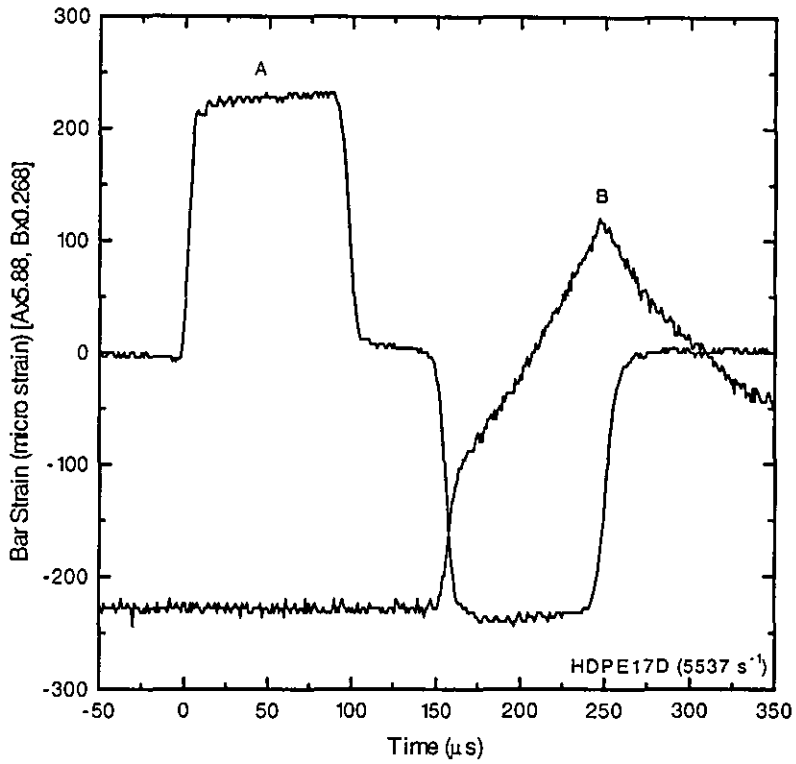


Figure (4.1.1c) DSO record for an HDPE tested at an impact speed of 17.4 m/s.

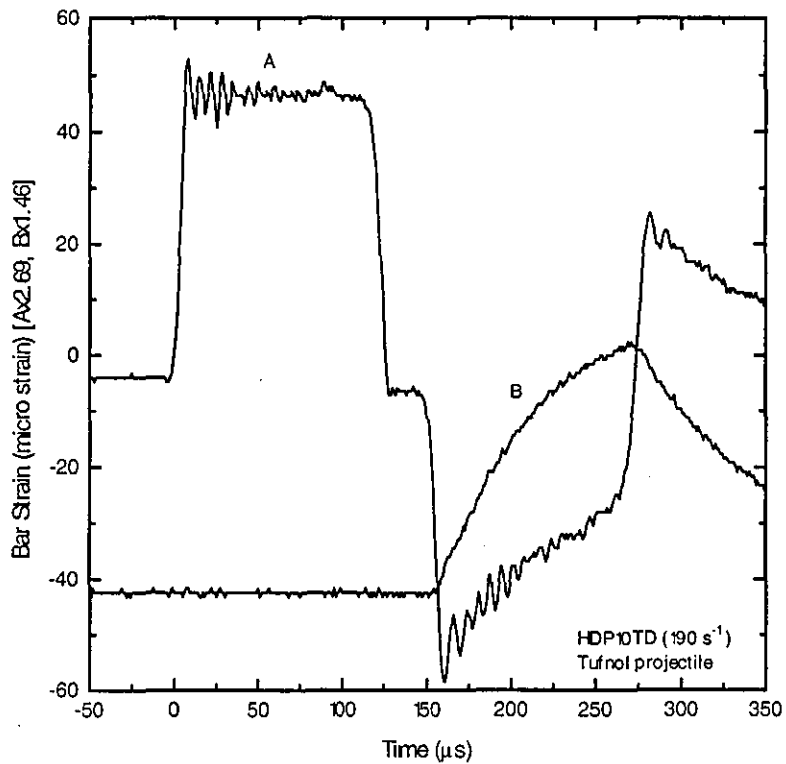


Figure (4.1.2) DSO record for an HDPE tested at an impact speed of 9.8 m/s using a tufnol projectile.

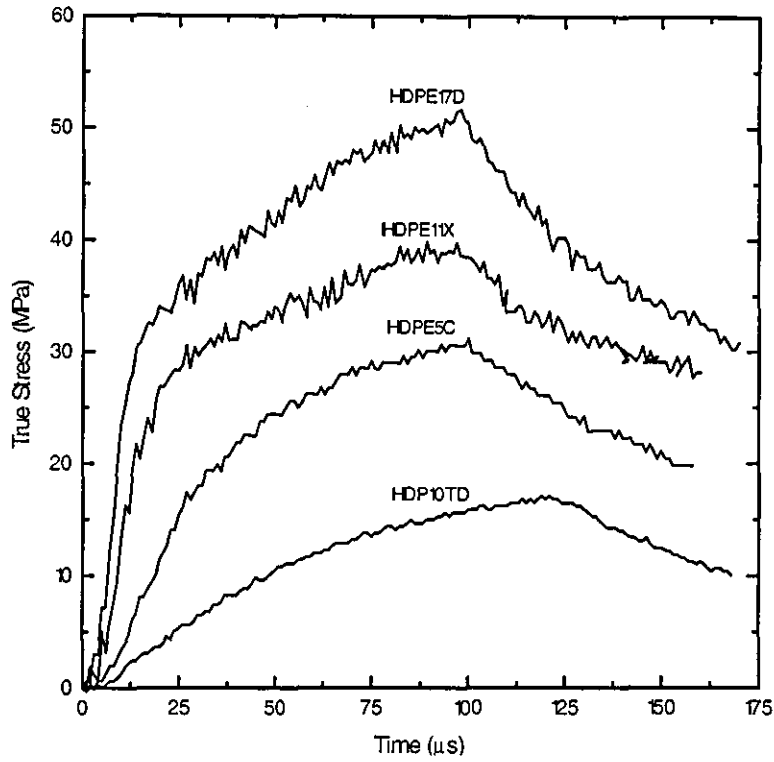


Figure (4.1.3) Stress/time curves calculated from the records in Figures (4.1.1a, b, c) and (4.1.2).

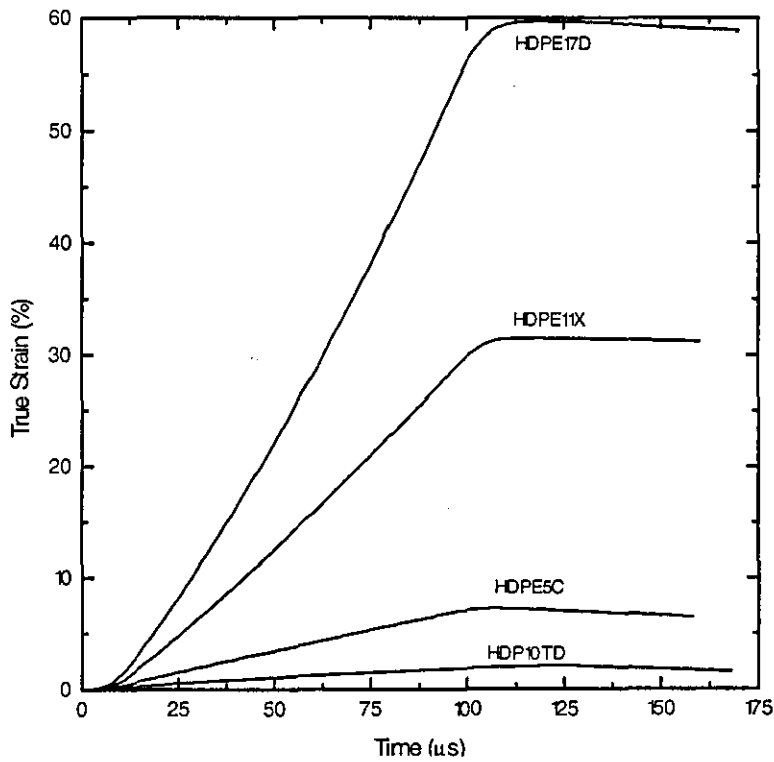


Figure (4.1.4) Strain/time curves for the corresponding records in Figures (4.1.1a, b, c) and (4.1.2).

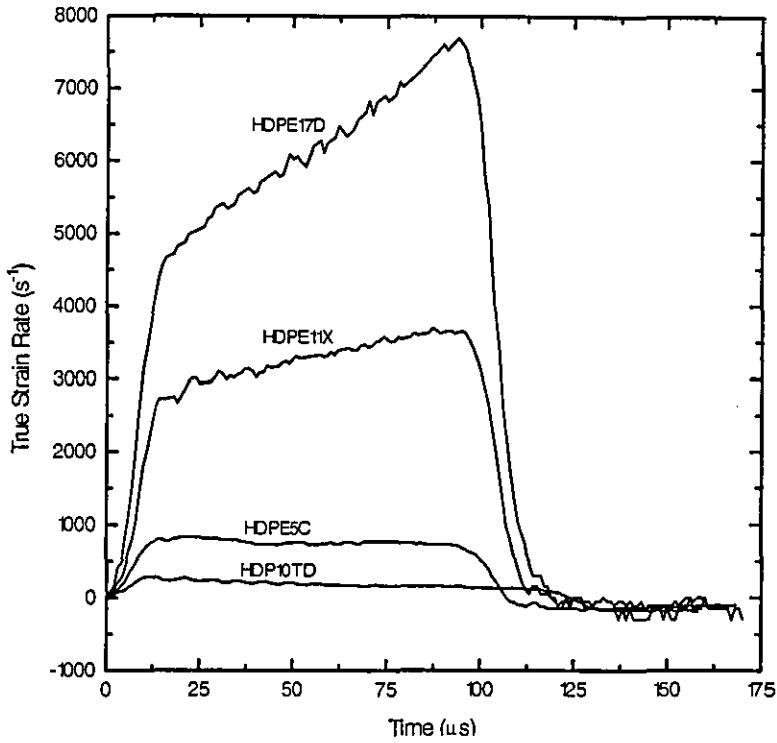


Figure (4.1.5) True strain rate histories.

All the plotted stress-strain results have been smoothed using the **HOPK.BAS** program, described in Chapter 3, to minimise any high frequency oscillations. Figure (4.1.6) shows a typical stress-strain plot showing the smoothed and unsmoothed curves.

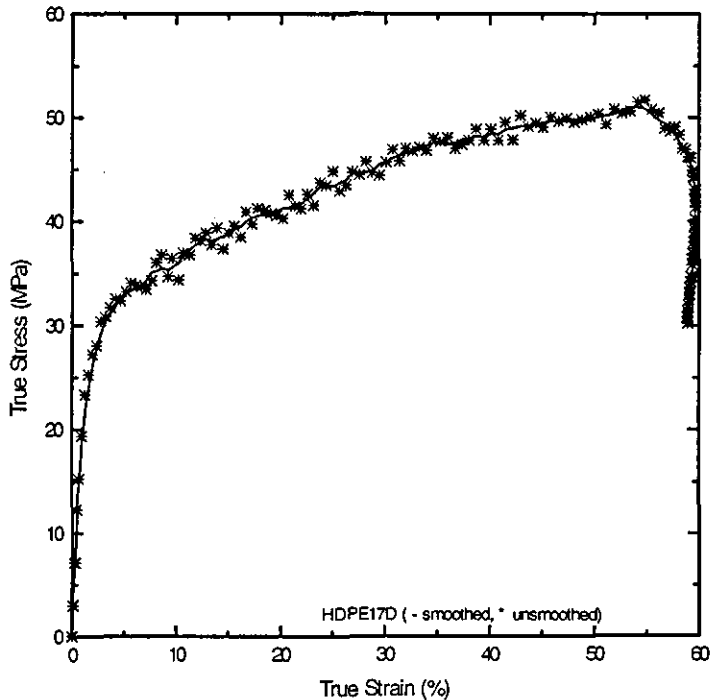


Figure (4.1.6) Typical stress-strain curve showing the smoothing effect on the results.

Figure (4.1.7) shows the true stress against true strain plots at different strain rates and a typical quasistatic curve at a strain rate of  $1 \times 10^{-2} \text{ s}^{-1}$ . These plots show that the flow stress increases with increasing strain rate. The elastic region in which the material obeys Hooke's law only lasts for a strain of about 1%. The gradient of the curves then continuously decreases up to a strain of about 10% after which it becomes reasonably constant. The elastic modulus, which is determined from the slope of the first linear part of the stress-strain curves, increases with increasing strain rate as tabulated in Table (4.1). The flow stresses at 5% and 10% strains are also tabulated for different strain rates. The strain rates which are used in this study are average strain rates calculated from the true strain-time curves between  $12 \mu\text{s}$  after the start of the test (the rise time of the loading pulse) and the time at which a strain of 30% is reached. For the experiments in which a strain of 30% is not reached, the strain rate was calculated by dividing the sample strain by the total length of the loading pulse, excluding the strain and time associated with the rise and decay of the loading pulse.

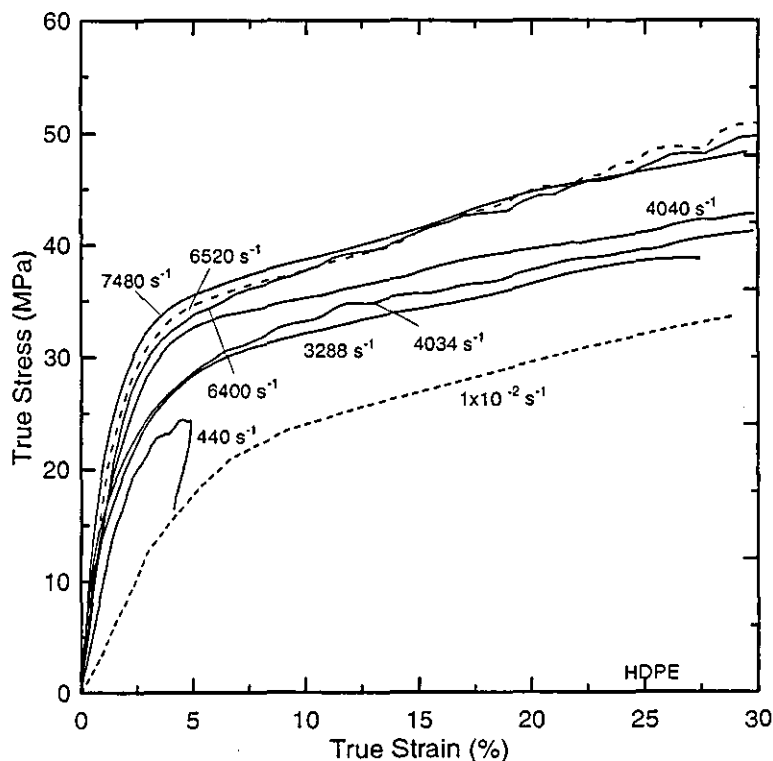


Figure (4.1.7) Stress-strain curves of HDPE at different strain rates.

**Table ( 4.1 ) HDPE results.**  
(T 18 cm Tufnol projectile is used)

Impact speed (m/s)	Sample dimensions		$\dot{\epsilon}_{\text{upto } 30\%}$ ( $\text{S}^{-1}$ )	E (GPa)	$\sigma_{5\%}$ (MPa)	$\sigma_{10\%}$ (MPa)
	L(mm)	D(mm)				
9.7 T	5.308	10.035	190	0.98	-	-
9.1 T	3.820	9.945	238	1.06	-	-
8.8 T	3.949	7.835	256	1.09	-	-
9.1 T	3.904	9.950	272	1.03	-	-
15.4 T	4.046	7.845	445	1.23	24.45	-
15.7 T	3.790	9.980	440	1.10	24.00	-
5.4	5.025	10.09	762	1.12	28.24	33.00
4.9	4.050	7.930	1000	1.36	29.00	32.50
5.3	4.303	7.516	1000	1.20	28.80	33.30
11.1	3.970	10.02	2250	1.69	28.00	34.00
10.8	3.740	9.880	2200	1.41	28.00	32.10
10.7	3.095	5.572	3292	1.93	28.79	32.00
18.1	4.800	10.20	3946	2.22	33.50	35.60
18.1	4.670	10.36	4208	1.55	31.78	34.82
19.8	3.983	9.900	4095	2.00	30.46	37.95
17.8	3.943	10.04	4080	2.26	28.66	33.15
21.3	4.017	7.518	5426	2.29	32.00	36.70
17.4	3.015	5.856	5557	2.27	33.00	35.64
17.4	3.069	5.889	5334	2.28	33.14	37.60
21.3	4.020	7.861	6171	2.12	32.37	36.50
25.0	3.800	9.962	6427	2.42	34.00	39.50
25.3	3.969	7.504	6543	2.22	34.50	37.70
21.3	3.675	7.572	6344	2.39	35.00	37.15
26.4	3.302	5.964	7741	2.23	35.30	38.50
$\pm 0.5$	$\pm 0.015$	$\pm 0.020$	$\pm 50$	$\pm 0.2$	$\pm 1.5$	$\pm 1.3$

At a strain rate of  $3292 \text{ s}^{-1}$  in the SHPB test the flow stress at 5% strain is 28.79 MPa, and the elastic modulus is 1.93 GPa. In the Hounsfield test the flow stress at 5% strain is 17 MPa, and the elastic modulus is 0.43 GPa at a strain rate of  $1 \times 10^{-2} \text{ s}^{-1}$  (see Table (4.1)). The Young's modulus increases with increasing strain rate as shown in Figure (4.1.8).

Figure (4.1.9) shows the calculated temperature rise against strain at various strain rates for HDPE. The maximum temperature rise reached here is about  $5^\circ\text{C}$  at a strain of 30%. Thus there is no significant effect of the temperature rise on the HDPE properties at this level of strain. However, a larger temperature rise would effect the HDPE behaviour.

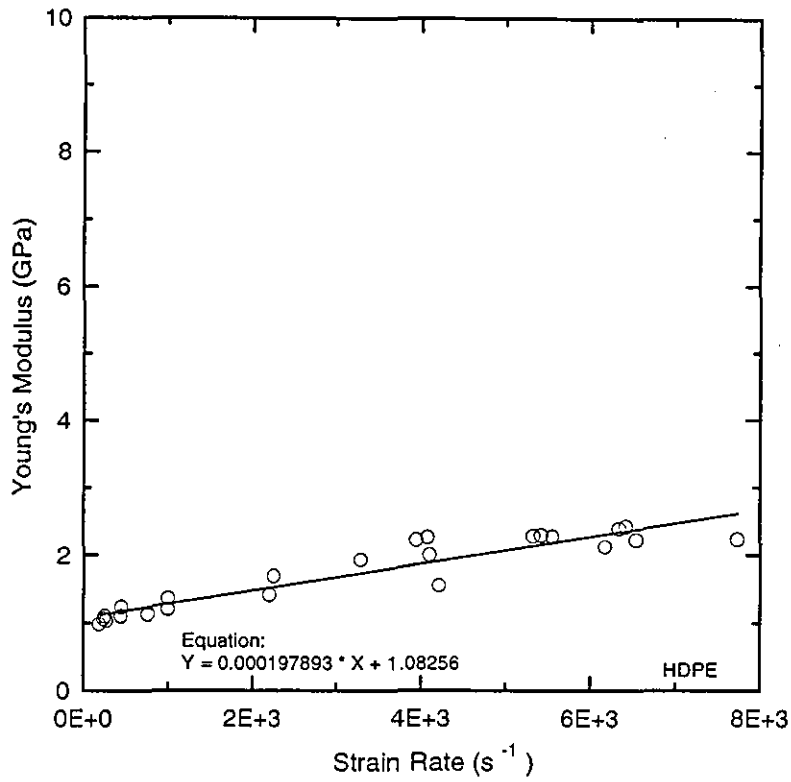


Figure (4.1.8) Young's modulus against strain rate for HDPE.

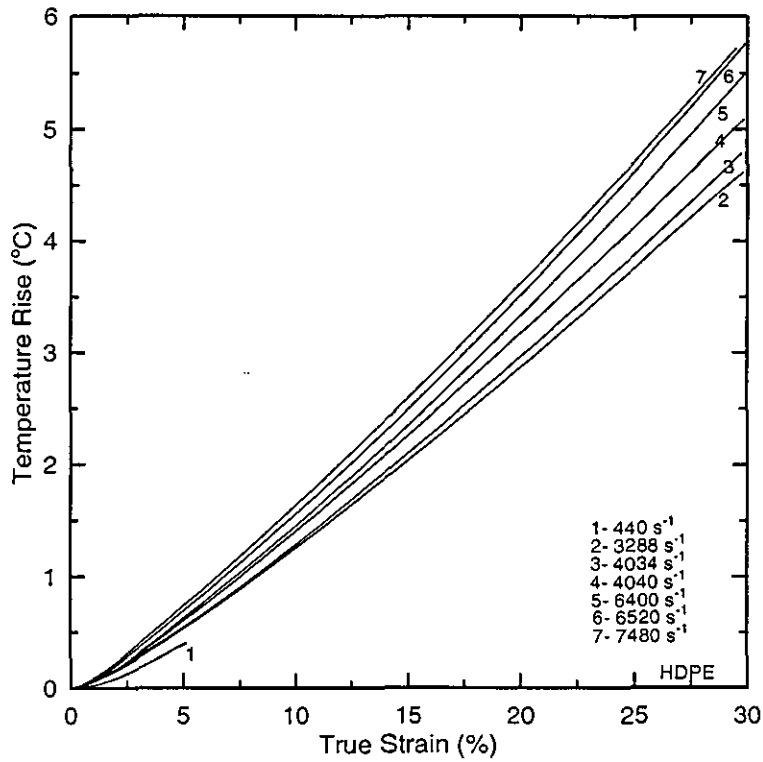


Figure (4.1.9) Plot of temperature rise against true strain at various strain rates.

## 4.2 UHMWPE results

UHMWPE material has also been tested at different strain rates using the SHPB system. Figures (4.2.1 a, b, and c) show typical DSO records for UHMWPE samples tested at strain rates of 1120, 1750, and 3411  $s^{-1}$  respectively. True stress and strain histories are shown in Figures (4.2.2) and (4.2.3). Figure (4.2.4) shows typical strain rate histories. Figure (4.2.5) shows stress-strain plots at various strain rates, while Figure (4.2.6) shows the temperature rise against strain calculated from the area under the stress-strain curves in Figure (4.2.5).

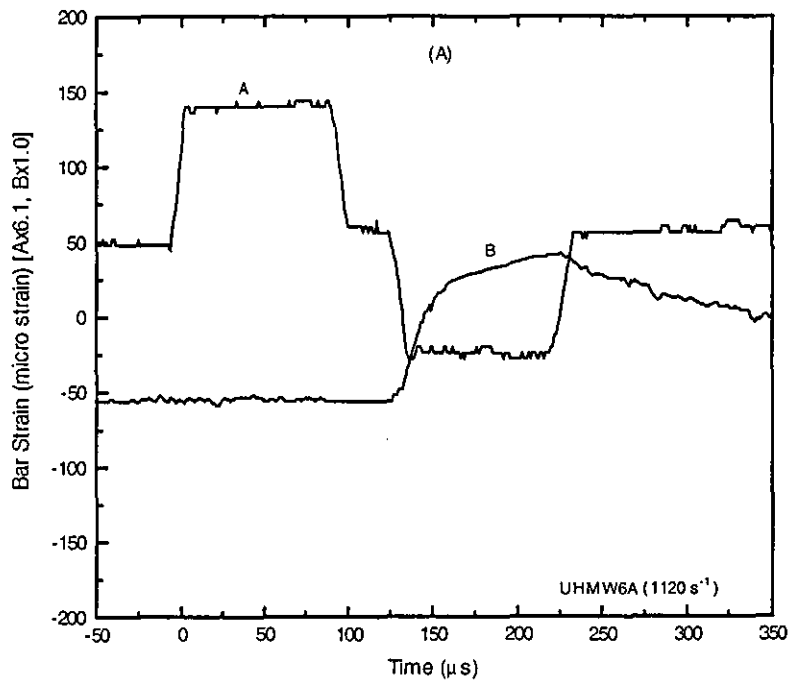


Figure (4.2.1a) DSO record for UHMWPE at an impact speeds of 6.3 m/s.



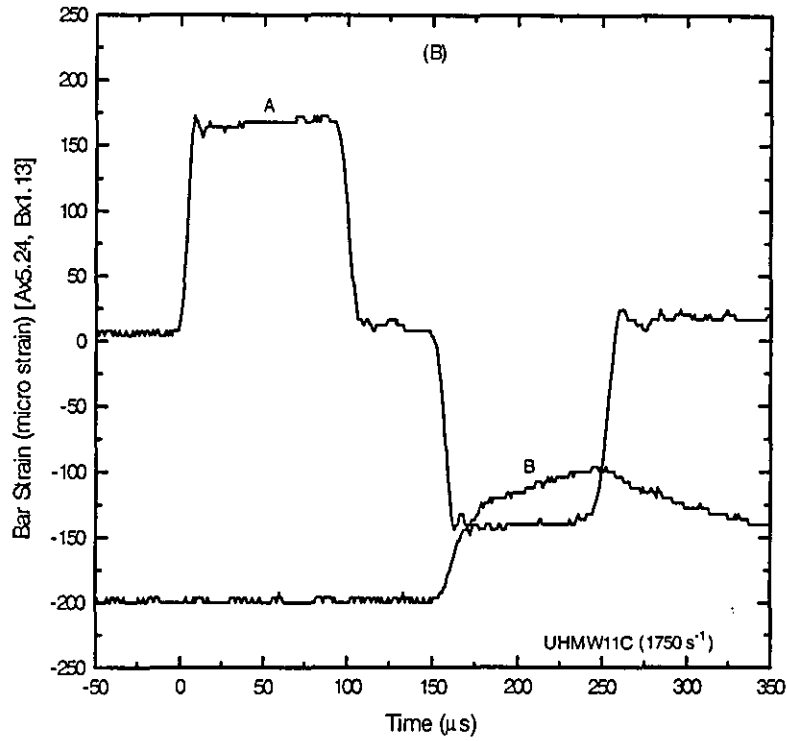


Figure (4.2.1b) DSO record for UHMWPE at an impact speed of 11 m/s.

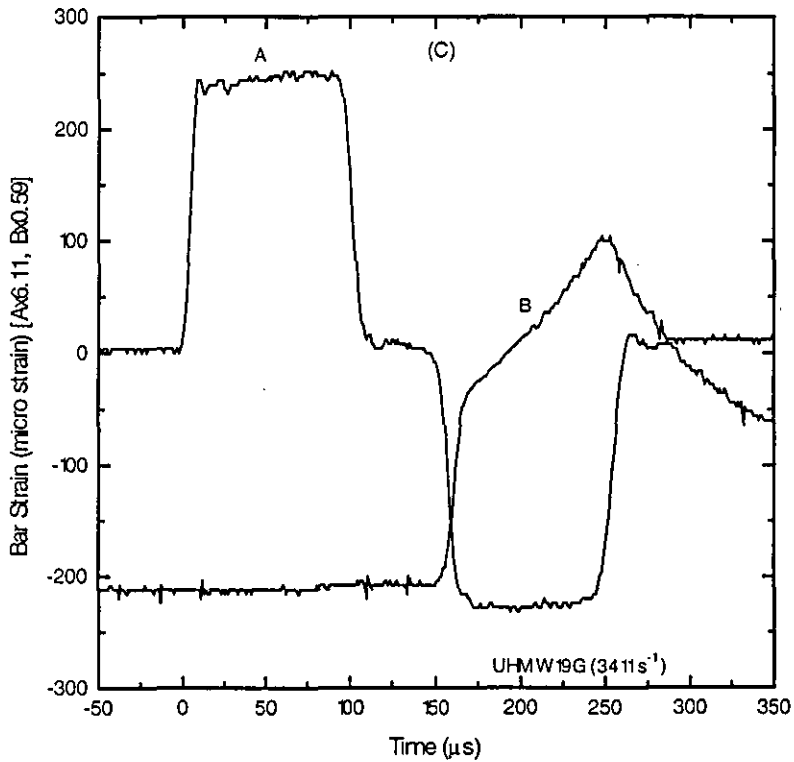


Figure (4.2.1c) DSO record for UHMWPE at an impact speed of 19 m/s.

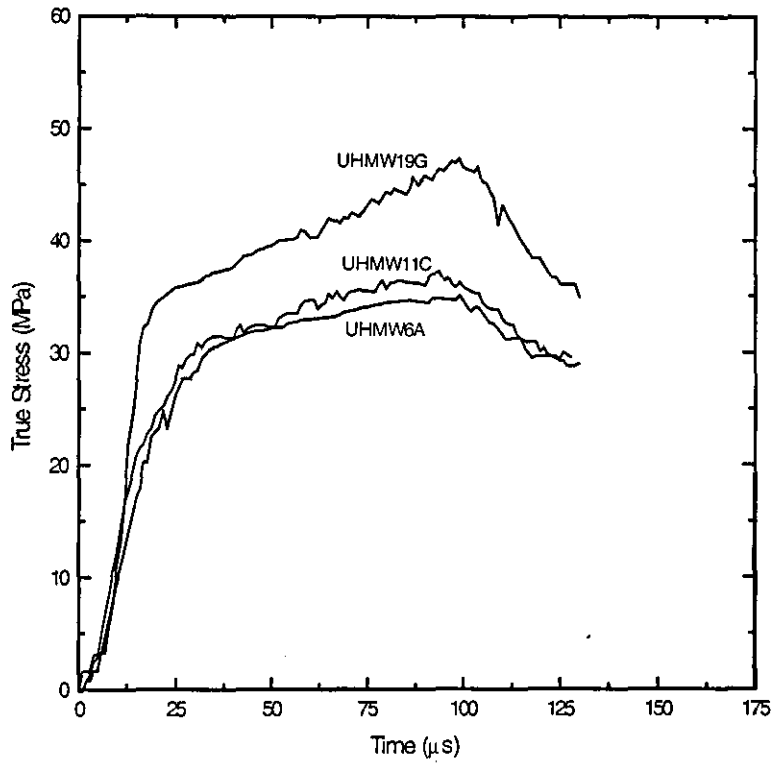


Figure (4.2.2) True stress histories for UHMWPE.

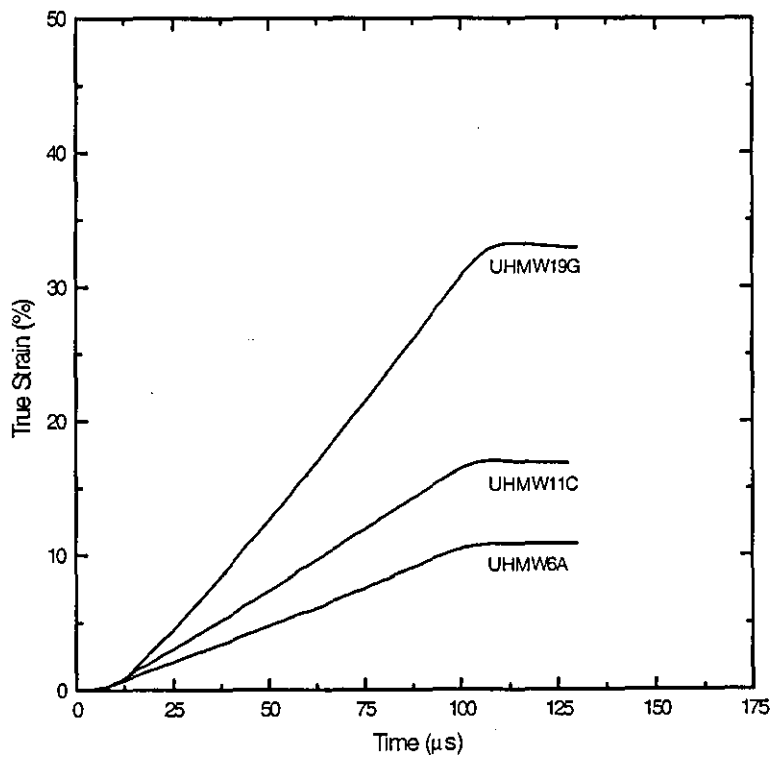


Figure (4.2.3) True strain histories for UHMWPE.

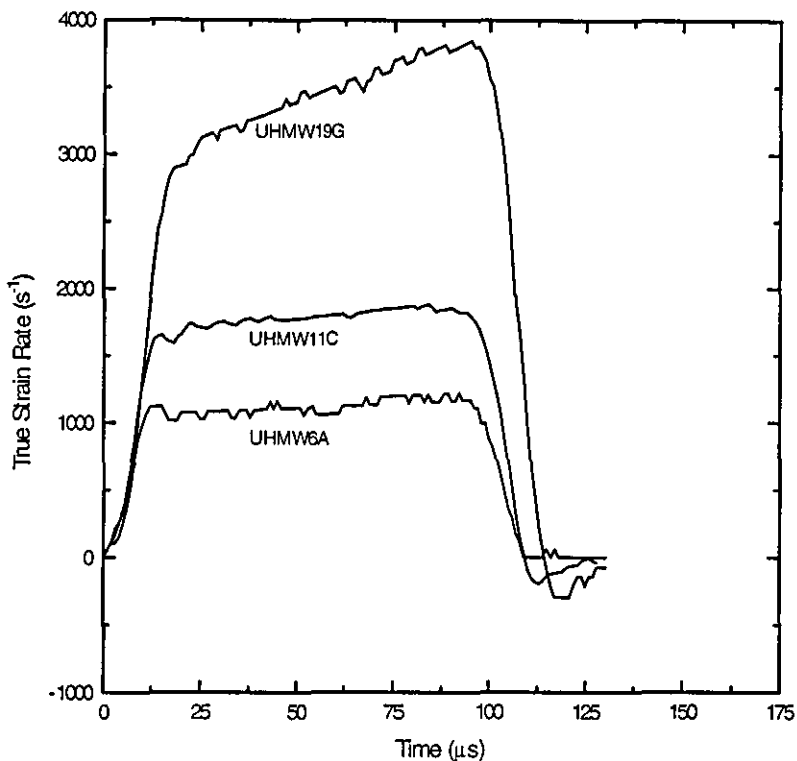


Figure (4.2.4) True strain rate profiles for UHMWPE tests at different impact speeds.

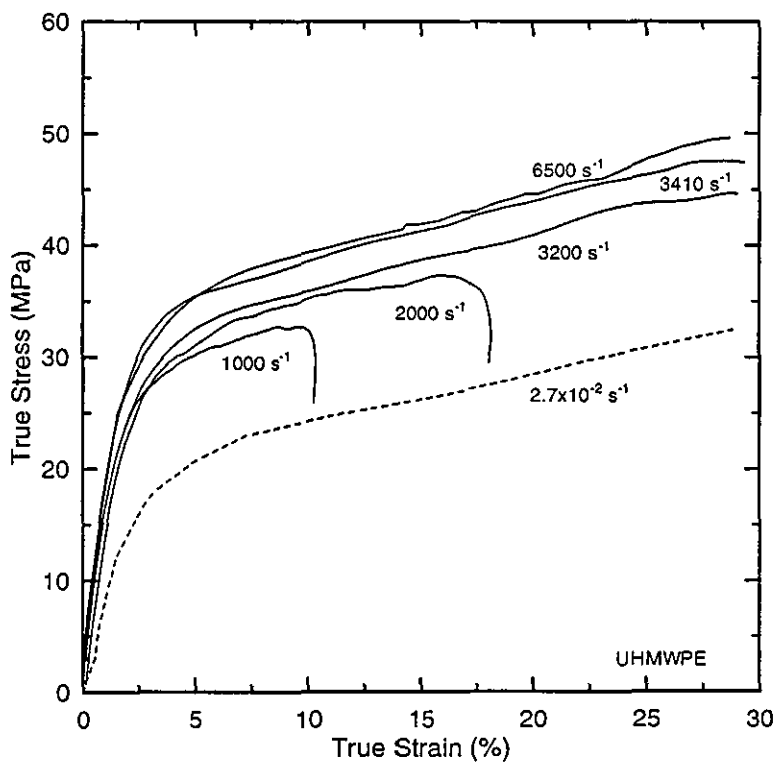


Figure (4.2.5) Stress-strain curves for UHMWPE tested at different strain rates.

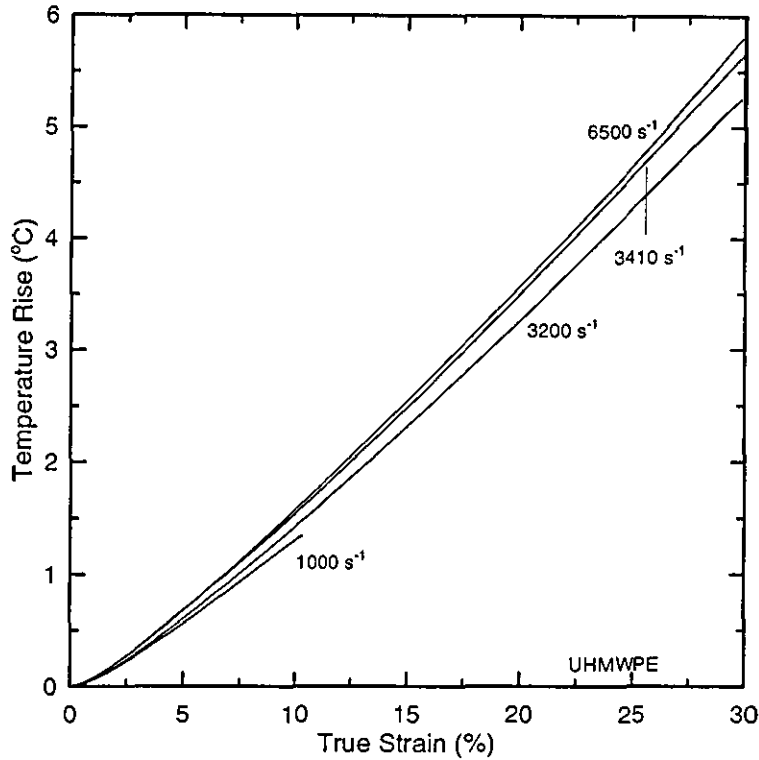


Figure (4.2.6) Curves of temperature rise for UHMWPE at different strain rates.

**Table (4.2) UHMWPE results.**

(T 18 cm Tufnol, S 30 cm steel projectile is used)

Impact speed (m/s)	Sample dimensions		$\dot{\epsilon}_{\text{upto30\%}} \text{ (s}^{-1}\text{)}$	E (GPa)	$\sigma_{5\%}$ (MPa)	$\sigma_{10\%}$ (MPa)
	L(mm)	D(mm)				
22.0 T	4.151	7.918	777	1.80	27.00	30.00
6.3	4.828	9.649	1120	1.91	30.15	32.20
6.4	4.869	9.905	1200	1.90	30.30	32.36
12.3	4.990	10.034	1722	1.78	34.60	39.20
11.1	4.931	9.450	1750	2.20	31.84	35.53
12.3	4.582	9.788	2200	1.75	33.30	37.70
19.3	4.960	9.996	3040	2.20	34.50	37.40
18.2	4.900	8.800	3252	2.18	33.42	36.30
17.9	4.930	9.600	3300	1.90	32.60	36.30
19.8	4.920	9.660	3400	2.11	35.00	38.50
19.4	4.888	9.895	3411	2.12	35.80	38.20
20.0	4.995	10.110	3725	1.80	35.40	37.30
19.9	3.840	8.060	4371	2.13	36.67	39.70
27.0	3.915	7.730	6045	2.18	33.00	35.70
21.3 S	3.630	7.544	6113	2.25	33.70	37.00
27.0	3.976	8.142	6285	2.25	33.70	37.00
$\pm 0.5$	$\pm 0.015$	$\pm 0.020$	$\pm 50$	$\pm 0.2$	$\pm 1.5$	$\pm 1.3$

The temperature rise for the UHMWPE samples is similar to that for the HDPE as shown in Figures (4.1.9) and (4.2.6). Tables (4.1) and (4.2) show that the Young's modulus of UHMWPE is 2.18 GPa compared to that for HDPE of 1.93 GPa at the same strain rate of 3250 s<sup>-1</sup>, which is almost 13% higher than that of

HDPE. The flow stress of UHMWPE at 10% strain and  $3252 \text{ s}^{-1}$  strain rate is about 36 MPa, while for HDPE it is 32 MPa. Figure (4.2.7) shows the increase in the Young's modulus with increasing the strain rate for UHMWPE.

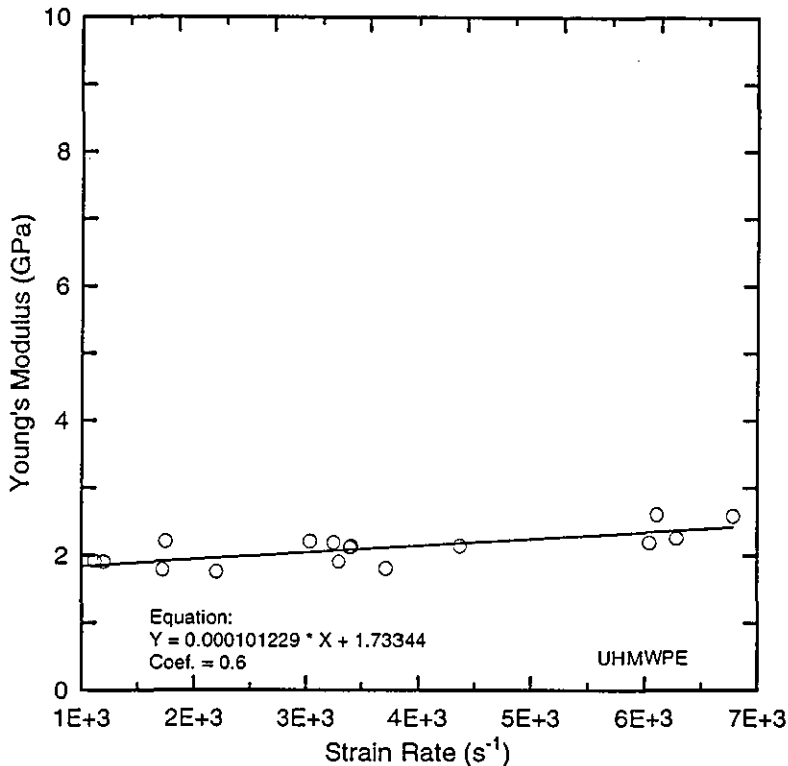


Figure (4.2.7) Young's modulus against strain rate for UHMWPE.

A 30 cm steel projectile has been used to provide a longer stress pulse (about  $120 \mu\text{s}$ ) and hence to give larger compressive strains in the sample. The reflected part of the loading pulse A travels back to the loading end of the incident bar and then reflects to act as a second loading pulse A'. This is shown in Figure (4.2.8), which also shows that the sample is fractured by the second loading pulse. Figure (4.2.9) shows the true stress, strain and temperature rise histories calculated from Figure (4.2.8). Calculating the first and second loading stress-strain curves shows that the UHMWPE sample is fractured at a strain level of 120% as indicated in Figure (4.2.10). The stress and strain values for the second loading are calculated by considering that the second pulse A' is the incident pulse, and that the pulse B' is the transmitted pulse as shown in Figure (4.2.8). The first transmitted pulse B travels toward far end of the transmitter bar, then partially reflects back toward the sample as a tensile pulse and helps to pull the bar away from the sample. The tail of the first transmitted pulse is extrapolated to meet the second transmitted pulse at where the baseline is obtained.

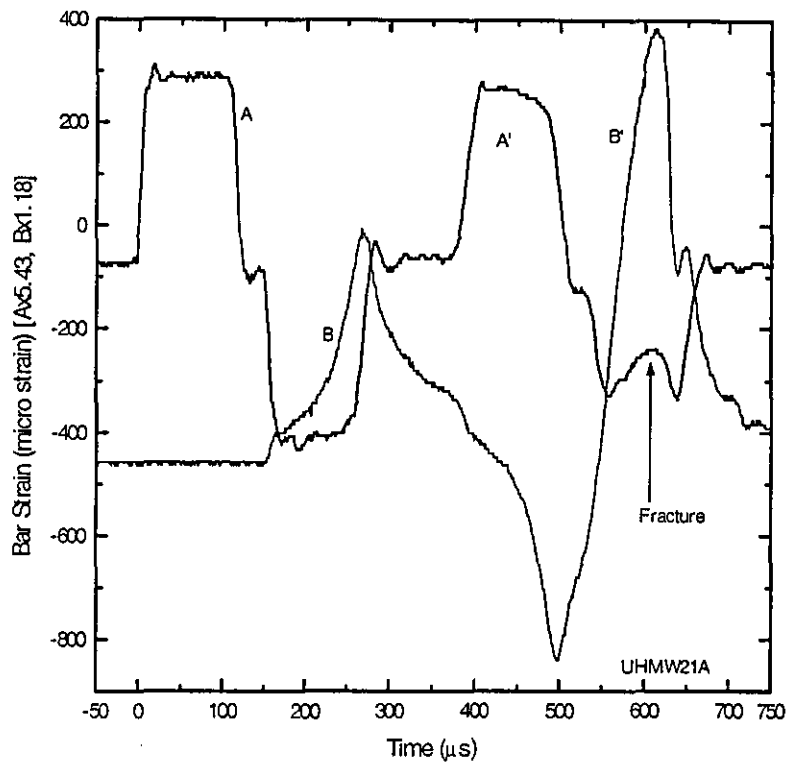


Figure (4.2.8) DSO record for UHMWPE sample using 30 cm long steel projectile.

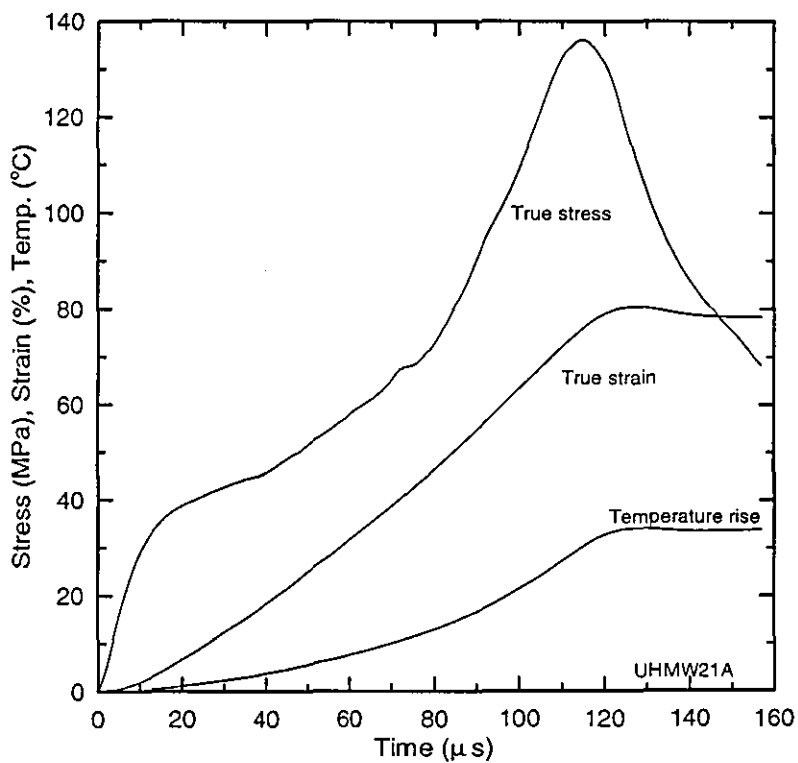


Figure (4.2.9) Stress, Strain and Temperature rise histories of the first loading of a UHMWPE sample using a 30 cm long projectile.

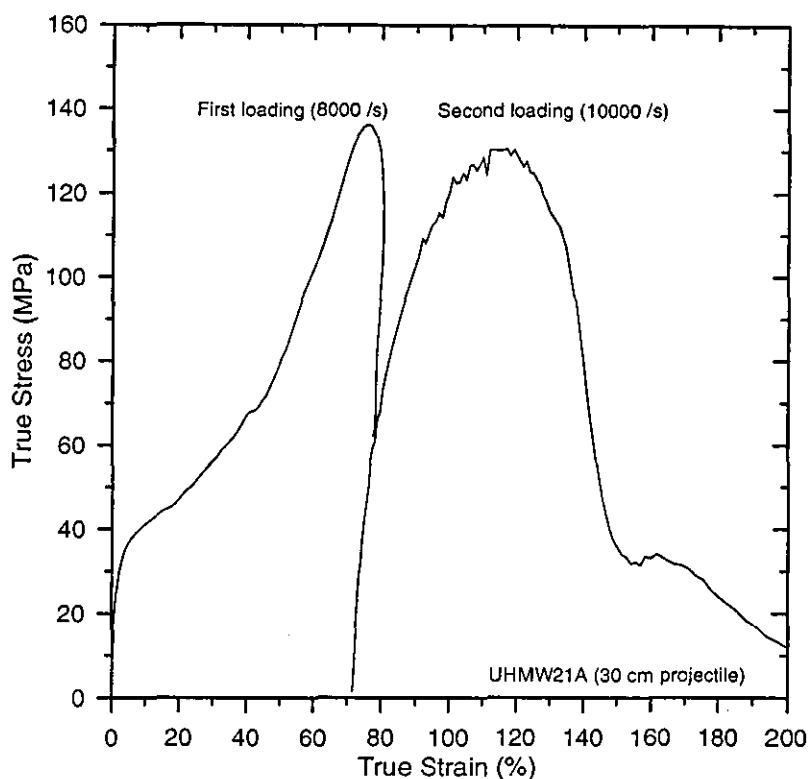


Figure (4.2.10) Stress-strain plot for the first and second loading.

In this experiment, the calculated bulk temperature rise up to fracture was 100°C. This level of temperature rise would cause some softening to the material and hence reduce the flow stress. However, the temperature rise up to 30% strain was small, and hence the softening was also small. The strain hardening is large, so the small thermal softening effect is not clear during the plastic deformation of soft polymers like UHMWPE.

### 4.3 Nylatron results

Nylatron GS (which is a modified nylon 66) has also been tested using the SHPB system. Figures (4.3.1a,b c, d and e) show typical SHPB records for nylatron samples tested at impact speeds of 5, 11, 17, 29, and 27 m/s. Plots of true stress, strain, and strain rate histories are shown in Figures (4.3.2), (4.3.3), and (4.3.4) respectively for various impact speeds. Some of the SHPB results for nylatron are shown in Table (4.3). The predicted temperature rise against strain curves for different strain rates are shown in Figure (4.3.6). The plot scaled up to strain of 30% and temperature of 20 °C.

To calibrate the program that calculates temperature rise in the sample during deformation, a K-type thermocouple was inserted in to the nylatron sample for a test at an impact speed of 20 m/s and strain rate of  $4313 \text{ s}^{-1}$ . The thermocouple recorded a temperature rise profile with a maximum temperature rise of  $38.1 \text{ }^\circ\text{C}$  compared with the computed value of  $38.8 \text{ }^\circ\text{C}$  at strain of 47%. The close agreement between these values validates the calculation of the temperature rise from the stress-strain curves for all the adiabatic tests.

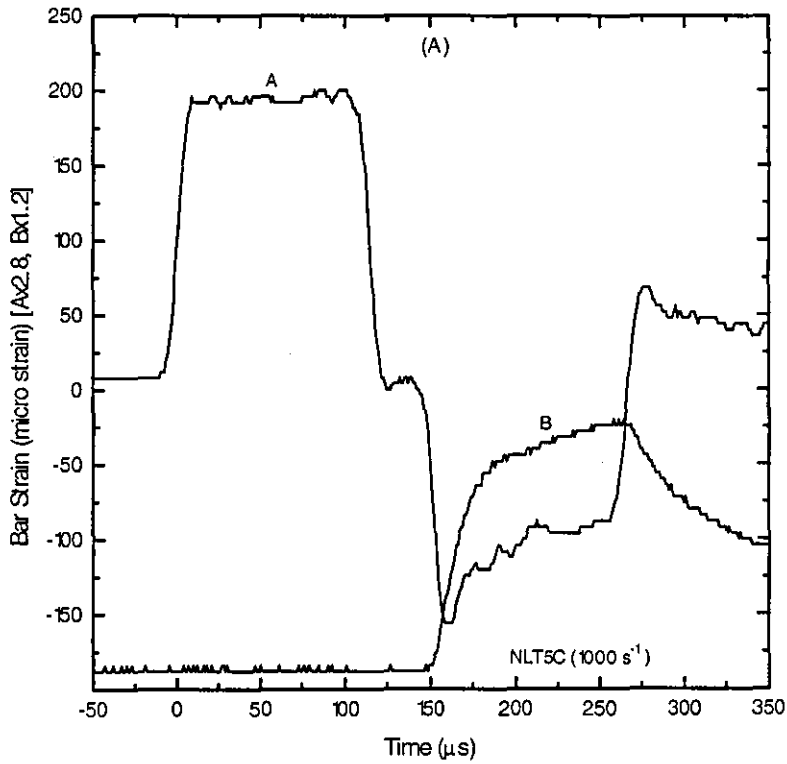


Figure (4.3.1a) DSO record for a nylatron sample at an impact speed of 5 m/s.



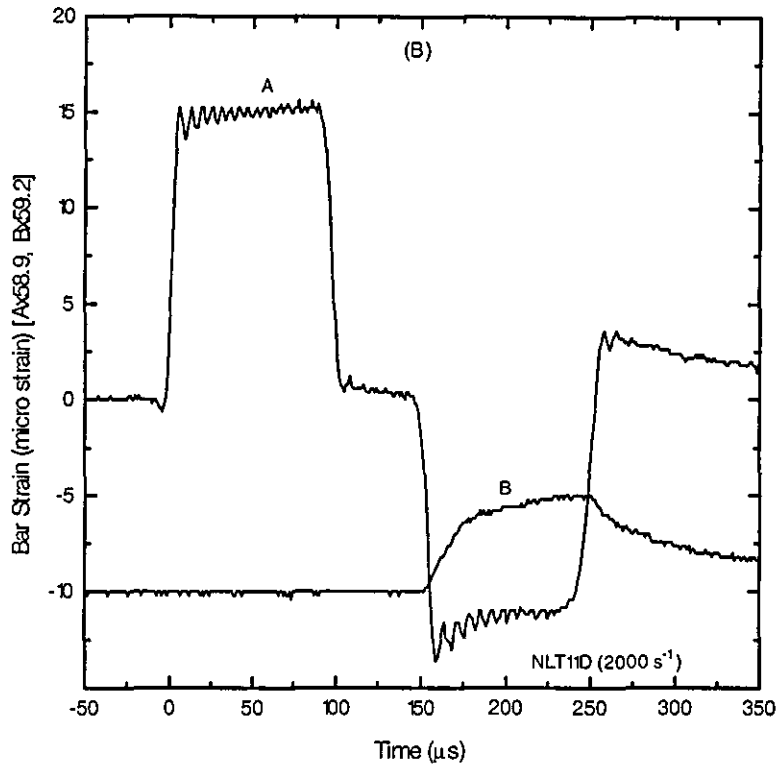


Figure (4.3.1b) DSO record for nylatron tested at an impact speed of 11 m/s.

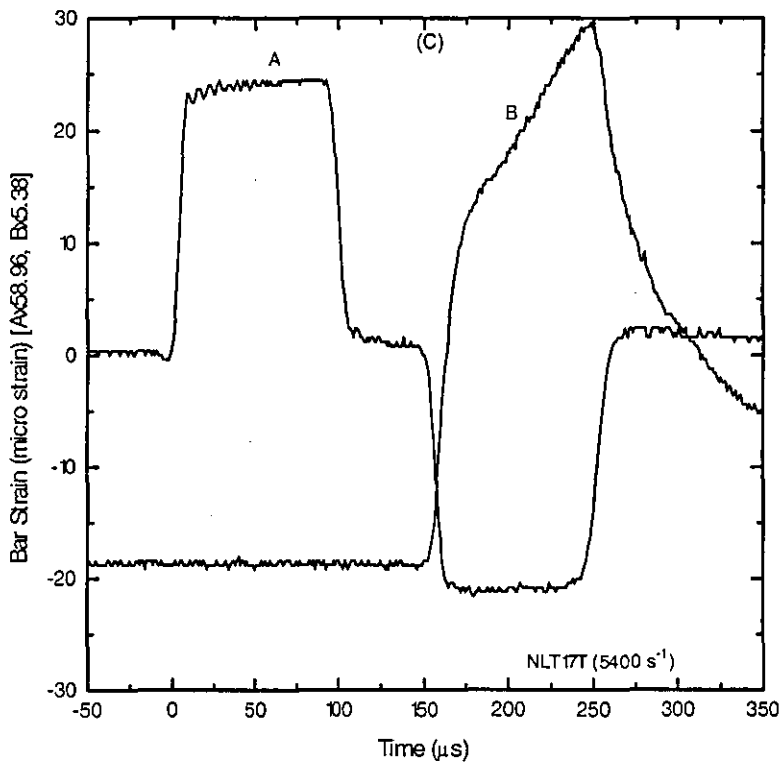


Figure (4.3.1c) DSO record for nylatron tested at an impact speed of 17 m/s.

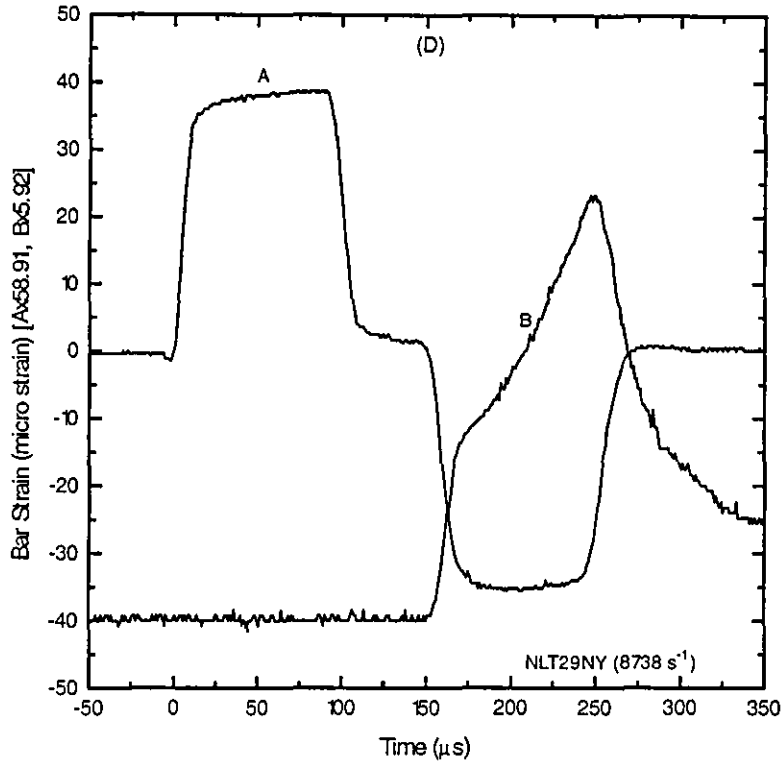


Figure (4.3.1d) DSO record for nylatron tested at an impact speed of 29 m/s.

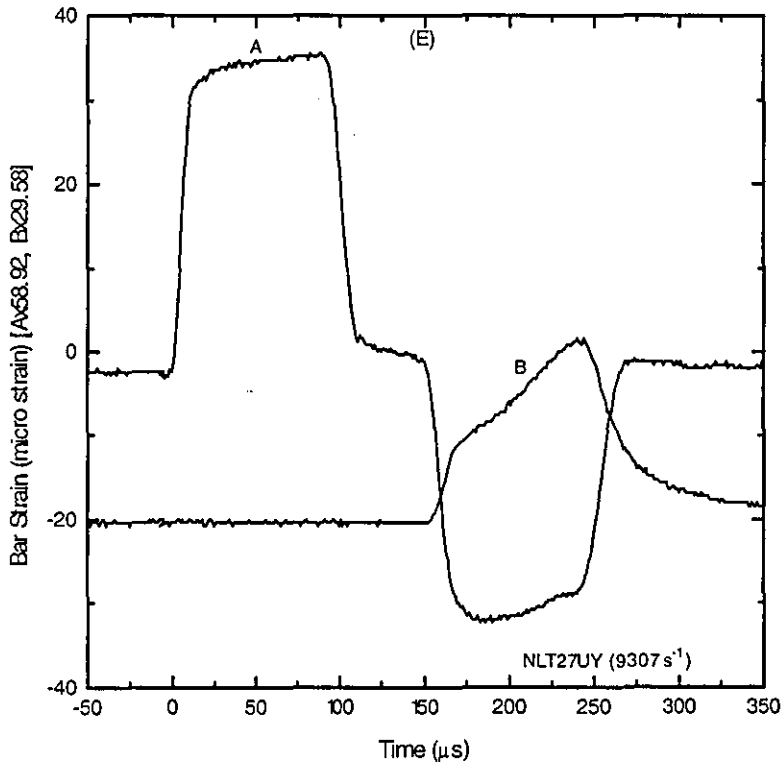


Figure (4.3.1e) DSO record for a nylatron tested at an impact speed of 27 m/s.

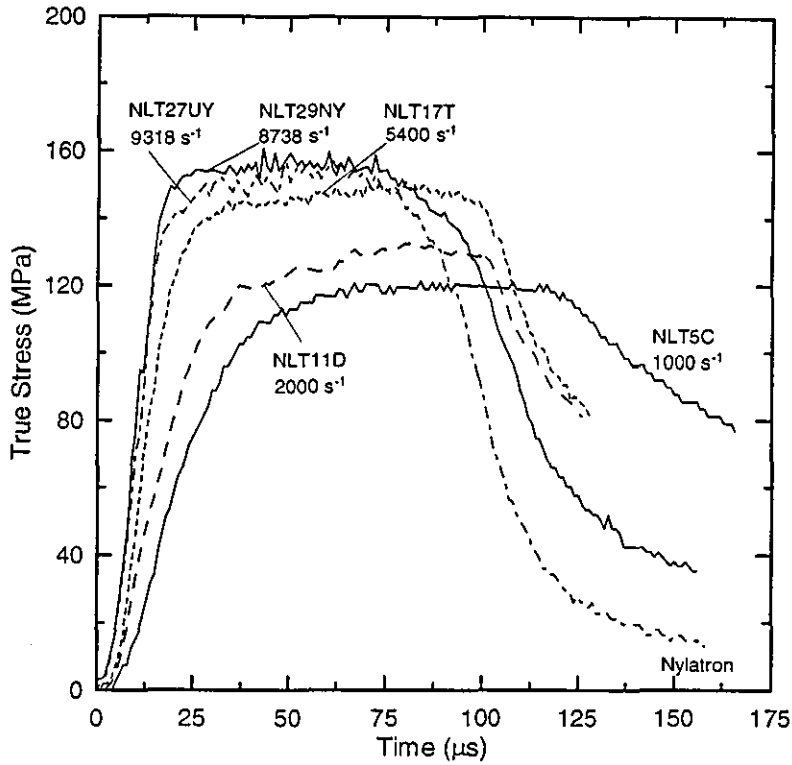


Figure (4.3.2) True stress histories for nylatron calculated from the records in Figure (4.3.1).

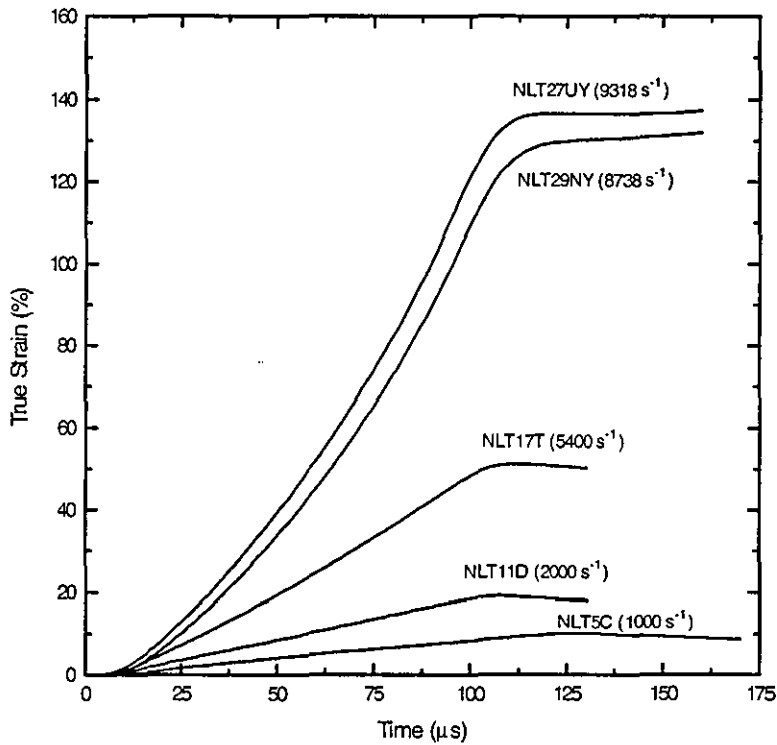


Figure (4.3.3) True strain histories for nylatron calculated from the signals in Figure (4.3.1).

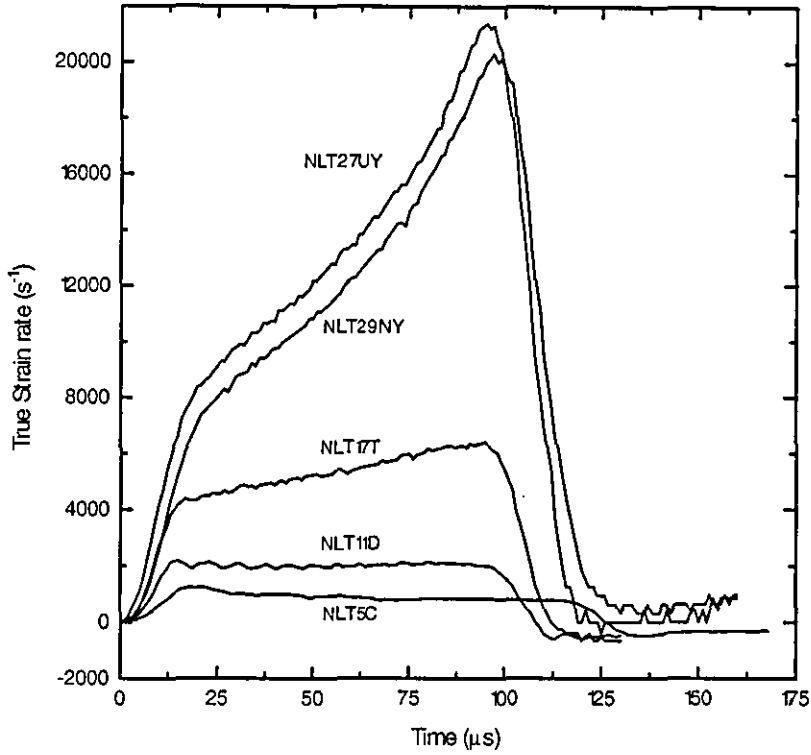


Figure (4.3.4) True strain rate profiles for the records shown in Figure (4.3.1).

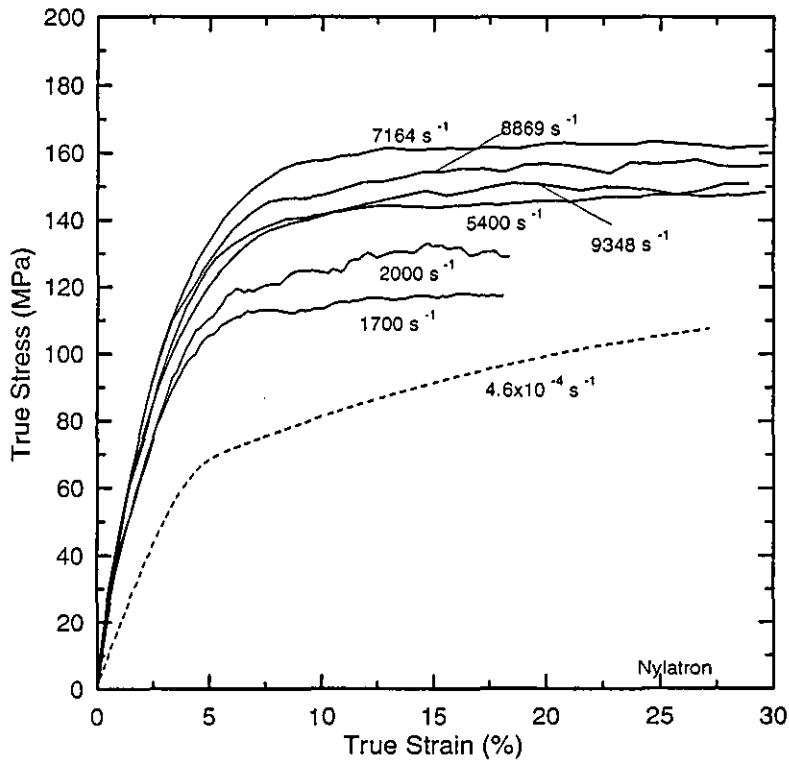


Figure (4.3.5) True stress-strain curves of nylatron tested at various strain rates.

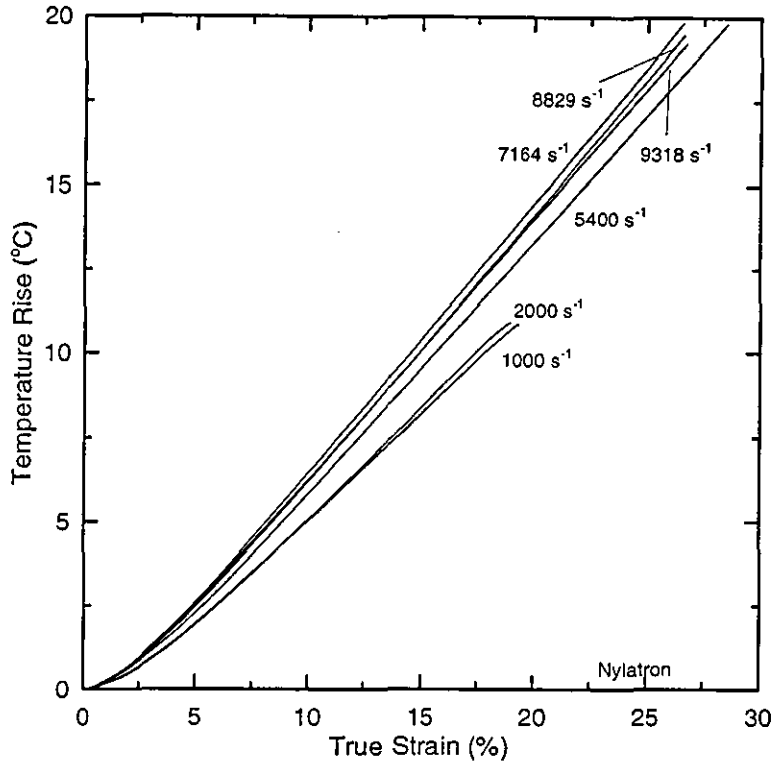


Figure (4.3.6) Temperature rise for nylatron tested at different strain rates.

**Table (4.3) Nylatron results.**  
(T Tufnol, S 30 cm Steel projectile)

V (m/s)	Dimension L(mm) D(mm)		$\dot{\epsilon}_{30\%}$ (s <sup>-1</sup> )	E (GPa)	$\sigma_{5\%}$ (MPa)	$\sigma_{10\%}$ (MPa)
5.0 T	3.952	7.922	150	3.18		
5.0 T	4.115	8.036	150	3.39		
11.0 T	4.072	8.171	231	3.25		
5.4	5.080	10.00	750	3.20	112.0	120.0
6.4 S	3.972	8.050	1000	4.09	115.0	117.7
11.1	4.996	9.920	1100	3.85	117.5	127.0
10.9	5.000	10.03	1250	3.04	112.0	128.7
11.0 S	3.928	8.020	1699	4.23	112.2	120.3
11.4 S	3.932	8.000	1700	4.68	113.4	117.6
10.8	3.934	8.050	2000	3.98	114.0	124.0
10.4	2.970	6.044	3203	4.23	121.0	144.0
19.3	3.992	8.010	3408	4.70	132.5	141.2
18.7 S	3.420	6.000	4183	4.00	121.8	146.4
19.1 S	3.199	6.224	4313	4.08	123.6	144.4
21.3	4.130	7.621	4800	4.30	128.0	146.2
16.5	3.031	6.070	5059	4.10	120.0	141.6
16.5	3.108	6.175	5400	4.65	121.0	142.0
28.4	3.649	8.244	6221	4.60	130.0	143.5
23.8 S	3.090	6.114	7210	4.29	127.6	159.0
29.2	3.166	5.963	8221	4.45	123.0	142.4
28.6	2.908	5.723	8738	4.10	129.0	152.1
24.7 S	2.406	6.006	8920	4.40	127.5	147.0
27.5	2.312	7.960	9318	4.67	128.0	145.7
±0.5	±0.015	±0.020	±50	±0.2	±1.5	±1.3

Figure (4.3.5) shows stress-strain curves at various strain rates. As for HDPE and UHMWPE materials, the flow stress for nylatron increases with strain rate. However, at the highest strain rates the flow stress for nylatron unexpectedly drops with increasing strain rate. Figure (4.3.6) shows the calculated temperature rise against true strain for nylatron samples tested at different strain rates. The Young's modulus increases with the increase of strain rate as shown in Figure (4.3.7).

Nylatron has been tested to high strain levels using a 30 cm long projectile to give the required longer loading pulse at impact speed of 24.7 m/s. A typical analysis of this test gives stress, strain and temperature rise against time curves as shown in Figure (4.3.8). In this test, the strain level reaches about 120%, and the maximum temperature rise is approximately 80°C which is high enough to soften the sample. This also takes the nylatron beyond its glass transition temperature of about 50°C.

Nylatron is a stronger polymer than HDPE and UHMWPE. At a strain rate of 3400 s<sup>-1</sup>, nylatron has a Young's modulus of about 4.7 GPa, and a flow stress at 10% strain of about 141 MPa compared to 2.1 GPa and 38 MPa respectively for UHMWPE.

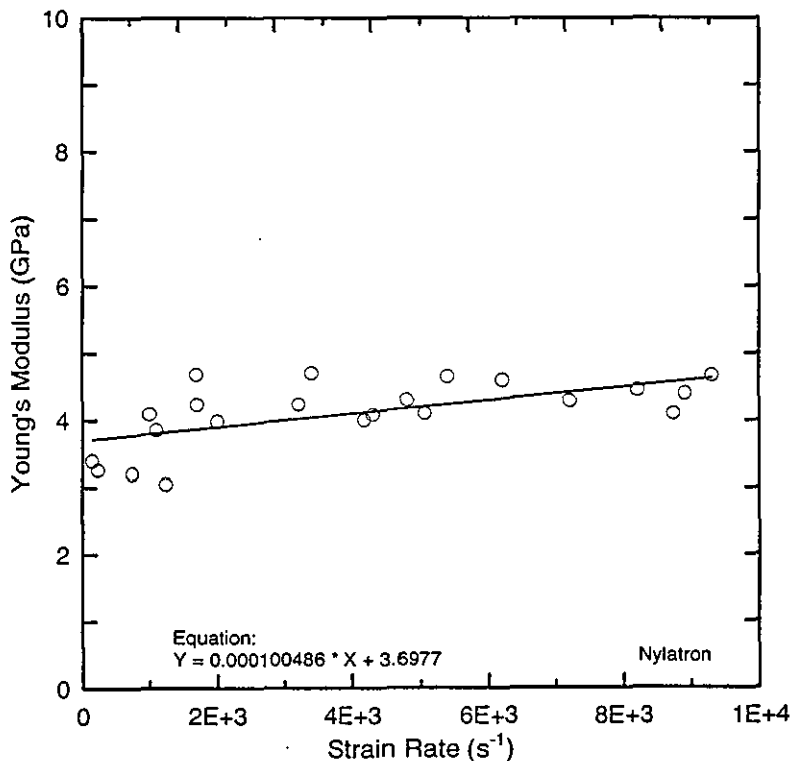


Figure (4.3.7) Plot of Young's modulus variation with strain rate.

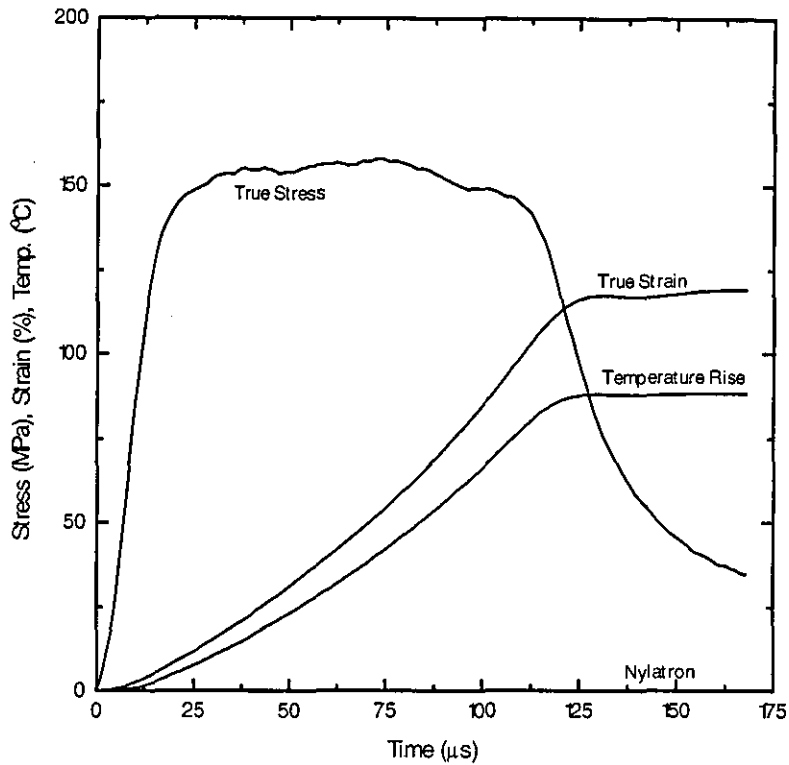


Figure (4.3.8) True stress, strain and temperature rise histories of a nylatron sample tested by the SHPB at  $\dot{\epsilon}_{30\%} = 8920\text{s}^{-1}$  and  $\bar{\dot{\epsilon}}_{\text{max}} = 13000\text{s}^{-1}$ .

#### 4.4 PEEK results

SHPB compressive tests have been performed on samples made of Victrex PEEK of grade 150G, supplied by ICI. Figures (4.4.1 a, b, c, d and e) show the SHPB records for PEEK samples tested at impact speeds of 6, 15, 15, 26 and 37 m/s. The true stress, strain and strain rates histories are also shown in Figures (4.4.2), (4.4.3), and (4.4.4) respectively. Beside the normal 25 cm long steel projectile, a 12 cm long steel projectile is used as well as a 15 cm long aluminium projectile to obtain loading pulses with different durations and amplitudes. By using some of the stress - strain curves shown in Figure (4.4.5), the calculated temperature rise generated within the plastically deformed samples has been plotted against true strain in Figure (4.4.6).

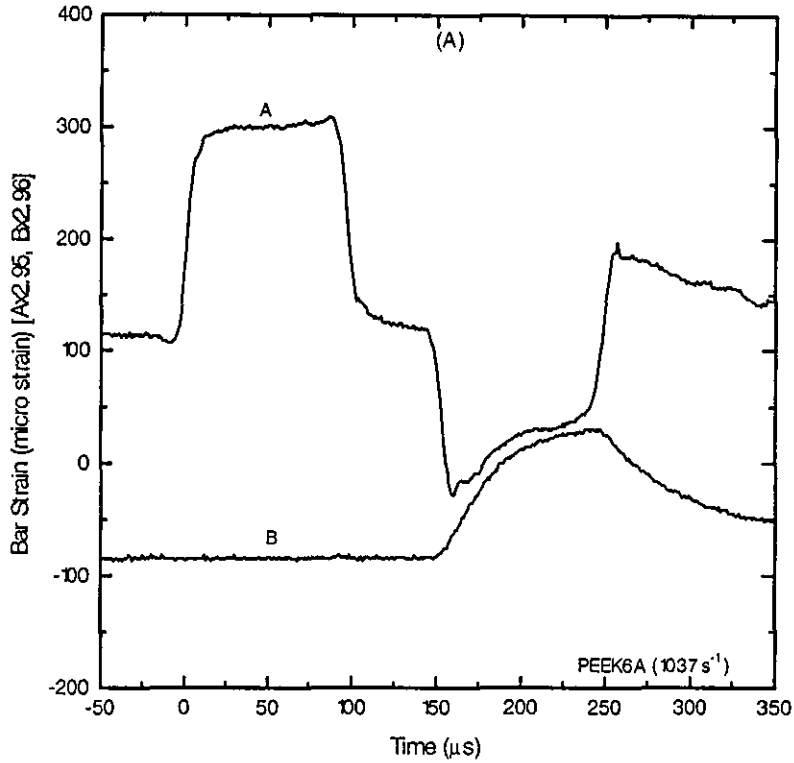


Figure (4.4.1a) DSO record for PEEK tested at an impact speed of 6 m/s.

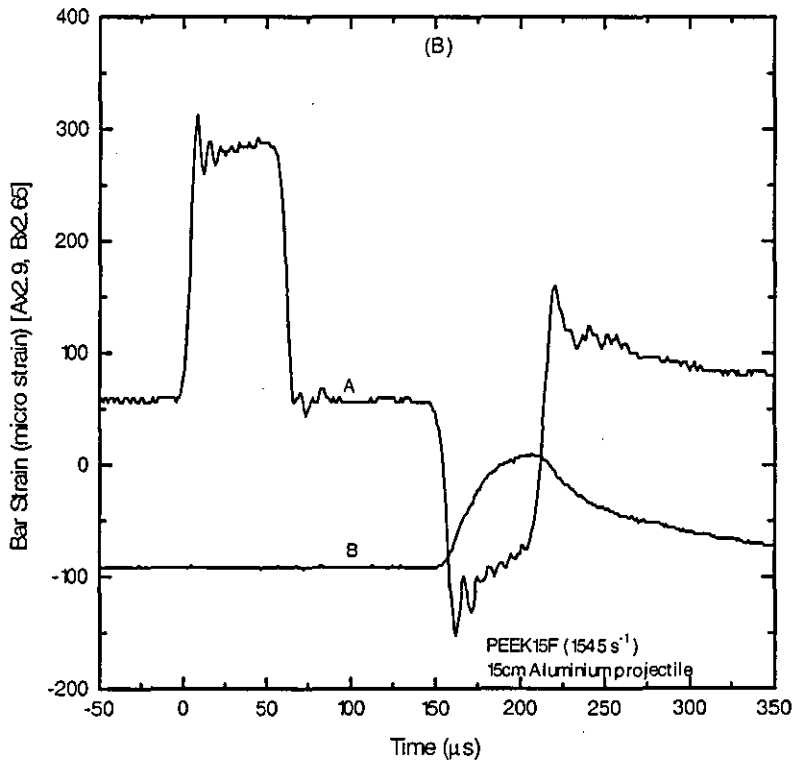


Figure (4.4.1b) DSO record for PEEK tested at an impact speed of 15 m/s using a 15 cm aluminium projectile.



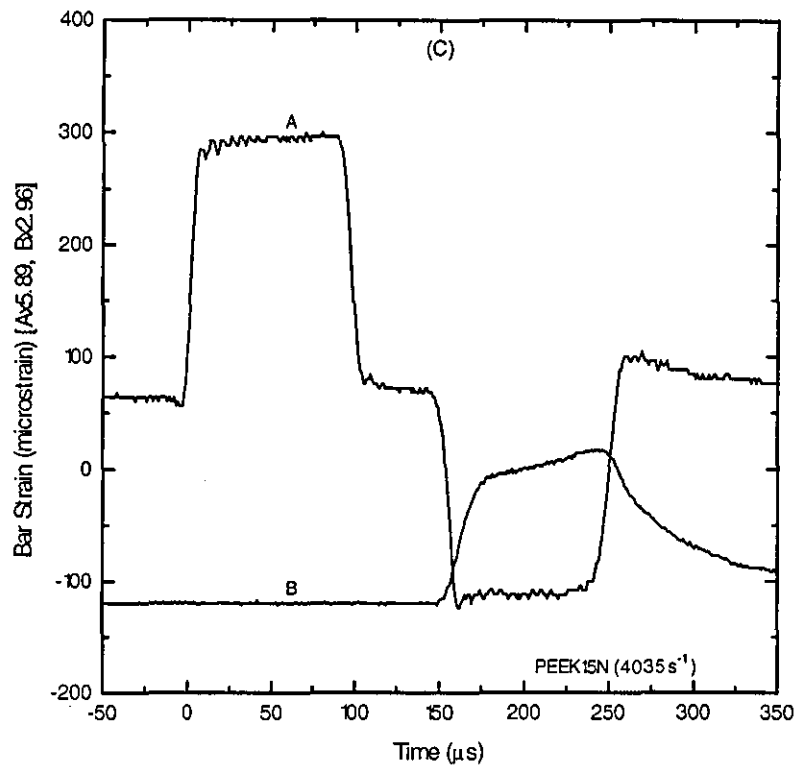


Figure (4.4.1c) DSO record for PEEK tested at an impact speed of 15 m/s.

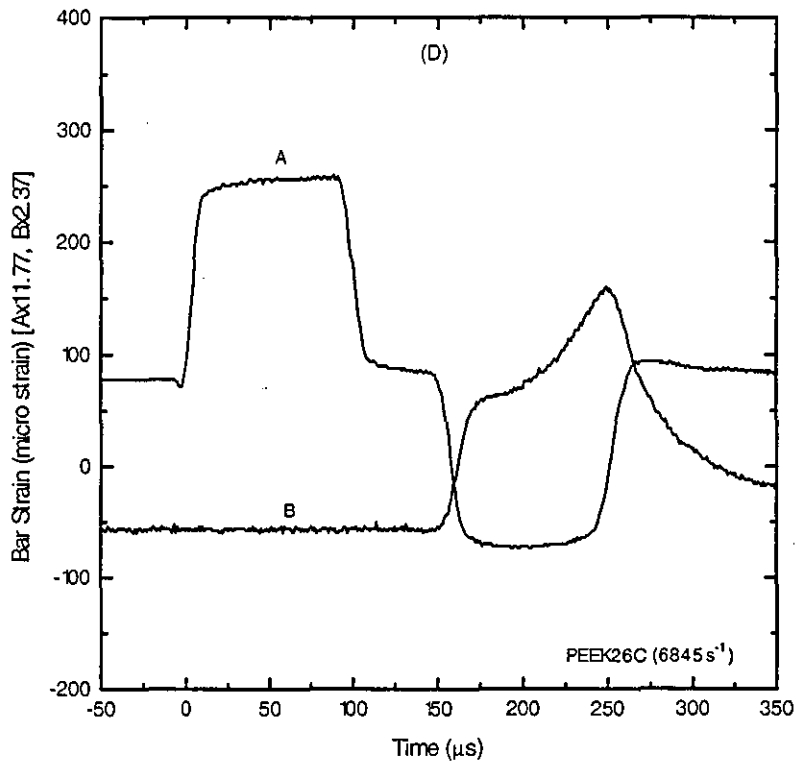


Figure (4.4.1d) DSO record for PEEK tested at an impact speed of 26 m/s.

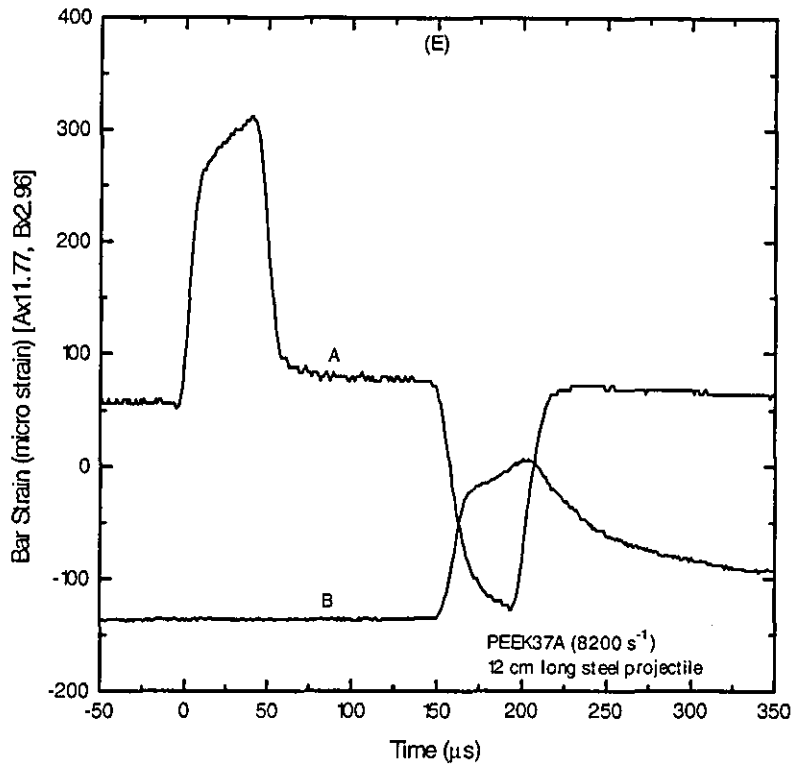


Figure (4.4.1e) DSO record for PEEK tested at an impact speed of 37 m/s.

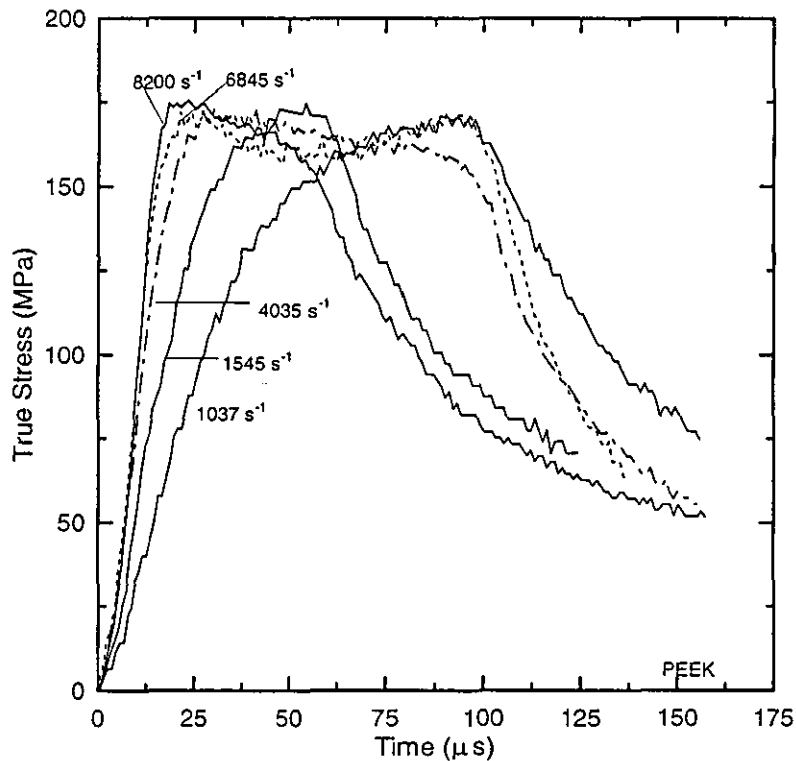


Figure (4.4.2) True stress histories for PEEK tested at different strain rates.

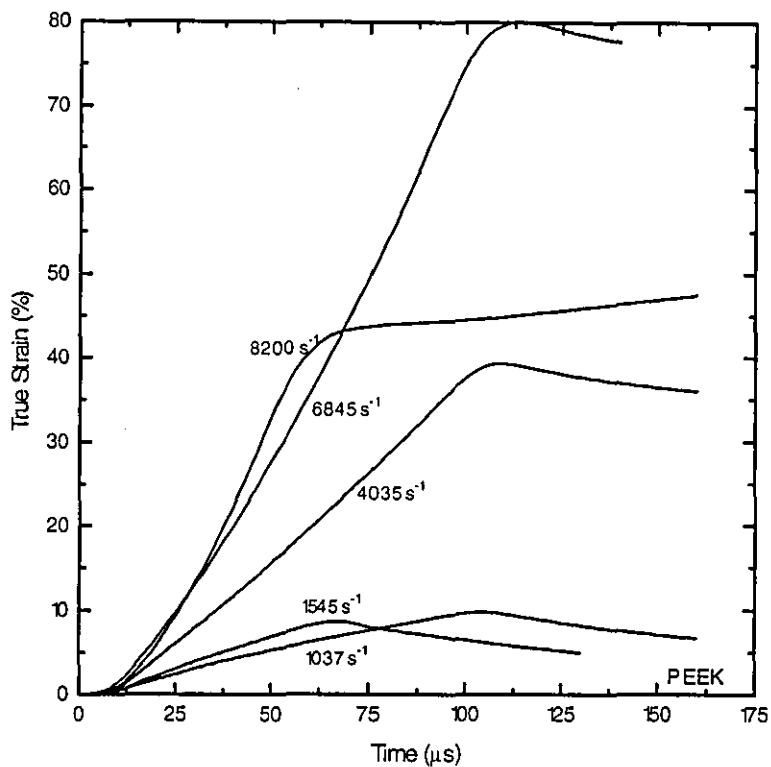


Figure (4.4.3) True strain histories for PEEK tested at different strain rates.

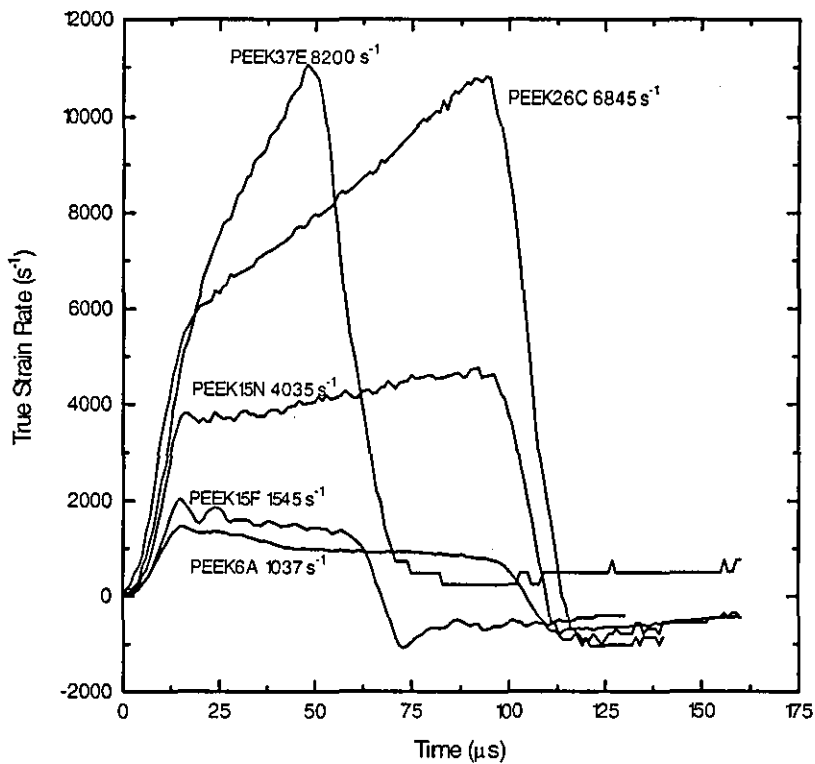


Figure (4.4.4) True strain rate profiles for PEEK tested at different impact speeds.

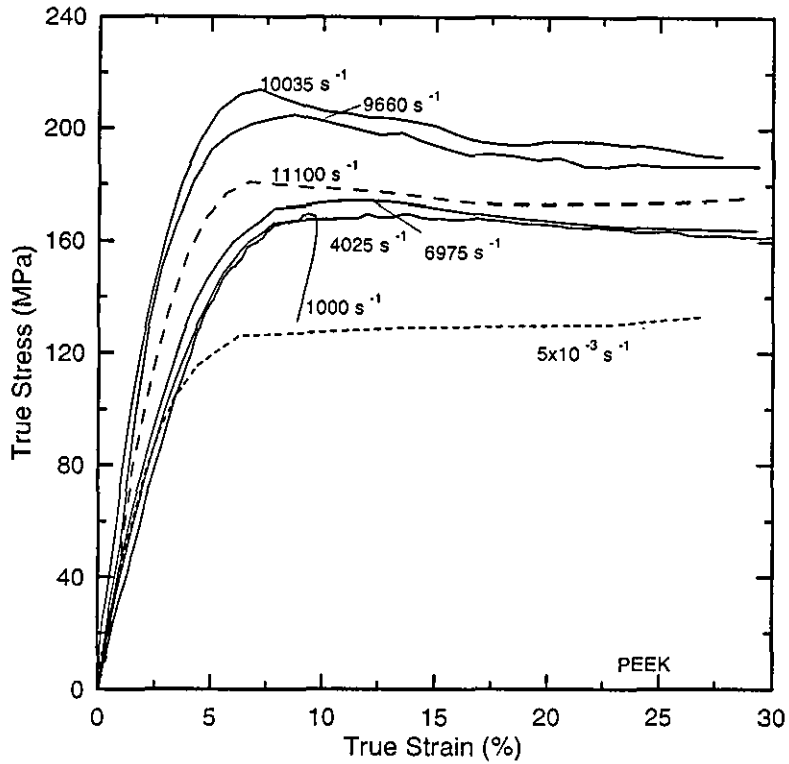


Figure (4.4.5) Stress-strain curves for PEEK 150 g tested at various strain rates.

**Table (4.4) SHPB results for PEEK**  
(A 15 cm aluminium projectile, s 12 cm steel projectile)

V (m/s)	Dimension L(mm) D(mm)		$\dot{\epsilon}_{\text{upto } 30\%}$ ( $\text{s}^{-1}$ )	E (GPa)	$\sigma_{5\%}$ (MPa)	$\sigma_{10\%}$ (MPa)
8.3	3.184	6.892	1000	3.30	138.0	-
6.0	3.189	7.863	1037	3.32	137.6	169 est.
15.3 A	3.167	6.822	1545	4.03	154.0	165.0
9.8	3.180	6.990	1919	3.86	138.3	164.6
9.8	3.180	6.992	1986	3.70	141.0	169.0
15.0	3.202	7.821	4035	4.19	137.0	170.1
17.6	3.168	6.964	4312	4.58	147.0	180.1
17.8	3.170	6.975	4330	4.61	144.2	174.2
18.5	3.176	6.839	4726	4.28	135.0	164.5
21.7	3.192	7.822	6552	4.34	147.8	171.9
26.5	3.178	6.972	6845	4.39	142.5	168.7
27.2	3.166	6.982	6928	4.57	149.4	174.0
24.0	3.136	7.845	6931	4.65	146.1	166.7
25.0	3.182	7.868	6952	4.27	148.8	169.6
25.0	3.168	7.863	7148	4.43	145.2	166.8
24.7	3.193	7.862	7266	4.76	151.5	172.0
37.1 s	3.141	7.843	7866	5.14	153.0	166.3
37.1 s	3.089	7.833	8200	5.60	162.7	174.5
28.5	3.186	7.767	9960	5.80	192.2	202.0
28.0	3.214	6.056	10035	5.90	190.0	206.0
29.2	3.220	6.053	10761	5.40	173.2	201.1
33.1	3.175	6.850	10294	5.85	185.0	190.0
32.4	3.242	6.071	11100	5.00	162.5	176.6
$\pm 0.5$	$\pm 0.015$	$\pm 0.020$	$\pm 50$	$\pm 0.2$	$\pm 1.5$	$\pm 1.3$

Testing PEEK at various strain rates using the SHPB system gives the elastic moduli and flow stresses shown in Table (4.4). The PEEK is stronger than the previous three materials, and has a well defined yield point. From Figure (4.4.5) the yield point of PEEK is higher and more defined than for nylatron. The flow stress at a strain of 10% for PEEK is 170 MPa at a strain rate of  $4 \times 10^3 \text{ s}^{-1}$ , while for nylatron at the same strain rate it is 145 MPa. As with nylatron, a similar anomalous high strain rate behaviour occurs for PEEK as shown in Figure (4.4.5). The flow stress increases with strain rate up to a strain rate of about  $10,000 \text{ s}^{-1}$ , above which a drop in the flow stress occurs.

From the stress-strain curves, the temperature rise in the PEEK samples has been computed, as shown in Figure (4.4.6). Figure (4.4.7) shows increases in the elastic modulus with increasing of strain rate.

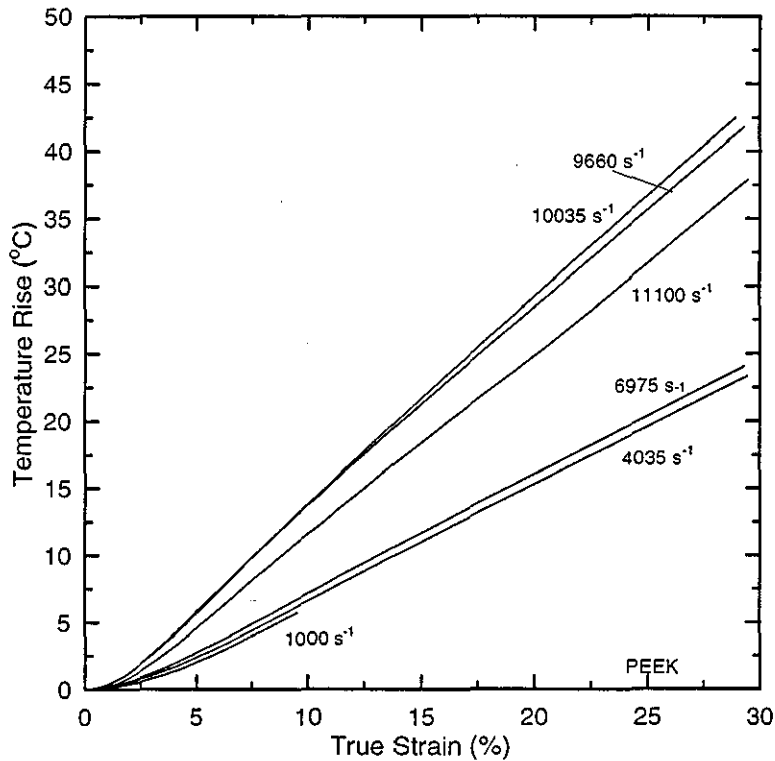


Figure (4.4.6) Calculated temperature rise-strain curves for PEEK at different strain rates.

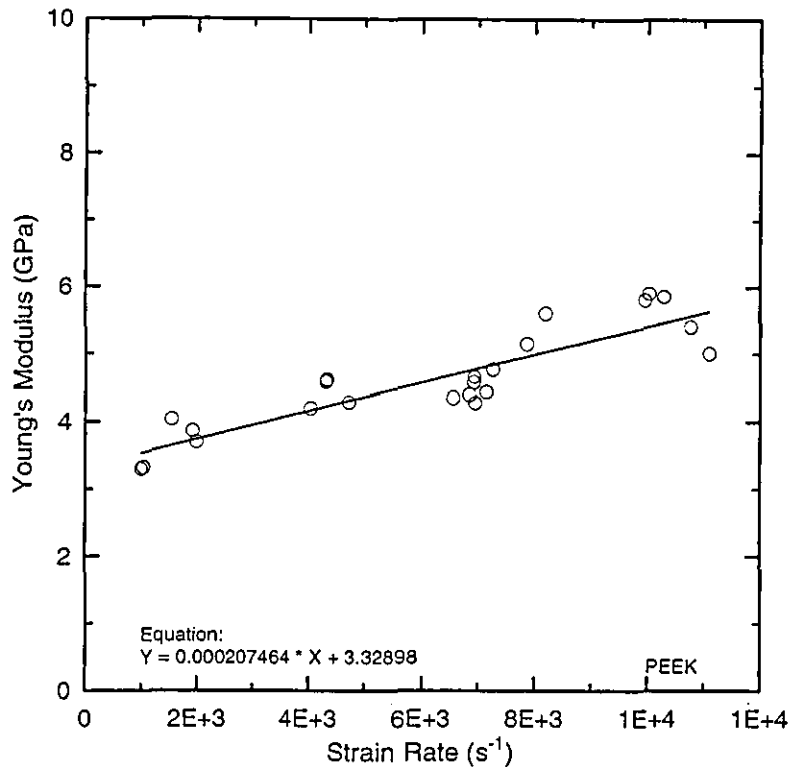


Figure (4.4.7) Variation of Young's modulus with strain rate for PEEK.

#### 4.5 Conclusions

The split Hopkinson pressure bar (SHPB) system has been used to study four engineering polymers (HDPE, UHMWPE, nylatron, and PEEK). HDPE and UHMWPE show almost the same behaviour except that the HDPE is slightly softer than UHMWPE and has a lower Young's modulus.

The nylatron material (modified nylon 66) has a more pronounced yield transition between the elastic and plastic parts of its stress-strain curves and is a stronger material than HDPE and UHMWPE. In the SHPB compressive tests the samples do not fracture except for the very high strain rates performed with UHMWPE. This is due to the thermal softening because of the high temperature rise within the sample during the test. However, nylatron fractures in tensile tests as described elsewhere in this thesis.

PEEK is stronger than nylatron and has higher upper yield points. All the polymers studied show an increase in flow stress with increasing strain rate. However, for nylatron and PEEK at very high levels of strain rate the flow stress starts to drop. This behaviour has also been noticed by other researchers (such as Walley et al (1991)) for PEEK and nylon. A satisfactory explanation for this transition to negative strain rate sensitivity has not yet been put forward. One

possibility is that the very high strain rates causes an increase in brittleness which could result in localised high stresses due to micro-fractures. It is known that there are very high temperatures ( e.g. 530 °C for PMMA, and 700 °C for PC (Swallowe et al (1984, 1986))) associated with these fractures which could therefore cause softening and rapid decrease in the flow stress.

As it will be seen in Chapter 6, the system reaches 90% of its equilibrium value at time between 4 and 6  $\mu$ s after the starting point of the loading pulse for all materials tested. This may cause inaccuracy in measuring the Young's modulus, which is measured at the initial part of the stress-strain curves. Theoretically, these inaccuracies are estimated add an error of around 1% compared to the error if equilibrium was fully achieved. However, the experimental values agreed to within about 3% of the values obtained by other researchers such as Ahmad (1988) who used the wave propagation method in his calculations. Also all the experimental results quoted (except for very high strain rates) are from stress-strain curves where the elastic region lasts much longer than the time required to achieve the full equilibrium.

## **CHAPTER 5**

### **THE VISCOELASTIC BEHAVIOUR OF POLYMERS**

#### **5.1 Introduction**

A material is said to be viscoelastic if it exhibits some of the deformation characteristics of viscous materials and elastic materials (Peapell (1985)).

Polymers are viscoelastic materials due to the time dependence in their stress-strain relationship. This behaviour makes the polymers more complicated to study. The phenomenon of viscoelasticity depends on several parameters, particularly stress ( $\sigma$ ), strain ( $\epsilon$ ), temperature (T) and time (t), and hence can be described by the relation:

$$f(\sigma, \epsilon, T, t) = 0 \qquad 5.1$$

Generally, viscoelastic behaviour is extremely complicated and only in the case of relatively simple problems can the response be predicted accurately by existing theories (Ahmad (1988)). Few theories have been put forward to predict the viscoelastic behaviour of materials, such as the Boltzman superposition principle, which could be called the integral representation of linear viscoelasticity because it defines an integral equation. Linear differential equations for solving specific problems in the deformation of viscoelastic solids have also been used (Lee (1960)).

#### **5.1.1 Basic elements**

Two simple models have been proposed which, if they are applied in the right way, enable the characteristics of real materials to be simulated. These are: the Kelvin-Voigt solid and the Maxwell solid. The basic elements of these models are:

a) A Hookean solid. The stress-strain relationship is that for a spring for which stress  $\sigma$  is linearly related to strain  $\epsilon$  (Benham and Warnock (1979)):

$$\sigma = E\epsilon \qquad (5.2)$$

where E is Young's modulus.



b) A Newtonian liquid. Stress is proportional to strain rate  $\dot{\epsilon}$  and the constant of proportionality is  $\eta$  the viscosity coefficient of the liquid. This model is represented by a dashpot in which a piston is moved through the Newtonian fluid. The formula for this model is :

$$\sigma = \eta \dot{\epsilon} \quad (5.3)$$

### 5.1.2 Kelvin-Voigt solid

This model is a simple combination in parallel of the elements mentioned above, as in Figure (5.1).

Relating the stress  $\sigma_1$  and the strain  $\epsilon_1$  in the spring,

$$\sigma_1 = E_v \epsilon_1 \quad (5.4)$$

Relating the stress  $\sigma_2$  and the strain  $\epsilon_2$  in the dashpot,

$$\sigma_2 = \eta_v \dot{\epsilon}_2 \quad (5.5)$$

The total strain applied on the two elements is the same as the strain on each one, while the total stress is distributed between the two elements.

$$\epsilon = \epsilon_1 = \epsilon_2 \quad (5.6)$$

$$\sigma = \sigma_1 + \sigma_2 \quad (5.7)$$

The general Kelvin solid stress-strain relationship is then represented by

$$\sigma = E_v \epsilon + \eta_v \dot{\epsilon} \quad (5.8)$$

The difference between this type of solid and a purely elastic solid is the time dependence. With three interrelated quantities, stress, strain, and time, if one conducted a simple compression test on a viscoelastic material, the resulting stress-strain curve would vary in shape and position depending on the strain rate.

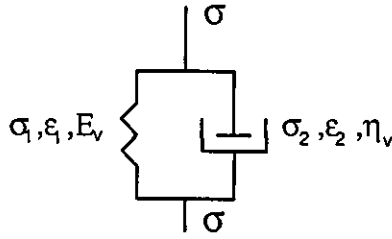


Figure (5.1) Kelvin-Voigt model.

Consider the model for two test conditions.

a) At a constant strain rate of  $\dot{\epsilon} = R$ .

From equation (5.8) by substituting  $R$ , we will get

$$\sigma = E_v \epsilon + \eta_v R \quad (5.9)$$

This equation has a linear curve with slope  $E_v$  and intercept with the stress axis of  $\eta_v R$  as shown in Figure (5.2a).

b) at constant stress rate  $\dot{\sigma} = K$  and  $\sigma = K t$ , Equation (5.8) can be written as

$$\sigma - E_v \epsilon = \eta_v \frac{d\epsilon}{dt}$$

or  $-\frac{E_v}{\eta_v} \frac{dt}{dt} = \frac{d(-E_v \epsilon)}{\sigma - E_v \epsilon}$ , which is the differential equation of

$$\frac{-E_v}{\eta_v} t = \ln(\sigma - E_v \epsilon)$$

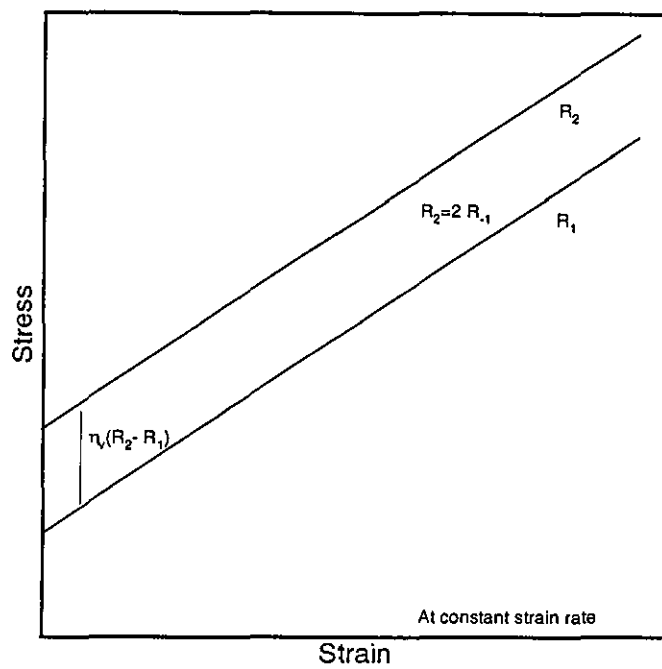
This equation gives an exponential form

$$\epsilon = \frac{\sigma_0}{E_v} \left( 1 - \exp\left(-\frac{E_v \sigma}{\eta_v K}\right) \right) \quad (5.10)$$

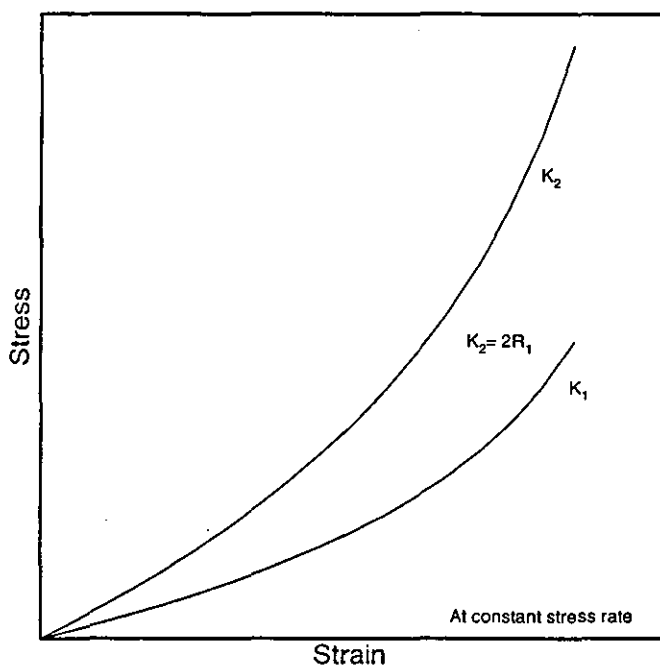
or  $\sigma = \frac{\eta_v K}{E_v} \ln\left(\frac{\sigma_0}{\sigma_0 - E_v \epsilon}\right)$

where  $\sigma_0$  is the stress at  $t=0$  (beginning of creep).

The stress-strain curves for Equations (5.9) and (5.10) at two strain-rates,  $R_1$  and  $R_2$  ( $R_2 > R_1$ ), and two stress-rates,  $K_1$  and  $K_2$  ( $K_2 > K_1$ ) under these conditions are shown in Figures (5.2a, b).



(a) at a constant strain rate



(b) at a constant stress rate

Figure (5.2) Kelvin-Voigt solid behaviour.

The Kelvin solid model (Findley et al (1976)) does not show a time dependant relaxation as in Equation (5.8) for stress relaxation where  $\dot{\epsilon} = 0$  (constant strain), and the material behaves as an elastic solid.

If  $\varepsilon$  is kept constant and hence  $\dot{\varepsilon} = 0$ , the Kelvin model (Equation (5.8)) gives  $\sigma = E_v \varepsilon$ , i.e. a constant stress.

On the other hand, the Kelvin model does show creep behaviour to a first approximation. For creep under constant stress  $\sigma = \sigma_0$ , Equation (5.8) give

$$\varepsilon = \frac{\sigma_0}{E_v} (1 - \exp\frac{-E_v}{\eta_v} t) , \text{ where } \sigma = \sigma_0, \text{ and } \dot{\varepsilon} = 0 \text{ at } t=0.$$

The recovery response, where  $\sigma = 0$ , which gives

$$E_v \varepsilon + \eta_v \dot{\varepsilon} = 0$$

This equation gives a solution for strain as

$$\varepsilon = \varepsilon_0 \exp\frac{-t}{\tau'}$$

where  $\tau' = \eta_v / E_v$  is the time constant called as the retardation time.

### 5.1.3 Maxwell solid

This consists simply of a spring in series with a dashpot as shown in Figure (5.3).

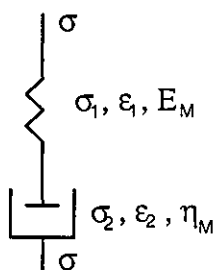


Figure (5.3) Maxwell model.

The equations for the stress-strain relations are

$$\sigma_1 = E_M \varepsilon_1 \tag{5.11}$$

$$\sigma_2 = \eta_M \dot{\varepsilon}_2 \tag{5.12}$$

which relates the stress  $\sigma_1$  and the strain  $\varepsilon_1$  in the spring and the stress  $\sigma_2$  and strain  $\varepsilon_2$  in the dashpot.

$$\text{The total stress } \sigma = \sigma_1 = \sigma_2 \tag{5.13}$$

$$\text{and the total strain } \varepsilon = \varepsilon_1 + \varepsilon_2 \tag{5.14}$$

The stress in the dashpot is linearly related to strain rate; therefore the total strain equation must be differentiated with respect to time to give:

$$\begin{aligned} \dot{\varepsilon} &= \dot{\varepsilon}_1 + \dot{\varepsilon}_2 \\ \text{or} \quad \dot{\varepsilon} &= \frac{\dot{\sigma}}{E_M} + \frac{\sigma}{\eta_M} \end{aligned} \quad (5.15)$$

Consider the model under two test conditions.

a) at a constant strain rate,  $\dot{\varepsilon} = R$

$$\therefore \varepsilon = Rt \quad (5.16)$$

Then from equation (5.15)

$$\dot{\sigma} = E_M \left( R - \frac{\sigma}{\eta_M} \right)$$

After integration and putting  $\sigma=0$  at  $t=0$ , the equation will be (Ahmad 1988):

$$\sigma = R\eta_M \left( 1 - \exp\left(\frac{-E_M \varepsilon}{\eta_M R}\right) \right) \quad (5.17)$$

The values of  $\eta_M$  and  $E_M$  can be determined from the experimental stress-strain curve.

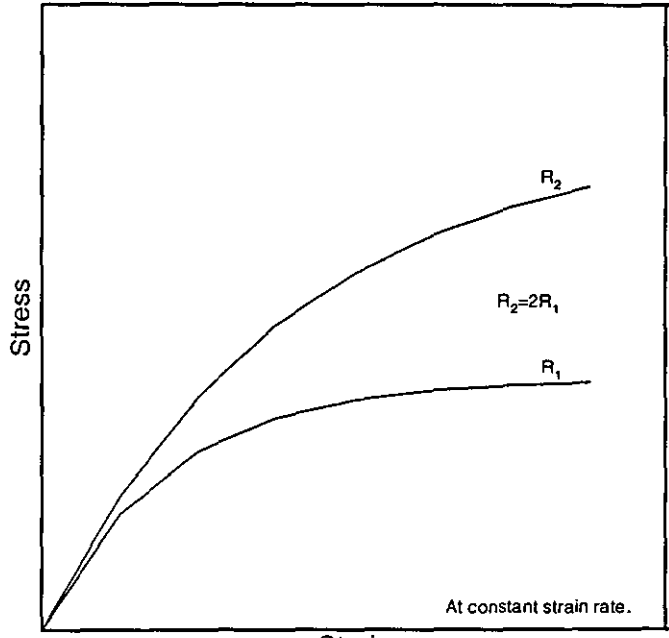
b) At a constant stress rate,  $\dot{\sigma} = K$ , then  $\sigma = Kt$ .

From Equation (5.15), by integrating, and putting  $\varepsilon = 0$  at  $t = 0$ , the relation will be

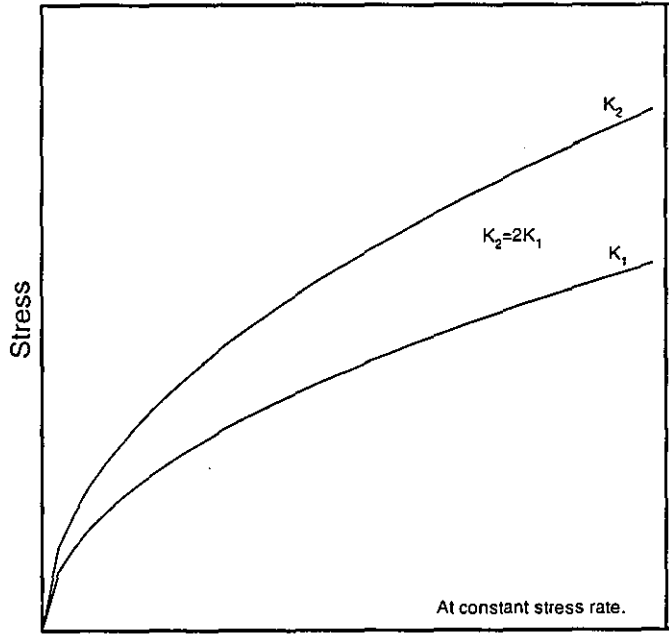
$$\varepsilon = \frac{\sigma}{E_M} + \frac{\sigma^2}{2\eta_M K} \quad (5.18)$$

The stress-strain curves for Equations (5.17) and (5.18) are shown in Figure (5.4).

The Maxwell model describes the stress relaxation of a viscoelastic solid to a first approximation, and the Kelvin model the creep behaviour, but neither model is adequate for the general behaviour of a viscoelastic solid where it is necessary to describe both stress relaxation and creep.



(a) at constant strain rate



(b) at constant stress rate

Figure (5.4) Maxwell solid behaviour.

Another way to study the Maxwell model is to consider stress relaxation. In this case where  $\dot{\epsilon} = 0$  (constant strain), Equation (5.15) will be as

$$\frac{\dot{\sigma}}{E_M} + \frac{\sigma}{\eta_M} = 0$$

Thus

$$\frac{d\sigma}{\sigma} = -\frac{E_M}{\eta_M} dt$$

At time  $t=0$ ,  $\sigma = \sigma_0$  the initial stress, and integrating this equation gives

$$\sigma = \sigma_0 \exp\left(-\frac{E_M}{\eta_M} t\right)$$

This shows that the stress decays exponentially with a time constant  $\tau = \eta_M / E_M$ :

$$\sigma = \sigma_0 \exp\left(-\frac{t}{\tau}\right)$$

where  $\tau$  is the relaxation time.

Under conditions of constant stress i.e.  $\dot{\sigma} = 0$ ,  $\dot{\epsilon} = \sigma / \eta_M$ , and Newtonian flow is observed (creep behaviour).

## 5.2 Standard linear solid

A more realistic model for viscoelastic behaviour is the standard linear solid model which is the main model used in this chapter.

This model consists of a Kelvin-Voigt model in series with a Hookean solid as shown in Figure (5.5).

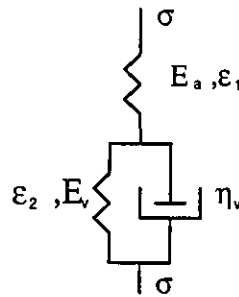


Figure (5.5) Standard linear viscoelastic model.

From Hooke's law for an elastic solid the equation for the stress-strain relation is

$$\sigma = E_a \epsilon_1 \quad (5.19)$$

and from the Kelvin model the equation is

$$\sigma = E_v \epsilon_2 + \eta_v \dot{\epsilon}_2 \quad (5.20)$$

$$\text{The total stress is } \sigma = \sigma_1 + \sigma_2, \quad (5.21)$$

$$\text{and the total strain is } \epsilon = \epsilon_1 + \epsilon_2 \quad (5.22)$$

$$\dot{\epsilon} = \dot{\epsilon}_1 + \dot{\epsilon}_2 \quad (5.23)$$

From Equations (5.19), (5.20) and Equation (5.23).

$$\begin{aligned} \dot{\epsilon}_1 &= \frac{\dot{\sigma}}{E_a} \\ \dot{\epsilon}_2 &= \frac{\sigma - E_v \epsilon_2}{\eta_v} = \frac{\sigma - E_v \left( \epsilon - \frac{\sigma}{E_a} \right)}{\eta_v} \\ \dot{\epsilon} &= \frac{\dot{\sigma}}{E_a} + \frac{\sigma - E_v \left( \frac{E_a \epsilon - \sigma}{E_a} \right)}{\eta_v} \end{aligned}$$



$$\dot{\epsilon} = \frac{\dot{\sigma} \eta_V + \sigma E_a - E_a E_V \left( \frac{E_a \epsilon - \sigma}{E_a} \right)}{E_a \eta_V}$$

$$E_a \eta_V \dot{\epsilon} = \dot{\sigma} \eta_V + \sigma E_V - E_a E_V \epsilon + \sigma E_a$$

$$\therefore \dot{\sigma} \eta_V + \sigma(E_a + E_V) = \dot{\epsilon} E_a \eta_V + E_a E_V \epsilon \quad (5.24)$$

Assuming the strain rate is constant  $\dot{\epsilon} = R$ , then  $\epsilon = Rt$

From Equation (5.24) substituting R and t will give

$$\dot{\sigma} \eta_V + \sigma(E_a + E_V) = R \eta_V E_a + Rt E_a E_V$$

Letting  $A = E_a \eta_V R$ ,  $B = R E_a E_V$ ,  $C = (E_a + E_V)$ , and  $D = \eta_V$ , the equation will be in the following form:

$$C \sigma + D \dot{\sigma} = A + Bt$$

$$\therefore \dot{\sigma} + \frac{C}{D} \sigma = \frac{A}{D} + \frac{B}{D} t$$

and putting  $E=C/D$ ,  $F=A/D$ , and  $G=B/D$  then

$$\dot{\sigma} + E\sigma = F + Gt$$

This equation can be written as

$$\frac{\partial}{\partial t} (\sigma \exp(Et)) = (F + Gt) \exp(Et)$$

$$\sigma \exp(Et) = \int_0^t (F + Gt) \exp(Et) dt + K$$

Where K is a constant of integration.

$$\therefore \sigma = \exp(-Et) \int_0^t (F + Gt) \exp(Et) dt + K \exp(-Et)$$

$$= \exp(-Et) \left[ \frac{F}{E} (\exp(Et) - 1) + \frac{G}{E} \left( t - \frac{1}{E} \right) \exp(Et) + \frac{G}{E^2} \right] + K \exp(-Et)$$

At  $t=0$ ,  $\sigma=0$

$$\therefore K=0$$

$$\sigma = \exp(-Et) \left[ \frac{F}{E} (\exp(Et) - 1) + \frac{G}{E} \left( t - \frac{1}{E} \right) \exp(Et) + \frac{G}{E^2} \right]$$

$$= \frac{F}{E} (1 - \exp(-Et)) + \frac{G}{E} \left( t - \frac{1}{E} \right) + \frac{G}{E^2} \exp(-Et)$$

$$\begin{aligned}
 &= \frac{F}{E} [1 - \exp(-Et)] + \frac{Gt}{E} - \frac{G}{E^2} + \frac{G}{E^2} \exp(-Et) \\
 &= \frac{F}{E} [1 - \exp(-Et)] + \frac{Gt}{E} - \frac{G}{E^2} [1 - \exp(-Et)] \\
 &= [1 - \exp(-Et)] \left( \frac{F}{E} - \frac{G}{E^2} \right) + \frac{Gt}{E} \\
 &= [1 - \exp(-Et)] \left( \frac{FE - G}{E^2} \right) + \frac{Gt}{E}
 \end{aligned}$$

By substituting all the constants back, the equation will be

$$\sigma = \frac{E_a E_v}{E_a + E_v} \varepsilon + \frac{E_a^2 \eta_v R}{(E_a + E_v)} \left[ 1 - \exp\left\{-\left(\frac{E_a + E_v}{\eta_v R}\right)\varepsilon\right\} \right] \quad (5.25)$$

For  $E_v = 0$ , the above equation becomes

$$\sigma = \eta_v R \left[ 1 - \exp\left\{-\left(\frac{E_a}{\eta_v R}\right)\varepsilon\right\} \right]$$

Which is as for the Maxwell model.

Differentiating Equation (5.25) with respect to  $\varepsilon$  gives

$$\frac{d\sigma}{d\varepsilon} = \frac{E_a E_v}{E_a + E_v} + \frac{E_a^2 \eta_v R}{(E_a + E_v)^2} \left(\frac{E_a + E_v}{\eta_v R}\right) \exp\left\{-\left(\frac{E_a + E_v}{\eta_v R}\right)\varepsilon\right\}$$

at  $\varepsilon = 0$

$$\frac{d\sigma}{d\varepsilon} = \frac{E_a E_v}{E_a + E_v} + \frac{E_a^2}{E_a + E_v} = E_a \left(\frac{E_v + E_a}{E_v + E_a}\right) = E_a \quad (5.26)$$

$\therefore$  The slope of stress-strain curve at  $\varepsilon = 0$  gives the value of the elastic modulus  $E_a$ .

At  $\varepsilon = \infty$ , the exponential term in Equation (5.25) will be zero and

$$\begin{aligned}
 \sigma &= \frac{E_a E_v \varepsilon}{E_a + E_v} + \frac{E_a^2 \eta_v R}{(E_a + E_v)^2} \\
 \therefore \frac{d\sigma}{d\varepsilon} &= \frac{E_a E_v}{E_a + E_v} = E_\infty \quad (5.27)
 \end{aligned}$$

By knowing  $E_a$  the value of  $E_v$  can be found from the slope of the stress-strain curve at  $\varepsilon = \infty$ , as shown in Figure (5.6).

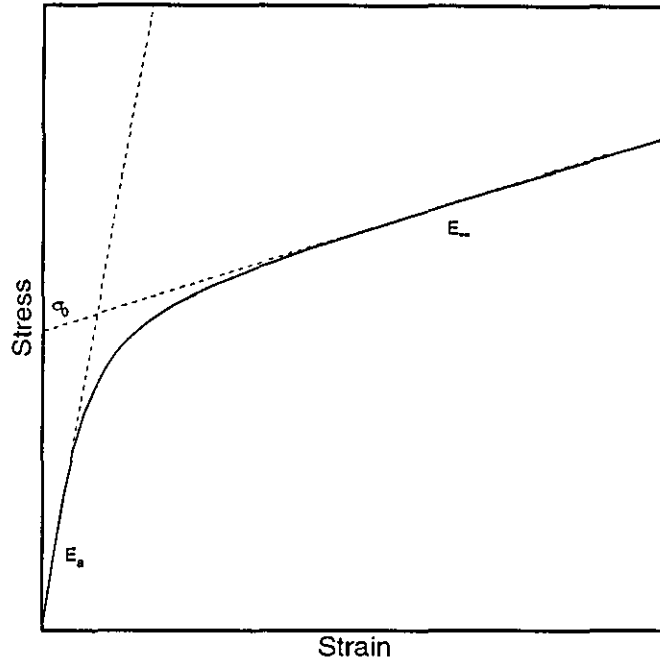


Figure (5.6) Stress-strain curve for standard linear model.

From equation (5.27) at  $\varepsilon = 0$ ,  $\sigma = \sigma_0$

Therefore

$$\eta_v = \frac{\sigma_0 (E_a + E_v)^2}{E_a^2 R} \quad (5.28)$$

which is the viscoelastic modulus.

$$\therefore \sigma = E_v \varepsilon + \sigma_0 \left[ 1 - \exp\left\{-\left(\frac{E_a + E_v}{\eta_v R}\right) \varepsilon\right\}\right] \quad (5.29)$$

By obtaining the values of  $E_a$ ,  $E_v$ , and  $\sigma_0$  from the stress-strain curve, Equation (5.29) can be applied for any strain rate.

### 5.3 Bi-linear elasto-plastic model

Stress-strain behaviour can be described by an elasto-plastic model called the bi-linear model. This model is represented by the nonlinear stress-strain relationship used by Richard and Blacklock (1969) and based on theoretical work done by Ramberg and Osgood (1943) to describe the shape of stress - strain curves by three parameters.

The constitutive equation for this relationship is

$$\sigma = \frac{E_a \varepsilon}{\left[1 + \left(\frac{E_a \varepsilon}{\sigma_0}\right)^n\right]^{1/n}} \quad (5.30)$$

where  $\sigma$  is the stress,  $E_a$  is the Young's modulus,  $\varepsilon$  is the strain,  $\sigma_0$  is the plastic stress,  $\sigma_y$  is the yield stress and  $n$  is a parameter defining the shape of the nonlinear stress-strain relationship related to the ratio  $\sigma_0/\sigma_y$ . A nondimensional plot of  $\sigma_0/\sigma_y$  against  $n$  will obtain the three parameters for the material;  $E_a$ ,  $\sigma_0$ , and  $n$ .

The differential of Equation (5.30) is

$$d\sigma = \left( \frac{E_a}{\left(1 + [E_a \varepsilon / \sigma_0]^n\right)^{\frac{n+1}{n}}} \right) d\varepsilon \quad (5.31)$$

Thus, the tangent modulus can be obtained and is

$$E_t = E_a / \left[1 + (E_a \varepsilon / \sigma_0)^n\right]^{\frac{n+1}{n}} \quad (5.32)$$

Since the relationship is nonlinear for a material demonstrating plastic behaviour, the constant change of the stiffness of the material has to be taken into account in the analysis (Hsu and Bertels (1974)). In order to overcome this difficulty, piecewise linearity has been assumed by Hsu and Bertels (1974) in dealing with the plasticity analysis, so that the linear theory of elasticity can be used.

Almost all the published results from the incremental finite element theories use predetermined piecewise linear approximations of stress-strain curves. Such approaches necessitate the use of the concept of the initial yield functions and rely on the elastic behaviour of the material up to this initial yield.

The yield is measured practically at a fixed percentage of deformation (i.e. 0.2% offset of strain for ductile materials). So, complications may arise when the state of some parts of the structure is very near the elasto-plastic transition. Therefore, it is necessary to make an accurate estimate and iterations of the next load increment so that the state of stress in these parts will not deviate from its stress-strain relation.

Richard and Blacklock (1969) suggested a simple solution to this problem, that is to make use of continuous approximations of the measured stress-strain

behaviour. The constitutive relation proposed by Richard and Blacklock is for the use of an approximate inelastic method of finite element structural analysis, but not based on the incremental method. Therefore their model is limited to the nonhardening ideally plastic materials, which is not practical as most engineering materials at large plastic strains usually exhibit linear work hardening.

A new constitutive stress-strain relation was proposed by Hsu and Bertels (1974) for the general behaviour of materials, and takes the form :

$$\sigma = \frac{E_a \varepsilon}{\left\{ 1 + \left[ \frac{E_a \varepsilon}{(1 - E_\infty / E_a) \sigma_0 + E_\infty \varepsilon} \right]^n \right\}^{1/n}} \quad (5.33)$$

where  $\sigma$ ,  $\varepsilon$  are the stress and strain, respectively;  $E_a$ ,  $E_\infty$  are the moduli of elasticity and plasticity, respectively;  $\sigma_0$  is the stress level at the intersection (kink) of the elasto-plastic curve as shown in Figure (5.7).

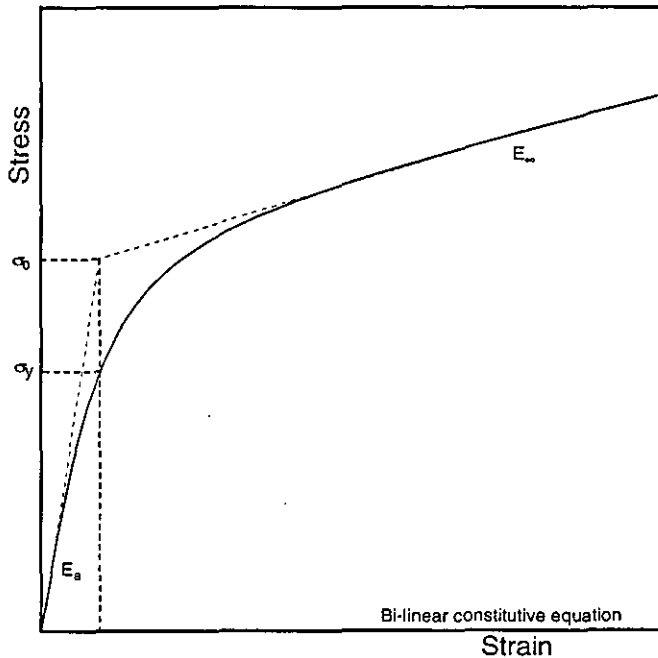


Figure (5.7) Identical stress-strain curve.

The stress power  $n$  may be estimated by the expression (Hsu and Bertels (1974):

$$n = \frac{\ln(2)}{\ln(\sigma_0 / \sigma_y)} \quad (5.34)$$

### 5.4 Four-element model

The uniaxial mechanical constitutive relation employed in this model is based on a simple four-element model. This nonlinear, four-element, elastic-viscoplastic model was developed by Chase and Goldsmith (1974) to describe the mechanical behaviour of anelastic polymers over a large range of strain rates ( $10^{-5}$  to  $3 \times 10^3 \text{ s}^{-1}$ ) and large strains (up to 40%). The model consists of spring, dashpot and friction element connected together in parallel, and these are connected in series with a spring element as shown in Figure (5.8).

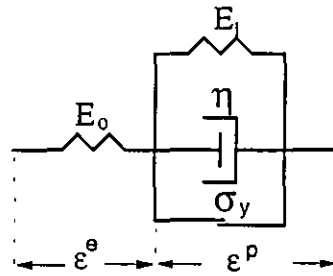


Figure (5.8) Four-element model of an elastic-viscoplastic solid.

Figure (5.9) shows a typical stress-strain curve for the four-element model. In the diagram (Figure (5.8))  $E_0$  and  $E_1$  are the elastic elements,  $\eta$  is a viscous element and  $\sigma_y$  is a rigid perfectly plastic element. The constitutive equations for the Chase and Goldsmith model are;

$$\dot{\epsilon} = \frac{\dot{\sigma}}{E_0}, \quad \text{at } \sigma \leq \sigma_s \quad (5.35)$$

$$\dot{\epsilon} = \frac{\dot{\sigma}}{E_0} + \frac{1}{\eta}(\sigma - \sigma_s), \quad \text{at } \sigma > \sigma_s \quad (5.36)$$

where the static stress  $\sigma_s = \frac{E_0}{E_0 + E_1}(\sigma_y + E_1 \epsilon)$ , where  $\eta = 0$ .

The constant strain rate response of the model for  $\sigma > \sigma_s$  is

$$\begin{aligned} \sigma = & \frac{E_0}{E_0 + E_1}(\eta_y + \bar{\eta}R + E_1 \epsilon)(1 - \exp[-\alpha(\epsilon - \epsilon_y)]) \\ & + [\sigma_y + \frac{E_0 E_1}{E_0 + E_1}(\epsilon - \epsilon_y)] \exp[-\alpha(\epsilon - \epsilon_y)] \quad \text{at } \sigma > \sigma_s \end{aligned} \quad (5.37)$$

where  $R = \dot{\epsilon} = \text{constant}$ ,  $\epsilon_y = \sigma_y / E_0$ ,  $\bar{\eta} = \frac{E_0}{E_0 + E_1} \eta$ , and  $\alpha = E_0 / \bar{\eta}R$ .

The initial slope ( $E_0$ ) of the bi-linear curve in Figure (5.9) is the elastic modulus, and the asymptotic slope ( $E_\infty = E_0 E_1 / (E_0 + E_1)$ ) is the plastic modulus. The stress in this model must exceed the static stress-strain curve before

viscoplastic flow occurs. The straight line of slope  $E_{\infty}$ , that intersects the response curve at  $\sigma_y$  is called the static stress-strain curve ( $\sigma_s$ , where  $\eta = 0$ ).

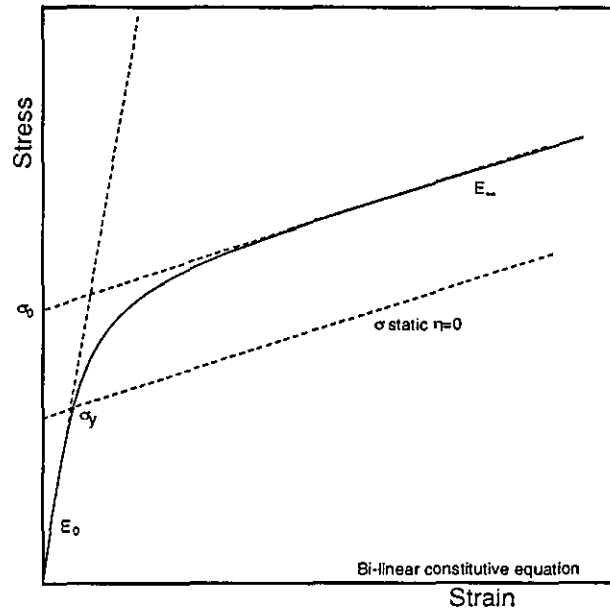


Figure (5.9) Constant strain-rate stress-strain curve for the four-element model (Chase and Goldsmith (1974)).

## 5.5 Examination of three models

### 5.5.1 Standard linear solid

#### A) HDPE results

The values of  $E_a$ ,  $E_\infty$ ,  $E_v$ ,  $\sigma_0$  and  $\eta_v$  in Table (5.1) for HDPE at various strain rates are calculated from the experimental stress-strain curves (Figure (5.10)) and plugged into Equation (5.29) to obtain a theoretical stress-strain relationships, where the units for the stress ( $\sigma$ ) are MPa, while strain ( $\epsilon$ ) is dimensionless. Errors quoted in Table (5.1) are calculated from the spread of experimental results and are applicable to all tables in this chapter.

1) at  $\dot{\epsilon} = 2.5 \times 10^{-3} \text{ s}^{-1}$

$$\sigma = 15.1\epsilon + 20.2(1 - \exp[-15.16\epsilon])$$

2) at  $\dot{\epsilon} = 3295 \text{ s}^{-1}$

$$\sigma = 38.2\epsilon + 29.6(1 - \exp[-51.2\epsilon])$$

3) at  $\dot{\epsilon} = 7523 \text{ s}^{-1}$

$$\sigma = 51.3\epsilon + 35.0(1 - \exp[-62.36\epsilon])$$

These expressions are plotted in Figure (5.10), and show good agreement with the experimental data for all strains, except that for  $\dot{\epsilon} = 2.5 \times 10^{-3} \text{ s}^{-1}$  where the theoretical stress is slightly below the experimental for strains from about 3% - 10%.

Table(5.1) HDPE results

$\dot{\epsilon} (\text{s}^{-1})$	$E_a$ (GPa)	$E_\infty$ (MPa)	$E_v$ (MPa)	$\sigma_0$ (MPa)	$\eta_v$ (MPa)
$2.5 \times 10^{-3}$	0.32	15.1	14.4	20.2	8824.6
3295	1.55	38.2	37.4	29.6	0.00942
7523	2.23	51.3	50.1	35.0	0.00486
$\pm 1\%$	$\pm 1\%$	$\pm 1\%$	$\pm 2\%$	$\pm 1.5\%$	$\pm 6\%$



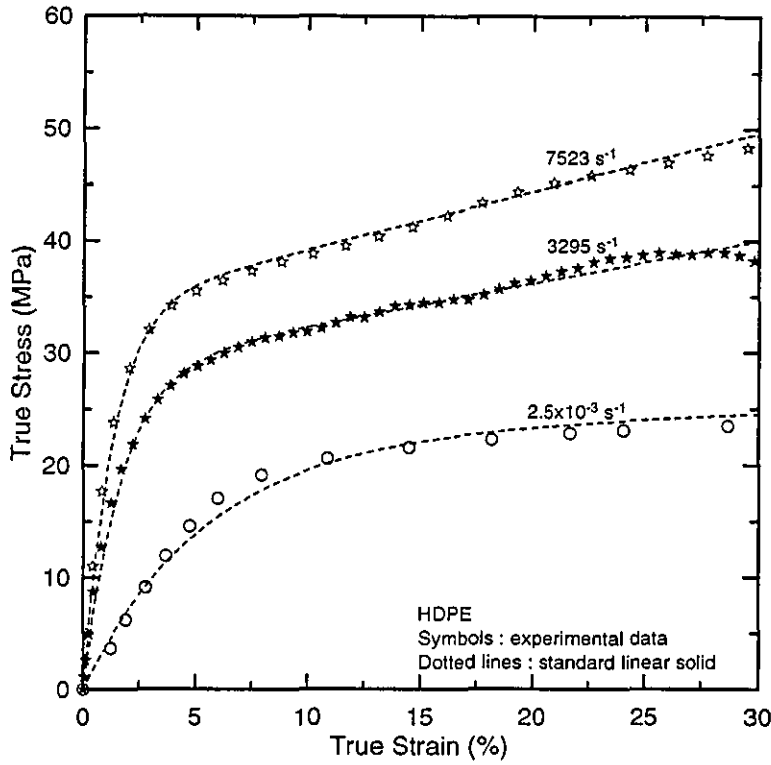


Figure (5.10) Experimental data and Standard Linear Solid curves for HDPE at various strain rates.

B) UHMWPE results

Table (5.2) shows the measured values of  $E_a$ ,  $E_{\infty}$ ,  $E_v$ ,  $\sigma_0$  and  $\eta_v$  for UHMWPE at various strain rates ( $\dot{\epsilon}$ ). The stress-strain relationships were obtained from Equation (5.29) as follows and plotted in Figure (5.11) with the experimental data. The calculated curves show a good agreement with experimental data at all strains.

- 1) at  $\dot{\epsilon} = 8.2 \times 10^{-4} \text{ s}^{-1}$   

$$\sigma = 25.0\epsilon + 16.0(1 - \exp[-24.86\epsilon])$$
- 2) at  $\dot{\epsilon} = 2.7 \times 10^{-2} \text{ s}^{-1}$   

$$\sigma = 39.9\epsilon + 21.42(1 - \exp[-35.65\epsilon])$$
- 3) at  $\dot{\epsilon} = 5 \times 10^{-2} \text{ s}^{-1}$   

$$\sigma = 39.92\epsilon + 22.25(1 - \exp[-34.32\epsilon])$$
- 4) at  $\dot{\epsilon} = 2000 \text{ s}^{-1}$   

$$\sigma = 38.73\epsilon + 32.0(1 - \exp[-46.06\epsilon])$$
- 5) at  $\dot{\epsilon} = 3410 \text{ s}^{-1}$   

$$\sigma = 49.4\epsilon + 34.0(1 - \exp[-60.6\epsilon])$$
- 6) at  $\dot{\epsilon} = 6746 \text{ s}^{-1}$   

$$\sigma = 50.3\epsilon + 38.85(1 - \exp[-55.52\epsilon])$$

Table (5.2) UHMWPE results

$\dot{\epsilon}$ (s <sup>-1</sup> )	$E_a$ (GPa)	$E_\infty$ (MPa)	$E_v$ (MPa)	$\sigma_0$ (MPa)	$\eta_v$ (MPa)
$8.2 \times 10^{-4}$	0.42	25.0	23.6	16.0	21766
$2.7 \times 10^{-2}$	0.80	39.9	38.0	21.4	870.5
$5.0 \times 10^{-2}$	0.80	39.9	30.0	22.3	488.3
2000	1.51	38.7	37.8	32.0	0.0168
3410	2.10	49.4	48.3	34.0	0.0104
6746	2.20	50.3	49.2	38.9	0.0060

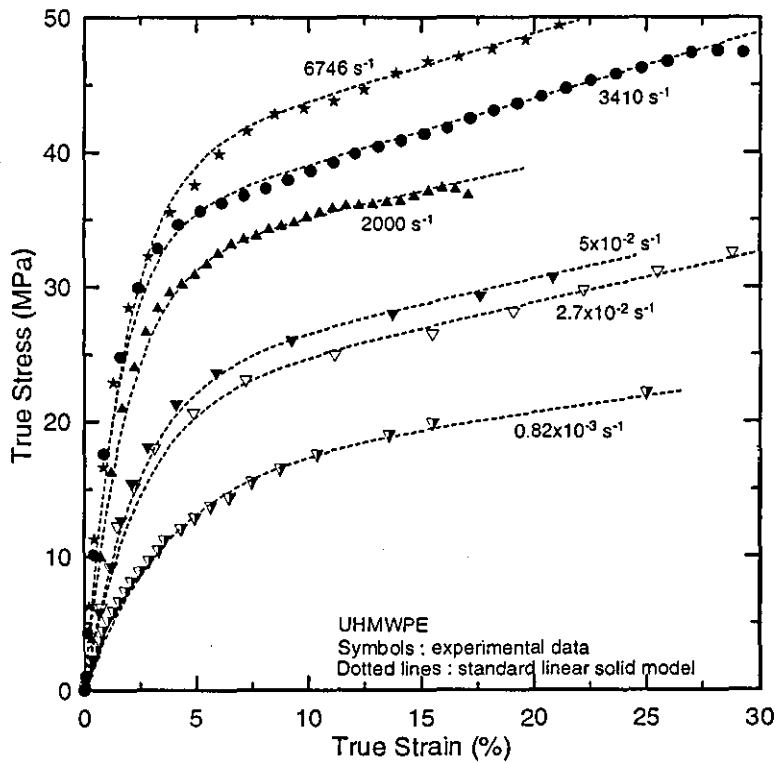


Figure (5.11) Experimental data and Standard Linear Solid curves for UHMWPE at various strain rates.

C) Nylatron results

The standard linear solid model has also been applied to the results for nylatron. Figure (5.12) shows the experimental and theoretical curves at various strain rates. Table (5.3) shows the calculated values of  $E_a$ ,  $E_\infty$ ,  $E_v$ ,  $\sigma_0$  and  $\eta_v$ . These values are used to obtain the following stress-strain relationships.

- 1) at  $\dot{\epsilon} = 1.77 \times 10^{-4} \text{ s}^{-1}$   
 $\sigma = 165.0\epsilon + 42.0(1 - \exp[-40.71\epsilon])$
- 2) at  $\dot{\epsilon} = 4.6 \times 10^{-4} \text{ s}^{-1}$   
 $\sigma = 155.0\epsilon + 66.0(1 - \exp[-26.77\epsilon])$
- 3) at  $\dot{\epsilon} = 2000 \text{ s}^{-1}$   
 $\sigma = 132.4\epsilon + 119.0(1 - \exp[-27.36\epsilon])$
- 4) at  $\dot{\epsilon} = 7164 \text{ s}^{-1}$   
 $\sigma = 10.3\epsilon + 161.0(1 - \exp[-27.98\epsilon])$
- 5) at  $\dot{\epsilon} = 8869 \text{ s}^{-1}$   
 $\sigma = 27.26\epsilon + 150.0(1 - \exp[-27.91\epsilon])$
- 6) at  $\dot{\epsilon} = 9318 \text{ s}^{-1}$   
 $\sigma = 35.0\epsilon + 143.0(1 - \exp[-29.48\epsilon])$

Figure (5.12) shows that the theoretical stresses are below the experimental ones in the region between strains of about 2% and 12% for all strain rates.

Table (5.3) Nylatron results

$\dot{\epsilon} \text{ (s}^{-1}\text{)}$	$E_a \text{ (GPa)}$	$E_\infty \text{ (MPa)}$	$E_v \text{ (MPa)}$	$\sigma_0 \text{ (MPa)}$	$\eta_v \text{ (MPa)}$
$1.77 \times 10^{-4}$	1.85	165.0	151.5	42.0	277740
$4.6 \times 10^{-4}$	1.90	155.0	143.3	66.0	165938
2000	3.38	132.4	127.4	119.0	0.0641
7164	4.40	10.3	10.3	161.0	0.0225
8869	4.23	27.3	27.1	150.0	0.0172
9318	4.25	35.0	34.7	143.0	0.0156

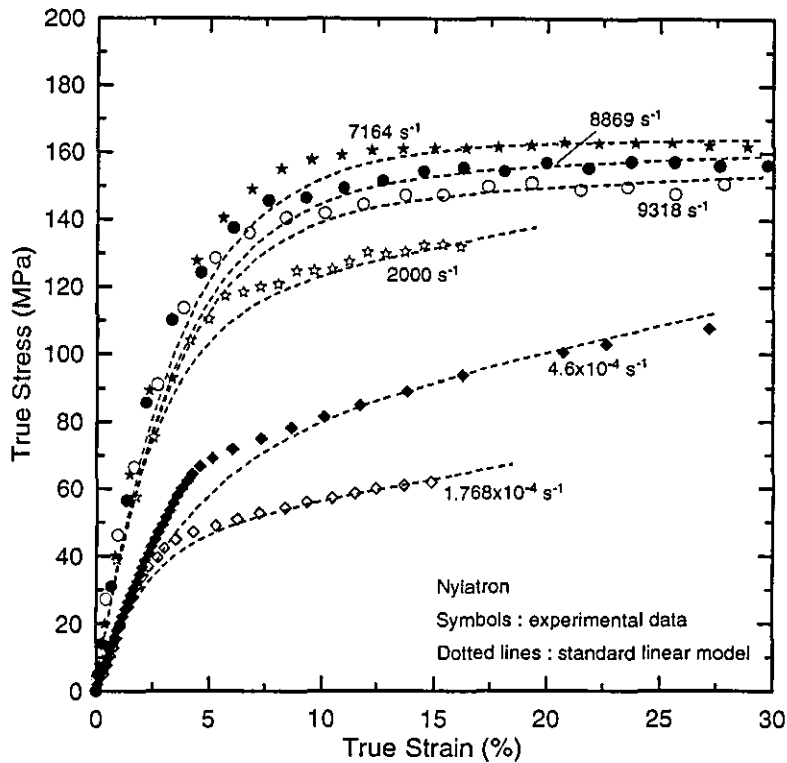


Figure (5.12) Experimental and standard linear solid curves for nylatron.

#### D) PEEK results

Using the same method, the values of  $E_a$ ,  $E_\infty$ ,  $E_v$ ,  $\sigma_0$  and  $\eta_v$  for PEEK at various strain rates are tabulated in Table (5.4). The values of  $E_\infty$  and  $E_v$  show a negative sign due to the upper and lower yield in the stress - strain curves of the PEEK especially at higher strain rates. As in Figure (5.12) for nylatron the calculated values for PEEK give theoretical curves below the experimental ones, as shown in Figure (5.13).

1) at  $\dot{\epsilon} = 5 \times 10^{-3} \text{ s}^{-1}$

$$\sigma = 30.0\epsilon + 124.23(1 - \exp[-26.33\epsilon])$$

2) at  $\dot{\epsilon} = 1.16 \times 10^{-2} \text{ s}^{-1}$

$$\sigma = -2.07\epsilon + 137.05(1 - \exp[-28.47\epsilon])$$

3) at  $\dot{\epsilon} = 4025 \text{ s}^{-1}$

$$\sigma = -35.76\epsilon + 172.63(1 - \exp[-25.04\epsilon])$$

4) at  $\dot{\epsilon} = 9660 \text{ s}^{-1}$

$$\sigma = -84.13\epsilon + 208.21(1 - \exp[-28.81\epsilon])$$

5) at  $\dot{\epsilon} = 11100 \text{ s}^{-1}$

$$\sigma = -17.1\epsilon + 178.8(1 - \exp[-30.87\epsilon])$$

Table (5.4) PEEK results

$\dot{\epsilon}$ (s <sup>-1</sup> )	$E_a$ (GPa)	$E_\infty$ (MPa)	$E_v$ (MPa)	$\sigma_0$ (MPa)	$\eta_v$ (MPa)
$5 \times 10^{-3}$	3.30	30.0	29.7	124.2	25295
$1.16 \times 10^{-2}$	3.90	-2.1	-2.1	137.1	11802
4025	4.29	-35.8	-36.1	172.6	0.0422
9660	5.90	-84.1	-86.2	208.2	0.0209
11100	5.50	-18.1	-17.2	178.8	0.0160

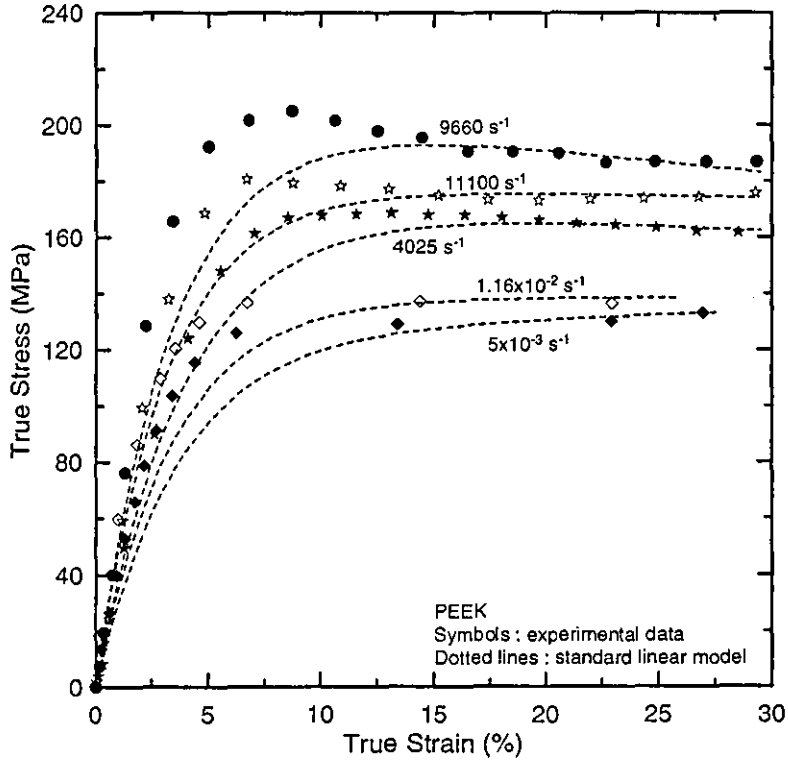


Figure (5.13) Experimental data and standard linear solid curves for PEEK.

### 5.5.2 Bi-linear model (BLM)

#### A) HDPE results

The bi-linear stress-strain Equation (5.33) was applied to obtain the theoretical stress-strain curves using the measured values of  $E_a$ ,  $E_\infty$ ,  $\sigma_0$ ,  $\sigma_y$  and  $n$  for HDPE at various strain rates (Table 5.5). Figure (5.14) shows the bi-linear stress-strain plots with the experimental data. A very good agreement between the experimental and the theoretical curves is shown in Figure (5.14).

Table (5.5) HDPE values for the BLM.

$\dot{\epsilon}$ (s <sup>-1</sup> )	$E_a$ (GPa)	$E_\infty$ (MPa)	$\sigma_0$ (MPa)	$\sigma_y$ (MPa)	$n$
$2.5 \times 10^{-3}$	0.32	15.1	20.2	17.0	4.02
3295	1.55	38.2	29.6	20.6	1.91
7523	2.23	51.3	35.0	25.4	2.16

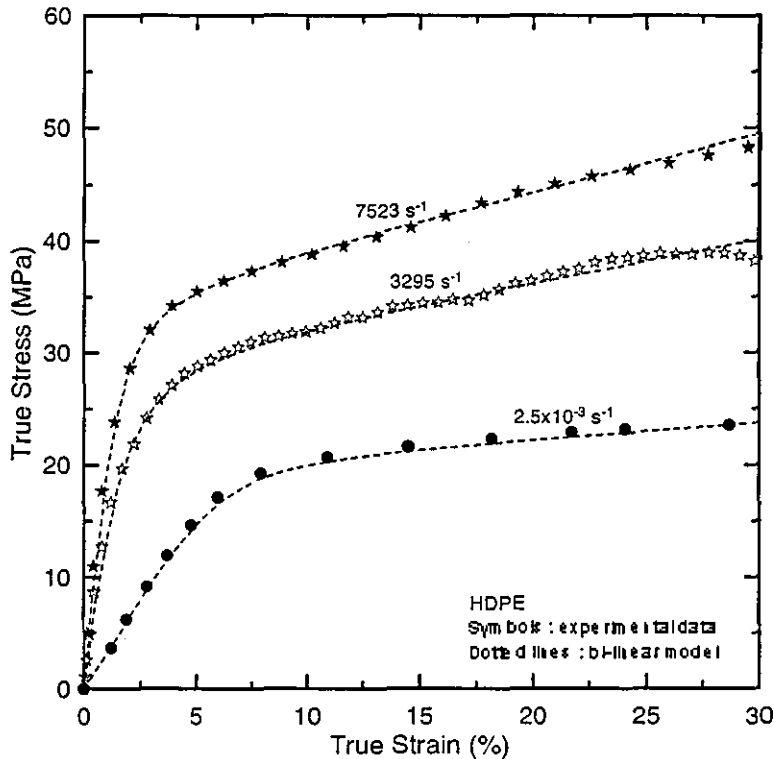


Figure (5.14) Experimental stress-strain curves and bilinear model for HDPE.

B) UHMWPE results

As with the HDPE results, the bi-linear model for the measured values of  $E_a$ ,  $E_\infty$ ,  $\sigma_0$ ,  $\sigma_y$  and  $n$  for UHMWPE at various strain rates (Table 5.6) fits very well the experimental data, as shown in Figure (5.15).

Table (5.6) UHMWPE values for the BLM.

$\dot{\epsilon}$ (s <sup>-1</sup> )	$E_a$ (GPa)	$E_\infty$ (MPa)	$\sigma_0$ (MPa)	$\sigma_y$ (MPa)	$n$
$8.2 \times 10^{-4}$	0.42	25.0	16.0	12.0	1.99
$2.7 \times 10^{-2}$	0.80	39.9	21.4	16.0	2.18
0.05	0.80	39.9	22.3	18.2	2.71
2000	1.51	38.7	32.0	23.8	2.34
3410	2.10	49.4	34.0	25.5	2.19
6746	2.20	50.3	38.9	28.0	1.95

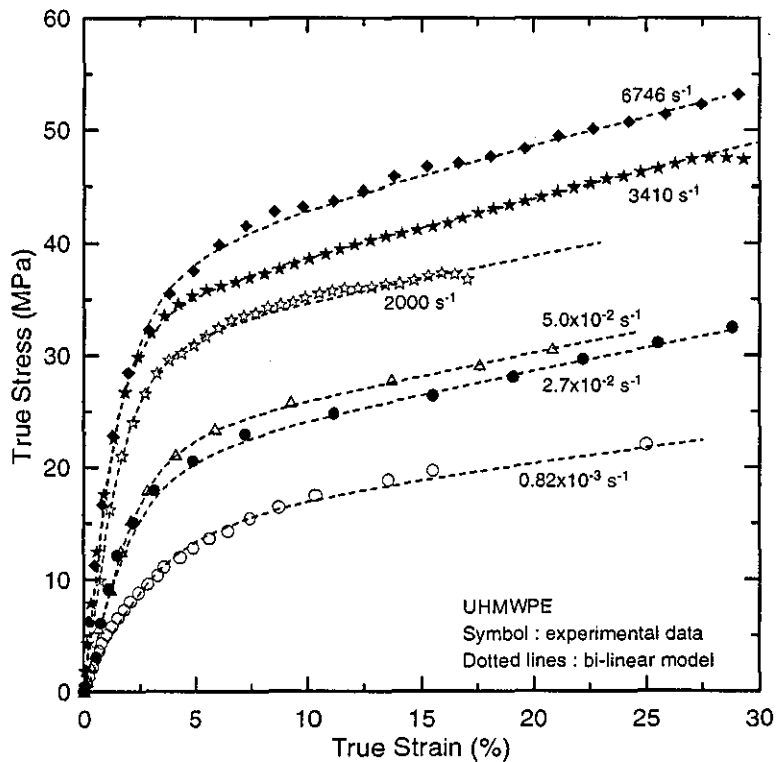


Figure (5.15) Experimental data and bilinear model curves for UHMWPE.

C) Nylatron results

The bi-linear model is designed to follow the shape of the stress-strain curve, as is shown by the good agreement with all the experimental curves at different strain rates. As shown in Figure (5.16), the bi-linear model curves for the values in Table (5.7) fit the experimental data for all strain rates and at all strains up to the strain hardening or softening which are outside the range of strain plotted.

Table (5.7) Nylatron values for the BLM.

$\dot{\epsilon}$ (s <sup>-1</sup> )	$E_a$ (GPa)	$E_\infty$ (MPa)	$\sigma_0$ (MPa)	$\sigma_y$ (MPa)	$n$
$1.77 \times 10^{-4}$	1.85	151.5	42.0	35.0	5.19
$4.6 \times 10^{-4}$	1.90	155.0	66.0	55.0	3.80
2000	3.38	132.4	119.0	96.0	3.23
7164	4.40	10.3	161.0	119.0	2.25
8869	4.23	27.3	150.0	28.0	2.39
9318	4.25	35.0	143.0	106.0	2.32

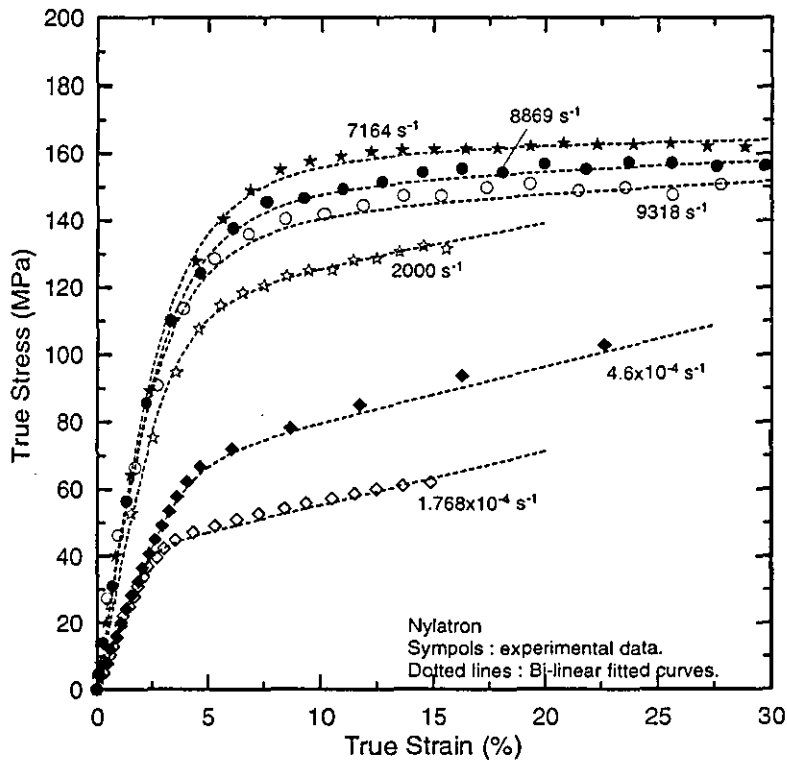


Figure (5.16) Experimental data and bilinear model curves for nylatron.

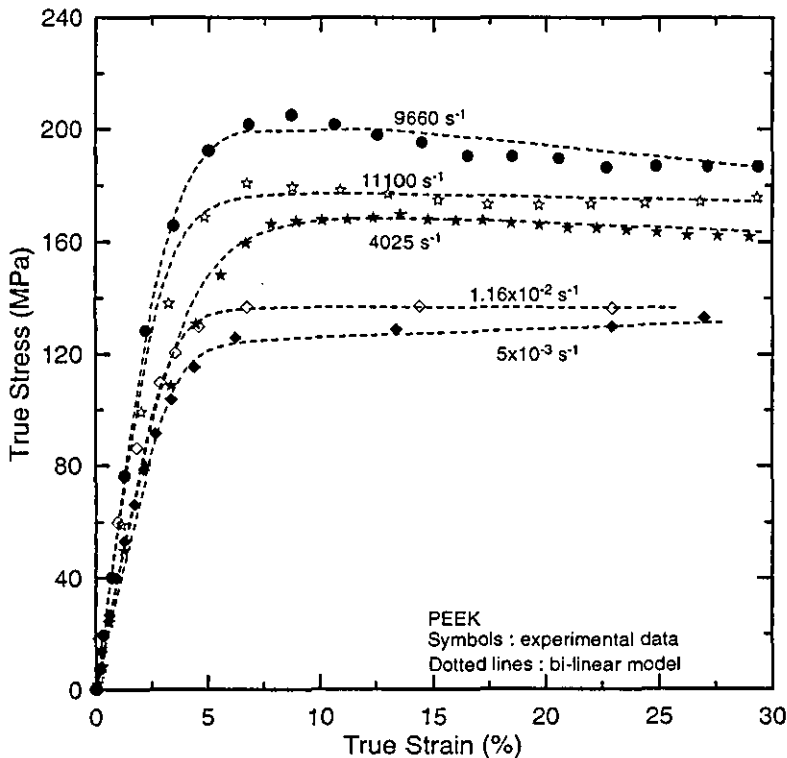


D) PEEK results

As observed from the experimental data, the PEEK has well-defined upper and lower yield points, especially at high strain rates. Therefore it is not easy to fit a simple model with the experimental data. Figure (5.17) shows that for low and medium strain rates the model is in a good agreement with the experimental data, but when the strain rate gets high, the model starts to miss the data particularly after the yield. However, the model follows the trends of the experimental data for all curves in the elastic region. The theoretical stress-strain curves calculated from Equation (5.33) using the values in Table (5.8), and the experimental data are plotted in Figure (5.17).

Table (5.8) PEEK values for the BLM.

$\dot{\epsilon}$ (s <sup>-1</sup> )	$E_a$ (GPa)	$E_{\infty}$ (MPa)	$\sigma_0$ (MPa)	$\sigma_y$ (MPa)	$\eta$ (MPa)
$5 \times 10^{-3}$	3.30	30.0	124.2	110.0	5.69
$1.16 \times 10^{-2}$	3.90	-2.1	137.1	120.0	5.22
4025	4.29	-35.8	172.6	140.0	3.31
9660	5.50	-84.1	208.2	170.0	3.42
11100	5.50	-18.1	178.8	150.0	3.85



Figure(5.17) Experimental data and bi-linear model curves for PEEK at various strain rates.

### 5.5.3 Four element model

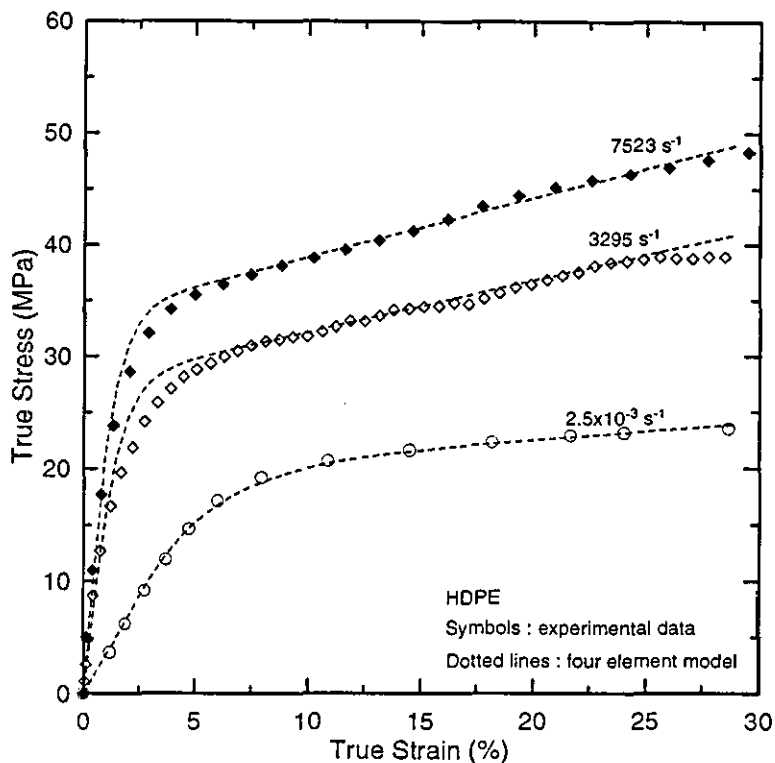
The four-element model (FEM) has also been studied (Equation 5.37) for the experimental data of HDPE, UHMWPE, nylatron and PEEK. This model is different from the standard linear solid and bi-linear model because it has the yield parameter in the equation, so it can fit the stiffer materials better than the softer due to the yield stress being better defined for the stiffer materials.

#### A) HDPE results

The values of  $E_a$ ,  $E_\infty$ ,  $\sigma_0$  and  $\sigma_y$  for HDPE in Table (5.9) were used to calculate the stress-strain curves for the FEM. The experimental data and the theoretical curves are shown in Figure (5.18). Figure (5.18) shows that at high strain rates the theoretical stress is higher than the experimental data in the elastic-plastic transition region due to the viscosity of this material.

Table(5.9) HDPE values for the FEM.

$\dot{\epsilon}(\text{s}^{-1})$	$E_a$ (GPa)	$E_\infty$ (MPa)	$\sigma_0$ (MPa)	$\sigma_y$ (MPa)
$2.5 \times 10^{-3}$	0.32	15.1	20.2	10.0
3295	1.55	38.2	29.6	14.7
7523	2.23	51.3	35.0	17.4



Figure(5.18) Experimental data and four element model curves for HDPE at various strain rates.

### B) UHMWPE results

Like HDPE, the UHMWPE results in Figure (5.19) show that in the yield region the theoretical curves do not follow the experimental data. Table (5.10) shows the calculated values of  $E_a$ ,  $E_\infty$ ,  $\sigma_0$  and  $\sigma_y$  for UHMWPE that are used to calculate the theoretical stress-strain curves at various strain rates.

Table(5.10) UHMWPE values for the FEM

$\dot{\epsilon}$ (s <sup>-1</sup> )	$E_a$ (GPa)	$E_\infty$ (MPa)	$\sigma_0$ (MPa)	$\sigma_y$ (MPa)
$8.2 \times 10^{-4}$	0.42	25.0	16.0	7.2
$2.7 \times 10^{-2}$	0.80	39.9	21.4	10.0
$5.0 \times 10^{-2}$	0.80	39.92	22.3	11.3
2000	1.51	38.73	32.0	15.0
3410	2.10	49.4	34.0	16.8
6746	2.20	50.3	38.9	19.5

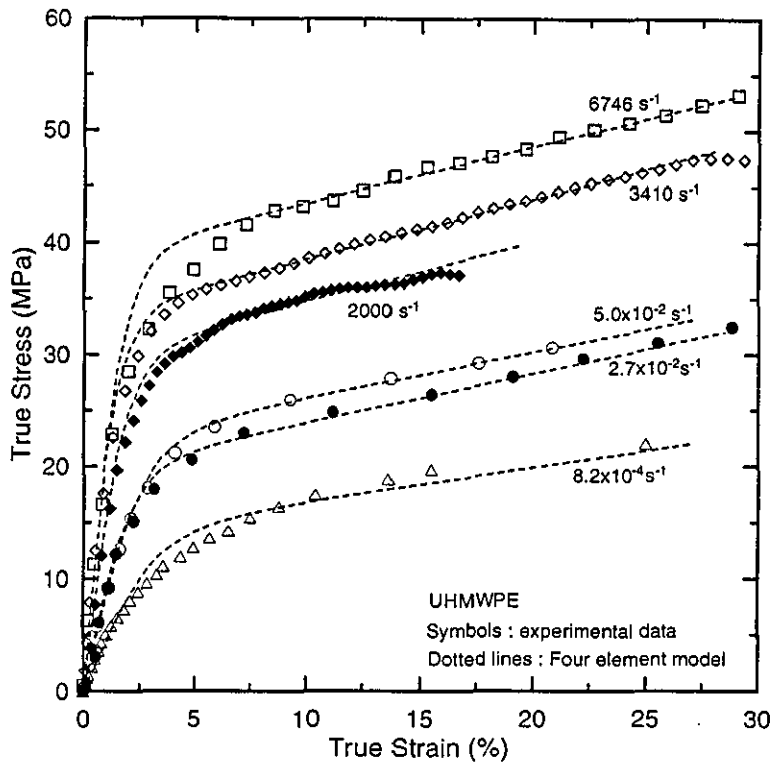


Figure (5.19) Experimental data and four element model curves for UHMWPE at various strain rates.

C) Nylatron results

The four-element model fits the nylatron experimental data very well as shown in Figure (5.20) using the measured values of  $E_a$ ,  $E_\infty$ ,  $\sigma_0$  and  $\sigma_y$  (Table 5.11) for nylatron samples tested at various strain rates.

Table(5.11) Nylatron values for the FEM.

$\dot{\epsilon}(\text{s}^{-1})$	$E_a$ (GPa)	$E_\infty$ (MPa)	$\sigma_0$ (MPa)	$\sigma_y$ (MPa)
$1.7 \times 10^{-4}$	1.85	151.5	142.0	22.0
$4.6 \times 10^{-4}$	1.90	155.0	66.0	35.0
2000	3.38	132.4	119.0	57.7
7164	4.40	10.3	161.0	79.2
8869	4.20	27.3	150.0	72.5
9318	4.25	35.0	143.0	69.0

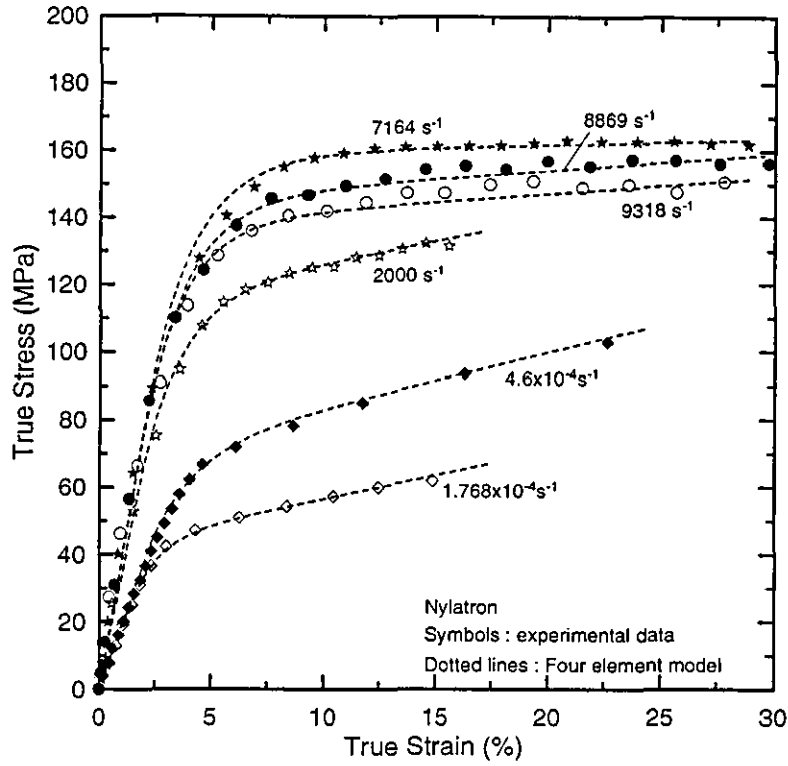


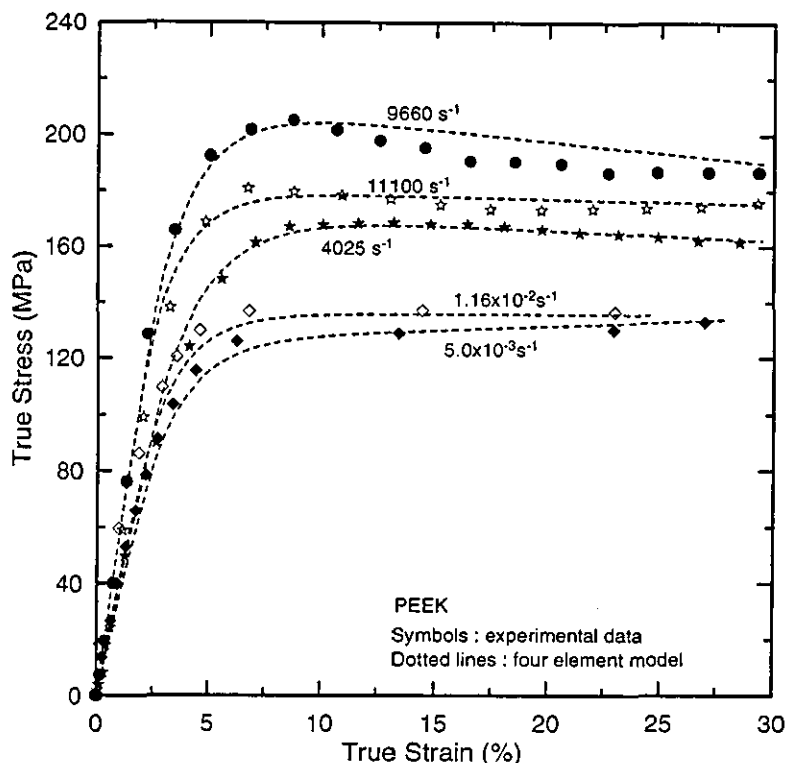
Figure (5.20) Experimental data and four-element model curves for nylatron at various strain rates.

#### D) PEEK results

Apart from the upper and lower yield point region at the high strain rates, the FEM curves are in good agreement with the PEEK experimental data as shown in Figure (5.21). The theoretical curves were calculated from the FEM using the tabulated values of  $E_a$ ,  $E_\infty$ ,  $\sigma_0$  and  $\sigma_y$  shown in Table (5.12).

Table (5.12) PEEK values for the FEM.

$\dot{\epsilon}$ (s <sup>-1</sup> )	$E_a$ (GPa)	$E_\infty$ (MPa)	$\sigma_0$ (MPa)	$\sigma_y$ (MPa)
$5 \times 10^{-3}$	3.3	30.0	124.2	63.0
$1.16 \times 10^{-2}$	3.9	-2.07	137.1	68.0
4025	4.3	-35.7	172.6	86.0
9660	5.5	-84.1	208.2	106.0
11100	5.5	-18.1	178.8	90.0



Figure(5.21) Experimental data and four-element model curves for PEEK at various strain rates.

## 5.6 Discussion

Measurements have been made from the stress-strain curves of HDPE, UHMWPE, nylatron and PEEK to obtain values of the parameters  $E_a$ ,  $E_\infty$ ,  $\sigma_0$ ,  $\eta_v$ ,  $\sigma_y$  and  $n$  at various strain rates. These values were used to calculate theoretical stress-strain curves for three models. In these measurements low and high strain rates have been obtained by using the Hounsfield machine and Hopkinson pressure bar (SHPB), respectively.

Applying the standard linear solid (Equation (5.29)) gives stress-strain curves which fit quite well the experimental stress strain curves for HDPE and UHMWPE for all strain rates. However the standard linear solid does not fit the whole range of strain for nylatron and PEEK due to their greater stiffness and the sharp, short elastic-plastic transition in their stress-strain curves.

A bi-linear model has also been applied for the above materials. It gave a good agreement with the experimental data for all materials except for PEEK at high strain rates where the upper and lower yield feature occurs.

The last model used was the four-element model. This model fits well most of the data for nylatron, and the low and medium strain rates curves for HDPE and UHMWPE. The four-element model agrees with the low and medium stress-strain curves of PEEK, but at high strain rates where the upper and lower yield points occur, then the theoretical curves could not follow the trends of the data.

The definition of the yield point is different between the four-element model and the bi-linear model, i.e. it is lower for the FEM than it is for the bi-linear model.

Comparison of the fits to the three theoretical model helps in the choice of the most suitable model for each polymer. The most appropriate model can then be used by engineers to predict the polymer behaviour under a range of conditions. Knowing expressions for the constants used, such as Young's modulus and yield stress as a function of strain rate will help to produce a complete predictive description of the material.

In conclusion the measured values of the parameters  $E_a$ ,  $E_\infty$ ,  $\sigma_0$ ,  $\eta_v$ ,  $\sigma_y$  and  $n$  are not very easy to obtain from the experimental data due to the viscosity of the soft polymers.

## **CHAPTER 6**

### **MULTIPLE REFLECTION EFFECT ANALYSIS IN SHPB SAMPLES WITHIN THE ELASTIC LIMIT**

#### **6.1 Introduction**

The split Hopkinson pressure bar (SHPB) technique is a well established method for the determination of high strain rate properties of materials (discussed in Chapter 3). In the SHPB test, the sample (a small solid cylinder of the test material) is sandwiched between two long, high strength steel bars. The sample can be compressed by a stress pulse generated by impacting the end of one of the steel bars (incident bar) using a steel projectile. The projectile has the same diameter as the steel bars, and a length that is appropriate for providing a suitable loading pulse duration.

The stress pulses in the bars are recorded by strain gauges placed equidistant from the sample. The stress-strain properties can be derived from the amount of the stress pulse reflected and transmitted by the sample, assuming that stress equilibrium exists throughout the sample.

When the stress wave travels along the incident bar in a positive direction, it hits the first interface between the incident bar and the sample. The difference in impedance between the bars and the sample makes the wave partially reflect back in the -ve direction as a reflected pulse  $\sigma_R$ , while the rest of the wave passes through the first interface as a transmitted pulse (from the first interface) at time zero  $\sigma_{T0}$ . The  $\sigma_{T0}$  travels toward the second interface between the sample and the transmitter bar and again due to the impedance mismatch, part of  $\sigma_{T0}$  will reflect back toward the first face and the rest will transmit into the transmitter bar.

The time required for the  $\sigma_{T0}$  pulse to reach the second face of the sample, or in other words the time required for the pulse to travel between the two faces of the sample is called the traverse time  $tt$ , which defined as:

$$tt = \frac{\ell}{c_s}$$

where  $\ell$  is the sample length and  $c_s$  is the wave speed in the sample.

So, after one period of traverse time the reflection occurs at the second face of the sample creating  $\sigma_{R1}$  and  $\sigma_{T1}$ . This process continues, so that multiple



reflections occur within the sample and a succession of reflected waves become "trapped" inside the sample propagating back and forth between the two interfaces (Dixon (1990)).

Theoretically, reflected waves thus "trapped" in this manner will undergo an infinite number of reflections between the interfaces; however at each reflection the intensity of the reflected stress will decrease since a portion of the wave is transmitted each time. Eventually, the trapped wave will have decayed to a negligible amplitude. The effect of multiple reflections within the sample is to cause a dispersion of the incident wave. Thus, if the incident wave has a sharp rise time before reaching a constant maximum stress, the transmitted wave will have a less sharp rise time. These multiple reflections cause a non-uniform stress distribution, that may lead to inaccurate estimates of the initial stress/strain properties of the sample (A-Maliky and Parry (1994)).

The theory of SHPB analysis is based on the equation  $\epsilon_T = \epsilon_I + \epsilon_R$ . This equation is only true if the forces and therefore the stresses are equal on both sides of the sample. This equilibrium condition will not arise immediately a stress wave is incident on a SHPB sample, but occurs after several reflections have taken place inside the sample.

## 6.2 Theory

Consider a compressive stress  $\sigma_x$  on one face of an element of a bar as in Figure (6.1); passing through a distance  $dx$ , the stress on the other face will be given by  $\sigma_x + \frac{\partial \sigma_x}{\partial x} dx$ . If the displacement of the element is  $u$ , then from Newton's second law of motion (Kolsky (1963), and Graff (1975))

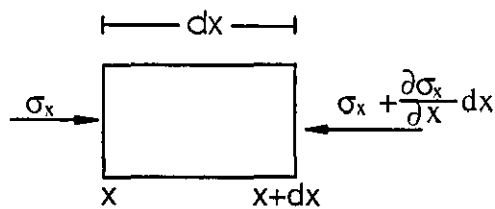


Figure (6.1)

$$\begin{aligned}
 ma &= F \\
 \rho A dx \frac{\partial^2 u}{\partial t^2} &= -A \frac{\partial \sigma_x}{\partial x} dx
 \end{aligned}
 \tag{6.1}$$

where  $\rho$  and  $A$  are density and cross-sectional area respectively.

The ratio between the stress  $\sigma_x$  and the strain  $\frac{\partial u}{\partial x}$  in the element is Young's modulus  $E$ , using a negative sign since  $\sigma_x$  is compressive, i.e.

$$\begin{aligned}
 E &= \frac{-\sigma_x}{\partial u / \partial x} \\
 \therefore \sigma &= -\frac{\partial u}{\partial x} E \\
 \text{or } \frac{\partial \sigma}{\partial x} &= -\frac{\partial^2 u}{\partial x^2} E
 \end{aligned}
 \tag{6.2}$$

Then from equation (6.1)

$$\begin{aligned}
 \rho \frac{\partial^2 u}{\partial t^2} &= E \frac{\partial^2 u}{\partial x^2} \\
 \text{or} & \\
 \frac{\partial^2 u}{\partial t^2} &= c^2 \frac{\partial^2 u}{\partial x^2}
 \end{aligned}
 \tag{6.3}$$

This equation corresponds to the propagation of longitudinal waves along the bar with a speed  $c = \sqrt{E/\rho}$  for linear elastic materials. Equation (6.3) has a solution that can be written as  $u = f(x - ct) + g(x + ct)$  where  $f$  and  $g$  are arbitrary functions in the directions of increasing and decreasing  $x$  respectively (Johnson (1972)).

Assuming the wave is travelling in the positive  $x$  direction only (compressive), then the displacement  $u$  due to the incident pulse is:

$$u = f(x - ct) \tag{6.4}$$

$$\frac{\partial u}{\partial x} = f'(x - ct)$$

$$\frac{\partial u}{\partial t} = -cf'(x - ct) = -c \frac{\partial u}{\partial x}$$

$$\sigma = -E \frac{\partial u}{\partial x} = \frac{-E}{-c} \frac{\partial u}{\partial t} = \rho c \frac{\partial u}{\partial t}$$

$$\text{or } \sigma = \rho c v \tag{6.5}$$

Thus  $\sigma$  is linearly related to the particle velocity  $v$ , where  $\rho c$  is the acoustic impedance or the mechanical impedance of the bar denoted by ( $Z$ ).

$$\therefore \sigma = Zv \quad (6.6)$$

When the end of the bar is free, then the shape of the reflected pulse is the same as that of the incident pulse, but inverted; thus a compression pulse will be reflected as a similar pulse in tension.

Consider an impact between two bars of unequal cross-sectional area and made from different materials. If the bar  $s_1$  (Figure 6.2) of speed  $V_1$  impacts the bar  $s_2$  of speed  $V_2$ , where  $V_1 > V_2$  and both travel in the same direction, then the common speed will be  $V_3$  after impact at time  $0 < t < 2\ell_1/c_1$  or  $2\ell_2/c_2$ , where  $\ell_1$ , and  $\ell_2$  are the length of  $s_1$ , and  $s_2$  respectively.

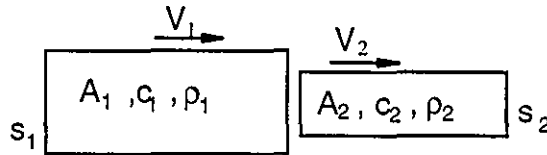


Figure (6.2)

The force acting on both bars at the common interface is the same, and if  $\sigma_1$  and  $\sigma_2$  denote the stresses generated, then

$$\begin{aligned} A_1\sigma_1 &= A_2\sigma_2 \\ A_1Z_1(V_1 - V_3) &= A_2Z_2(V_3 - V_2) \end{aligned} \quad (6.7)$$

Solving this equation for  $V_3$  gives

$$V_3 = \frac{\frac{A_1Z_1}{A_2Z_2} V_1 + V_2}{\frac{A_1Z_1}{A_2Z_2} + 1} \quad (9.8)$$

Substituting  $V_3$  in equation (6.7) and solving the left hand side for  $\sigma_1$  as

$$\begin{aligned} A_1\sigma_1 &= A_1Z_1(V_1 - V_3) \\ \text{or} & \\ \sigma_1 &= Z_1(V_1 - V_3) \end{aligned} \quad (6.9)$$

$$\sigma_1 = Z_1 V_1 - Z_1 \left( \frac{V_2 + \frac{A_1 Z_1}{A_2 Z_2} V_1}{1 + \frac{A_1 Z_1}{A_2 Z_2}} \right)$$

$$\sigma_1 = \frac{Z_1 V_1 \cdot (1 + \frac{A_1 Z_1}{A_2 Z_2}) - Z_1 V_2 - \frac{A_1 Z_1 V_1 \cdot Z_1}{A_2 Z_2}}{1 + \frac{A_1 Z_1}{A_2 Z_2}}$$

$$\sigma_1 = \frac{Z_1 V_1}{1 + \frac{A_1 Z_1}{A_2 Z_2}} \left( 1 + \frac{A_1 Z_1}{A_2 Z_2} - \frac{V_2}{V_1} - \frac{A_1 Z_1}{A_2 Z_2} \right)$$

$$\therefore \sigma_1 = \frac{Z_1 V_1}{1 + \frac{A_1 Z_1}{A_2 Z_2}} \left( 1 - \frac{V_2}{V_1} \right) \quad (6.10)$$

Equation (6.10) corresponds to the stress in the bar  $s_1$  after the impact, and similarly the stress in the second bar can be derived as:

$$\sigma_2 = \frac{Z_2 V_2}{1 + \frac{A_1 Z_1}{A_2 Z_2}} \left( \frac{V_1}{V_2} - 1 \right) \cdot \frac{A_1 Z_1}{A_2 Z_2} \quad (6.11)$$

Consider an incident elastic wave of compressive stress  $\sigma_1$  moving to the right as in Figure (6.3), through the bar  $s_1$  of cross-sectional area  $A_1$ . This wave is partially reflected and partially transmitted at the surface of discontinuity AB where another bar  $s_2$  of cross-sectional area  $A_2$  is perfectly attached to  $s_1$ . If  $A_2$  were zero, the wave would be reflected completely, whilst if  $s_1$  and  $s_2$  were of identical area and material, then the incident wave would be totally transmitted. But since  $s_1$  and  $s_2$  have different areas and are of different materials, then at AB the incident wave must be reflected and transmitted.

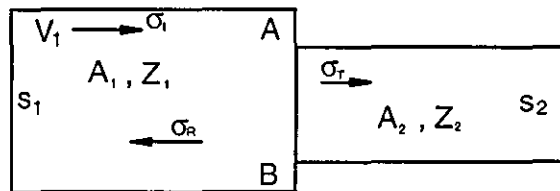


Figure (6.3)

The stress wave transmitted through  $s_2$  is  $\sigma_T$ , and reflected back through  $s_1$  is  $\sigma_R$ . Where the initial stress in  $s_1$  is  $\sigma_i = Z_1 v_i$  at the plane AB the following conditions are satisfied :

i) the forces acting on the plane AB acting from  $s_1$  and  $s_2$  are equal at all times, and,

ii) the particle velocity in plane AB, in the material for  $s_1$  and  $s_2$  are equal.

According to (i) we have, assuming  $\sigma_i$ ,  $\sigma_R$  and  $\sigma_T$  are taken to be compressive, then

$$A_1(\sigma_i + \sigma_R) = A_2\sigma_T, \quad (6.12)$$

$\sigma_i$ , and  $\sigma_R$  are associated with waves travelling in opposite directions, therefore, ii gives

$$v_i - v_R = v_T \quad (6.13)$$

where  $v$  denotes particle speed and subscripts I, R, and T refer to incident, reflection, and transmission. In general the stress ( $\sigma$ ) is related to density ( $\rho$ ), sound speed ( $c$ ), and particle speed ( $v$ ) by:

$$\sigma = \rho c v \quad \text{or} \quad v = \frac{\sigma}{\rho c} = \frac{\sigma}{Z} .$$

Therefore from equation (6.13) we have:

$$\frac{\sigma_i}{Z_1} - \frac{\sigma_R}{Z_1} = \frac{\sigma_T}{Z_2} \quad (6.14)$$

and from equation (6.12)

$$\sigma_i = \frac{A_2}{A_1}\sigma_T - \sigma_R \quad (6.15)$$

$$\sigma_R = \frac{A_2}{A_1}\sigma_T - \sigma_i \quad (6.16)$$

$$\sigma_T = \frac{A_1}{A_2}(\sigma_i + \sigma_R) \quad (6.17)$$

From equations 6.14 and 6.16,  $\sigma_T$  can be expressed as:

$$\frac{\sigma_T}{Z_2} = \frac{1}{Z_1} \left( \sigma_i - \frac{A_2}{A_1}\sigma_T + \sigma_i \right)$$

$$\frac{\sigma_T}{Z_2} + \frac{A_2 \sigma_T}{A_1 Z_1} = \frac{2\sigma_1}{Z_1}$$

or

$$\sigma_T \left( \frac{A_1 Z_1 + A_2 Z_2}{Z_2 A_1 Z_1} \right) = \frac{2\sigma_1}{Z_1}$$

$$\therefore \sigma_T = \frac{2A_1 Z_2}{A_1 Z_1 + A_2 Z_2} \sigma_1 \quad (6.18)$$

In a similar way from equation 6.14 and 6.17, the reflected stress is obtained as:

$$\therefore \sigma_R = \frac{A_2 Z_2 - A_1 Z_1}{A_1 Z_1 + A_2 Z_2} \sigma_1 \quad (6.19)$$

### 6.3 Analysis and computation

From Chapter 3, the theory of SHPB shows that the sample engineering strain  $\epsilon_s$ , strain rate  $\dot{\epsilon}$ , and stress  $\sigma_s$  are given by the following equations:

$$\epsilon_s = \frac{-2c_b}{\ell} \int_0^t \epsilon_R dt \quad (6.20)$$

$$\dot{\epsilon} = \frac{-2c_b}{\ell} \epsilon_R \quad (6.21)$$

$$\sigma_s = \frac{A_b}{A_s} E_b \epsilon_T \quad (6.22)$$

where  $\ell$ , and  $A_s$  are the length and the cross-sectional area of the sample, while  $c_b$ ,  $A_b$ , and  $E_b$  are the wave speed, cross-sectional area and Young's modulus for the bar respectively. The above equations have been derived assuming that stress equilibrium exists in the sample.

The theory in Section 6.2 can be applied to the SHPB system where the sample is a solid cylinder sandwiched between the incident and transmitter bars as shown in Figure (6.4), where:-

$Z_s$  and  $c_s$  are the mechanical impedance and sound speed in the sample, and  $Z_b$  and  $c_b$  are the mechanical impedance and sound speed in the bars.

The cross-sectional area of the sample and the bars are  $A_s = \pi d_s^2 / 4$  and  $A_b = \pi d_b^2 / 4$ , where  $d_s$  and  $d_b$  are the sample and bars diameters respectively.

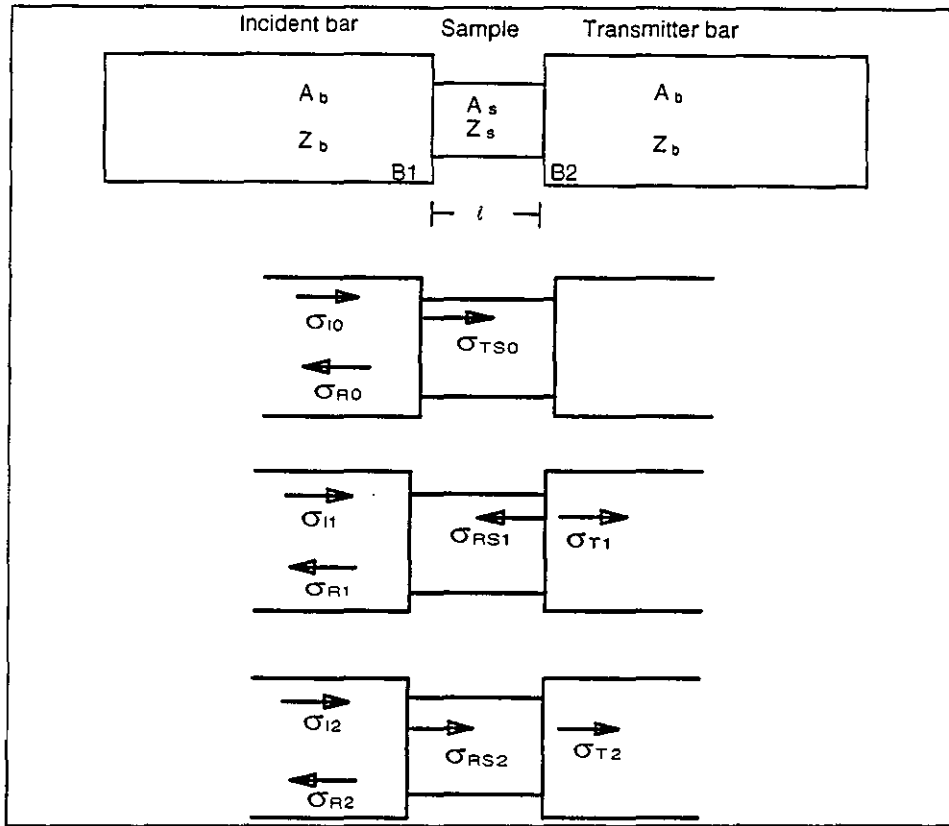


Figure (6.4) Pressure bars and sample.

Consider an elastic stress wave incident on the first interface (B1). The first reflection from this interface occurs at time  $t=0$  as in Figure (6.4), where :

$\sigma_{i0}$  = incident stress,

$\sigma_{r0}$  = reflected stress at B1,

$\sigma_{t1}$  = transmitted stress at the interface B2 at time  $t=l/c_s$ , which is called the traverse time (tt), and,

$\sigma_{rs1}$  = reflected stress at B2 at time tt.

If the incident stress wave has a finite duration, then the stress  $\sigma_i$  may be time dependent.

Using equations 6.18 and 6.19, the transmitted and reflected stresses can be calculated as:

$$\sigma_T = T\sigma_i, \tag{6.23}$$

and,

$$\sigma_R = R\sigma_i \tag{6.24}$$

where T and R are transmission and reflection coefficients and are:

$$T = \frac{2A_1Z_2}{A_1Z_1 + A_2Z_2} \quad (6.25)$$

and

$$R = \frac{A_2Z_2 - A_1Z_1}{A_1Z_1 + A_2Z_2} \quad (6.26)$$

At  $t = 1$  traverse time, the stress is transmitted into the sample. It is important to note at this stage that if  $\sigma_{i0}$  is compressive (+ve), then according to equation (6.18)  $\sigma_{T1}$  will also be compressive (+ve), while from equation (6.19)  $\sigma_{R0}$  may be compressive (+ve) or tensile (-ve) depending on the mechanical impedance  $Z_s$  of the sample and its cross-sectional area  $A_s$ .

Equations 6.18 and 6.19 can be written again for the SHPB as;

$$\sigma_T = \frac{2A_bZ_s}{A_sZ_s + A_bZ_b} \sigma_i \quad (6.27)$$

$$\sigma_R = \frac{A_sZ_s - A_bZ_b}{A_sZ_s + A_bZ_b} \sigma_i \quad (6.28)$$

and the transmission and reflection coefficients can be written at the interface B1 as:

$$T_1 = \frac{2A_bZ_s}{A_sZ_s + A_bZ_b} \quad (6.29)$$

$$R_1 = \frac{A_sZ_s - A_bZ_b}{A_sZ_s + A_bZ_b} \quad (6.30)$$

At the interface B2 the reflection will occur inside the sample, so the coefficient is denoted as  $R_2$  and the transmission coefficient as  $T_2$  (where the stress wave has transmitted partially into the transmitter bar).

$$R_2 = \frac{A_bZ_b - A_sZ_s}{A_sZ_s + A_bZ_b} = -R_1 \quad (6.31)$$

$$T_2 = \frac{2A_sZ_b}{A_sZ_s + A_bZ_b} \quad (6.32)$$

For a compressive incident stress, the transmitted stress will always be compressive; while the reflected stress can be tensile or compressive. Usually  $A_bZ_b > A_sZ_s$  making  $R_1$  negative and  $R_2$  positive (Parry et al (1994)).



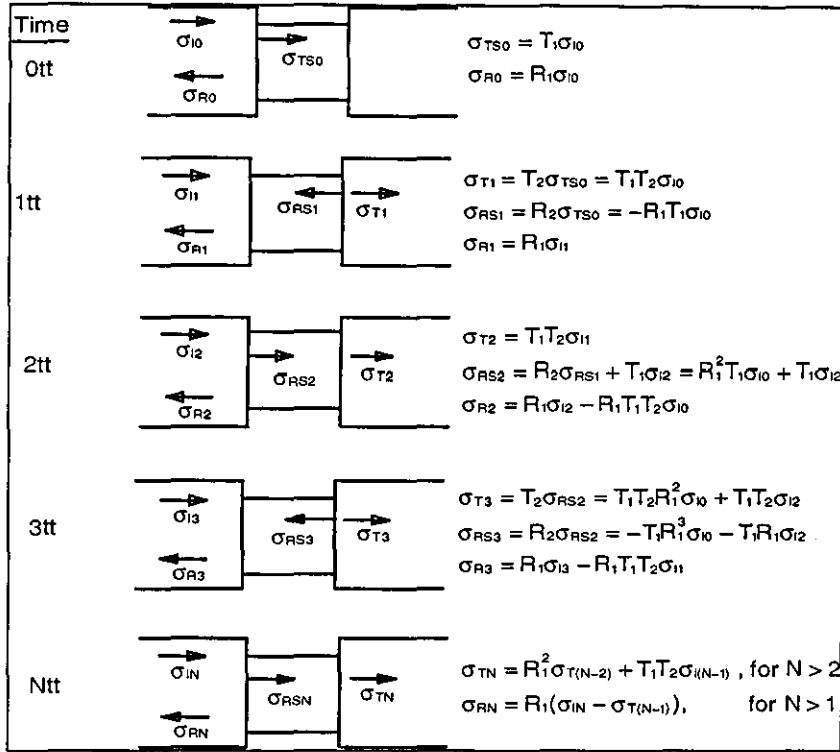


Figure (6.5) The build up of the reflected and transmitted stresses in an SHPB sample.

Figure (6.5) shows the build-up of the reflected and the transmitted pulses in the pressure bars caused by the multiple reflections between the interfaces. The stress expressions of the multiple reflections can be derived for the N'th traverse time as

$$\sigma_{TN} = R_1^2 \sigma_{T(N-2)} + T_1 T_2 \sigma_{I(N-1)}, \text{ where } N > 2 \quad (6.33)$$

$$\sigma_{RN} = R_1 (\sigma_{IN} - \sigma_{T(N-1)}), \text{ where } N > 1 \quad (6.34)$$

The first terms of  $\sigma_{TN}$  series (N=0 to 2) are unique and can be generated independently as:

$\sigma_{T0} = 0$  (no transmitted stress up until the first traversal time).

$\sigma_{TN} = T_1 T_2 \sigma_{I(N-1)}$ , for N = 1 and 2, because up until the third reflection there are no multiple reflections to be considered in the transmitted stress as illustrated in Figure (6.5).

The reflected stress is derived via conservation at the interface B1, and the first term (N=0) for the  $\sigma_{RN}$  series is a special case as no transmitted pulse has yet passed into the transmitted bar, so  $\sigma_{RN}$  can be calculated as:

$$\sigma_{RN} = R_1 \sigma_{IN} \quad , \quad \text{where } N = 0$$

In standard SHPB theory, the transmitted stress  $\sigma_T$  is proportional to the actual stress of the sample. This cannot be correct unless stress equilibrium has been achieved. Stress equilibrium occurs when the equation  $\sigma_I + \sigma_R = \sigma_T$  is satisfied. So, the equilibrium condition can be achieved when the ratio  $\frac{\sigma_T}{\sigma_I + \sigma_R} \cong 1$  is satisfied.

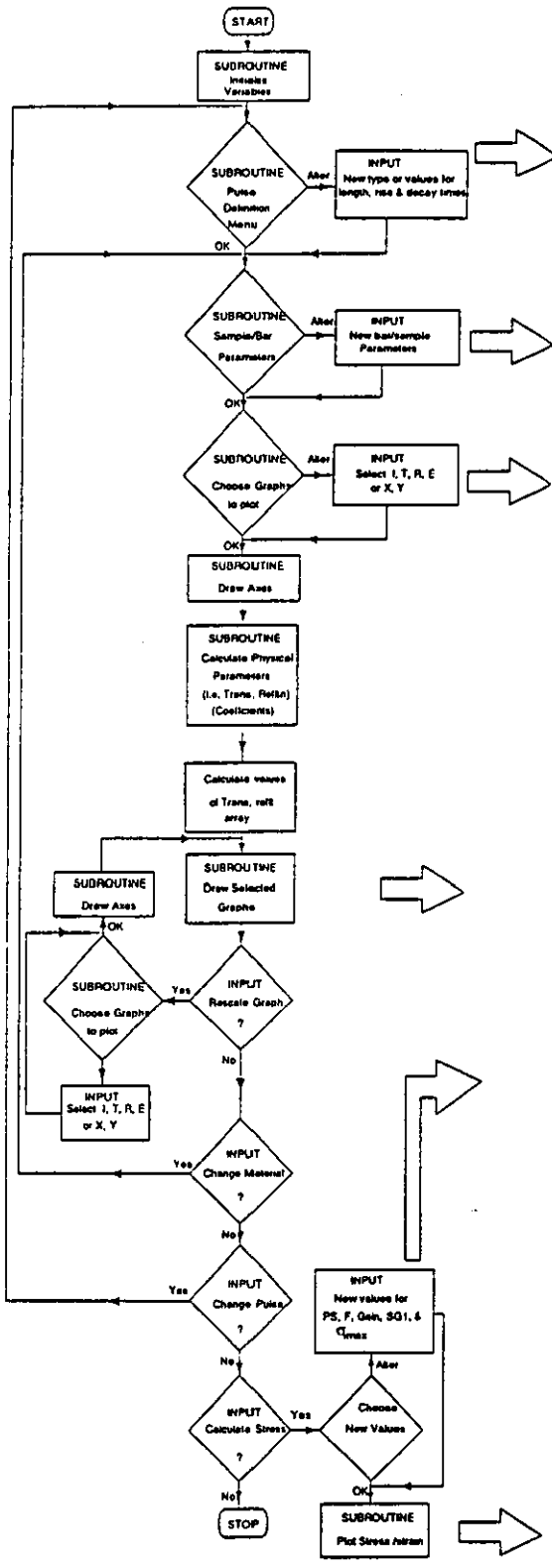
#### **6.4 Computer simulation of SHPB multiple reflections**

A BASIC computer program has been written for generating a step, ramp or smooth pulse with variable rise times, fall times and duration. By knowing the density, dimensions, elastic modulus and sound speed in the sample and the bars, the program predicts the transmitted and reflected pulses within the elastic limit of the sample.

Figure (6.6) shows a flow chart of the SHPB program which is divided into subroutines; the main subroutines generate the incident pulse, calculate the transmitted and the reflected pulses, and produce a plot of the pulses. The menu and the resulting graphs are also shown beside the corresponding subroutine in Figure (6.6).

In a real SHPB test, the pulse consists of a short rise time of about 10  $\mu\text{s}$  with a flat-topped constant loading section and a short decay time. The pulse duration is about 100  $\mu\text{s}$ . The experimental pulse has some oscillations in the flat-topped part (Pochhammer-Chree). However, to a good approximation the pulse is assumed to be flat-topped in this program.

In generating the ramp and the rectangular or step pulses, a linear function has been used for the rise and the fall part combined with the flat top, while the smooth pulse consists of a cosine type rise and fall combined with a flat top.



```

Pulse Definition Menu
-----
1. Type of Pulse      : Smooth
2. Length of Pulse   (us) : 120
3. Rise Time of Pulse (us) : 10
4. Decay Time of Pulse (us) : 12
   (-1 & No decay)

Press (1-4) to alter property
or (SPACE) to continue.
How many points to be saved ? 1200  E

Sample and Bar Definition Menu
-----
(( SAMPLE PROPERTIES ))      (( BAR PROPERTIES ))
1. Density (g/cm3) : 1.139      5. Density (g/cm3) : 7.72
2. Sound Speed (m/s) : 1689.2    6. Sound Speed (m/s) : 5248
3. Diameter (mm) : 8             7. Diameter (mm) : 12.7
4. Length (mm) : 4

Press (1-7) to alter property
or (SPACE) to continue.
Do you want to save the data in a file ? y
Input file name Gshp. 7 Mjst  E

Graph Plotting Menu
-----
(C) PLOT INCIDENT PULSE      : Yes
(E) PLOT TRANSMITTED PULSE   : Yes
(H) PLOT REFLECTED PULSE    : Yes
(X) PLOT T/(C+R) EQUILIBRIUM RATIO : Yes
(Y) CHANGE SCALE OF X-AXIS  : 90 traverse times
(Z) CHANGE SCALE OF Y-AXIS  : 1:1 to 1

Press (SPACE BAR) to plot graph.

Normalized Stress
1.00
0.80
0.60
0.40
0.20
0.00
-0.20
-0.40
-0.60
-0.80
-1.00
Time (in units of traverse times)
0 5 10 15 20 25 30 35 40 45 50 55 60 65 70 75 80 85 90 95 100

Press (R)rescale, (N)ew material, (P)ulse def, (E)xtension/strain or (RETURN) to end.
-----
Stress/Strain parameter Menu
-----
(( Experimental parameters ))
1. PSU voltage (V) : 90
2. SGI voltage (V) : 8.783
3. Gain factor : 2.14
4. SGI Gain : 22.761
5. wave number (V) : .076

Press (1-5) to alter property
or (SPACE) to continue.

90.00
81.00
72.00
63.00
54.00
45.00
36.00
27.00
18.00
9.00
0.00
0.40 0.80 1.20 1.60 2.00 2.40 2.80 3.20 3.60 4.000
STRESS-MPa
STRAIN (%)

Press (R)rescale, (N)ew material, (P)ulse def, (E)xtension/strain or (RETURN) to end.
    
```

Figure (6.6) Flow chart of SHPB multiple reflections program.

The program is designed to be run on IBM PC computer with a display resolution of at least 640x480 Pixels. As shown in the flow chart (Figure 6.6), the program initially defines all the variables, and then asks the user to define the stress pulse, type, duration, rise and fall times if required. By pressing <SPACE BAR> to continue, the program displays the next options menu by which the user can define, if required, the bar and the sample properties e.g. the density, diameter length and sound speed. The next section of the menu is used for plotting any or all of the incident, transmitted, and reflected pulses and the equilibrium ratio

$$\frac{\sigma_T}{\sigma_I + \sigma_R}$$

### 6.5 The pulse parameter and the plot resolution

Defining the incident pulse requires three parameters, the total pulse length, the rise time and the fall time. These limits will be used to generate the pulse array using P points (Hodson (1992)). It is best to use as many points as there are available in the conventional memory of the computer. To convert the pulse parameters from time units to data points, the following expressions have been used:

$$\text{Rise length } ri = \frac{\text{rise time}(\mu\text{s})}{\text{pulse length}(\mu\text{s})} \times P \quad \text{data points} \quad (6.35)$$

$$\text{Decay length } dy = \frac{\text{decay time}(\mu\text{s})}{\text{pulse length}(\mu\text{s})} \times P \quad \text{data points} \quad (6.36)$$

$$\text{The flat top length} = P - (ri + dy) \quad (6.37)$$

These three equations define the data resolution of the three parts of the pulse.

The effective data resolution, the number of points per traverse time **tt**, is then:

$$\text{ptsptt} = \frac{P}{\text{pulse length}} \times \text{tt} \quad (6.38)$$

The pulse plot on the screen is scaled according to the user choice of the number of traverse times on the x-axis (**x<sub>tt</sub>**), when the x-axis total length is 580 pixels:

$$\text{pixels per traverse time } \text{pptt} = \frac{580}{\text{x}_{\text{tt}}} \quad (6.39)$$

The x-axis scaling factor **xscale** is:

$$xscale = \frac{pptt}{ptsptt} = \frac{580}{xtt} \times \frac{\text{pulse length}}{P \times tt} \quad (6.40)$$

To choose a suitable number of points **P** conventional memory should be considered. In an experimental SHPB test, a typical pulse for example has a total length of about 100  $\mu\text{s}$  with a rise time of 10 $\mu\text{s}$  and a fall time of about 12 $\mu\text{s}$ . Performing the calculations for an aluminium sample of 4 mm length and sound speed ( $c_s$ ) of 5000 m/s, gives:

$$\text{traverse time } tt = \frac{4 \times 10^{-3}}{5000} = 0.8 \mu\text{s}$$

The rise phase of the pulse represents a total number of pixels given by:

$$\begin{aligned} \text{rise pixels} &= ri \times xscale = \frac{\text{rise time}}{\text{pulse length}} \times P \times \frac{580}{xtt} \times \frac{\text{pulse length}}{P \times tt} \\ &= \frac{7250}{xtt} \end{aligned} \quad (6.41)$$

The pulse has an average gradient of :

$$\text{gradient} = \frac{y - \text{axis length}}{\text{rise pixels}} = \frac{400}{7250} \times xtt = 0.0552 \times xtt \quad (6.42)$$

Consider a single traverse time exactly at the middle of the rise phase as shown in Figure (6.7). The stress values in the beginning and the end of the traversal can be calculated as:

$$y1 = \text{gradient} \times (\text{rise pixels} - pptt) / 2 \quad (6.43)$$

$$y2 = \text{gradient} \times (\text{rise pixels} + pptt) / 2 \quad (6.44)$$

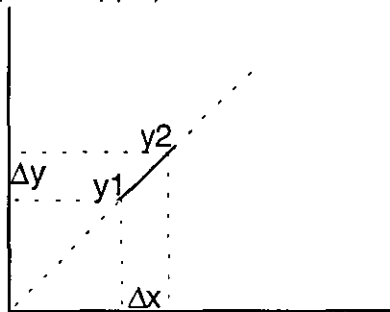


Figure (6.7)

assuming the gradient is constant over this range as in the ramp pulse, which it is for the COS function close to the range of 0,  $\pi$ ,  $2\pi$  etc. - the region we are considering.

$$\Delta y = y_2 - y_1 = \text{gradient} \times \text{pptt} = \text{gradient} \times \frac{580}{\text{xtt}} \quad (6.45)$$

For a typical plot, the x-axis length **xtt** might be 20 traverse times, so,

$$\Delta y = 32.016 = 32 \text{ pixels.}$$

This number of pixels is situated in one traverse time; so over a range of pixels per **tt**

$$\text{pptt} = \frac{580}{\text{xtt}} = \frac{580}{32} = 18.125$$

The number of data points representing these pixels is:

$$\text{ptsptt} = \text{data resolution} = \frac{\text{tt}}{\text{pulse length}} \times P = \frac{0.8}{100} \times P = 0.008 \times P \quad (6.46)$$

From this, it is clear that the data resolution depends linearly on the number of points. From the calculation above,  $\Delta y = 32$  occurs over the range of  $\text{pptt} = 18$ , bearing in mind that it is impossible to have a non - integer pixel number. In the case of poorest resolution at least two points are required to plot the line at one traverse time, and that gives:

$$2 = 0.008 \times P$$

$\therefore P = 250$ , for the minimum case.

For higher resolutions we require a much greater number of points, identical to the number of pixels. For the data resolution of 32, the value of  $P$  will be:

$$32 = 0.008 \times P$$

$\therefore P = 4000$

This value of  $P$  requires a lot of memory, as the array `pulse(P)`, the data array `refl(3P)` and `trans(3P)` array make a total of 28000 data points.

Between these two extremes, 2500 points have been chosen as the number to be used in the program. This allows the program to run with no problems using a 640kByte conventional computer memory. To have a suitable sampling rate for the saved data, equal to pulse length/number of points, the number of points and the length of the pulse should be chosen correctly.

## 6.6 Results and discussion

Understanding the way the SHPB system operates helps to make some predictions about the nature of the computed results, such as:

- 1) The transmitted pulse always has the same sign as the incident pulse as can be seen from Equation (6.27) while from Equation (6.28), the reflected pulse does not always have the same sign, but rather depends on the value of the cross-sectional area and the impedance of the sample compared with those of the bars. If  $A_s Z_s < A_b Z_b$ , the reflected pulse will be of opposite sign to the incident pulse.
- 2) After the stress pulse passes through the sample the multiple reflections inside the sample take a long time to decay, hence equilibrium no longer exists between the bar and the sample until the time tends to infinity. So the equilibrium ratio  $\sigma_T / (\sigma_I + \sigma_R)$  will oscillate with a period of  $2tt$  -the time required for the pulse to return to the interface.
- 3) Because of the time required for the pulse to propagate through the sample, the transmitted pulse starts one traverse time ( $tt$ ) after the reflected pulse. This delay can be compensated experimentally by appropriate positioning of the strain gauges, but would be inconvenient for samples of different thicknesses.
- 4) In general, the smaller the cross-sectional area of the sample, the greater the reflected pulse and the smaller the transmitted pulse.
- 5) The trend for all the computed results is that the normalised transmitted pulse tends to 1 and the reflected pulse vanishes to zero (Dixon (1990)). The time this process takes depends on the cross-sectional area and the mechanical impedance of the sample and bars.

The program may be used to produce a number of stress wave curves for different  $A_s, Z_s, A_b,$  and  $Z_b$  values, and square, ramp, and smooth pulse types with different rise time, fall time and duration. In the Loughborough University SHPB system the fixed values of the bars are diameter  $d_b=12.7\text{cm}$ ,  $c_b=5240\text{m/s}$  and  $\rho_b=7.72\text{g/cm}^3$  for 431-steel bars or  $\rho_b=8.05\text{ g/cm}^3$  and  $c_b=4818\text{ m/s}$  for maraging-steel bars.

The first test simulation compares the transmitted, reflected and equilibrium pulses using a fixed bar (431 steel) and a fixed sample length of 4 mm, but varying the pulse shape using 2:1 or 4:1 cross-sectional area ratios. The pulse shapes tested are the square pulse (zero rise time and fall time), and the smooth pulse with rise and fall time near the experimental values of 10 $\mu$ s and 12 $\mu$ s respectively. The ramp pulse was not used because it lies between the previous two pulses with a linear gradient rise time. These pulses were tested with the same length of 120 $\mu$ s, and used to produce graphs for different material such as HDPE, Nylatron, PEEK, and CFC (carbon fibre composite).

Figure (6.8a,b) shows the transmitted pulses  $\sigma_T$  and the reflected pulses  $\sigma_R$  using a smooth loading pulse  $\sigma_I$  of 120 $\mu$ s duration, 10 $\mu$ s rise time, and 12 $\mu$ s fall time. The samples tested in this simulation are HDPE(H) ( $E=2.30$  GPa,  $\rho=924.70$  kg/m<sup>3</sup>,  $c=1577$  m/s), Nylatron(N) ( $E=3.25$  GPa,  $\rho=1139.15$  kg/m<sup>3</sup>,  $c=1689.2$  m/s), PEEK(P) ( $E=3.30$  GPa,  $\rho=1312.00$  kg/m<sup>3</sup>,  $c=1586.00$  m/s), and CFC(C) ( $E=10.56$  GPa,  $\rho=1570.00$  kg/m<sup>3</sup>,  $c=2593.50$  m/s) with cross-sectional area ratios  $A_b/A_s=2$  and 4. Figure (6.9a,b) shows the reflected and transmitted pulses obtained using a rectangular loading pulse (4mm sample). Figures (6.8) and (6.9) show that the rectangular incident pulse has a higher initial reflection; this is due to a large mismatch in stress because this pulse has an infinite gradient at its half-period points. The higher the material impedance the higher the transmitted pulse and the smaller the reflected pulses, and these pulses recover faster than those in lower material impedance such as HDPE. For Figures (6.8) and (6.9) the samples have the same length of 4 mm, so the traverse times for HDPE, Nylatron, PEEK, and CFC are 2.536, 2.368, 2.522, and 1.542  $\mu$ s respectively. The transmitted pulses for all the materials are delayed by one traverse time after the reflected pulse; this delay is the propagation time required for the stress wave to pass through the sample from one face to the other.

The extreme square pulse is not ideal for drawing comparisons between the experimental and predicted results because the square pulse generates a high oscillation and the stress takes too long to reach equilibrium. Thus, the fundamental theory of the SHPB is not satisfied, since equation  $\epsilon_T = \epsilon_I + \epsilon_R$  is only applicable if force equilibrium exists at the sample-bar boundaries.

Figures (6.10) shows the equilibrium ratios for smooth pulse predictions for HDPE, Nylatron, and CFC with a cross-sectional area ratio of two. Figure (6.11)



shows the equilibrium ratios for CFC, and HDPE with cross-sectional area ratios of 2 and 4 using a rectangular loading pulse. These figures show that in hard materials like CFC the equilibrium is reached faster than in soft materials like HDPE. The time taken for  $\sigma_T / (\sigma_I + \sigma_R) = 1$  is important for correct stress-strain analysis. The results show that for the smooth incident pulse the equilibrium time is less than for the square pulse due to the continuity of the smooth pulse function. From the graph of the equilibrium ratio it can be seen that for the rectangular pulse (and also for short rise time pulses), the ratio curve rises quickly to a value greater than one; the initial reflected pulse is highly negative (tensile) as mentioned before and this reduces the denominator of the equilibrium expression, the ratio oscillates and settles down to unity as the stress mismatch is decreased at each reflection.

The transmitted pulse graph in Figure (6.12) and the reflected pulse graph in Figure (6.13) for HDPE, Nylatron, and CFC show that with increasing area ratio, greater dispersion of the incident pulse is seen. This occurs because a high area ratio increases the fraction of the pulse that will be reflected from either interface between bar and sample, and hence more multiple reflections will occur which leads to greater dispersion and less transmission. In particular, a large proportion of the incident pulse will be reflected if the area mismatch is great.

Another interesting observation is that for high area ratios the reflection takes longer to die out after the incident pulse has finished. This is due to more of the pulse being reflected at a higher area mismatch. The forces either side of the interface are more likely to be equal due to less stress being lost through transmission, so the magnitude of the equilibrium ratio oscillates again.

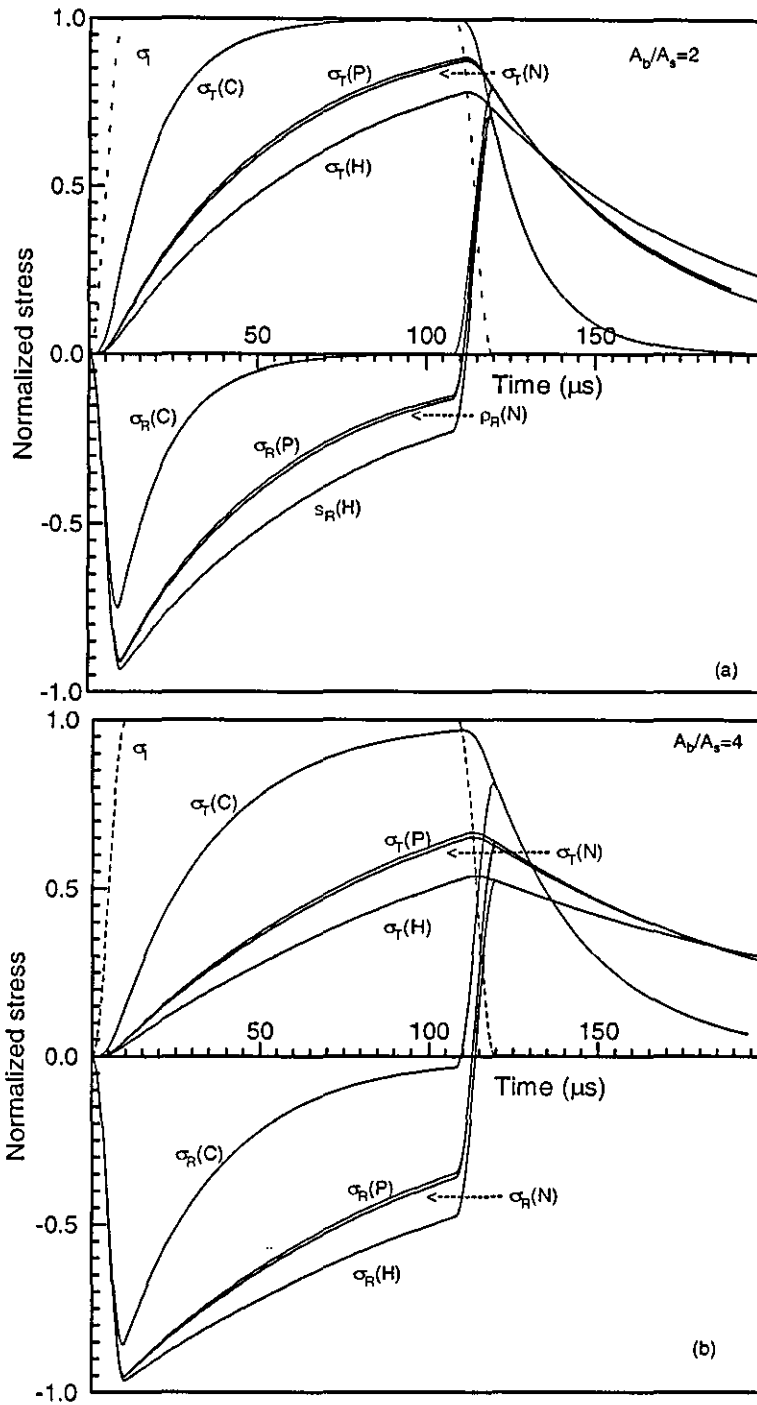


Figure (6.8) The predicted stress pulses for HDPE(H), nylatron(N), PEEK(P), and CFC(C) samples using a  $10\mu\text{s}$  rise time and  $12\mu\text{s}$  fall time smooth incident pulse of  $120\mu\text{s}$  duration with cross-sectional area ratios of (a) 2, and (b) 4.

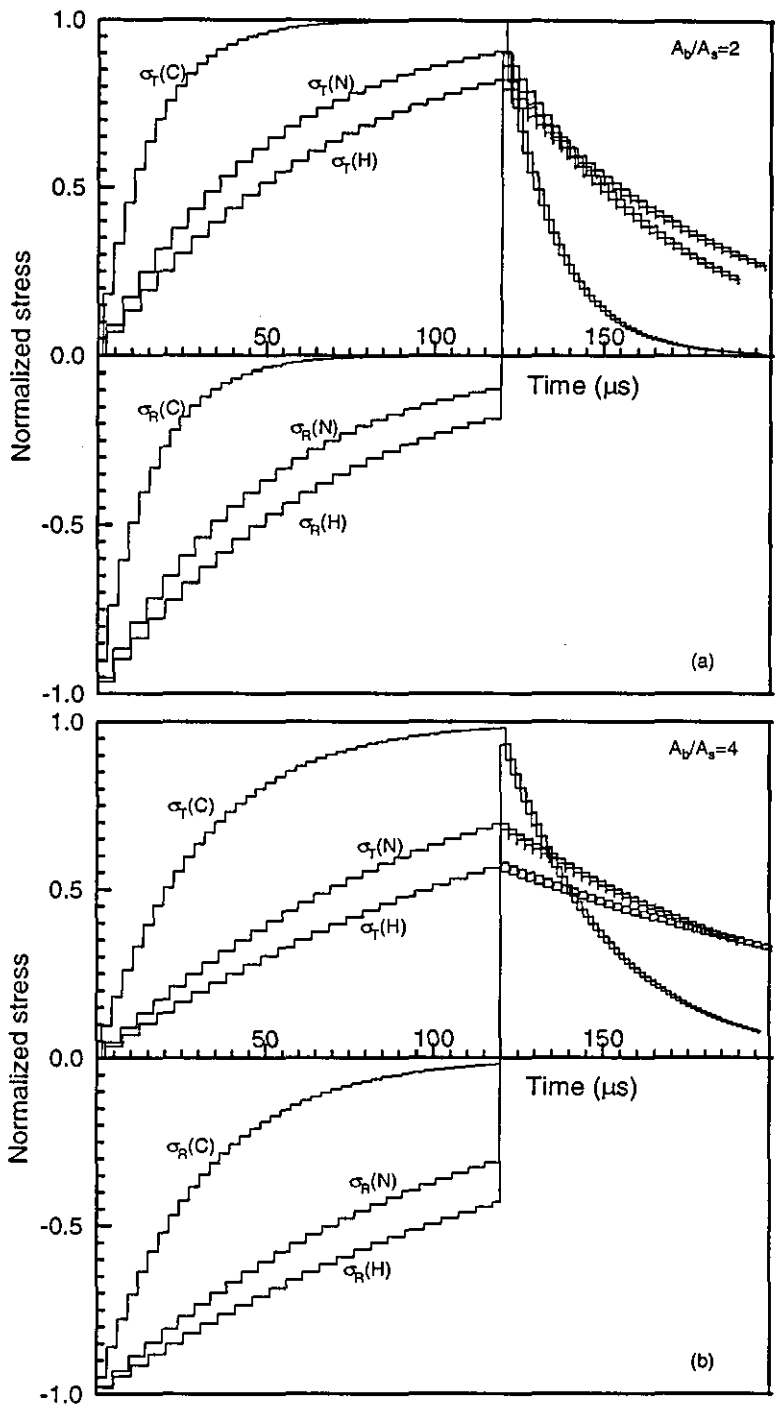


Figure (6.9) The predicted stress pulses for HDPE(H), nylatron(N), and CFC(C) samples using a rectangular incident pulse of  $120\mu\text{s}$  duration with cross-sectional area ratios of (a) 2 and (B) 4.

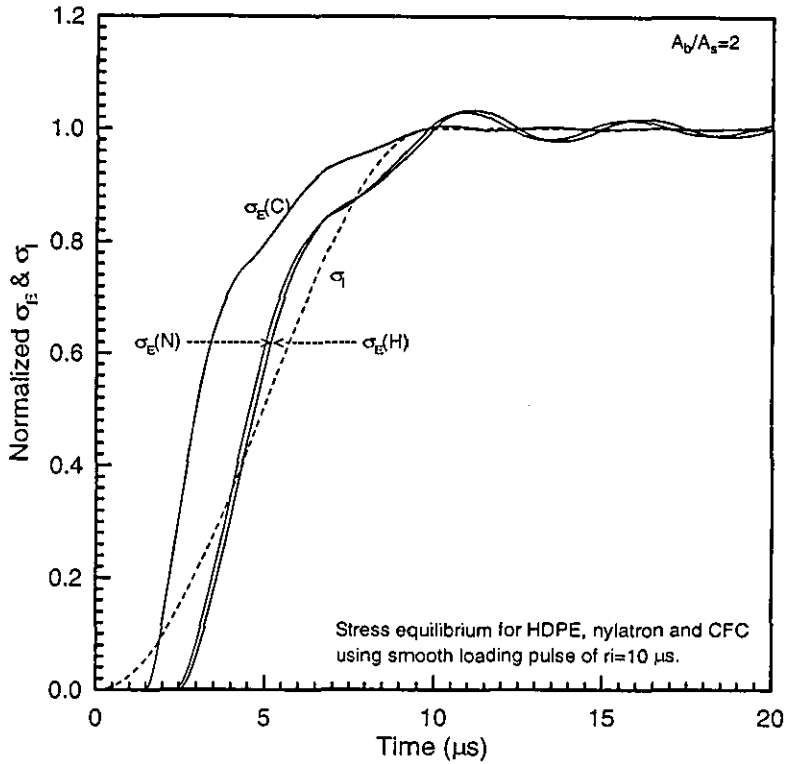


Figure (6.10) Stress equilibrium  $\sigma_E$  for 4 mm length HDPE(H), nylon(N), and CFC(C) samples using  $10\mu\text{s}$ -rise time smooth incident pulse.

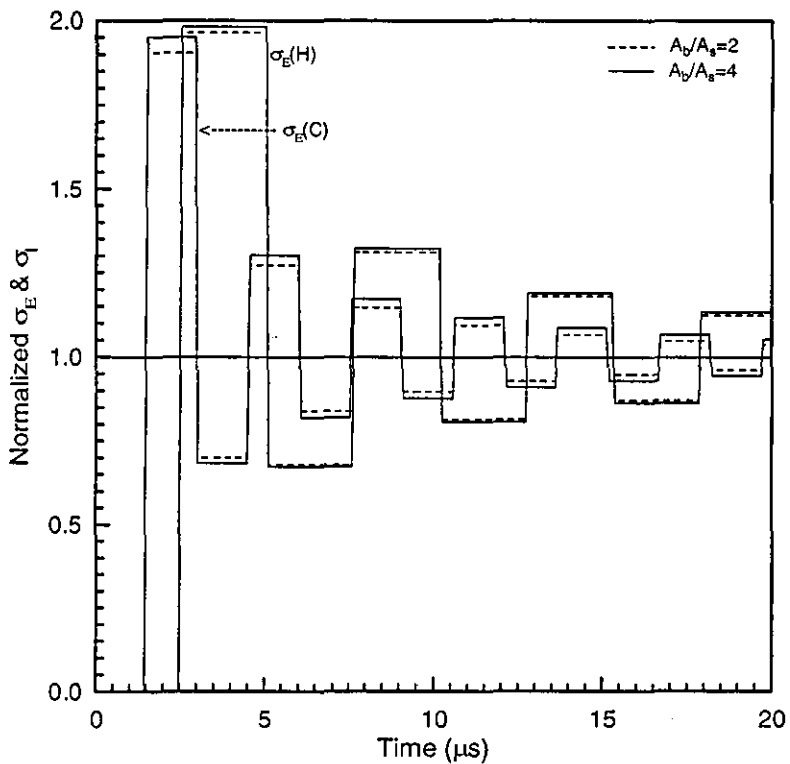


Figure (6.11) Stress equilibrium  $\sigma_E$  for 4 mm length HDPE(H) and CFC(C) samples using a rectangular incident pulse.

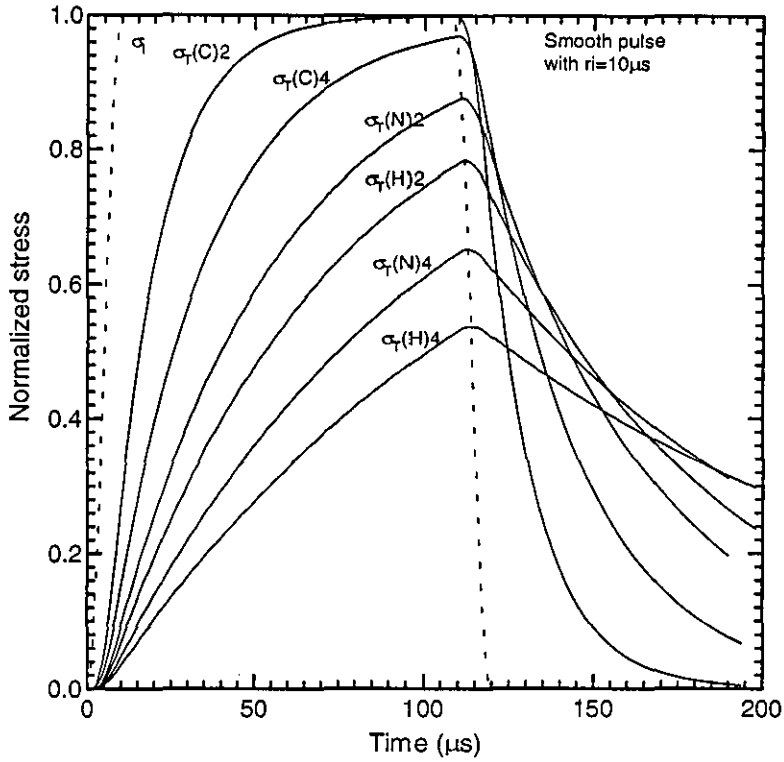


Figure (6.12) The predicted transmitted pulses for 4 mm length HDPE(H), nylatron(N), and CFC(C) samples with cross-sectional area ratios of 2 and 4.

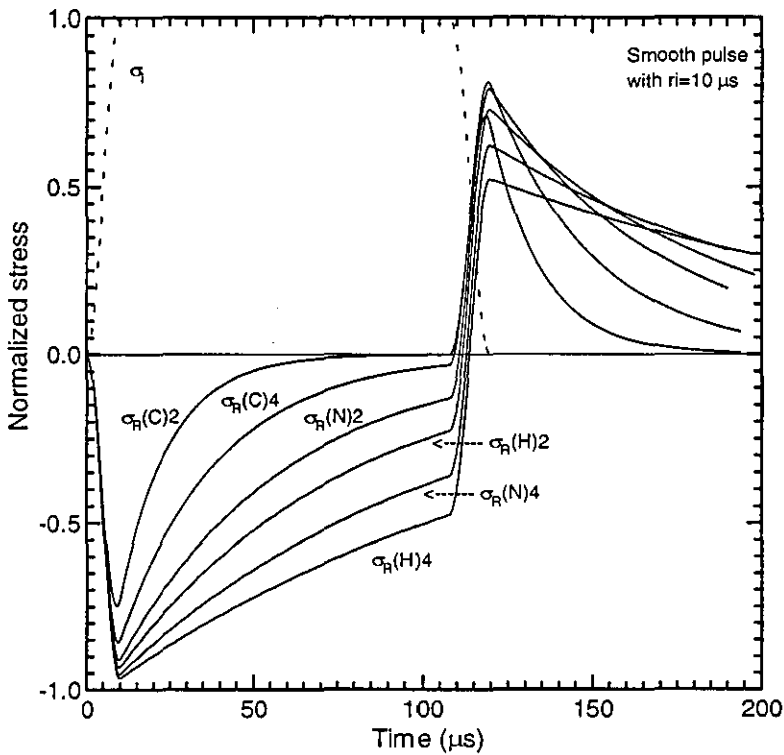


Figure (6.13) The predicted reflected pulses for 4 mm length HDPE(H), nylatron(N), and CFC(C) samples with cross-sectional area ratios of 2 and 4.

## **6.7 Comparison with experimental results**

These theoretical predictions were compared with the experimental results. Figures (6.14a), (6.15a), and (6.16a) show the experimental SHPB pulses for samples of Nylatron, Poyetheretherketone(PEEK), and a quasi-isotropic carbon-fibre/thermoplastic composite (CFC supplied by ICI), while Figures (6.14b), (6.15b), and (6.16b) show the predicted corresponding pulses using the actual sample dimensions and a smooth incident pulse of the same shape (omitting any oscillations), amplitude and duration as the actual pulse. The experimental pulse was restricted to an appropriate level of amplitude to enable the material response to remain within the elastic region.

The wave speed in each sample was obtained from the experimentally measured Young's modulus. A normal SHPB analysis was carried out for the predicted data, after conversion from normalised values by multiplying the data by the maximum value of the experimental incident pulse. Any sampling rate can be used by selecting the ratio pulse length/number of points, which equals the time interval for the predicted data.

Figures (6.14a, and b) show the experimental and the predicted pulses for Nylatron sample ( $d=8.17\text{mm}$ ,  $\ell=4.072\text{mm}$ ,  $\rho=1.139\text{ g/cm}^3$ ,  $E=3.25\text{ GPa}$ , and  $c_s=1687.2\text{ m/s}$ ). Analysis of these pulses shows a good agreement between the theoretical and the experimental stress-strain plots, as in Figure (6.14c). Both theoretical and experimental plots give the same value of Young's modulus (the same value used to predict the theoretical data). A similar analysis has been made for PEEK (Figure (6.15a, b, and c), and CFC (Figures 6.16a, b, and c).

As mentioned previously, the predicted transmitted pulse always comes one traverse time after the reflected pulse. Analysing these pulses with no shifting of the starting points of the transmitted pulses (one traverse time delay), gives stress-strain curves with a smaller Young's modulus than the actual values which were used. Shifting the transmitted pulse one traverse time to start at the same time as the reflected pulse gives a higher value of Young's modulus. The best results for measured values of Young's modulus are at half traverse time shifts as shown in Figures (6.14c, 6.15c, and 6.16c). This point should be considered by experimenters using the SHPB system. Table (6.1) shows the measured values used for Nylatron, PEEK, and CFC. The  $c_s$  values are obtained from the measured values of  $E$ .

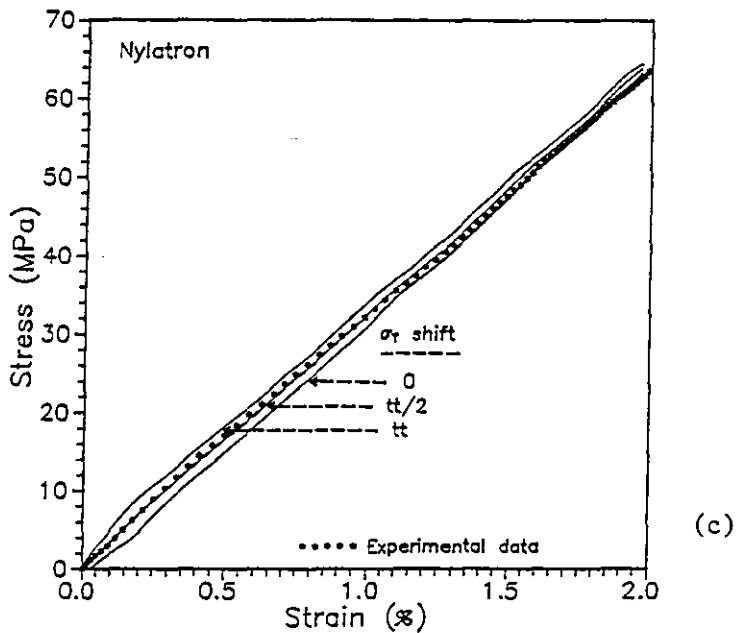
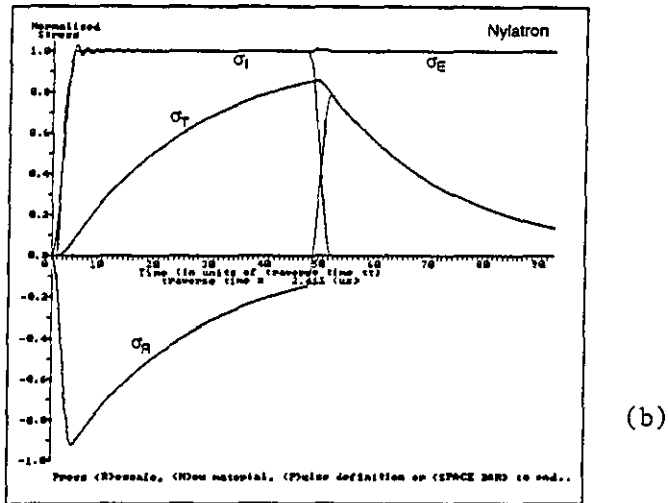
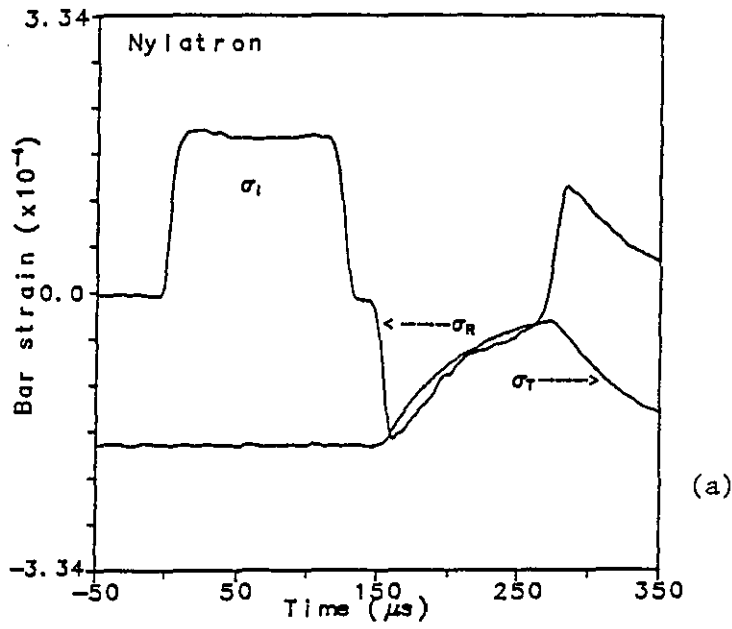


Figure (6.14) (a) Experimental pulses for nylatron; (b) predicted pulses; (c) comparison of the theoretical and experimental stress/strain plots.

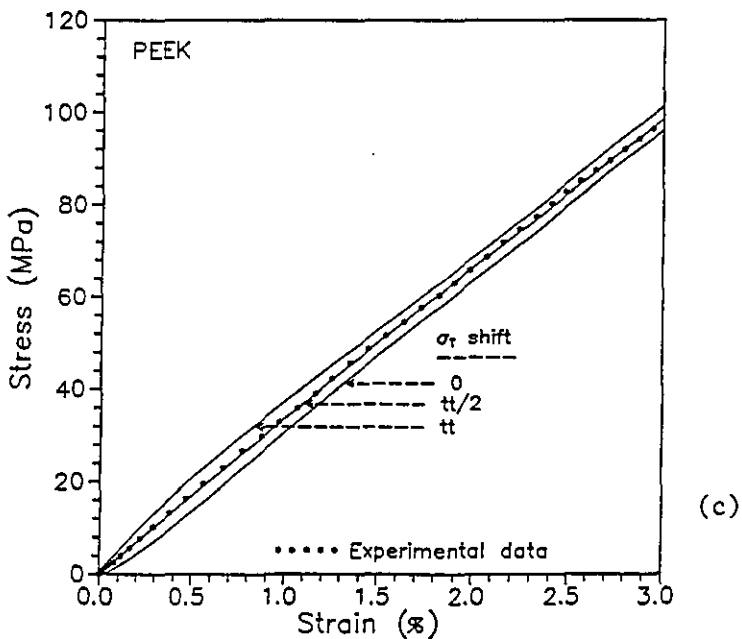
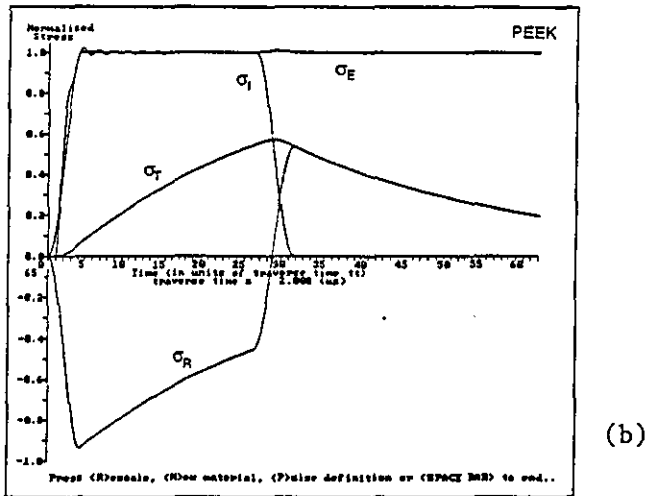
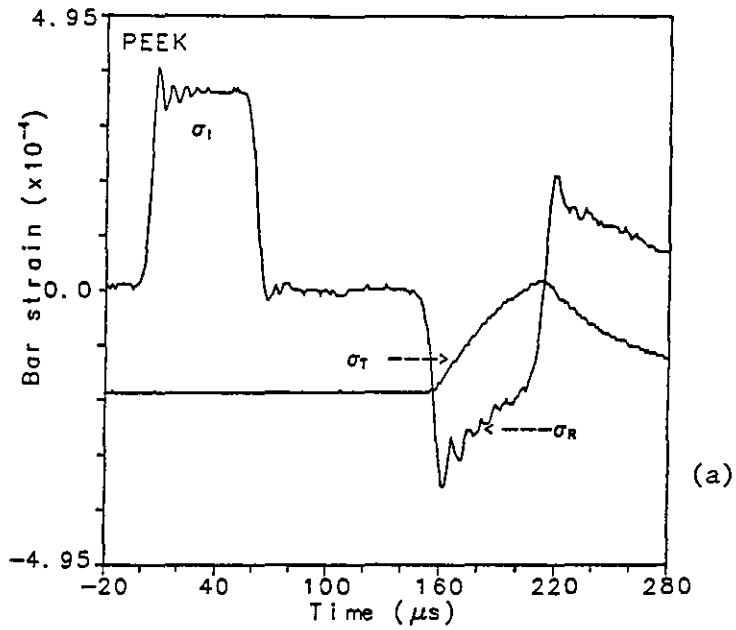


Figure (6.15) (a) Experimental pulses for PEEK; (b) predicted pulses; (c) comparison of the theoretical and experimental stress/strain plots.



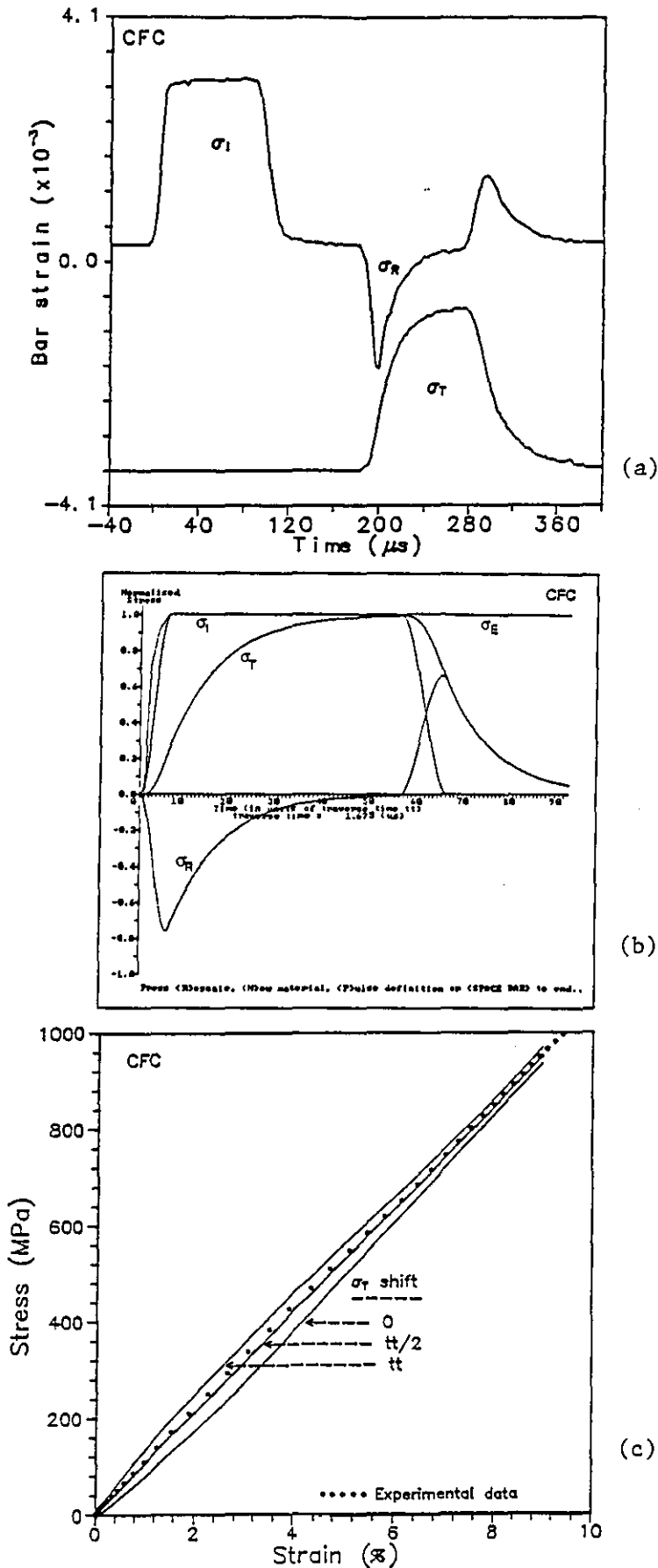


Figure (6.16) (a) Experimental pulses for CFC; (b) predicted pulses; (c) comparison of the theoretical and experimental stress/strain plots.

Table (6.1)  
The measured values used to predict the stress pulses  
for Nylatron, PEEK and CFC.

Material	$\rho_b$ (kg/m <sup>3</sup> )	$C_b$ (m/s)	$l_s$ (mm)	$D_s$ (mm)	$\rho_s$ (kg/m <sup>3</sup> )	$C_s$ (m/s)
Nylatron	7720	5240	4.072	8.17	1139.15	1689.2
PEEK	7720	5240	3.184	6.892	1312.0	1586.0
CFC	8050	4818	4.345	8.20	1570.0	2593.5

## 6.8 Conclusions

Profiles of transmitted and reflected SHPB-like waves have been successfully predicted when a flat-topped incident wave of known rise time is simulated by a computer program. The program indicates the time taken for stress equilibrium to occur in the sample, when the stress on the first face of the sample equals that on the second face for a given set of bar and sample parameters. Consideration of the time it takes to achieve the equilibrium is highly pertinent to SHPB testing, since the theory assumes it is achieved instantaneously. Thus the results of the program may be able to explain any observed differences in the rate of the build-up of the transmitted and the reflected pulses. The transmitted stress is regarded as being proportional to the actual sample stress in standard SHPB theory, but this cannot be true before stress equilibrium has been achieved. A realistic measure of the sample stress in the first few microseconds after the arrival of the incident pulse at the sample is a mean of the stresses on the first face ( $\sigma_i + \sigma_R$ ) and the second face ( $\sigma_T$ ) of the sample. With this in mind, it is interesting to note that other investigators have found the elastic modulus value (determined by the computer analysis) was always less than the actual value. This is probably due to the non-equilibrium conditions which prevail during the first few microseconds.

The results show that the pulse shape has a marked effect on the time taken for the sample to reach equilibrium at its boundaries. The smooth pulse produces results with a more realistic shape for the reflected and transmitted pulses, and equilibrium is achieved faster than for the square incident pulse, thus the program is nearer to the proper physical model of the SHPB system.

The cross-sectional area ratio also effects the equilibrium condition as shown by the results; the smaller the ratio the faster equilibrium will be achieved.

Using the normal SHPB method to analyse the theoretical pulses in the same way as the experimental ones, ignoring the sample thickness gives a stress-strain with zero shift as shown in Figures (6.14c, 6.15c, and 6.16c). These analyses show that the starting of the reflected pulse before the transmitted pulse causes the initial parts of the plots to have a downward curvature in the stress-strain graph, making the Young's modulus less than the actual value. Shifting the transmitted pulse forward by one traverse time ( $t_t$  shift) (so it starts at the same time as the reflected pulse), produces a stress-strain curve with an initial upward curvature making the modulus higher than the actual value. However, if the transmitted pulse is shifted forward by half a traverse time ( $t_t/2$  shift), the stress-strain curve becomes a straight line through the origin with a constant slope equal to the actual value of Young's modulus used previously to predict the pulses.

Practically, when a  $t_t/2$  shift is used with SHPB analysis of the experimental traces, the results show good agreement with the corresponding theoretical stress-strain results.

The theoretical analysis described in this chapter has been shown to predict accurately the shape of the experimental pulses resulting from wave reflections at SHPB sample. It also indicates that elastic stress equilibrium is effectively achieved within a sample after a few wave reflections, irrespective of the type of material.

In metallic materials the traverse times are as short as  $1\mu\text{s}$ , so they are likely to produce a smaller error in calculating the Young's modulus; in non-metallic materials such as polymers these traverse times cannot be neglected and will have a significant bearing on the interpretation of the incident and transmitted pulses, as will any non equilibrium effects. The program could prove helpful in choosing the appropriate point at which the transmitted pulse may be compared with the reflected pulse for a valid computation of stress-strain and stress or strain versus time. Also the program can be used to design a suitable incident pulse shape in order to control the strain rate. The typical pulses in the Loughborough SHPB system have a rise time of about  $10\mu\text{s}$ . This rise time can be made longer to produce a lower strain rate within the sample by placing a dummy sample in an extra split in the Hopkinson bar in front of the actual sample under test (Ellwood (1983)).

## **CHAPTER 7**

### **EXPLODING WIRE TECHNIQUE**

#### **7.1 Introduction**

In addition to low strain rate testing using the Hounsfield machine, and the high strain rate tests using the split Hopkinson pressure bar (SHPB), an exploding wire technique has also been used by the author to provide high strain rates. The exploding wire technique (EWT) provides a high rate of loading by producing cylindrical blast waves of high reflection pressure with short duration. These waves are used for internal loading of hollow polymeric cylindrical samples. The EWT overcomes the small size restrictions of other high strain rate methods like the SHPB.

A further development of the EWT is the freely expanding ring technique for studying the tensile stress-strain behaviour of materials. The technique requires a thin ring to be placed as a sliding fit on a thick-walled cylinder. The cylinder protects the ring from the temperature of the explosion and enables free flight of the ring to take place after the explosion inside the cylinder. From the ring deceleration, in the absence of a driving pressure, the true stress can be calculated.

#### **7.1.1 Exploding wires**

The exploding wires technique is used by several researchers such as Bennett (1958a,b, 1962, 1965, and 1971) and also with co-workers (1970, 1974) who studied exploding wire effects. Streak cameras as well as oscillographic systems were used to monitor the wire explosion process and the shock wave expansion in air. Bennett also determined the temperature behind the head of the shock wave generated by an exploding wire by employing blast wave theory. He and his co-workers developed some geometrical techniques and mathematical relations upon which subsequent analyses of metal flow in the exploding wire are based.

Cassidy et al (1968) used the exploding wire in their investigation as a source for high temperature studies. In their studies Cassidy and co-workers found that pulsed electrical discharges in metal wires produce high energy molecules and ions corresponding to high temperature.

Schofer et al (1977) recorded the pressure profile of shock waves of underwater wire explosions, using piezoresistive pressure probes at different distances from the wire.

Nakumura et al (1980) used a Schlieren system with high sensitivity and a high speed camera to measure high velocity flow propagating through gases due to a shock wave produced by wire explosions in air. So-Young and Kim (1984) employed oscillographic recordings and Schlieren - streak photography to observe the dwell, explosion, and arc discharge stages.

Isuzugawa and Fujimura (1982) proposed a simulation model considered to be appropriate to the behaviour of a copper wire heated by the passing of an impulse current until the wire's temperature reaches boiling point at atmospheric pressure when it violently evaporates.

Suhara (1986) initiated an arc discharge by exploding a wire in a static short gap between two electrodes. This experiment was performed to describe the voltage-current characteristics of the discharge and to calculate the arc duration time of opening electrical contacts for inductive circuits.

Yakimura (1987) gave an estimation of the pressure and energy of shock waves produced by a thin wire disintegration during the vaporisation stage. He compared the results obtained in air explosions with those for underwater explosions.

### **7.1.2 Expanding cylinders**

The high amplitude stress waves produced by the exploding wire technique were first used by Ensminger and Fyfe (1966) in a study of the behaviour of hollow cylinders. Swift and Fyfe (1970) used the exploding wire technique in two types of experiment to examine elastic/viscoelastic constitutive theory in radial cylindrical configurations. One experiment examined the plane strain plastic response of hollow cylinders subjected to an internal finite rise-time pressure pulse; the other experiment examined the decay behaviour of the cylindrical elastic precursor associated with high stress level impact loading. They considered the viscoplastic strain rate function in a linear and exponential form. Dynamic fracture of thick hollow cylinders has been studied by Schmit and Fyfe (1973) and Forrestal et al (1980) using the exploding wire technique. In their

investigation they examined the influence of biaxial strain on the dynamic fracture of metals.

Dirwish (1979) used a method proposed by Ensminger and Fyfe (1966) to measure the small displacements of the outer surfaces of thick nylon cylinders subjected to internal pressure waves due to the reflection of blast waves from an exploding wire. This involved monitoring the cylinder displacement using a laser beam which was interrupted by the outer surface of the cylinder. Ahmad (1988) used a strain gauge method to study the deformation of polymer cylinders by using exploding wires to provide a high internal impact loading.

Griffiths, Parry and Stewardson (1986), Parry et al (1988, 1990), Al-Maliky (1991), and Al-Maliky and Parry (1994, 1996) used an exploding wire as a method for impact loading to study material behaviour up to and including fracture. They produced a radial stress wave of high amplitude (>1 kbar), short rise time (< 2 $\mu$ s) and short duration ( $\approx$ 5 $\mu$ s) in hollow cylindrical samples.

### **7.1.3 Expanding rings**

The expanding ring method was used by Clark and Duwez (1950) to test materials at high strain rates. They placed a ring around a thin-walled hollow cylinder and obtained a uniform high strain rate by inducing a circumferential strain using a piston moving at a constant velocity to produce an internal fluid pressure. This gives the stress  $\sigma$  as

$$\sigma = p \frac{r_a}{d} \quad (7.1)$$

where  $p$  is the pressure,  $d$  is the wall thickness, and  $r_a$  is the average radius of the cylinder.

Forrestal and Walling (1972, 1973) used a magnetic pressure pulse caused by a current discharge to impulsively load an aluminium ring with an axisymmetric short duration pressure pulse. They measured the ring response by strain gauges and made comparisons between the measured strain-time history and two theoretical predictions, one using an elastic-perfectly plastic stress-strain law, and the other using a law suggested by Lindberg (1968, 1970). The first prediction gave the closest comparison to their measured results. Walling et al (1972) utilised a fast discharge capacitor bank and a current pulse shaping

technique to provide a pressure pulse with a duration of about  $2\mu\text{s}$  to be used as an impulsive loading system for structural rings.

Niordson (1965) developed a dynamic deformation method for a ring using the electromagnetic force generated by a 24 windings coil supplied by a discharge current from a  $12\mu\text{F}$  capacitor.

Hoggatt et al (1967, 1969) used the deformation caused by an explosive charge to study the behaviour of materials under impact conditions, using the freely expanding ring method.

Carden et al (1980) used an expanding ring method in which they subjected an aluminium ring to uniaxial loading by an electromagnetic pressure pulse to obtain the stress-strain dependence from the radial velocity versus time behaviour measured by a VISAR system. In 1981 Daniel et al tested a composite material at strain rates in the range of  $100\text{s}^{-1}$  to  $500\text{s}^{-1}$  employing thin ring samples loaded by an internal pressure pulse applied explosively through a liquid. Their analysis was based on a numerical solution of the equation of motion and involved smoothing and approximation of strain data, strain rate, and strain accelerations.

The expanding ring method was improved by Warnes et al (1981) and then in 1985 for determining dynamic material properties by using a direct velocity measuring device (laser velocity interferometer) to measure the velocity of the expanding ring. They determined the stress-strain behaviour of copper at large strains and high strain rates by pressing the ring onto a high strength steel driving cylinder. In their experiments they used three rings instead of one to reduce the time required for the central ring (under test) to achieve the one dimensional motion necessary for the stress equation to be correctly applied.

The properties of copper and tantalum rings have also been studied by Gourdin (1989a,b) and Gourdin et al (1989) at high strain rates using the electromagnetically expanding ring method. The magnetic pressure pulse was produced by a capacitor discharge current passed through a solenoid around which the ring under test was placed. The speed of expansion of the ring was recorded by a velocity interferometer (VISAR) system.

The main purpose of using the exploding wire in the work described in this thesis is to generate shock waves of high amplitude which can be used for loading HDPE, UHMWPE, nylatron and PEEK to study their behaviour under impact conditions.

## **7.2 Loughborough system**

### **7.2.1 The exploding wire set-up**

Basically the exploding wire system consists of a charging unit, switch and capacitor as shown in Figure (7.1) (see Al-Maliky (1991), Al-Maliky and Parry (1994, 1996)). The Loughborough University / Department of Physics exploding wire facility consists of two separate groups of equipment. The first one is the control unit in the main laboratory. This controls the second group which is inside a room called the exploding wire laboratory and which contains the charging units, the capacitor bank, and the flash gun. The charging unit contains a variac transformer which is supplied by 240 V mains AC through fortress safety and mode selector switches. The variac is followed by a DC unit which charges the capacitor bank through a series of high resistors of 100k $\Omega$  in total and 180 W each. These resistors limit the current through 10 rectifiers.

The capacitor bank has a capacitance of 13.2 $\mu$ F, a combined inductance of 30nH, and a maximum current rating of 500 kA peak. It can be operated at a maximum voltage (energy) of 40 kV (10 kJ). The capacitor windings use an oil/paper dielectric system housed in a metallic rectangular case with dimensions of 1.12 x 0.4 x 0.39 m. The capacitor elements are connected in parallel to H.T terminals in the centre of an insulating lid to obtain a low inductance configuration by using external parallel plate transmission lines.

The charging and discharging of the capacitor was made through contactor switches which were controlled by the control unit by means of position sensors and two-way valves which employ pressurised dry air supplied from two gas cylinders. The discharging switches, called earth switches, are used for bleeding the residual charge on the bank to earth after the experiment.



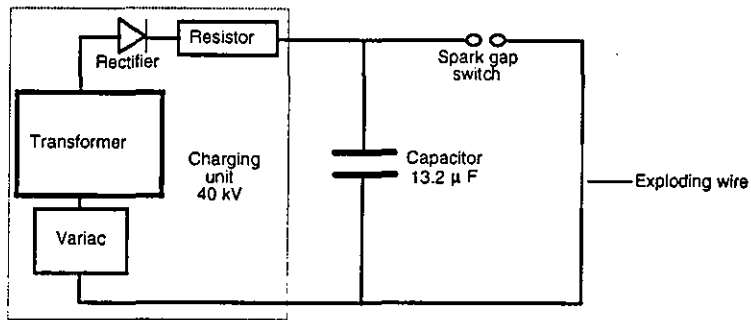


Figure (7.1) Basic diagram for the exploding wire system.

Discharging the bank requires a fast low inductance switch and therefore a spark gap switch (Figure 7.2) is employed in the exploding wire system. This switch is a pressurised dry-air filled type, which is triggered by an external high voltage pulse supplied to the third electrode in the gap to ionise the air between the main electrodes and so cause a rapid discharge.

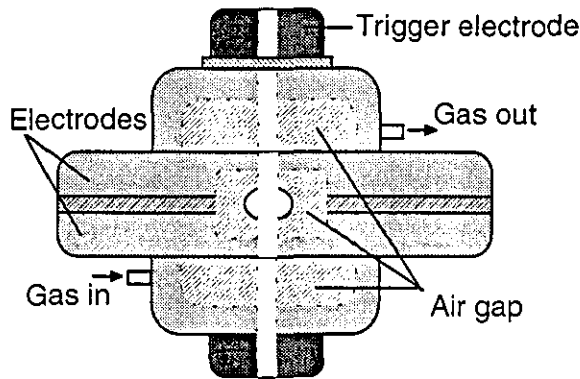


Figure (7.2) Spark gap switch.

As indicated above, the main laboratory, which is outside the exploding wire room, contains a control unit that controls all the system. This unit controls the bank charging voltage, the triggering of the spark gap via the E.H.T and H.V. trigger units, and the pneumatic control unit. It also controls the triggering of the recording system (high speed camera, flash gun and oscilloscope) through pulse generators. For a successful experiment correct synchronisation of the whole system is made using three delay units, which also act as pulse generators (Al-Maliky 1991). Figure (7.3) shows a block diagram for the synchronisation set-up.

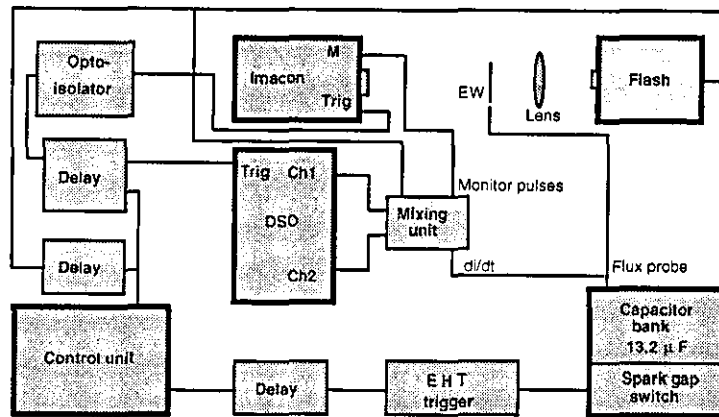


Figure (7.3) Block diagram of the exploding wire set-up.

### 7.2.2 The recording equipment

A high speed electronic image converter camera (IMACON) was used to capture the fast deformations of the samples under test. The images were recorded on a 3000 ASA flat Polaroid film loaded in the camera back. The exposure time is related to the framing rate of the camera which is determined by interchangeable plug-in modules. This time equals  $0.2/\text{framing rate}$ , i.e. one-fifth of the total time between each frame. The image resolution is 10 line pairs/mm for exposure times down to  $0.1\mu\text{s}$  ( $2 \times 10^6 \text{ f/s}$ ), and 5 line pairs/mm for shorter times. The high speed photograph has two rows of frames in the sequence shown in Figure (7.4). The Imacon camera was associated with a Schlieren set-up, flash gun, and an opto-isolator triggering unit to trigger the camera at chosen delay times. These devices are essential for the demands of this study, which requires short duration flash and a high speed camera.

To record the electrical signals such as the  $dI/dt$  profile and the synchronisation pulses for the whole event, a two-channel digital storage oscilloscope (DSO) was used. These pulses are fed to the DSO through a mixing unit shown in Figure (7.5) which is used for attenuating the many pulses, and displaying them together on the two-channel DSO. A typical DSO record is shown in Figure (7.6), indicated are the pulses which help the timing of the high speed photography and the test.

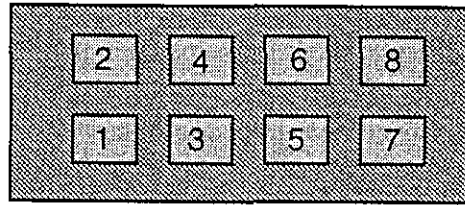


Figure (7.4) Sequence of frames in the high speed photograph.

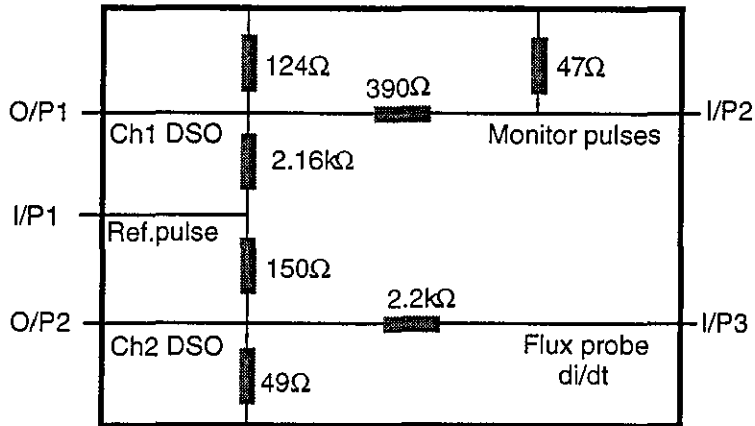


Figure (7.5) Circuit diagram of mixing unit.

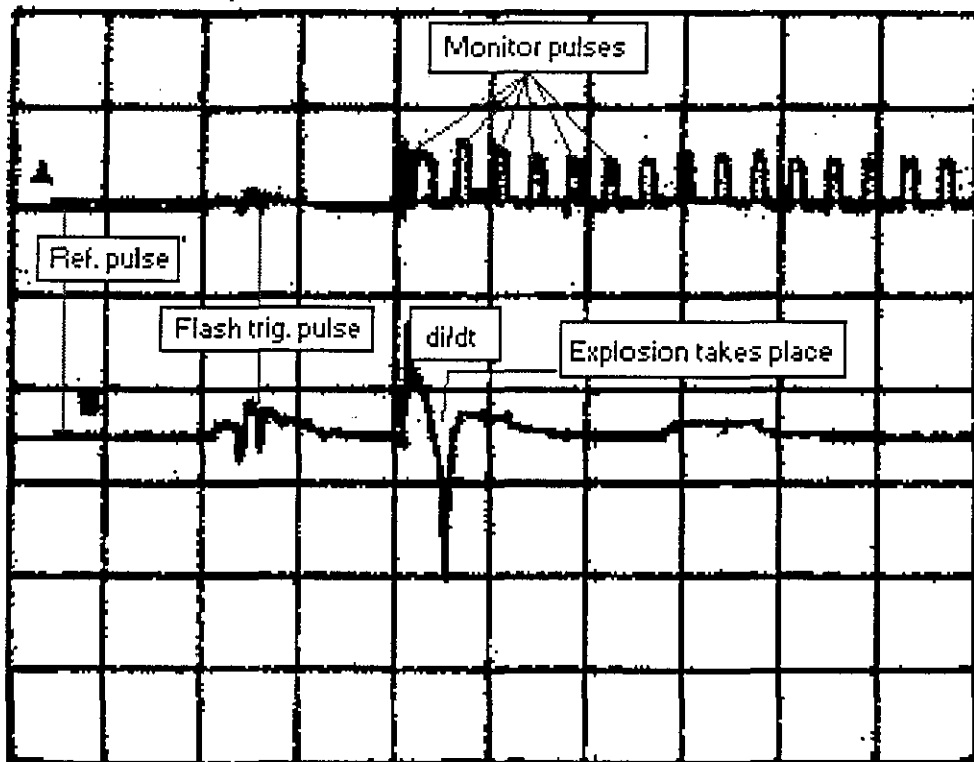


Figure (7.6) Typical DSO record of exploding wire pulses.

### 7.3 Expanding cylinder

As mentioned above, one of the methods used to determine the mechanical behaviour of materials is that in which a hollow cylinder is expanded by means of an internal pressure generated by an exploding wire. In this chapter, a study of HDPE, UHMWPE, and nylatron cylinders is described. High speed photography in association with the Schlieren technique is employed to monitor the radial displacements of the cylinders. Figure (7.7) shows the loading arrangement.

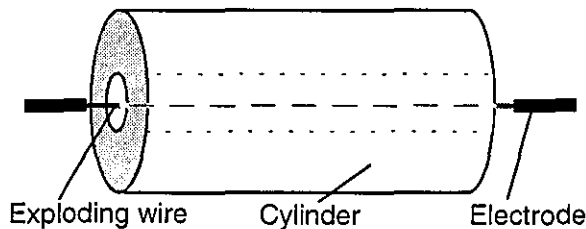


Figure (7.7) Diagram of expanding cylinder configuration.

### 7.4 Freely expanding rings

The freely expanding ring technique involves placing a thin ring of polymer as a sliding fit around a hollow thick-walled cylinder as shown in Figure (7.8). The blast wave generated by the exploding wire results in an internal reflected pressure pulse on the internal wall of the cylinder. This stress pulse propagates through the cylinder wall and is partially transferred into the ring. The ring consequently moves almost instantaneously at a high velocity away from the cylinder and then decelerates as a result of the almost uniaxial tensile hoop stress. By photographing the ring using the high speed camera, the true stress-strain properties can be determined, as shown below. The ring can be considered as under a state of uniaxial stress, while the cylinder is in a state of plane strain when loaded with a symmetrical radial pressure.

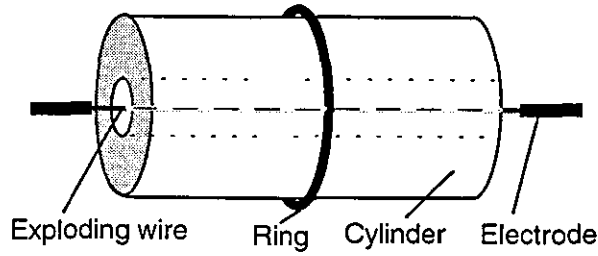


Figure (7.8) Freely expanding ring configuration.

The free expansion ring theory of Hoggatt and Recht (1969) states that if the ring is impulsively loaded, that is the duration of loading is very short, then the dynamic stress-strain relations of the material are obtained from the free flight deceleration of the ring after the initial high radial velocity due to the impulse. Using the equation of motion for a freely expanding ring, the true hoop stress in the absence of a driving pressure is easily shown to be

$$\sigma = -\rho R \ddot{R} \quad (7.2)$$

where  $\rho$  is the mass density of the material,  $R$  is the outer radius of the ring, and  $\ddot{R}$  is the radial deceleration of the ring flight. The true strain is given by

$$\varepsilon = \ln\left(\frac{R}{R_0}\right) \quad (7.3)$$

which gives a true strain rate of

$$\dot{\varepsilon} = \frac{\dot{R}}{R} \quad (7.4)$$

where  $R$ , and  $R_0$  are respectively the outer radius at any time and the initial radius and  $\dot{R}$  is the ring velocity.

## 7.5 Results and discussion

### 7.5.1 Exploding wire results

An extensive series of experiments has been carried out in which blast waves were generated by exploding copper wires of length 80 mm and diameter 0.71 mm (22swg) at voltages of 20, 25, and 30 kV. The length and diameter have been chosen for efficient energy transfer into the wire to produce required blast waves (Al-Maliky (1991)). These experiments involved measurements of the radial expansion of the shock front, from which the velocity was obtained and used to determine the maximum pressure of the reflected blast wave on the inner surface of a cylinder. Real-gas shock theory had to be employed in the

calculation of pressure to take into account the vibration and dissociation effects which are present at high Mach numbers. Typical results are shown in Table (7.1)

Table (7.1) Typical results for 8 cm/22 swg wire.

Voltage (kV)	Max. Velocity (km/s)	Max. Mach No.	Max reflection pressure (kbar)
20	2.95	8.60	0.80
25	3.95	11.50	1.67
30	4.86	14.00	2.86

A typical photographic sequence of an explosion is shown in Figure (7.9). This is for a shock wave expansion which is generated by a 22 swg (0.71 mm) diameter copper wire of length 80 mm fired at 25 kV. As can be seen, the blast wave expansion is cylindrically symmetric, which is an essential requirement. Figures (7.10) and (7.11) show plots of the radius against time, and velocity against radius for the shock fronts generated at 20, 25 and 30 kV.

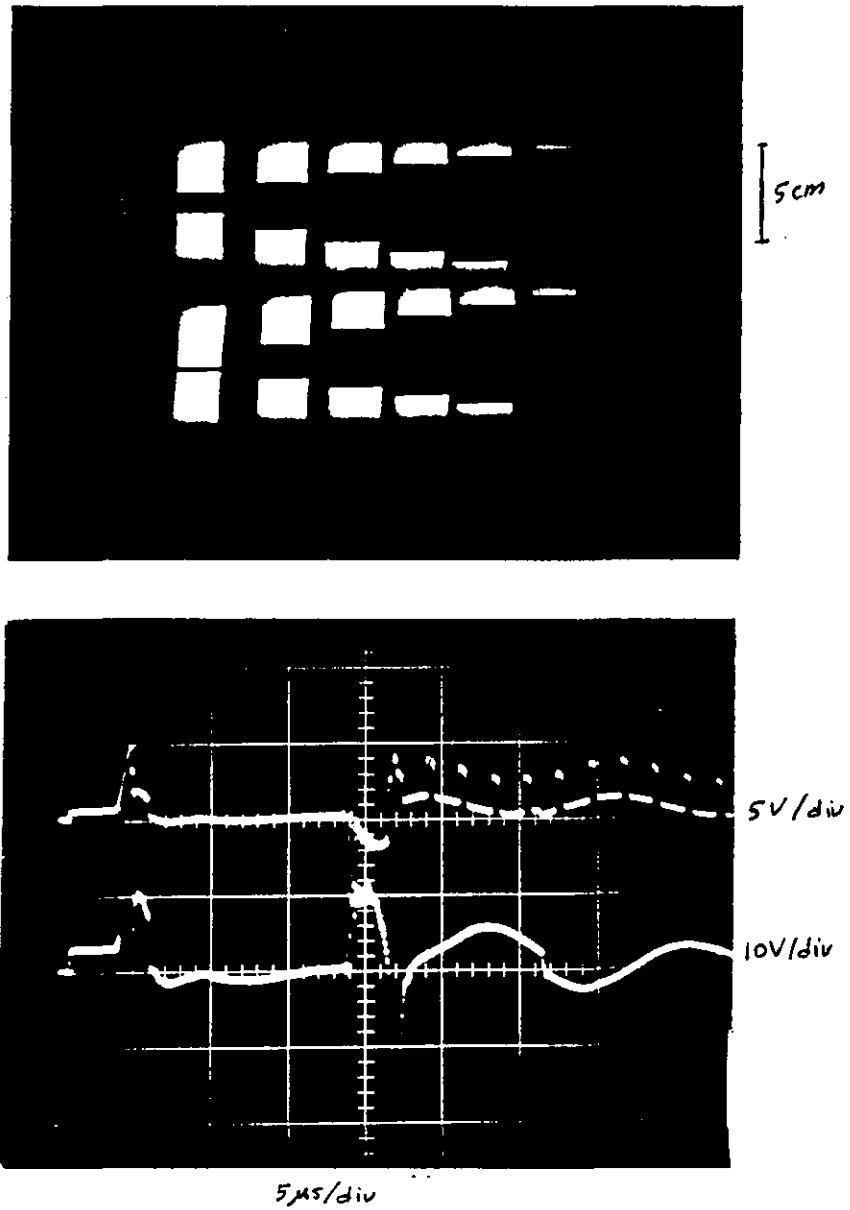


Figure (7.9) High speed photograph (top print) of shock wave expansion at a framing rate of  $10^6$  f/s, and the corresponding CRO record (bottom print) for an 80 mm/22 swg wire exploded at 25 kV.

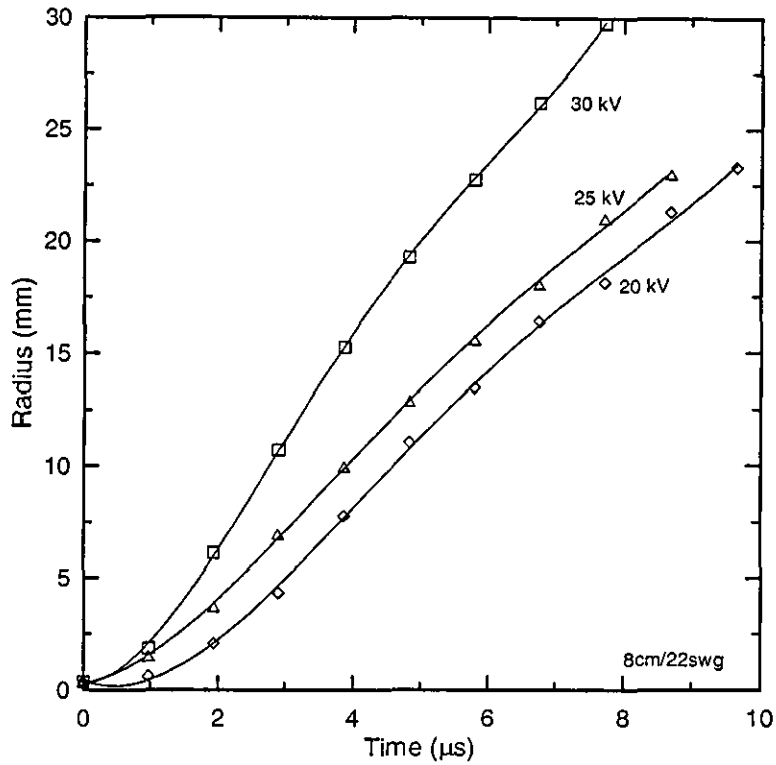


Figure (7.10) Radial expansion against time of shock waves generated by 8 cm/ 22 swg exploding wire at 20, 25, and 30 kV.

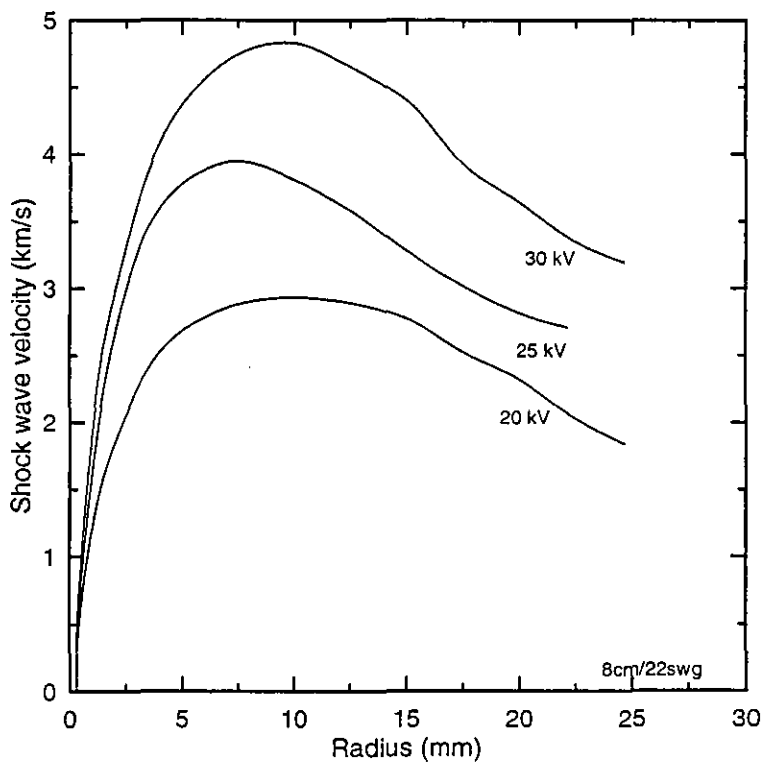


Figure (7.11) Shock wave velocities in air against the radial distance from the centre of the wire at different voltages.

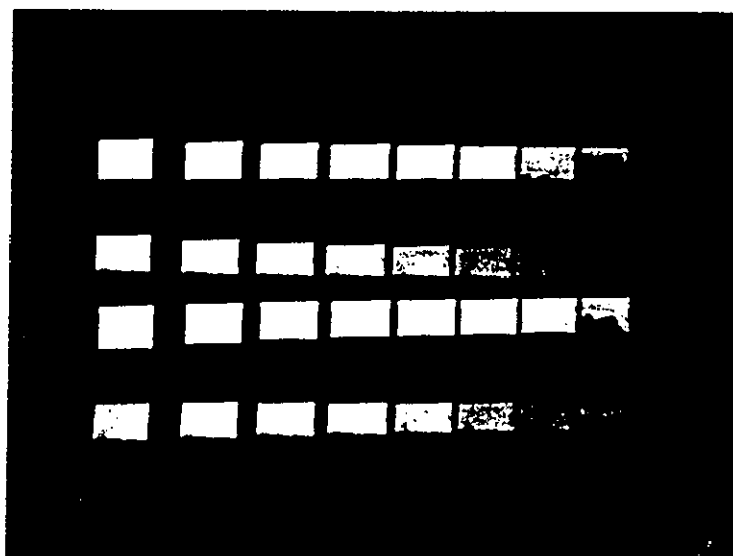


### **7.5.2 Expanding cylinder results**

In order to examine the suitability of different cylinder materials for expanding ring tests, UHMWPE HDPE and nylatron cylinders have been internally subjected to the shock waves of the wire explosion. The expansion of the cylinders was photographed by the high speed camera at framing rates of  $10^5$  and  $5 \times 10^5$  f/s in conjunction with Schlieren photography. Measurements of the radial displacements have been made from the high speed photographs using an eye-piece magnifier which can be used to measure small distances to about  $\pm 0.1$  mm, which corresponds to  $\pm 0.5$  mm in actual diameter.

Figure (7.12a) shows a high speed record for a UHMWPE cylinder of length 100 mm, inner diameter 9 mm, and outer diameter 26 mm, loaded by an 8 cm/22 swg wire explosion at 25 kV. The radius against time is plotted in Figure (7.12b) and from the gradient of this curve, the velocity of the outer radius can be obtained. Figure (7.12c) shows that the velocity against radius of the UHMWPE cylinder reaches a maximum of 60 m/s at a radius of 14.7 mm. Also the hoop strain is calculated and plotted as in Figure (7.12d). The measurements also give the strain at which the cylinder fractures. From the plot in Figure (7.12b) the fracture of the cylinder can be seen to be when the radius increases rapidly after about  $120 \mu\text{s}$ , and at a strain of about 26%. The strain rate is about  $4 \times 10^3 \text{ s}^{-1}$  over the first  $40 \mu\text{s}$ , while it is  $10^3 \text{ s}^{-1}$  at the time from  $40 \mu\text{s}$  to  $120 \mu\text{s}$ .

HDPE behaves similarly to the UHMWPE except that the HDPE fractures earlier, after about  $70 \mu\text{s}$  at strain of 20%.



A= 5 V B= 10 V TB= 20us TD= 1D

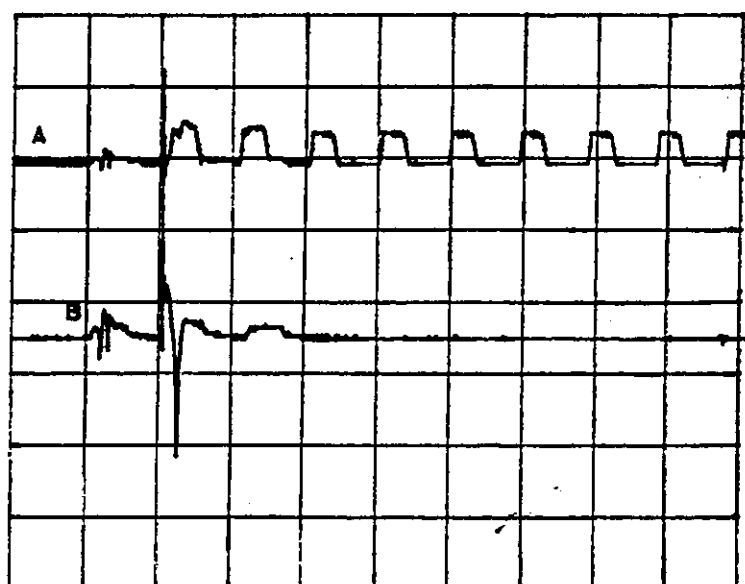


Figure (7.12a) High speed photograph at a framing rate of  $10^5$ f/s (top print) and DSO record (bottom print) for an UHMWPE cylinder loaded by an 8 cm/22 swg wire fired at 25 kV.

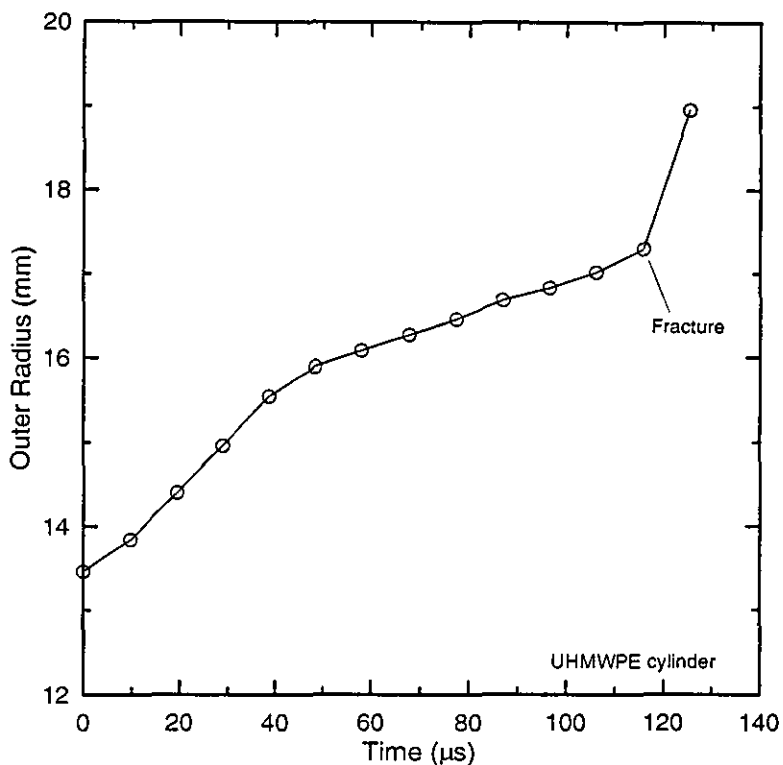


Figure (7.12b) Radius-time plot for the UHMWPE cylinder.

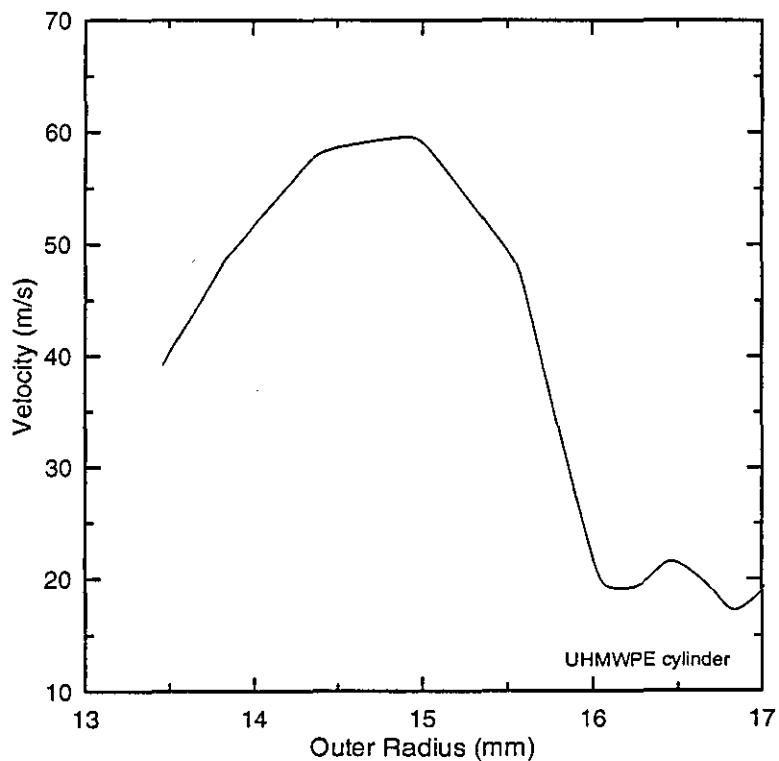


Figure (7.12c) Velocity-radius plot for the UHMWPE cylinder.

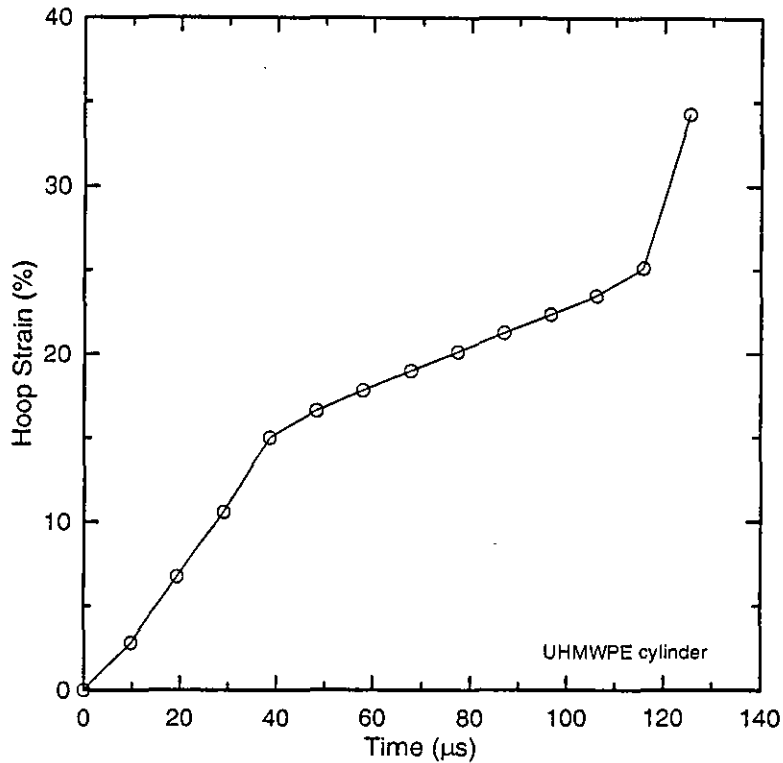
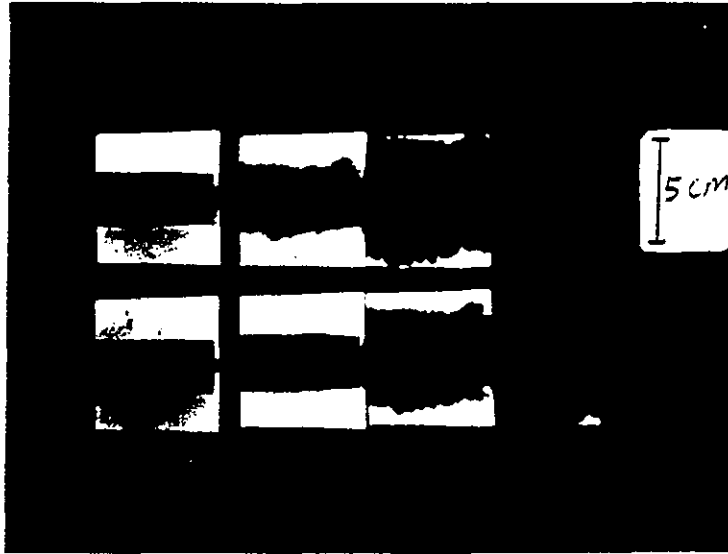


Figure (7.12d) True hoop strain against time for the UHMWPE cylinder.

Figure (7.13) shows a high speed photograph at a framing rate of  $10^5$  f/s for a nylatron cylinder of outer diameter 25 mm, wall thickness 9 mm, and length 100 mm. The photograph includes the right hand end of the cylinder together with a cylindrical brass electrode which holds one end of an 80 mm length, 22 swg wire inside the cylinder. The wire has exploded shortly after the first frame. By the second frame the cylinder has started to expand uniformly in the central region around the wire and copper vapour can be seen emerging from the open end. The cylinder has suddenly disintegrated by the fourth frame (about  $20\mu\text{s}$  after the start of the explosion) when the hoop strain is about 10% (third frame). An examination of the pieces of the cylinder recovered after the experiment confirmed that brittle fracture had occurred at this high strain rate of about  $6 \times 10^3 \text{ s}^{-1}$ .



A= 5 V B= 10 V TB= 10us TD= 10

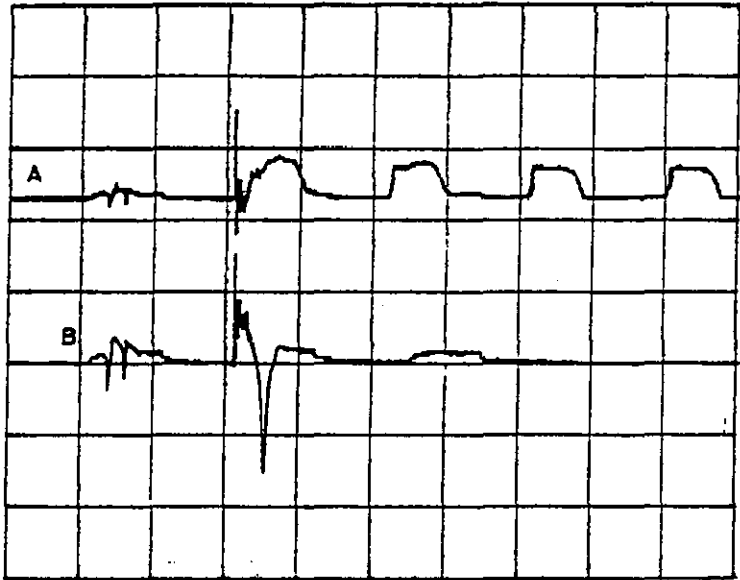


Figure (7.13) High speed photograph at a framing interval of  $10\mu\text{s}$  and a DSO record for a nylatron cylinder loaded by an exploding wire at a voltage of 25 kV.

Nylatron cylinders fractured after about  $20\mu\text{s}$  –  $30\mu\text{s}$  using the voltages 20, 25 and 30 kV giving hoop strain within a range of about 10%-12%. These strains are much lower than the quasistatic tensile values quoted by the manufacturer.

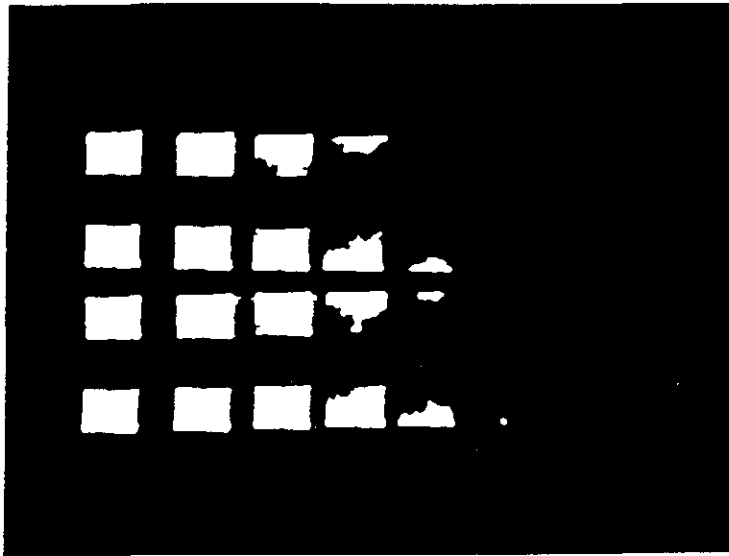
### **7.5.3 Expanding ring results**

In the expanding cylinders method, a pressure profile must be measured in order to calculate the stress. To avoid the difficulties in measuring the pressure, the freely expanding ring method has been used to determine the stress and strain without the need of knowing the reflected pressure profile. This method involved as mentioned before, placing a thin ring of the material to be tested on a thick-walled cylinder.

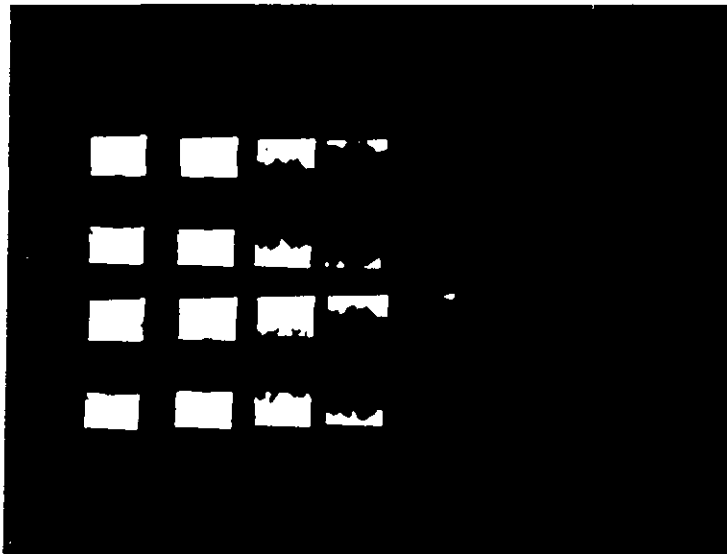
The choice of material for the driving cylinder for a ring experiment is important, so that sufficient momentum is transferred into the ring. A polymeric cylinder of the same material as the ring provides the best impedance match, but numerous experiments of the type described above and later have shown that this is not the most important criterion at the actual strain rates of about  $10^3 \text{ s}^{-1}$  for cylinders under impact conditions. It is important that the cylinders do not fracture during the time of observing the ring deformation. It is also essential to have an appropriate thickness of the cylinder wall so the cylinder expands more slowly than the ring allowing a separation between the cylinder and the ring to occur.

Nylatron appeared to be a good choice as a suitable cylinder material to be used with polymer rings because its acoustic impedance is a good match for the rings, it has high tensile strength and stiffness compared with many other thermoplastic polymers, and it is inexpensive (a useful feature since the cylinders can be used once only) (Al-Maliky and Parry (1996)).

Rings have been successfully launched using nylatron cylinders, but the useful observation time is limited to less than  $30 \mu\text{s}$  because pieces of the fractured cylinders overtake the rings resulting in secondary impacts followed by obliteration of the field of view, as shown in Figure (7.14 a, b).



(a)



(b)

Figure (7.14) Nylatron cylinders and ring fractured by an exploding wire at 20 kV, and photographed at  $10^5$  f / s.

Pieces from a fractured cylinder can overtake the expanding ring obliterating the field of view and also cause unwanted secondary impacts. UHMWPE did not fracture at least until  $110\mu\text{s}$  with a strain of about 26%. Aluminium cylinders were also tried and they did not fracture but there was no measurable ring movement because of the impedance mismatch with the polymer rings.

After the experiments described above, the most satisfactory cylinder material was therefore found to be UHMWPE, which has a very high impact strength. Although these cylinders did fracture, a high strain was required in order to

fracture them (>26%) and the fracture occurred after the required observation time of the ring movement had elapsed. Also, the cylinders remained relatively intact at the end of the experiment, in contrast to nylatron's complete disintegration.

### 1) HDPE results

High speed photographs at framing rates of  $5 \times 10^5$  f/s and  $10^5$  f/s are shown in Figure (7.15a) and (7.15b) respectively with their corresponding DSO records for HDPE rings of 0.53 mm thickness, 13.07 mm outer radius, and 4.72 mm length placed on an HDPE cylinder of 3.47 mm and 12.55 mm inner and outer radii respectively and length of 65 mm. The higher framing rate of  $5 \times 10^5$  f/s ( $2 \mu\text{s}$  between frames) gives better resolution of the ring expansion. These rings were loaded by 8 cm/22 swg wires fired at 25 kV. The mean diameter of the ring, taken over its complete length parallel to the cylinder, was measured as a function of time by using, a calibrated graticule to observe magnified images of the ring on the Polaroid print. The measurement error in the diameter was about  $\pm 0.1$  mm. Figure (7.15c) shows a combined plot of the outer radius (R) expansion against time (t) of two separate experiments. It was possible to combine the experiments because of the excellent shot-to-shot consistency. A second order polynomial gives an excellent fit to the radius-time data.

$$R(\text{mm}) = 12.897 + 0.178t - 1.493 \times 10^{-3} t^2$$

where t is the time in  $\mu\text{s}$ .

The first derivative gives the expansion velocity as

$$\dot{R}(\text{mm} / \mu\text{s}) = 0.178 - 2.987 \times 10^{-3} t$$

and the deceleration as

$$\ddot{R}(\text{mm} / \mu\text{s}^2) = -2.987 \times 10^{-3}$$

Equations (7.2), (7.3) and (7.4) give respectively the hoop stress, strain and strain rate by substituting R,  $\dot{R}$  and  $\ddot{R}$  from the polynomial equations for a given time of observation.

Figure (7.15c) shows the velocity and strain rate against time, and indicated that the ring has an initial velocity of about 178 m/s. The strain rate varies between  $1.3 \times 10^4 \text{ s}^{-1}$  at the beginning of the measurements to zero at time  $60 \mu\text{s}$  as shown



in Figure (7.15c). The tensile hoop stress increases during the expansion causing the deceleration of the ring. The velocity decreases to zero, and hence the strain rate ( $\dot{\epsilon} = \dot{R}/R$ ) becomes zero, at the maximum strain.

The hoop strain, stress and radius against time curves are shown in Figure (7.15d). The stress-strain curve obtained is plotted in Figure (7.15e) up to 30% strain. However, there is uncertainty in the polynomial fit for the first few microseconds, so the results have been plotted only after about 3% strain for all materials. Also shown in Figure (7.15e) is a quasistatic stress-strain curve for comparison.

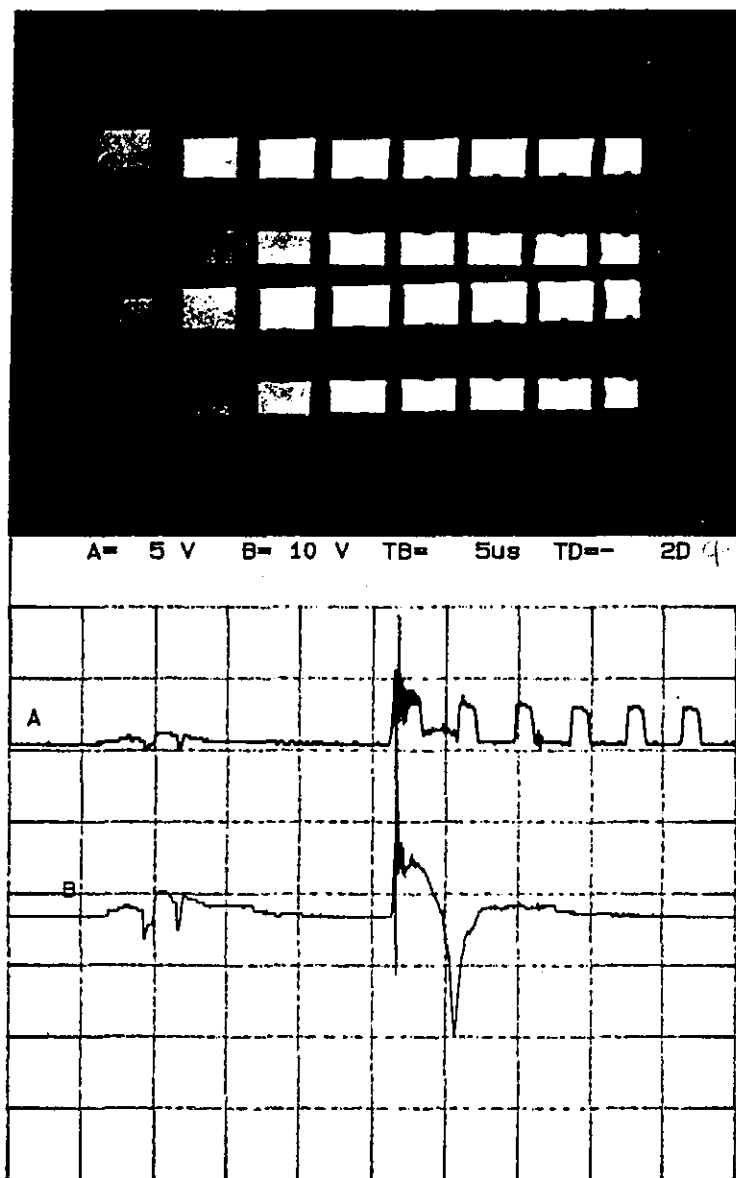
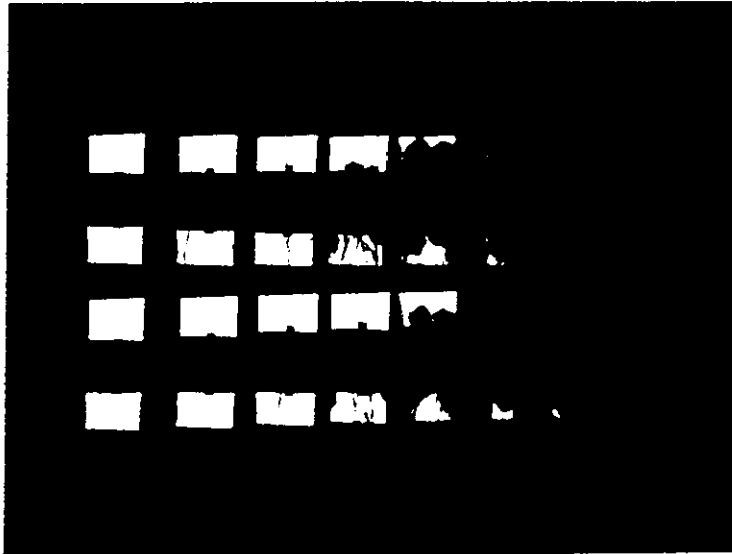


Figure (7.15a) High speed photographs at a framing rate of  $5 \times 10^5$  f/s (top print) and DSO record (bottom print) for an HDPE ring placed on an HDPE cylinder.



A= 5 V B= 10 V TB= 10us TD= 1D

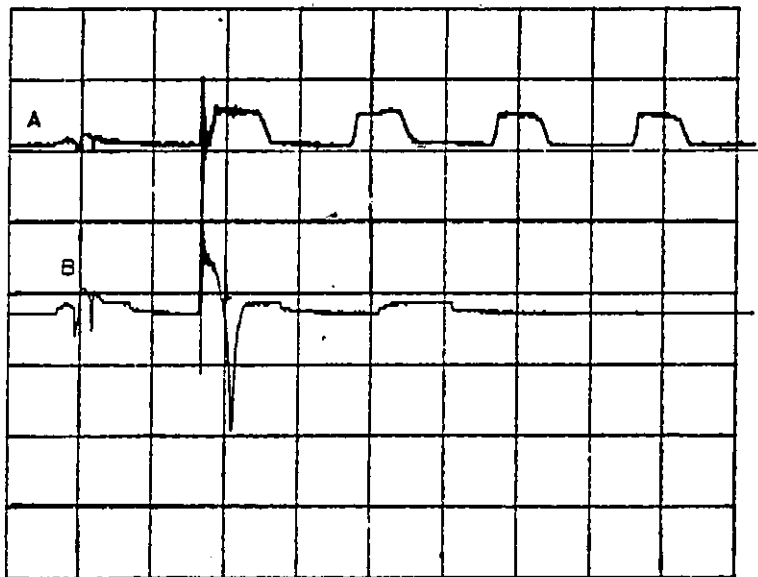


Figure (7.15b) High speed photograph and DSO record for the HDPE ring placed on HDPE cylinder. Frame rate =  $10^5$  f/s.

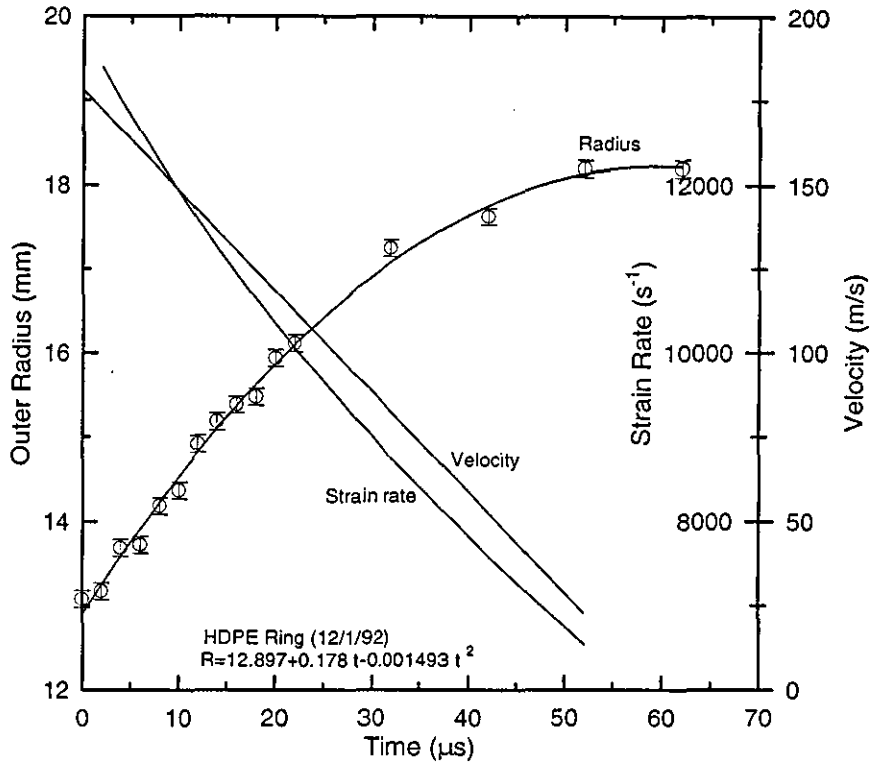


Figure (7.15c) Outer radius-time plot for the HDPE ring placed on an HDPE cylinder.

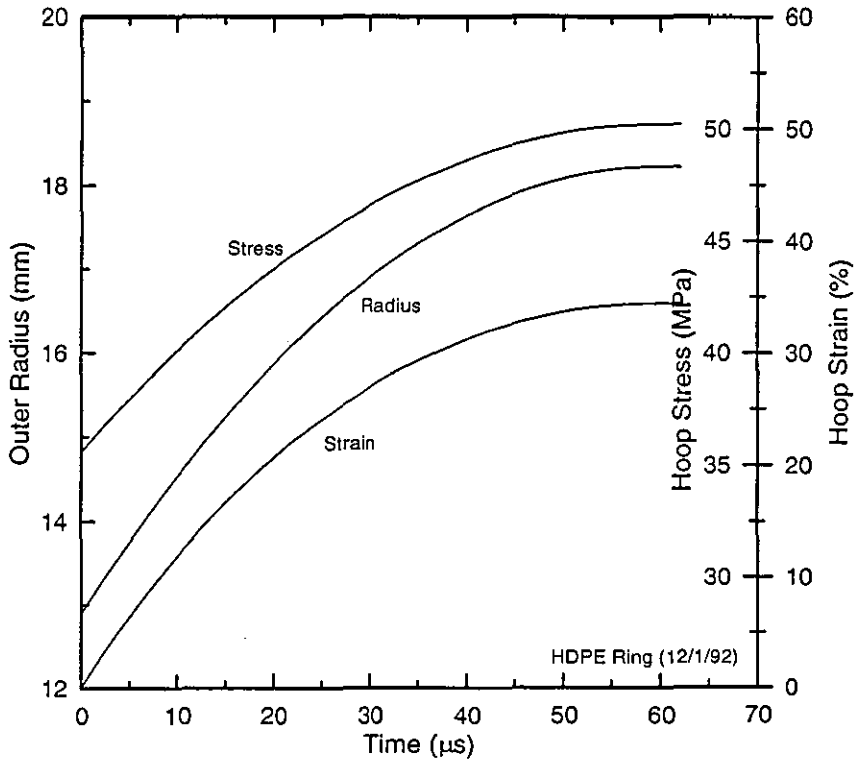


Figure (7.15d) Plot of radius, strain and stress for the HDPE ring.

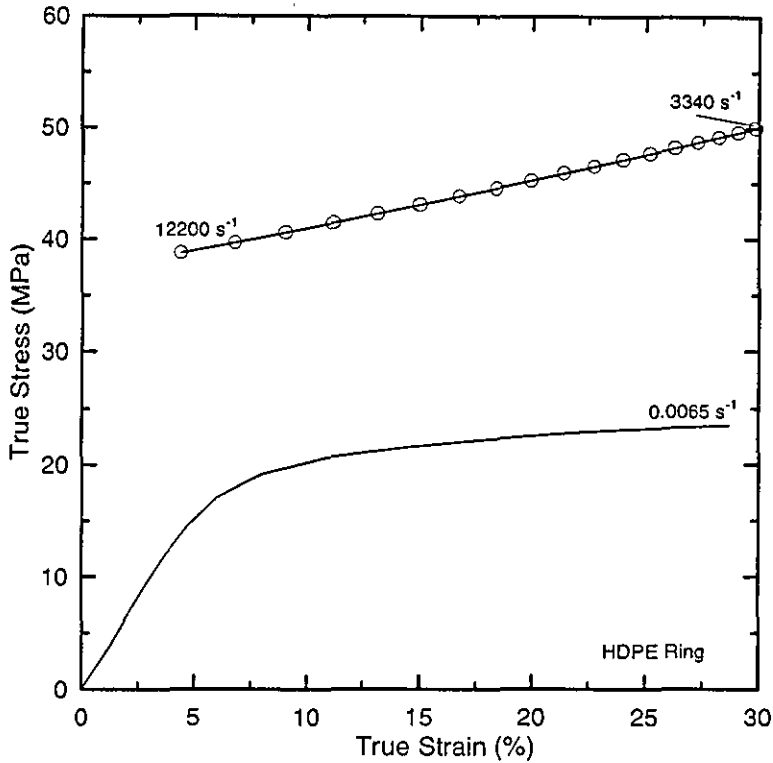
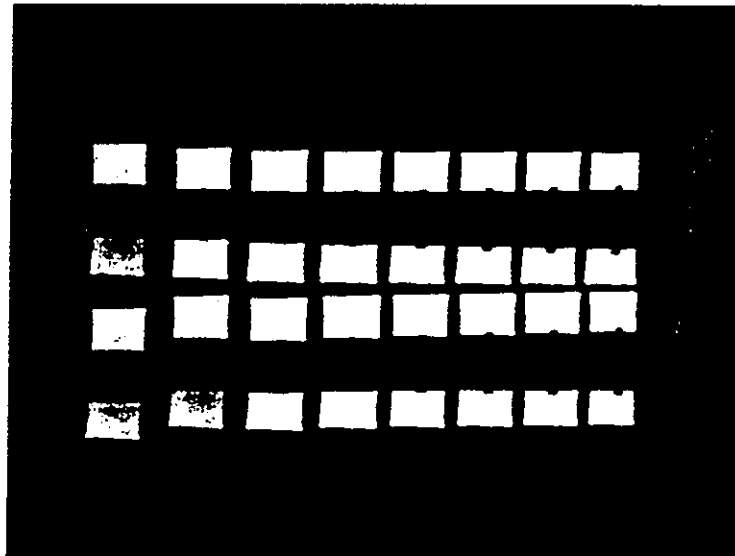


Figure (7.15e) Stress-strain curve for the HDPE ring together with a quasistatic curve.

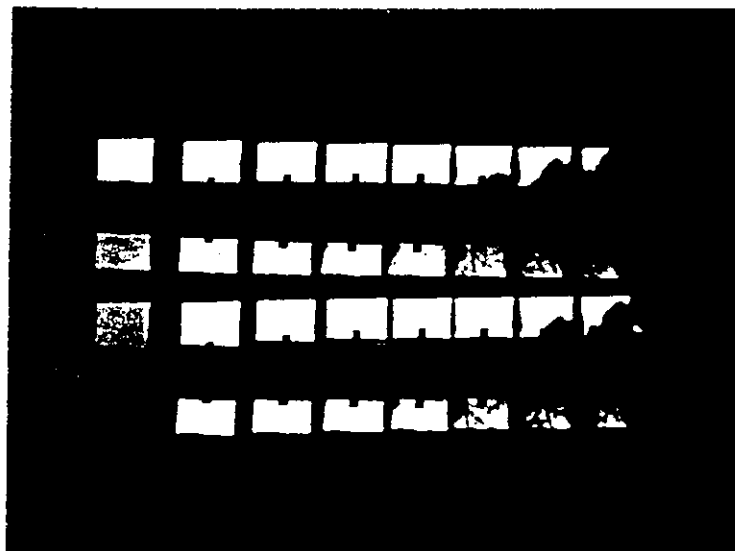
## 2) UHMWPE results

UHMWPE was tested by placing thin rings of UHMWPE on UHMWPE cylinders of outer diameter of about 25 mm. Figure (7.16a) shows high speed photographs taken at framing rates of  $5 \times 10^5$  f/s for an UHMWPE ring 0.5 mm thick, 4.90 mm long, and 26.0 mm inner diameter placed on a 70 mm long UHMWPE cylinder, with outer diameter of 25.0 mm and wall thickness of 9.2 mm. The loading was produced by an 8 cm /22 swg wire fired at 25 kV. From the original print of high speed photograph in conjunction with the corresponding DSO record it has been determined that the wire exploded at the fourth frame (at about  $6 \mu\text{s}$ ), then the expansion started after the blast wave propagates thorough the air, cylinder wall and then transmitted into the ring (about  $4 \mu\text{s}$ ). Figure (7.16b) shows high speed photographs at a framing rate of  $10^5$  f/s for an expanding UHMWPE ring 4.92 mm long, 0.5 mm thick, and 26.3 mm outer diameter on a 70 mm long UHMWPE cylinder of thickness 9.2 mm, and outer diameter of 25.3 mm, fired by an 8 cm/22 swg wire at 25 kV. The results of these experiments were combined in one graph as shown in Figure (7.16c), which shows experimental radius-time data and the second order polynomial fitting equation, as well as velocity-time and strain rate-time curves.

The ring has an initial maximum velocity of 218 m/s with a constant deceleration of  $3.2 \times 10^{-3} \text{ mm}/\mu\text{s}^2$ . The strain rate varies between  $15000 \text{ s}^{-1}$  at  $5 \mu\text{s}$  and zero at  $68 \mu\text{s}$ . Figure (7.16d) shows calculated radius, strain and stress against time curves. Figure (7.16e) shows the calculated stress-strain curve for the UHMWPE ring, as well as a quasistatic curve for comparison.



(a)



(b)

Figure (7.16) UHMWPE rings on UHMWPE cylinders at framing intervals of (a)  $2 \mu\text{s}$ , and (b)  $10 \mu\text{s}$ .

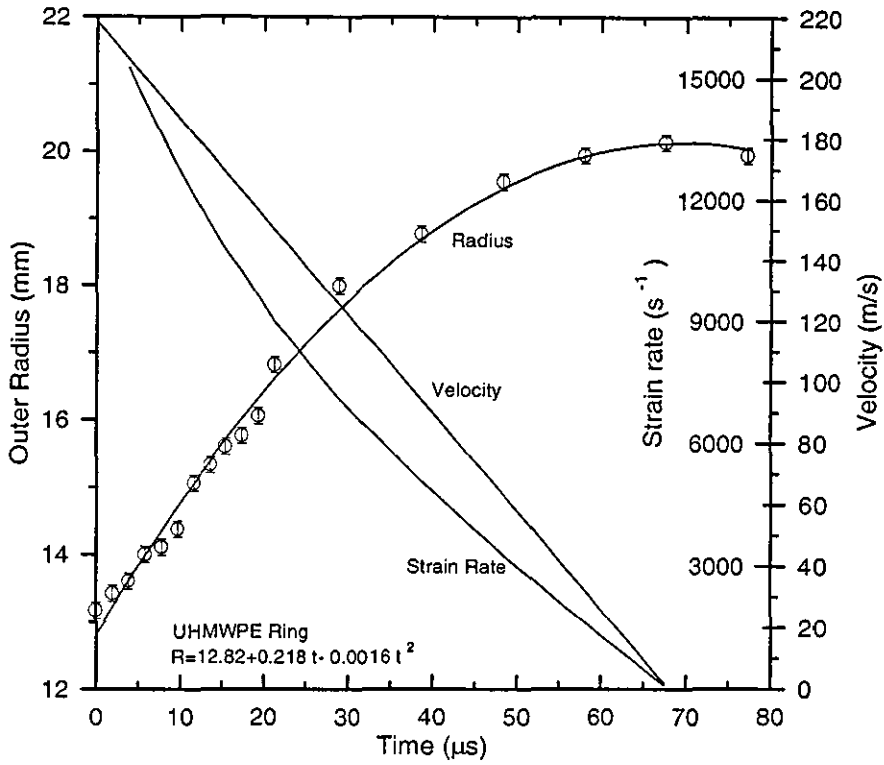


Figure (7.16c) Radius, velocity and strain rate against time for UHMWPE rings.

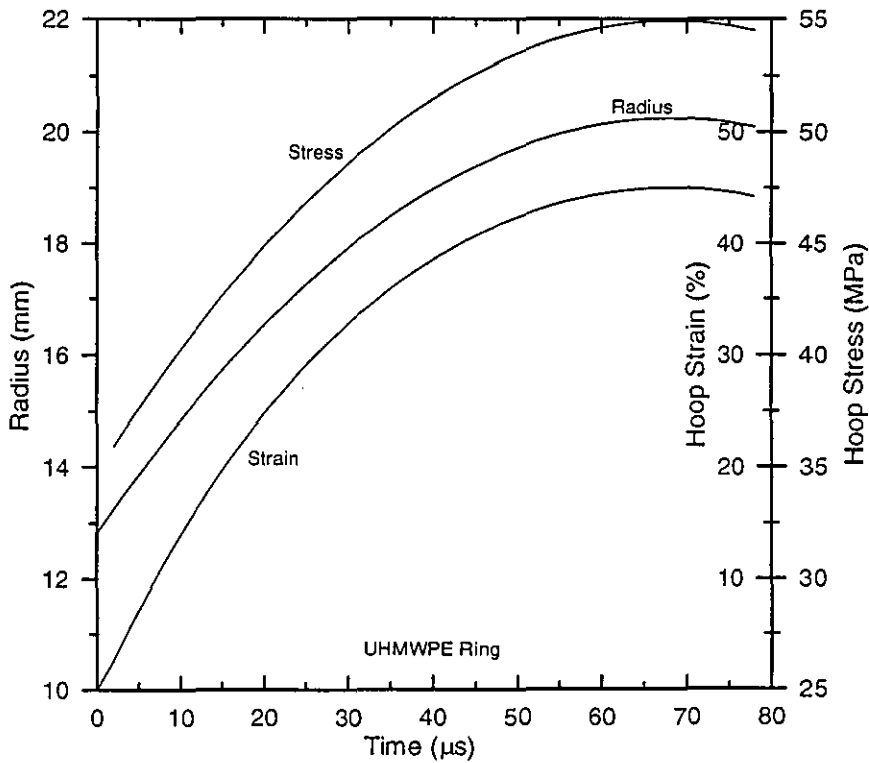


Figure (7.16d) Radius, strain and stress against time curves for the UHMWPE rings.

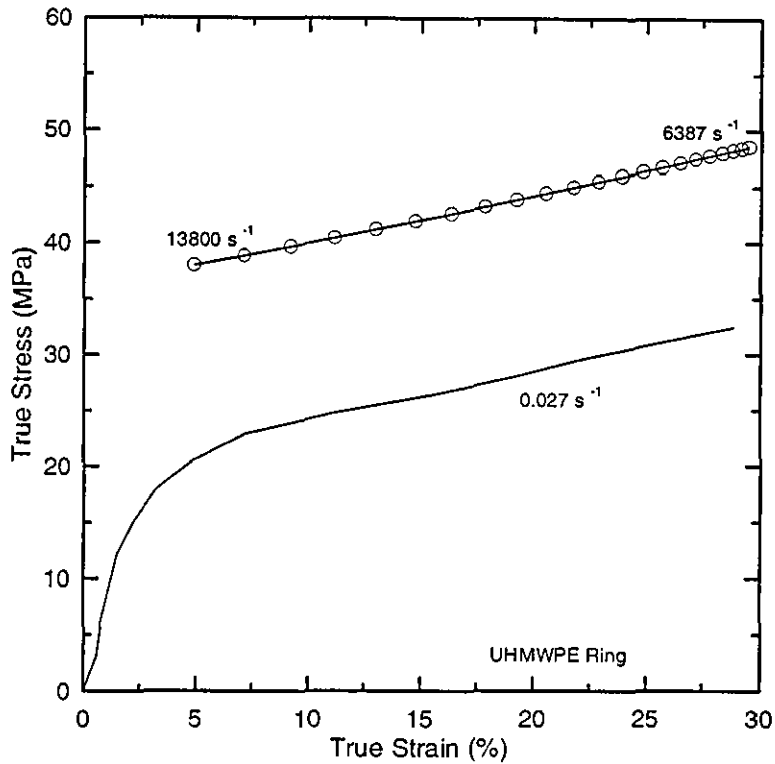


Figure (7.16e) True stress-strain curve for an UHMWPE ring as well as the quasistatic curve.

### 3) Nylatron results

Figures (7.17a,b) show high speed photographs of nylatron rings 0.5 mm thick, 5 mm long, and 26 mm outer diameter, placed on UHMWPE cylinders and fired by 8 cm/22 swg wires at 25 kV. The framing rates are  $5 \times 10^5$  f/s and  $10^5$  f/s for Figures (7.17a) and (7.17b) respectively. Nylatron rings show brittle fracture as shown in Figure (7.17b). Figure (7.17c) shows the second order polynomial equation imposed on the experimental data of radius expansion, in the region between the start of the expansion ( $10 \mu\text{s}$ ) and fracture (about  $25 \mu\text{s}$ ). The nylatron fractures after about 18% strain. Figure (7.17d) shows velocity, stress, strain and strain rate against time plots. The strain rate starts with an initial value of about  $14400 \text{ s}^{-1}$ , and then decreases. The calculated stress-strain curve is shown in Figure (7.17e), in which a quasistatic curve is also shown for comparison.

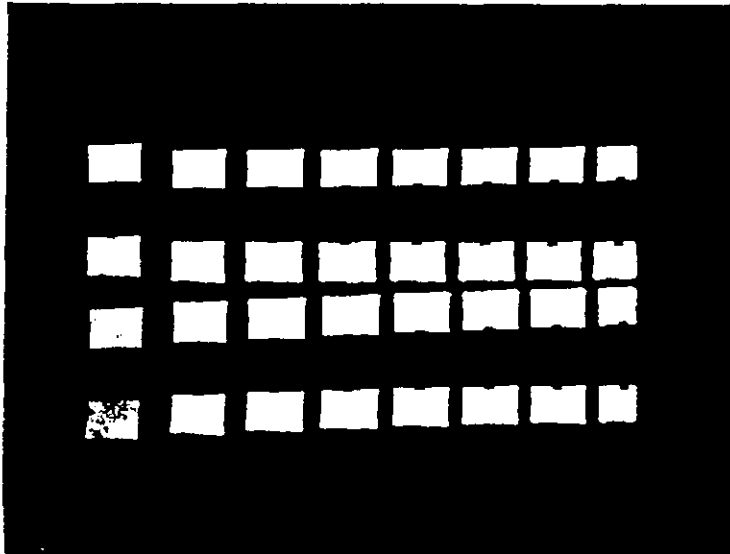


Figure (7.17a) High speed photograph at a framing rate of  $5 \times 10^5$  f/s for nylatron ring fitted on UHMWPE cylinder, and tested by 8 cm/22 swg wire at 25 kV.

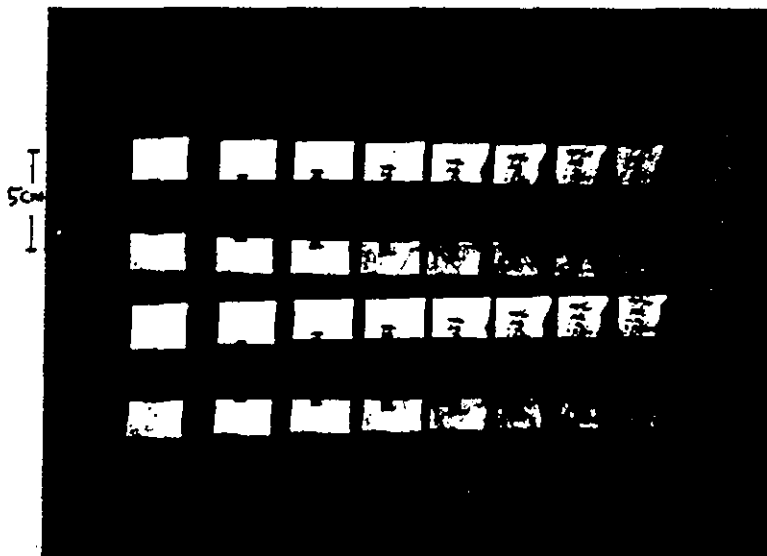


Figure (7.17b) High speed photograph at a framing rate of  $10^5$  f/s for nylatron ring fitted on UHMWPE cylinder, and tested by 8cm/22swg wire at 25 kV.



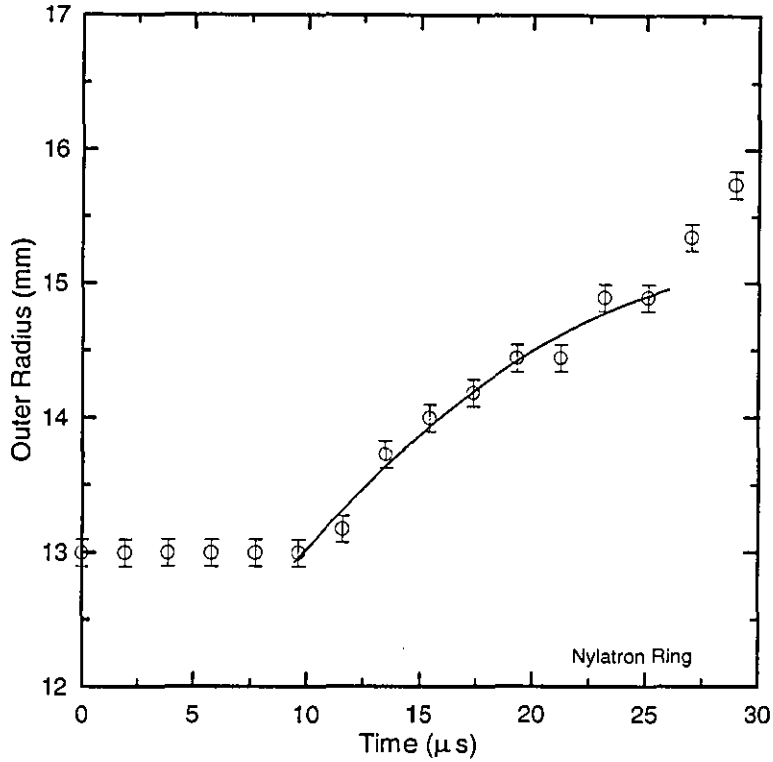


Figure (7.17c) Radius-time curve for a nylatron ring placed on an UHMWPE cylinder.

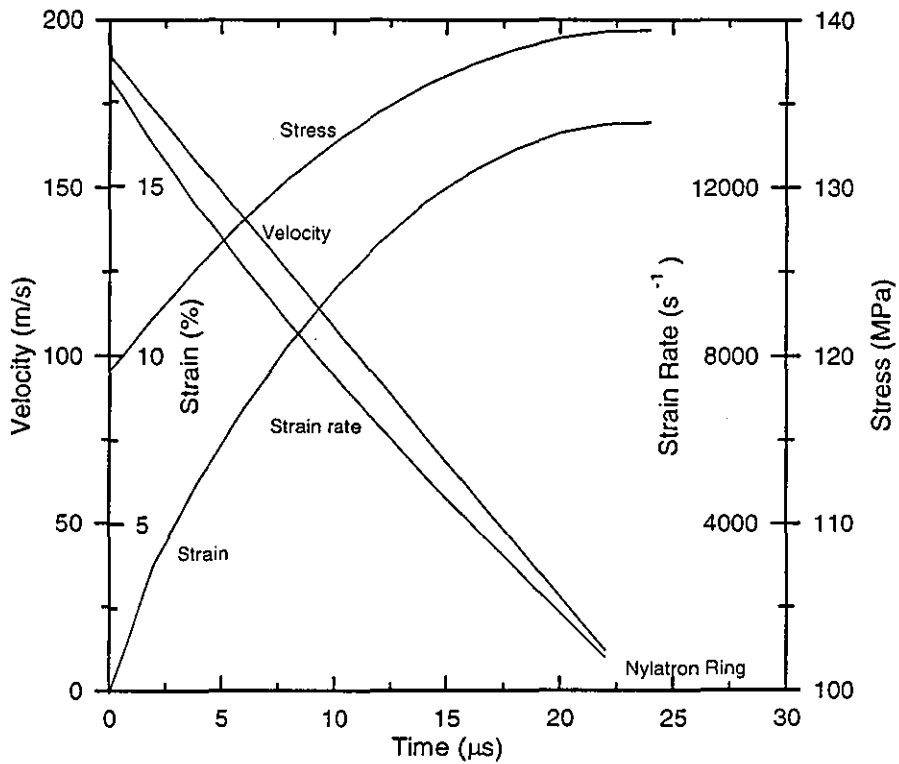


Figure (7.17d) Stress, strain, velocity and strain rate against time for a nylatron ring.

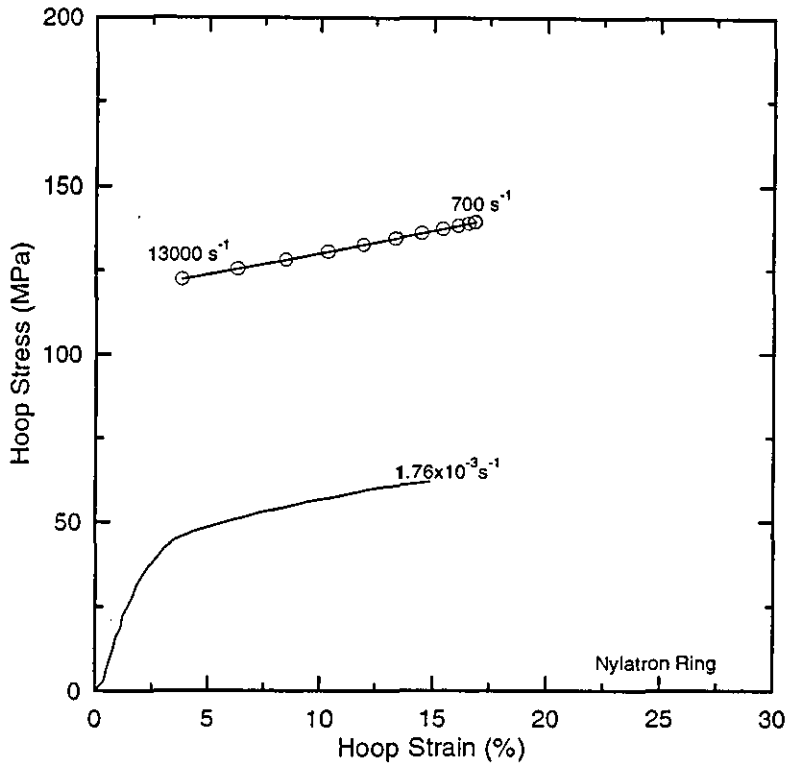


Figure (7.17e) Stress-strain curve for the nylatron ring, with the quasistatic curve for comparison.

#### 4) PEEK results

Figure (7.18a, b) show high speed photographs of PEEK rings 0.5 mm thick, 5 mm long, and 26 mm outer diameter, placed on UHMWPE cylinders loaded by 8 cm/22 swg wires fired at 25 kV. In Figure (7.18a), the framing rate is  $10^5$  f/s and from the original print of high speed photograph in conjunction with the corresponding DSO record, the wire exploded just after the first frame. In frame number 5 ( $40\mu\text{s}$  later), the ring has started to fracture and subsequent frames show the rapid disintegration of the ring. The sequence shown in Figure (7.18b) is at a higher framing rate of  $5 \times 10^5$  f/s and gives a much better resolution of the ring expansion. The wire explosion occurs in frame 3 and a few microseconds later, the ring moves uniformly away from the cylinder.

Figure (7.18c) shows an analysis for an experiment with a PEEK ring shown in Figure (7.18b). A second order polynomial gave an excellent fit to the radius-time data. This was then used to determine the velocity, strain rate and acceleration of the ring. As can be seen in Figures (7.18c) and (7.18d) the radius-time curve shows that after a short acceleration phase, the ring velocity decreased linearly with time from a maximum of 200 m/s after  $20\mu\text{s}$ . An initial

strain rate of about  $1.6 \times 10^4 \text{ s}^{-1}$  was reached, which decreased to about  $6 \times 10^3 \text{ s}^{-1}$  after  $20 \mu\text{s}$ . Figure (7.18e) shows stress-strain curves for PEEK rings tested at different strain rates. A quasistatic curve is also plotted for comparison.

Three PEEK rings have been placed beside each other on an UHMWPE cylinder and fired by an 8 cm/ 22 swg wire at 25 kV. In Figure (7.19) the high speed photograph shows that the rings expand parallel to each other. Also it can be seen that the middle ring expands faster than the others, which was a consequence of it being a better fit on the cylinder than the other two rings. The ring on the right hand side expands faster than the one on the left hand side for the same reason. So, it is important to make sure that the ring is in good contact and fits on the cylinder to transfer as much energy as possible before it separates from the cylinder.

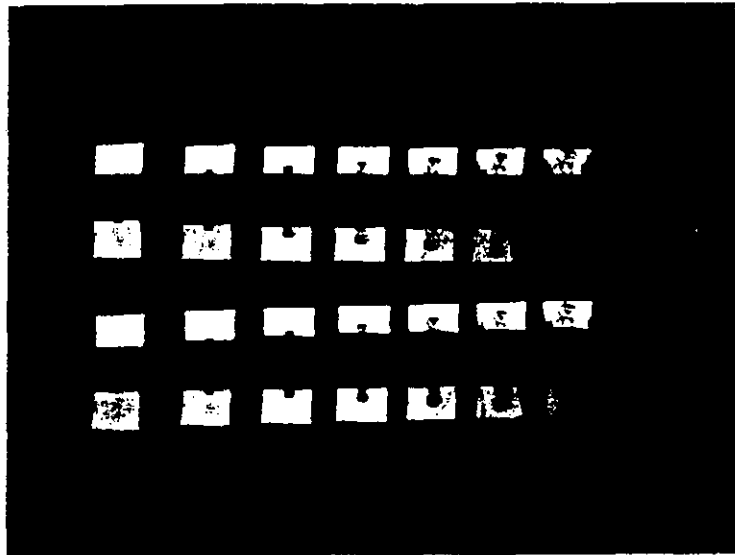


Figure (7.18a) High speed photographs at a framing rate of  $10^5 \text{ f/s}$  of a PEEK ring placed on an UHMWPE cylinder.

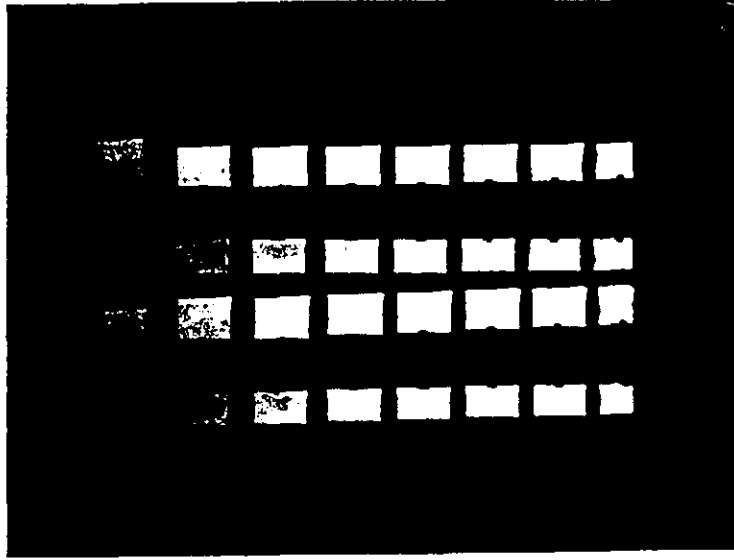


Figure (7.18b) High speed photographs at a framing rate of  $5 \times 10^5$  f/s of a PEEK ring placed on an UHMWPE cylinder.

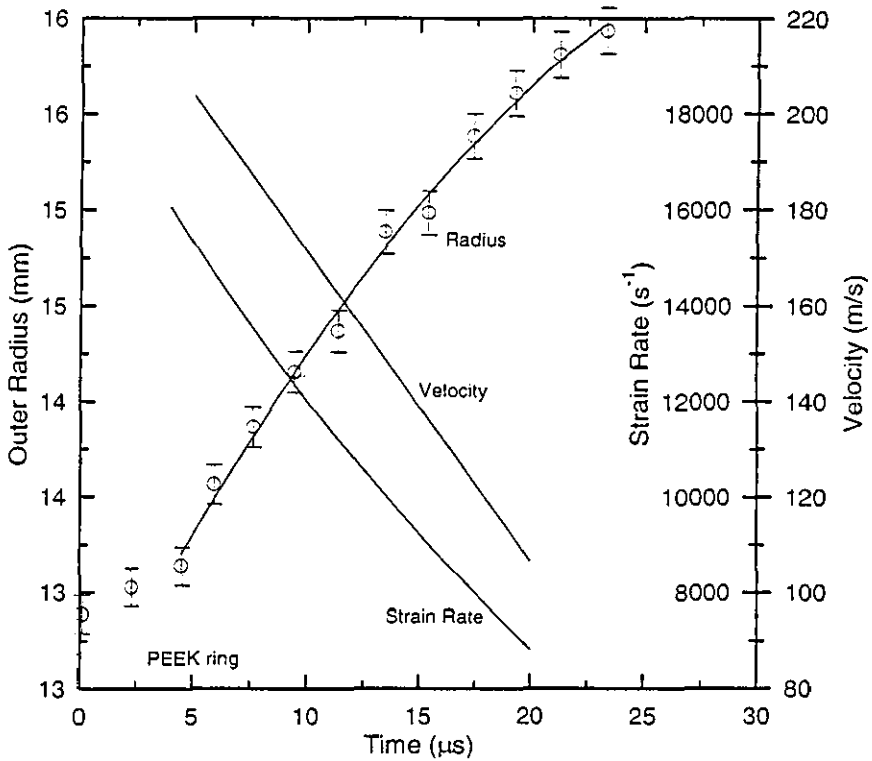


Figure (7.18c) Radius, velocity and strain-rate against time curves for the PEEK ring placed on an UHMWPE cylinder.

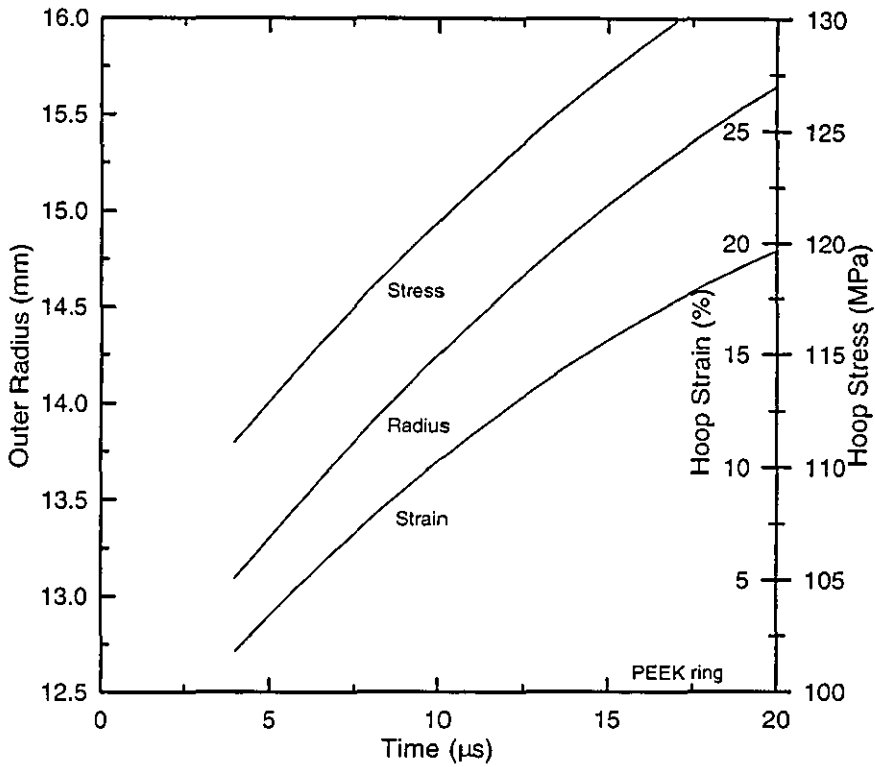


Figure (7.18d) The corresponding radius, stress and strain curves for the PEEK ring.

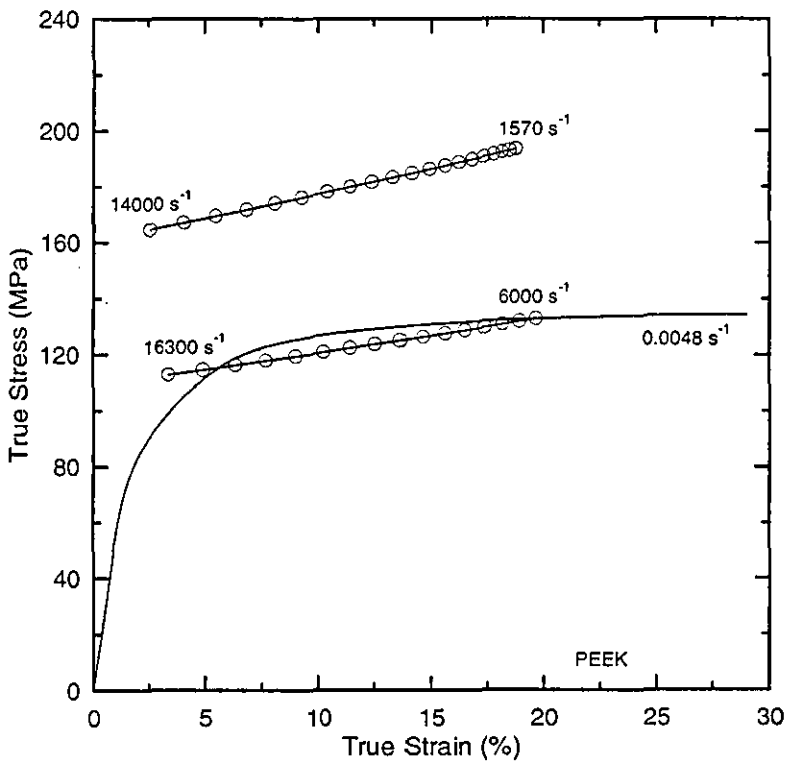


Figure (7.18e) Stress-strain curves for PEEK rings placed on UHMWPE cylinders together with quasistatic curve.

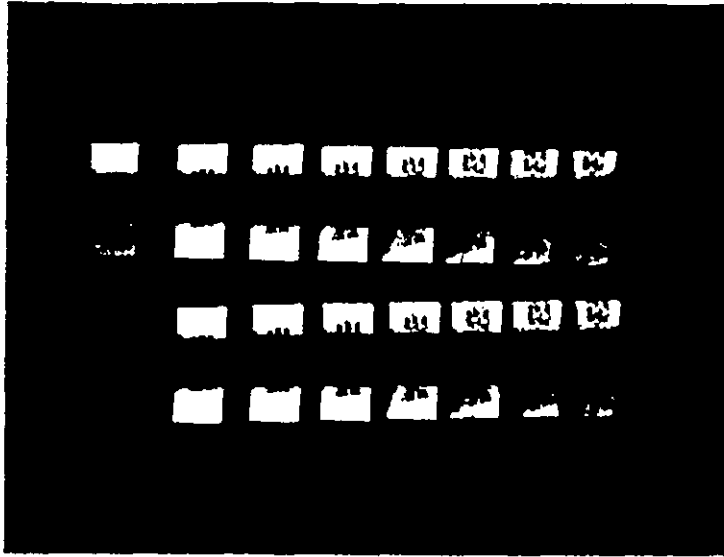


Figure (7.19) High speed photograph at a framing rate of  $10^5$  f/s of three PEEK rings fired by 8 cm/22 swg wire at 25 kV.

## 7.6 Conclusions

The experimental work in this chapter consisted of generating cylindrical blast waves produced in air at atmospheric pressure by exploding a copper wire. This copper wire was instantaneously vaporised by the conduction of a rapid discharge current from a  $13.2 \mu\text{F}$  capacitor with a stored energy of up to 10 kJ. Schlieren photography has been used in conjunction with a high speed image converter camera at framing rates of  $10^5$  f/s and  $5 \times 10^5$  f/s to study the high speed deformations of HDPE, UHMWPE, and nylatron thick-walled cylinders subjected to the impact of an internal explosion. The outer surface displacements, velocities, and hoop strains have been determined up and beyond fracture from the high speed photographs. The maximum radial velocity of thick-walled cylinders is about 60 m/s.

From the thick-walled cylinder tests it was possible to choose a suitable material to make the driving cylinders for the freely expanding rings. The nylatron cylinders show brittle fracture at small strains, therefore they were not suitable as driving cylinders. The HDPE and UHMWPE cylinders fracture after times which are long enough to observe the ring expansion. There was little difference

found between the HDPE and UHMWPE cylinders except that the UHMWPE cylinders fracture at high strains and after longer times. This makes the UHMWPE the most suitable material for the driving cylinders for the freely expanding ring method.

Few freely expanding ring experiments have been performed for each material, but they gave good consistent and repeatable results.

The nylatron and PEEK ring tests confirmed the marked drop in flow stress at strain rates above  $10^4 \text{ s}^{-1}$  shown in the SHPB results in Chapters 4 and 8.

HDPE, and UHMWPE were also tested using the freely expanding ring method.

A second order polynomial was used to fit the data since it provided a good smooth fit (see Figure (7.15)) for all materials. Higher order fits could be used but produce an oscillatory curve which when double differentiated to yield stress gives rise to oscillations on the deceleration-time curve. This was considered to be unrealistic. It is realised that the use of a second order polynomial forces the velocity term to be linear in time and hence the deceleration to be constant. Other researchers (Gourdin et al (1989), Carden et al (1980) and Warnes et al (1985)) who directly observed the velocity in a similar experiment found that it decreased linearly with time and this observation combined with the goodness of fit of the second order polynomial gives confidence in the results.

In conclusion, the exploding wire technique in combination with the freely expanding ring method has been used to enable the tensile stress-strain properties of polymers to be determined at very high strain rates. This method gave consistent results for HDPE, UHMWPE, nylatron, and PEEK and agreed well with other testing methods.

## **CHAPTER 8**

### **DISCUSSION OF RESULTS, CONCLUSIONS AND RECOMMENDATIONS**

#### **8.1 Discussion of results**

The main objective of this thesis was to study polymers tested at different strain rates at room temperature. To cover a wide range of strain rate, three test methods have been used: quasistatic, SHPB, and exploding wire techniques. Four thermoplastic materials have been studied: HDPE, UHMWPE, nylatron and PEEK. The author has described the results from these testing methods in separate chapters. The results from these methods are summarised and combined in this chapter to allow a comparison to be made between the results from the different test methods.

Principally, the measurement of the stress-strain properties of materials at high strain rates has been carried out using the split Hopkinson pressure bar system in which high compressive strain rates typically in the range of  $10^2 - 10^4 \text{ s}^{-1}$  were achievable with small solid cylindrical samples. The low strain rates were achieved for the same type of sample using a Hounsfield testing machine in compression (and also for a small number of tests in tension) for strain rates about  $10^{-4} - 10^{-2} \text{ s}^{-1}$ . Tensile stress-strain properties at strain rates around  $1.6 \times 10^4 \text{ s}^{-1}$  have been achieved using the expanding ring technique.

According to the Eyring theory, Walley and Field (1994) reported that the actual specimen strain rate can be related to temperature and measured strain rate by the following equation

$$\ln \dot{\epsilon}_1 = \frac{T_0}{T_0 + \Delta T} \ln \dot{\epsilon}_0$$

where  $T_0$  and  $\Delta T$  are the ambient temperature (about  $20^\circ\text{C}$ ) and the change of temperature in the sample respectively;  $\dot{\epsilon}_0$  is the strain rate at  $T_0$  and  $\dot{\epsilon}_1$  is the corrected strain rate after the temperature change. The points on a stress/ $\log(\dot{\epsilon})$  graph should then be shifted to the right of where they would be if there were no temperature change. However, the effect is small at a strain of 5%. The average value of the factor  $T_0 / (T_0 + \Delta T)$  at 5% strain for HDPE is 0.97, and 0.97 for UHMWPE, 0.89 for nylatron and 0.87 for PEEK. Therefore, the isothermal to adiabatic transition is unlikely to cause a noticeable change in the stress/ $\log(\dot{\epsilon})$  plot at a 5% strain level, especially for HDPE and UHMWPE.



1) HDPE

The HDPE results shown in Figure (8.1) represent stress-strain properties over a wide range of strain rate from quasistatic tests at about  $10^{-4} \text{ s}^{-1}$ , up to dynamic rates of  $10^4 \text{ s}^{-1}$ . The stress-strain curves have almost the same plastic modulus, while the Young's modulus varies between 0.4 GPa and 2.5 GPa over a range of strain rate of  $2 \times 10^{-3} \text{ s}^{-1}$  -  $1.2 \times 10^4 \text{ s}^{-1}$  as shown in Figure (8.2). For all the materials tested (except PEEK), the Young's modulus plots indicate a linear increase in E with strain rate for strain rate  $> 100 \text{ s}^{-1}$  i.e. for the SHPB results. In the quasistatic tests, the Young's modulus is much lower than the SHPB values, and hence could not be included in the linear regression line in the graph shown in Figure (8.2). This may be due to the high viscosity of these polymers at low strain rates. Figure (8.3) shows that the flow stress initially increases linearly with the logarithm of strain rate with a slope of 0.77 MPa, but after a strain rate of about  $3 \times 10^3 \text{ s}^{-1}$ , the flow stress starts to increase rapidly.

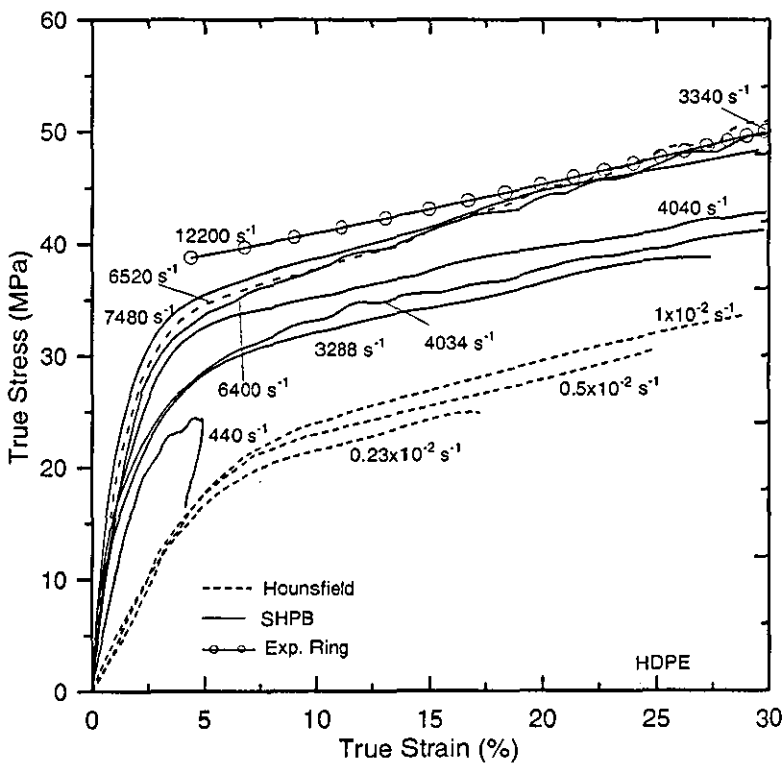


Figure (8.1) Stress-strain curves for HDPE at different strain rates.

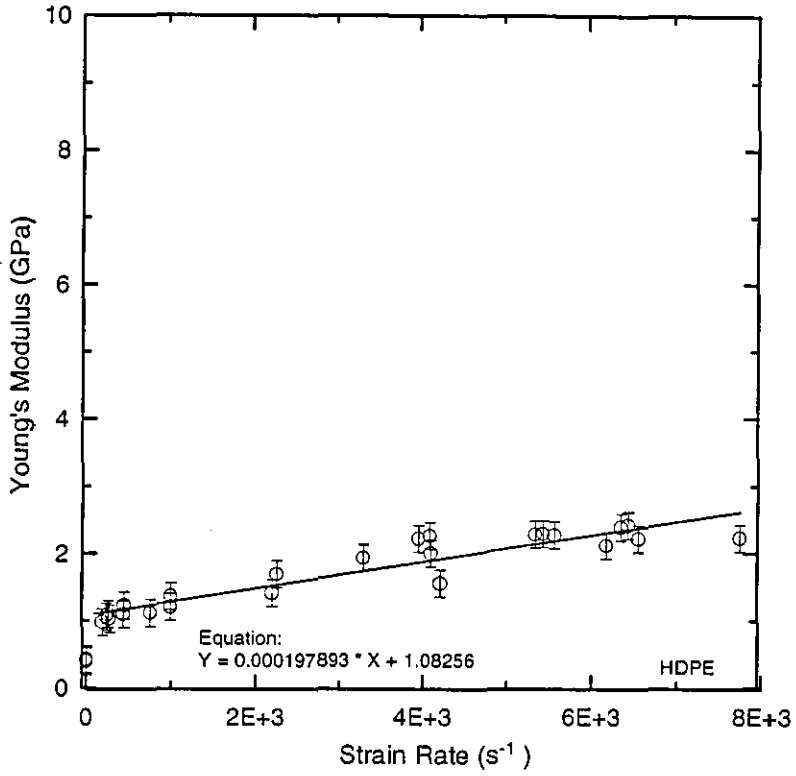


Figure (8.2) Young's modulus-strain rate plot for HDPE.

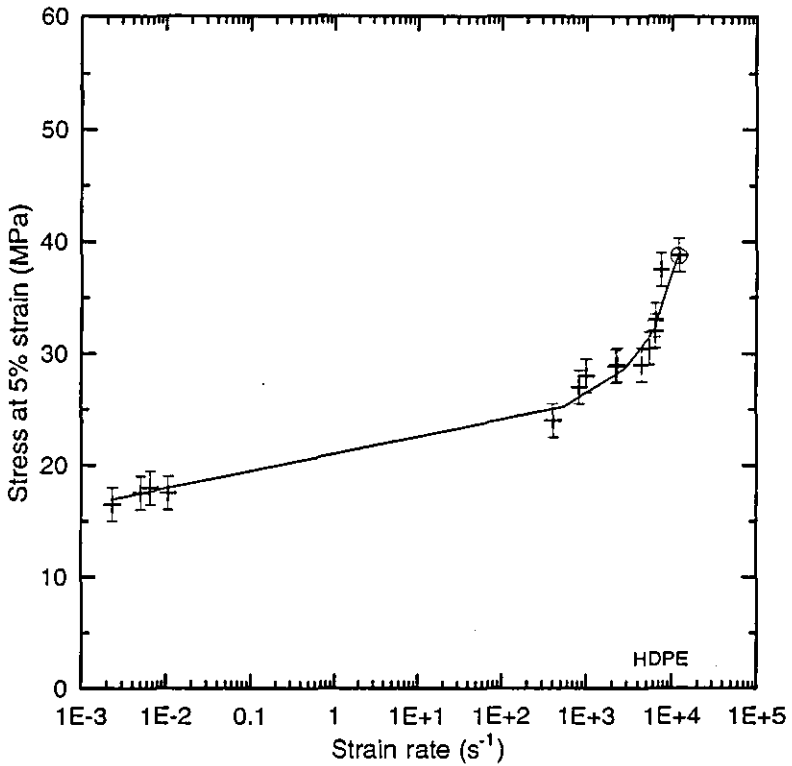


Figure (8.3) Strain rate sensitivity plot for HDPE at 5% strain.

## 2) UHMWPE

UHMWPE, a similar material to HDPE, as expected has mechanical properties similar to HDPE. Figure (8.4) shows the stress-strain curves for UHMWPE from the quasistatic, SHPB and freely expanding ring tests at different strain rates. These tests give different Young's modulus between 0.5 GPa and 2.6 GPa over a range of strain rate from  $2 \times 10^{-4} \text{ s}^{-1}$  to  $1.4 \times 10^4 \text{ s}^{-1}$  as shown in Figure (8.5). Flow stresses at 5% strain plotted against log strain rate are shown in Figure (8.6). As for HDPE, the UHMWPE results show a linear increase of the flow stress with strain rate up to  $3 \times 10^3 \text{ s}^{-1}$  after which the flow stress rises more rapidly with strain rates. The result from the freely expanding ring fit in well with this trend.

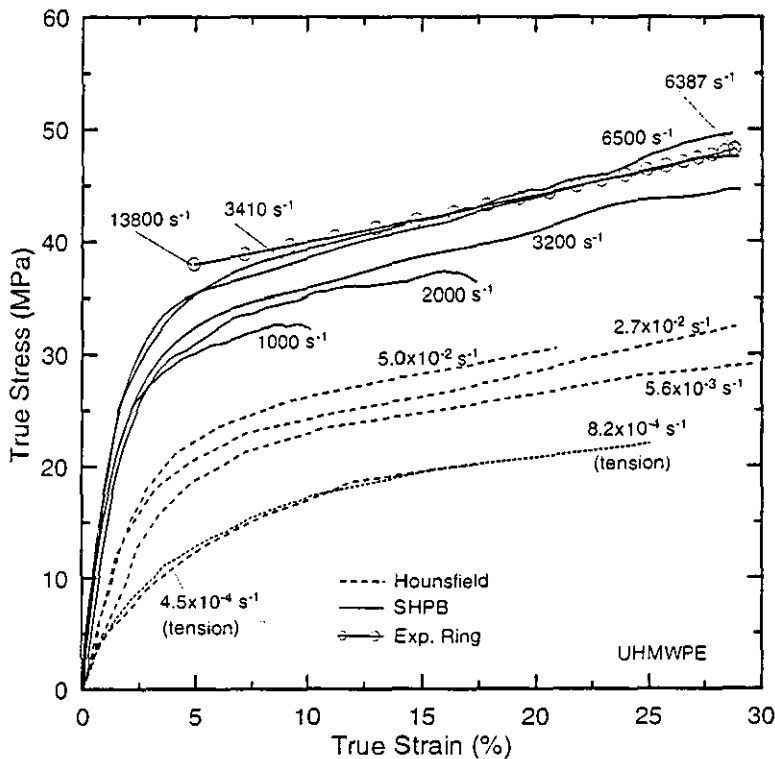


Figure (8.4) Stress-strain curve for UHMWPE at different strain rates.

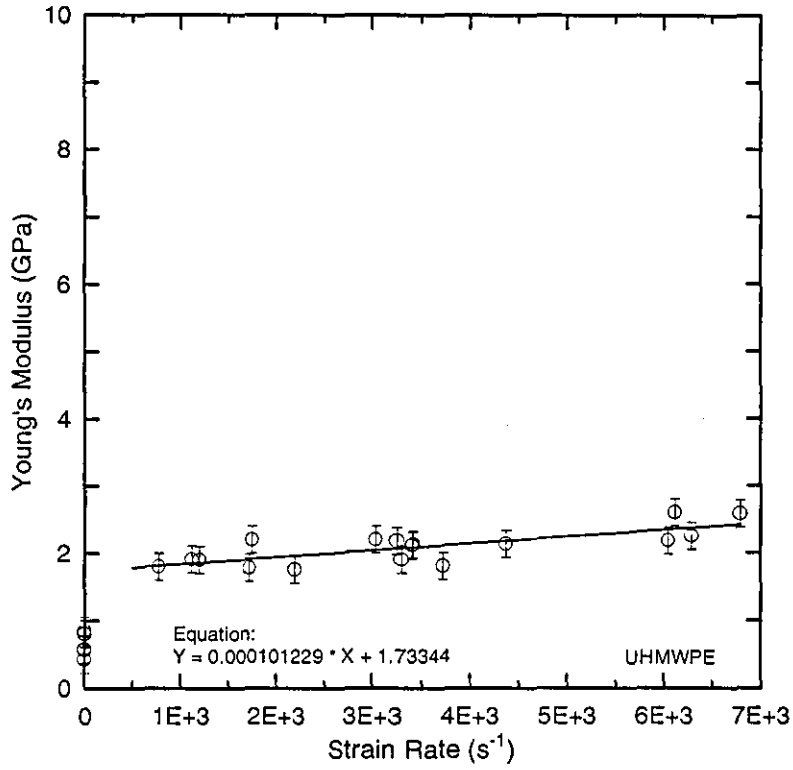


Figure (8.5) Young's modulus variation against strain rate for UHMWPE.

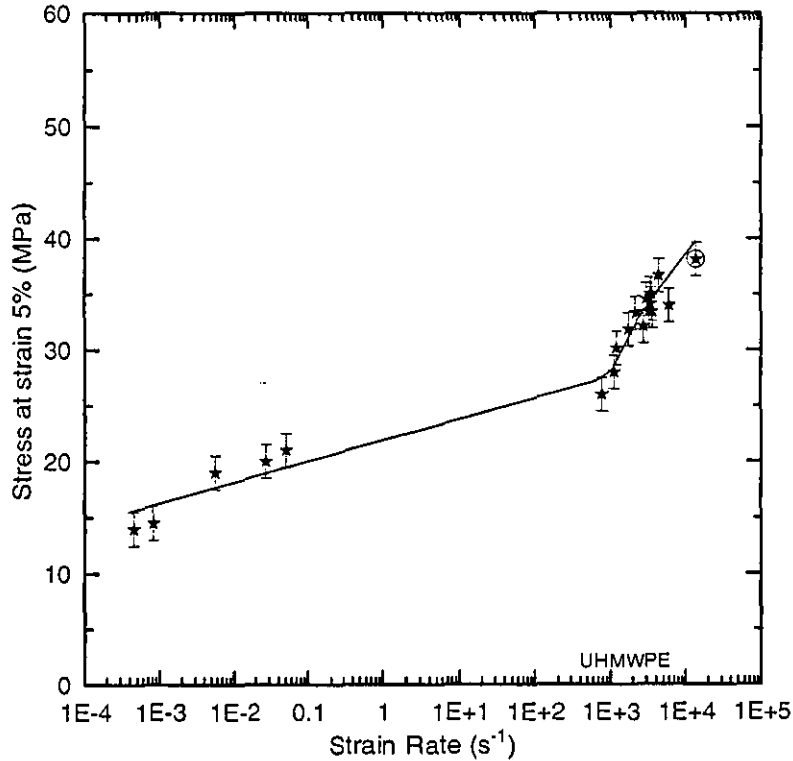


Figure (8.6) Strain rate sensitivity for UHMWPE at 5% strain.

### 3) Nylatron

Nylatron is also used in this study of strain rate behaviour. As can be seen from the stress-strain results in Figure (8.7), the elastic modulus and yield points are high than that for the previous materials. Figure (8.8) shows the Young's modulus varied between 2 GPa and 5 GPa when the strain rate increases from  $1 \times 10^{-4} \text{ s}^{-1}$  to  $1.4 \times 10^4 \text{ s}^{-1}$ . Figure (8.9) shows that the flow stress increases linearly with log strain rate (up to  $4 \times 10^3 \text{ s}^{-1}$ ), the flow stress then increases more rapidly up to  $7 \times 10^3 \text{ s}^{-1}$ , above which there is a sudden drop. This is in contrast to the HDPE and UHMWPE behaviour where no drops occur.

Figure (8.10) shows results from an SHPB test at a mean strain rate (up to 30% strain) of  $7710 \text{ s}^{-1}$ , in which a very high compressive strain was achieved. It can be seen that when the temperature of the sample exceeds the glass transition temperature of the nylatron ( $50^\circ \text{C}$ ), i.e. at a temperature increase of  $29^\circ \text{C}$  above the  $21^\circ \text{C}$  initial temperature, the stress-strain curve shows some clear strain softening.

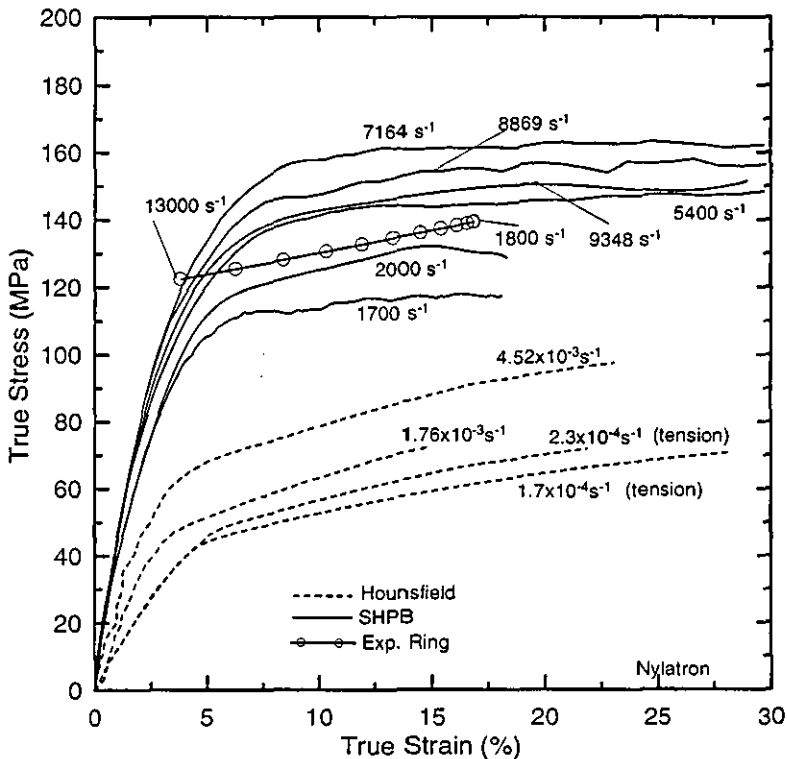


Figure (8.7) Stress-strain curves for nylatron at different strain rates.

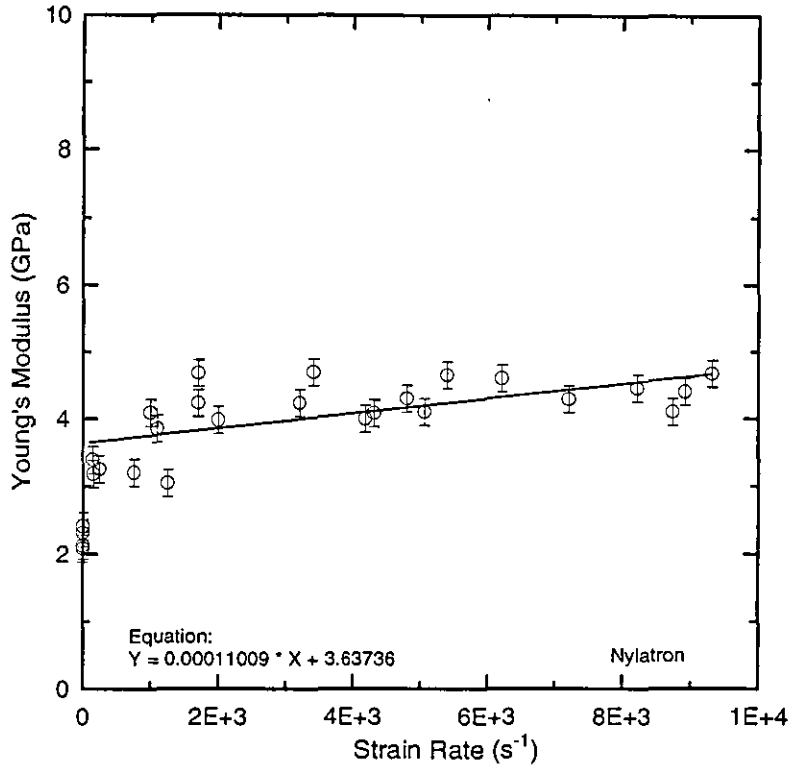


Figure (8.8) Young's modulus against strain rate for nylatron.

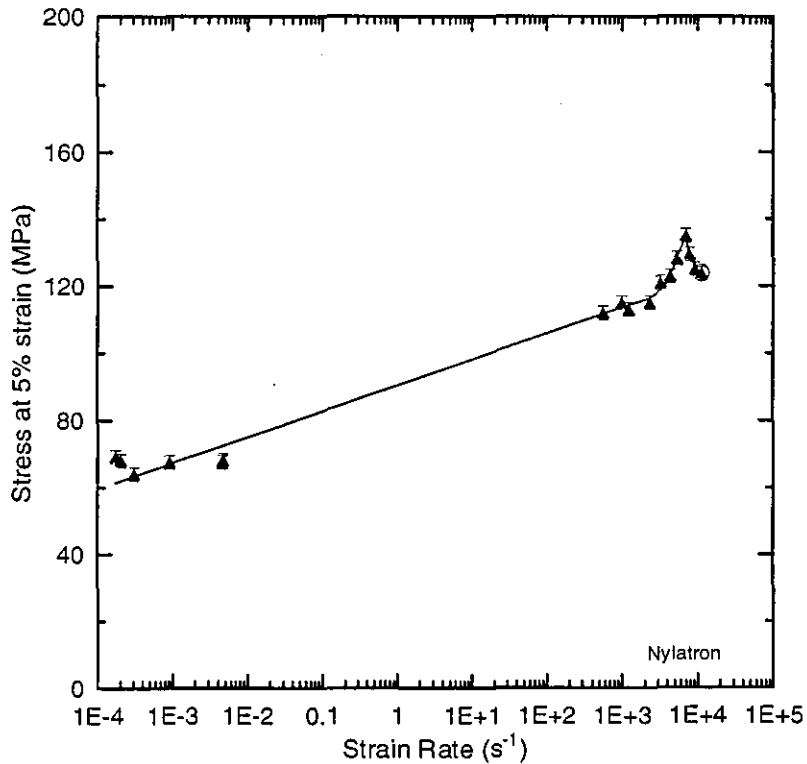


Figure (8.9a) Flow stress against strain rate for nylatron at 5% strain for a wide strain rate range.

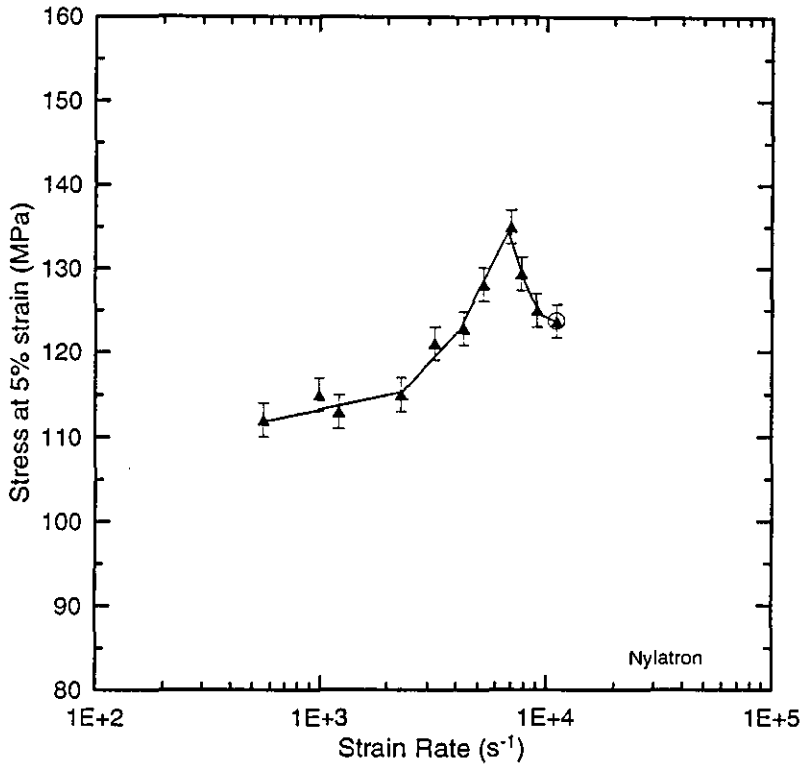


Figure (8.9b) Flow stress against strain rate for nylatron at 5% strain for high strain rates.

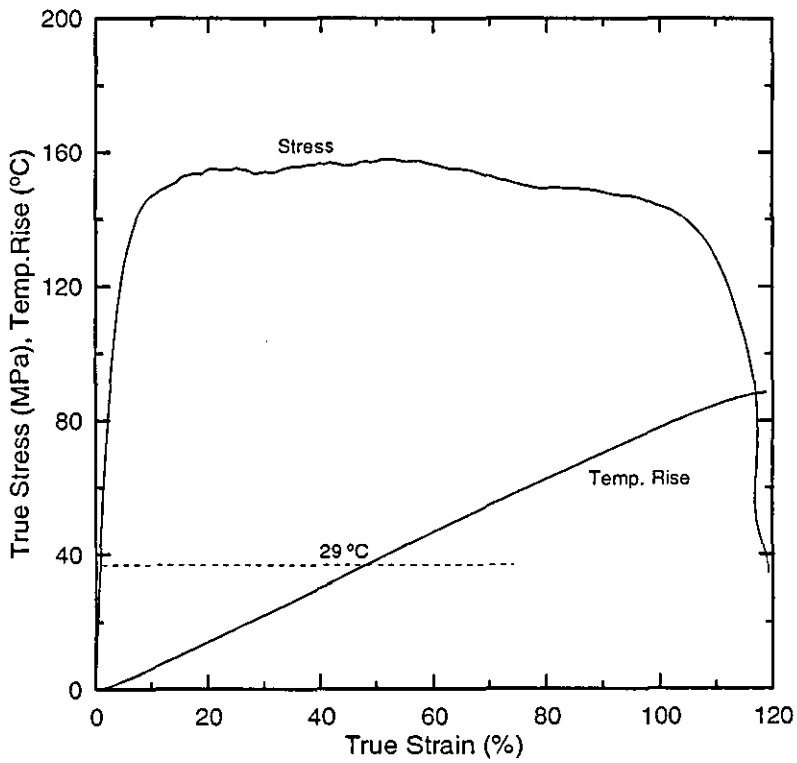


Figure (8.10) Stress and temperature rise against strain curves of nylatron tested at  $\dot{\epsilon}_{30\%} = 7210 \text{ s}^{-1}$ .

4) PEEK

The stress-strain results for PEEK given in Figure (8.11) show a well defined yield point at high strain rates. The Young's modulus of PEEK increases linearly with strain rate as shown in Figure (8.12). Figures (8.13a, b) show strain rate sensitivity plots for PEEK plotted in different scales for clarity. The flow stress increases linearly with log strain rate up to  $4 \times 10^3 \text{ s}^{-1}$ . It then increases more rapidly up to a strain rate of about  $10^4 \text{ s}^{-1}$ , above which a marked sharp drop occurs. This phenomenon is more pronounced in PEEK than in nylatron.

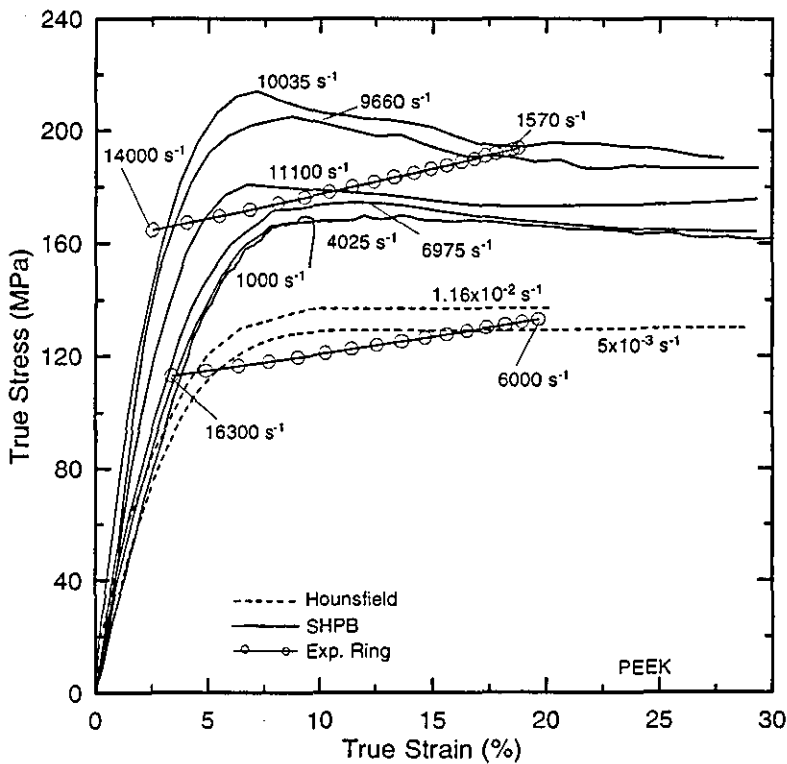


Figure (8.11) Stress-strain curve for PEEK at various strain rates.



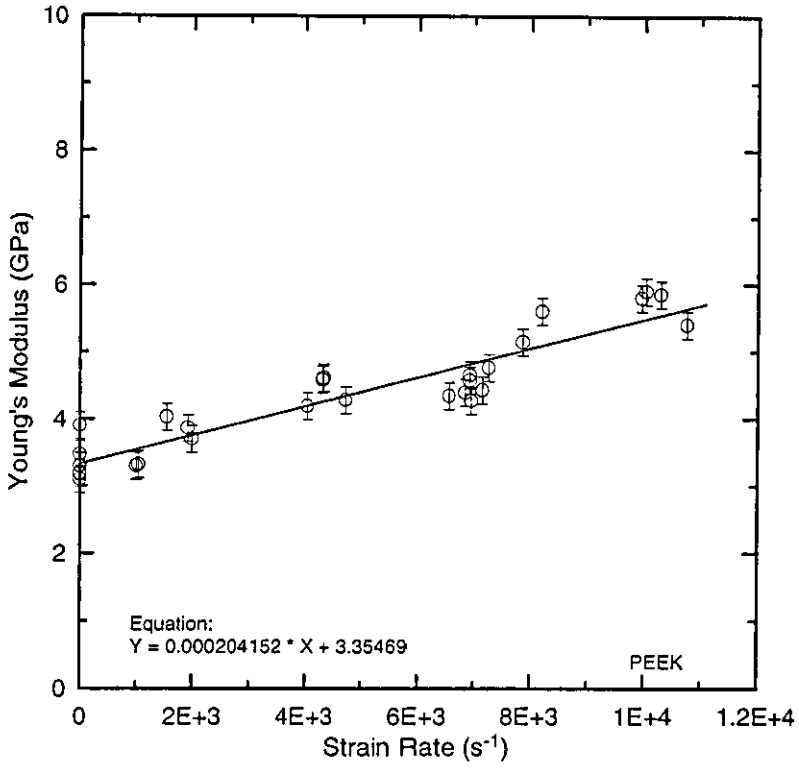


Figure (8.12) Young's modulus against strain rate for PEEK.

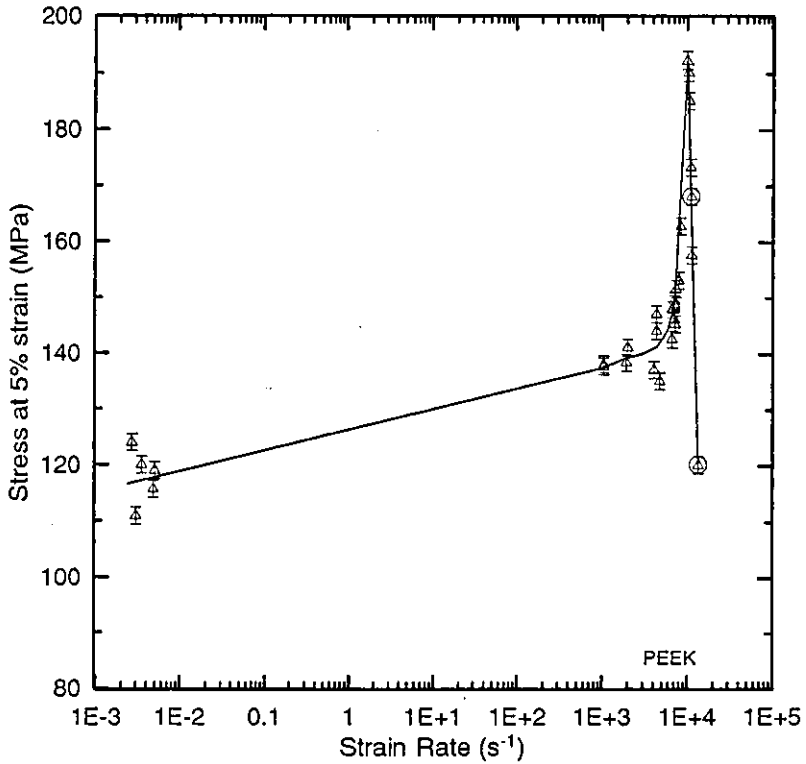


Figure (8.13a) Flow stress at 5% strain against strain rate for PEEK.

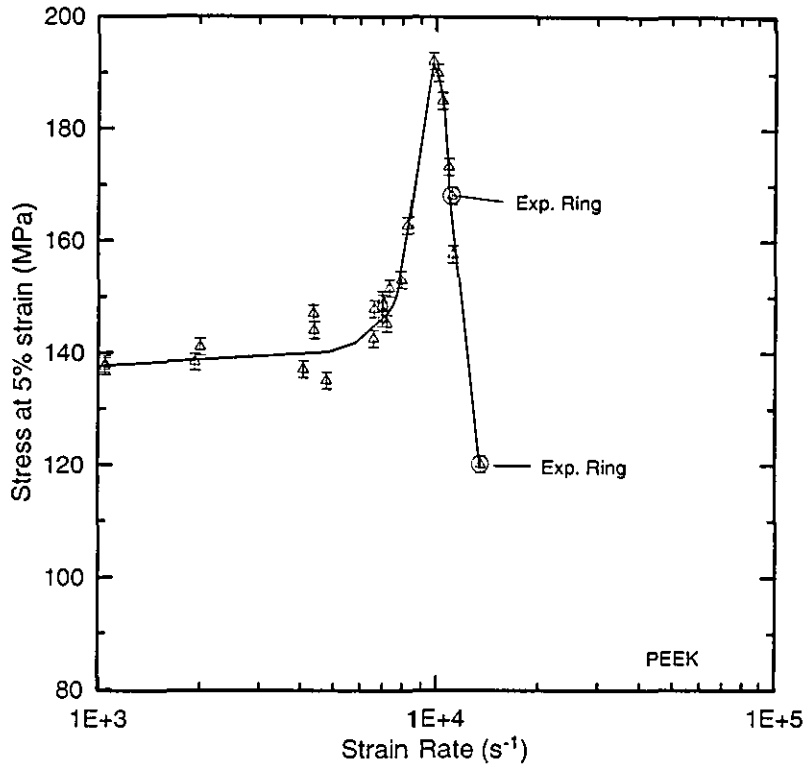


Figure (8.13b) Flow stress at 5% strain against strain rate for PEEK at high strain rates.

The  $\sigma / \log \dot{\epsilon}$  plots for all materials tested show a linear increase in the flow stress with the increase of  $\log$  strain rate up to strain rate of  $10^3 \text{ s}^{-1}$ . This behaviour obeys the thermal activation theory of Eyring which predicts the linear relationship of the flow stress and  $\log$  strain rate. Eyring theory proposed that the dependence of flow stress on strain rate follows the logarithmic form

$$\sigma = \frac{RT}{v_a} \left\{ \frac{\Delta H}{RT} + \ln \frac{2\dot{\epsilon}}{\dot{\epsilon}_0} \right\}$$

where  $R$  is the gas constant,  $T$  is temperature,  $v_a$  is the activation volume, which is the volume of the polymer segment that is considered to represent the volume of a polymer segment which has to move as a whole in order for plastic deformation to occur (Ward (1979)).

The sharp increase of the flow stress may be due to another thermal activation stage. This thermal activation theory extends the Eyring equation above by assuming that there is more than one activated rate process with all species of flow units moving at the same rate, the stress being additive as

$$\sigma = \frac{RT}{V_{a1}} \left\{ \frac{\Delta H_1}{RT} + \ln \frac{2\dot{\epsilon}}{\dot{\epsilon}_{01}} \right\} + \frac{RT}{V_{a2}} \sinh^{-1} \left\{ \frac{\dot{\epsilon}}{\dot{\epsilon}_{a2}} \exp \frac{\Delta H_2}{RT} \right\}$$

where the two activated processes are denoted by the subscript symbols 1 and 2 respectively. Gorham (1991) suggested that inertia may be an important mechanism behind the rapid increase in the flow stress at high strain rates. The deformation velocity, friction and wave propagation could also contribute. Diah et al (1993) believed that the observed increase in strain rate sensitivity at high strain rates is related to the sample thickness.

The drop in the compressive flow stress at very high strain rates for nylatron and PEEK has been observed, but not explained, by other researchers (Walley and Field (1994)). This dip cannot be an experimental error, especially when other polymers tested under the same conditions do not show this dip. Also this unexpected observation has been confirmed in the present work by using two different testing techniques: the freely expanding ring and the SHPB. Therefore, this drop in the flow stress is real, and is not due to sample thickness effects as reported by Diah et al (1993).

The flow stress data on the  $\sigma / \log \dot{\epsilon}$  graphs have been plotted at strains of 5% where the rise in the bulk temperature is negligible and so cannot be considered as a contributory factor to the stress drop at very high strain rate.

The flow stress drop may be caused by internal failure due to local micro fractures caused by the brittleness of the material at very high strain rates. Another possible explanation is that the localised temperature rise generated at the tips of micro-cracks in the sample may effect the material response (Swallowe et al 1984, 1986). The glass transition temperature of nylatron is 50° C and for PEEK it is 144°C, so if the localised temperature reaches this level the material becomes rubbery, and hence the flow stress could drop with increasing strain rate.

## **8.2 Conclusions**

The work described in this thesis has fulfilled the author's main objective to study the mechanical properties of a selection of thermoplastic materials. Mechanical tests have been performed on four polymeric materials; HDPE, UHMWPE, nylatron and PEEK 150g over a wide range of strain rates ( $\approx 10^{-4} \text{ s}^{-1} - 2 \times 10^4 \text{ s}^{-1}$ ).

To assist in the interpretation of the SHPB results, a theoretical computer analysis was undertaken which was based upon multiple elastic reflections within the sample. The analysis gave important insights into how long it takes for stress equilibrium to be reached in a sample. Using the analysis, there was excellent agreement between the predicted and measured stress-strain curves over the initial elastic region for all the polymers.

Three theoretical models; standard linear solid, bi-linear and four-element models were applied on the experimental stress-strain results. The standard linear solid model fit very well the HDPE and UHMWPE stress-strain curves, but does not fit the whole range of strain for nylatron and PEEK due to their greater stiffness and sharp elastic-plastic transition in their stress-strain curves. The bi-linear and four-element model gave a good agreement with the experimental data for all polymers except for PEEK at high strain rates where the upper yield feature clearly occurs

The exploding wire technique used in this project enabled a study to be made of the tensile behaviour of polymers in the form of hollow cylinders, up to and beyond fracture.

Although it was possible to measure the outer surface hoop strain, the stress/strain properties could not be determined without knowing the loading pressure. Due to the difficulties in measuring the pressure inside these cylinders, the freely expanding ring method was used to determine the stress-strain properties of the polymers without the need to measure the pressure profile. The freely expanding ring method enables measurements of tensile properties at very high strain rates to be made and cannot be achieved by other methods such as SHPB.

Combining the results of the quasistatic, SHPB and freely expanding ring methods in one set of graphs for each polymer has enabled material property variations over a wide range of strain rates to be visualised. The graphs clearly show that the flow stresses for HDPE and UHMWPE increase linearly with increasing log strain rate up to a strain rate of about  $10^3 \text{ s}^{-1}$ , above which the flow stress increases even more rapidly this behaviour possibly caused by thermal activation processes occurring in different stages, or by a rapid increase in the crystallinity of the polymers and hence these polymers become harder. Nylatron and PEEK behave in a similar manner except that at very high strain rates a rapid decrease occurs in the flow stress. This decrease could be associated with a transition to brittle behaviour or adiabatic shearing. Fractures caused by adiabatic shear have been observed to take place in metals at very high strain rates. Indications of shear fractures were noticed in the pieces found from the fractured rings after the experiments and this is the likely cause of the drop in flow stress.

### **8.3 Recommendations for future work**

- 1) Further work is needed on the freely expanding ring method to obtain properties of polymers in tension at different high strain rates. This can be achieved by using different input voltages for the exploding wires.
- 2) In addition to high speed photography, laser beam scanning could be used to record the radial displacement of the outer surface of expanding rings and cylinders. This would give a continuous recording of the displacement and also better resolution.
- 3) A wider range of polymers and other materials such as composites and metals could be tested using the freely expanding ring method. Comparisons could then be made between the high strain rate tensile behaviour and the high rate compressive behaviour obtained from SHPB system.
- 4) Properties of polymers should be studied using the SHPB system at low and high temperatures to examine, for example, the effects of the glass transition temperature on the polymer behaviour.
- 5) More tensile tests should be performed at low strain rates using the Hounsfield machine to be compared with the compressive tests at low strain rates.
- 6) The multiple wave reflection method used with the SHPB to predict the properties of materials up to the elastic limit should be extended to cover the plastic polymer response, which would involve taking into account the variations in the sample dimensions and Poisson's ratio during a test.
- 7) Multiple loading could be used in SHPB system by using a two-split bars projectile.
- 8) The nylatron and PEEK samples structure could be x-rayed to establish the structure associated with the flow stress drop at very high strain rates.

## **REFERENCES**

- Ahmad S H (1985)** Optical studies of cylindrical blast waves produced by exploding wires, Internal report.
- Ahmad S H (1988)** High strain rate behaviour of polymers using blast wave and impact loading methods. PhD thesis, Department of Physics, Loughborough University.
- Albertini C and Montagnani M (1974)** Testing techniques based on the split Hopkinson bar. in J. Harding (Ed) Mechanical properties at high rates of strain, Inst. of Physics, London, ser no. **21** 22-32.
- Al-Maliky N S (1991)** High speed photographic studies of blast waves impact phenomena. MPhil thesis, Department of Physics, Loughborough University.
- Al-Maliky N S (1992)** Theory and application of split Hopkinson pressure bar. Internal report, Department of Physics, Loughborough university.
- Al-Maliky N and Parry D J (1994)** Measurements of high strain rate properties of polymers using an expanding ring method, J. Physique IV **4** C8-71-6.
- Al-Maliky N and Parry D J (1996)** A freely expanding ring technique for measuring the tensile properties of polymers, Meas. Sci. Technol. **7** 746-752.
- Anderson J C, Leaver K D, Alexander J M and Rawlings R D (1974)** Materials science. Nelson and sons Ltd.
- Arruda E M and Boyce M C (1991)** Proceedings of the 8th international conference on deformation, yield and fracture of polymers, Cambridge, UK, 8-1-1991.
- Attwood T E, Dawson P C, Freeman J, Hoy L, Rose J and Staniland P (1981)** Synthesis and properties of polyaryletherketones. Polymer **22** 1096-1103.
- Bauwens-Crowet C (1973)** J. Matter. Sci. **8** pp968.
- Bauwens J C (1980)** Attempt to correlate the formation of free volume and plastic deformation process in glassy polymers. Polymer **21** 699-705.
- Bauwens-Crowet C, Bauwens J C and Holmes G (1969)** Tensile yield stress behaviour of glassy polymers. J. Polym. Sci. A-2 **7** 735-74.
- Bauwens-Crowet C, Ots J M and Bauwens J C (1974)** The strain rate and temperature dependence of yield of polycarbonate in tension, tensile creep and impact tests. J. Mat. Sci. **9** 1197-1201.
- Benham P D, and Warnock F V (1979)** Mechanics of solids and structure. Pitman Press.
- Bennett F D (1958a)** Cylindrical shock wave from exploding wire. Phys. Fluids **1**(4) pp34.
- Bennett F D (1958b)** Energy partition in the exploding wire phenomena. Phys. Fluids **1**(6) pp515.

## References

- Bennett F D (1962)** Shock producing mechanisms of exploding wires. *Phys. Fluids* 5(8) pp891.
- Bennett F D (1965)** High temperature cores in exploding wires, *Phys. Fluids* 8 (6) 1106-1108.
- Bennett P D (1971)** Current diffusion in cylindrical exploding wires and fuses during microsecond electrical pulses. *J. Appl. Phys.* 42 (7) 2835-2839.
- Bennett F D, Kahl G D and Weber F N (1970)** Qualitative interferometry of expanding metal vapor. *Phys. Fluids* 13(7) 1725-1730.
- Bennett F D, Burden H S and Shear D (1974)** Expansion of superheated metals. *J. Appl. Phys.* 45(8) 3429-3438.
- Beguelin P H and Kausch H H (1994)** The effect of the loading rate on the fracture toughness of poly(methylmethacrylate), polyacetal, polyether-etherketone and modified PVC. *J. Mat. Sci.* 29 91-98.
- Bertholf L D and Karnes C H (1975)** Two-dimensional analysis of the split Hopkinson pressure bar system. *J. Mech. Phys. Solids* 23 1-19.
- Bhusham B and Johsman W R (1978)** Measurement of dynamic material behaviour under nearly uniaxial strain conditions. *Int. J. Solids Structures* 14 pp739.
- Billington E W and Brissenden C (1971)** Dynamic stress-strain curves for various plastics and fibre-reinforced plastics. *J. Phys. D: Appl. Phys.* 4 272-286.
- Blundell D J, Mahendrasingam A, McKerron D, Turner A, Rule R, Oldman R and Fuller W (1994)** Orientation changes during the cold drawing and subsequent annealing of PEEK, *Polymer* 35 (18) 3875-3882.
- Bodner S R and Parton Y (1974)** A representation of elastic-viscoplastic strain hardening behaviour for generalized straining histories. *Inst. Physics Conf. Serial no.* 21 102-111.
- Booth M J and Hirst W (1970)** The rheology of oils during impact. I. Mineral oils. *Proc. Roy. Soc. Lon. A* 316 391-413.
- Booth M J and Hirst W (1970)** The rheology of oils during impact. II. Silicone fluids. *Proc. Roy. Soc. Lon. A* 316 314-429.
- Bowden P B (1973)** *Physics of glassy polymers.* ed. Haward R N, Applied Sci., London.
- Boyce M C and Arruda E M (1990)** An experimental and analytical investigation of the large strain compressive and tensile response of glassy polymers. *Polymer Eng. and Sci.* 30(21) 1288-1298.
- Brinson H F and DasGupta A (1975)** The strain rate behaviour of ductile polymers. *Exp. Mech.* 15 458-463.
- Briscoe B J And Nosker R W (1984)** The influence of interfacial friction on the deformation of (HDPE) in a split Hopkinson pressure bar. *Wear* 95 241-262.



References

- Briscoe B J And Nosker R W (1985)** The flow stress of high density polyethylene at high rates of strain, *Polymer Communications* **26** (October) 307-308.
- Briscoe B J and Hutchings I M,(1976)** Impact yielding of high density polyethylene. *polymer* **17** 1099-102.
- Brooks N W, Duckett R A and Ward I M (1992)** Investigation into double yield points in polyethylene. *Polymer* **33**(9) 1872-1879.
- Brown N and Ward I M (1968)** Load drop at the upper yield point of a polymer. ✱  
*J. Polymer Sci., A-2* **6** 607-620.
- Campbell J D and Dowling A R (1970)** The behaviour of materials subjected to dynamic incremental shear loading. *J. Mech. Phys. Solids* **18**, pp43.
- Cansfield D L, Ward I M, Woods D, Buckley A, Pierce J and Wesley J (1983)** Tensile strength of ultra high modulus linear polyethylene filaments. *Polymer communications* **24** 130-131.
- Carden A E, Williams P E and Karpp R R (1980)** Comparison of flow curves of 6061 aluminium alloy at high and low strain rates. In *Shock wave and high strain rate phenomena in metal, concepts and applications*, ed. Meyers M A and Lawrence E, Murr Plenum Press, New York, 37-50.
- Cassidy E C, Abramowitz S and Beckett C W (1968)** Investigations of the exploding wire process as a source for high temperature studies. NBS Monograph 109, US Dept of Commerce National Bureau of Standards.
- Cebe P, Chung S Y and Hong S (1987)** Effect of thermal history on mechanical properties of polyetheretherketone below the glass transition temperature. *J. Appl. Polymer Sci.* **33** 487-503.
- Channell A D, Clutton E and Capaccio G (1994)** Phase segregation and impact toughness in linear low density polyethylene. *Polymer* **35** (18) 3893-3899.
- Chase K W and Goldsmith W (1974)** Mechanical and optical characterisation of an anelastic polymer at large strain rates and large strains. *Exp. Mech.* **14** 10-18.
- Chiem C Y and Liu Z G (1986)** High strain-rate behaviour of carbon fibre composites. *Proc. of the Eur. Mech. Colloquium 214*, Sept 16-19 Kupari Yugoslavia, "Mechanical Behaviour of Composites and Laminates". ed. by Green W A and Micunovic, Elsevier Applied Sci. pub. Ltd. 45-53
- Chiu S and Neubert V (1967)** Difference method for wave analysis of the split Hopkinson pressure bar with a viscoelastic specimen. *J. Mech. Phys. Solids* **15** 177-193.
- Christensen R M (1967)** Application of the method of time-dependent boundary conditions in linear viscoelasticity. *J. Appl. Mech.* **34** 503-504.

## References

- Chou S C, Robertson K and Rainey (1973)** The effect of strain rate and heat developed during deformation on the stress-strain curve of plastics. *Exp. Mech.* **13** 422-432.
- Clark D S and Duwez P E (1950)** The influence of strain rate on some tensile properties of steel. *Proc. ASTM* **50** 560-575.
- Conn A F (1965)** On the use of thin wafers to study dynamic properties of metals. *J. Mech. Phys. Solids* **13** 311-327.
- Crochet M J (1966)** Symmetric deformations of viscoelastic-plastic cylinders. *J. Appl. Mech.* **33 E** 327-334.
- Daniel I M, LaBedz R H and Liber T (1981)** New method for testing composites at very high strain rates. *Exp. Mech.* **21** pp71.
- Davies R (1948)** A critical study of the Hopkinson pressure bar. *Phil. Trans. A*, **240** 375.
- Davies R (1956)** Stress waves in Solids. *British J. of Appl. Phys.* **7** 203-209.
- Davies E D and Hunter S C (1963)** The dynamic compression testing of solids by the method of the split Hopkinson pressure bar. *J. Mech. Phys. Solids* **11** 155-179.
- Dawson P C (1993)** The mechanical and thermal behaviour of polymers under high strain rate compression. Ph.D thesis, Department of Physics, Loughborough University.
- Dawson P C, Swallowe G M, Xinwu Z (1991)** Temperature rises during high rate deformation of polymers. *Colloque C3, Journal de Physique III* **1** C3-702 -C3-707
- Deopura B L, Sengupta A K, Verma Anu (1983)** Effect of moisture on physical properties of nylon. *Polymer Communications* **24** (September) 287-288.
- Dharan C K and Hauser F E (1970)** Determination of stress-strain characteristics at very high strain rates. *Exp. Mech* **10** 370-376.
- Dion N N, Leever P S and Williams J G (1993)** Thickness effects in split Hopkinson pressure bar tests. *Polymer* **34** (20) 4230-4234.
- Dirwish M (1979)** Ph.D thesis, Department of Physics, Loughborough University.
- Dixon P R (1990)** PhD thesis, Department of Physics, Loughborough University.
- Duffy J (1974)** Some experimental results in dynamic plasticity. *Inst. Phys. Conf.* **21** 72-80.
- Edelson H D and Korneef T (1966)** A comparative study of exploding wire in air and water, *J. Appl. Phys.* **37** (5) pp2166.
- Egorov E A, Zhizhenkov V, Marikhin V and Myasnikova L (1990)** Molecular mobility and fracture processes in ultimately drawn high density polyethylene. *J. Macromol. Sci. Phys.* **B29** (2&3) 129-137.
- Eisenberg M A and Yen C F (1983)** Application of a theory of viscoplasticity to uniaxial cyclic loading. *J. Eng. Mat. Tech.* **105** 106-111.
- Ellwood S H (1983)** PhD thesis, Department of Physics, Loughborough University.

## References

- Ellwood S, Griffiths L J and Parry D J (1982)** A tensile technique for materials testing at high strain rates. *J. Phys. E: Sci. Instrum.* **15** 1169-1172.
- Ensminger R R and Fyfe I M (1966)** Constitutive model evaluation using cylindrical stress wave propagation. *J. Mech. Phys. Solids* **14** 231-238.
- Field J E, Swallowe G M, Pope H and Palmer S (1984)** High strain rate properties of explosives. *Inst. Phys. Conf. ser. no 70 (3rd Conf. Mech. Prop. High rates of strain. Oxford 381-389).*
- Findley W N, Lai J and Onaran K (1976)** Creep and relaxation of nonlinear viscoelastic materials. North-Holland Publ. Co., Amsterdam.
- Fleck N A, Stronge W J, Liu J (1990)** High strain rate shear response of polycarbonate and polymethylmethacrylate. *Proc. R. Soc. London* **A429** 459-479.
- Follansbee P S (1986)** High strain rate deformation of FCC metals and alloys. In *Metallurgical applications of shock wave and high strain rate phenomena*, ed. Murr L E, Staudhammer and Meyers M A, Marcel Dekker, New York, p.451.
- Follansbee P S and Frantz C (1983)** Wave propagation in the split Hopkinson pressure bar. *J. Eng. Mat. Tech.* **105** 61-66.
- Follansbee P S and Kocks U F (1988)** A constitutive description of the deformation of copper based on the use of the mechanical threshold stress as an internal state variable. *Acta Metall.* **36(1)** 81-93.
- Follansbee P S, Regazzoni G and Kocks U F (1984)** In *Mechanical properties of materials at high rates of strain*, *Inst. Phys. Conf. ser.* **70**.
- Forrestal M J and Walling H C (1972)** Axisymmetric plastic response of rings to short duration pressure pulses. *AIAA J.* **10 (1)** 1382-1384.
- Forrestal M J, Duggin and Butler (1980)** An explosive loading technique for uniform expansion of 304 stainless steel cylinders at high strain rates, *J. Appl. Mech. trans. ASME* **47** 17-19.
- Fotheringham D and Cherry B (1978)** Strain rate effects on the ratio of recoverable to non-recoverable strain in linear polyethylene. *J. Mat. Sci.* **13** 231-238.
- Fotheringham D and Cherry B (1978)** The role of recovery forces in the deformation of linear polyethylene. *J. Mat. Sci.* **13** 951-964.
- Frounchi M, Chaplin R and Burford R (1994)** Mechanical and fracture properties of diethylene glycol bis(allyl Carbonate) resins. *Polymer* **35(4)** 752-757.
- Fyfe I M and Rajendran A M (1980)** Dynamic pre-strain and inertia effects on the fracture of metals. *J. Mech. Phys. Solids* **28** 17-26.
- Gent A N and Jeon J (1986)** Plastic deformation of crystalline polymers. *Polymer Eng. and Sci.* **26 (4)** 285-289.
- Gilat A and Pao Y (1988)** High rate decremental strain rate test. *Exp. Mech.* **28** 322-325.

## References

- Gilbert D G, Ashby M F and Beaumont P (1986)** Modulus maps for amorphous polymers. *J. Mat. Sci.* **21** 3194-3210.
- Gorham D A (1979)** Measurement of stress-strain properties of strong metals at very high rates of strain. *Inst. Phys. Conf. ser.* **47**, Chapter 1.
- Gorham D A (1989)** Specimen inertia in high strain rate compression. *J. Phys. D: Appl. Phys.* **22** 1888-1893.
- Gorham D A (1991)** An effect of specimen size in the high strain rate compression test. *J. de Physique III* **1** C3 411-419.
- Gorham D A, Pope P H and Cox O (1984)** Sources of error in very high strain rate compression tests. *Inst. Phys. ser.* **70** 151-158.
- Gottenberg W G, Bird J and Agrawal G (1969)** An experimental study of a non-linear viscoelastic solid in uniaxial tension. *J. Appl. Mech.* **36 E** 558-564.
- Gourdin W H (1989a)** VISAR analysis in the presence of large intensity change: Application to the expanding ring. *Rev. Sci. Instrum.*, **60(4)** 754-759.
- Gourdin W H (1989b)** Constitutive properties of copper and tantalum at high rates of tensile strain: expanding ring results. *Inst. Phys. Conf. Ser No* **102** pp221.
- Gourdin W H, Weinland S and Boling R (1989)** Development of the electromagnetically launched expanding ring as a high strain rate test. *Rev. Sci. Instrum.*, **60(3)** 427-432.
- Graff K F (1975)** Wave motion in elastic solids, Oxford.
- Griffiths L J and Martin D (1974)** A study of the dynamic behaviour of a carbon fibre composite using the split Hopkinson pressure bar. *J. Phys. D: Appl. Phys.* **7** 2329-2341.
- Griffiths L J, Parry D J and Stewardson H (1986)** Cylindrical blast waves for materials testing. *Proc. Int. Symp. on Intense Dynamic loading and its effects*, Beijing, ed. Z Zheng and J Ding (Beijing: Science Press) 269-75.
- Griffiths L J, Parry D J and Warthington R (1979)** A comparison of optical and strain gauge techniques in the determination of the dynamic mechanical behaviour of carbon fibre composite using a split Hopkinson pressure bar. *Proc. Conf. on mechanical properties at high strain rates*, ser no. **47** IOP, London, pp62.
- G'Sell C, Boni S and Shrivastava S (1983)** Application of the plane simple shear test for determination of the plastic behaviour of solid polymers at large strains. *J. Mat. Sci.* **18** 903-918.
- G'Sell C and Jonas J J (1979)** Determination of the plastic behaviour of solid polymers at constant true strain rate. *J. Mat. Sci.* **14** 583-591.
- G'Sell C and Jonas J J (1981)** Yield and transient effects during the plastic deformation of solid polymers. *J. Mat. Sci.* **16** 1956-1974.
- Hall I H (1968)** *J. Appl. Polymer Science* **12** 739-750.

## References

- Hamdan S (1994)** The thermomechanical properties of aromatic polymers. Ph.D thesis, Department of Physics, Loughborough university.
- Hartmann B, Lee G F and Cole Jr. R (1986)** Tensile yield in polyethylene. *Polymer Eng. Sci.* **26**(8) 554-559.
- Hasan O A, Boyce M C, Li X S and Berko S (1993)** An investigation of the yield and postyield behaviour and corresponding structure of poly(methylmethacrylate). *J. Polymer Sci.* **31 Part B: Polymer Phys.** 185-197.
- Hauser F E (1966)** Techniques for measuring stress-strain relations at high strain rates. *Exp. Mech.* **6**(8) 395-402.
- Hauser F E, Simmons J A and Dorn J E (1960)** Strain rate effects in plastic wave propagation. in *Response of metals to high strain velocity deformation.* Metallurgical Soc. Conf. **9**, ed. Sheumon P G and Zackay V F.
- Haward R N (1994)** The derivation of strain hardening modulus from true stress-strain curves for thermoplastics. *Polymer* **35** (18) 3858-3862.
- Haward R N and Thackray G (1968)** *Proc. Roy. Soc. London A* **302** 453.
- Haward R N, Murphy B and White E (1971)** Relationship between compressive yield and tensile behaviour in glassy thermoplastics. *J. Appl. Polymer Sci.A-2* **9** 801-814.
- Hawley R H and Powel W E (1967)** A grain boundary model for polycrystals and singled carbides. *Exp. Mech.* **7**(5) 242-247.
- Hillier K W (1949)** A Method of measuring some dynamic elastic constants and its applications to the study of high polymers. *Proc. Phys. Soc.* **B62** 701-713.
- Hillier K W, Kolsky H (1949)** An investigation of dynamic elastic properties of some high polymers. *Proc. Phys. Soc.* **B62** 111-120
- Hodson (1992)** Internal report, Physics Department, Loughborough University.
- Hoggatt C R, Orr W R and Recht R F (1967)** The use of an expanding ring for determining tensile stress-strain relationships as functions of strain rate. *Proc. First Intl. Conf. Centre for High energy forming, June 19-23, Estes Park, Dover.*
- Hoggatt C R and Recht R F (1969)** Stress-strain data obtained at high strain rates using an expanding ring. *Exp. Mech.* **9** 441-448.
- Hope P S, Ward I M, and Gibson A G (1980)** The hydrostatic extrusion of polymethylmethacrylate. *J. Mat. Sci.* **15** 2207-2220.
- Hsu T R and Bertels A (1974)** Improved approximation of constitutive elasto-plastic stress-strain relationship for finite element analysis. *AIAA J.* **12**(10) 1450-1452.
- Hwangbo C K, Kong H J and Lee S S (1980)** Inhomogeneous wire explosion in water. *New Phys. (Korean Phys. Soc.)* **20** (3) 149-153.
- Imai Y, Brown N (1976)** The effect of strain rate on craze yielding, shear yielding, and brittle fracture of polymer at 77°K. *J. Polymer Sci.* **14** 723-739.

## References

- Isuzugawa K and Fujimura T (1982)** Studies of exploding wires. Bull Univ. OSAKA PREFEZI ser. 31 (2) 111-116.
- Johnson W (1972)** Impact strength of materials. Edward Arnold Pub. Ltd, London.
- Johnson C V, and Goldsmith W (1969)** Optical and mechanical properties of birefringent polymers. Exp. Mech. 9(6) 263-268.
- Jahsman W E (1971)** Re-examination of Kolsky technique for measuring dynamic material behaviour. J Appl. Mech. 38 75-82.
- Kamei E and Brown N (1984)** Crazeing in polyethylene. J. Polymer Sci.: Polymer Physics edition 22 543-559.
- Klein P G, Ladizesky N H and Ward I M (1986)** Electron irradiated isotropic polyethylene: Structure and mechanical properties of oriented mono filament produced by drawing, J. Polymer Sci. 24 1093-1113.
- Kolsky H (1949)** An investigation of the mechanical properties of materials at very high rates of loading. Proc. Phys. Soc. B 62 676-700.
- Kolsky H (1963)** Stress wave in solids. Dover Pub.
- Kukureka S N and Hutchings I M (1984)** Yielding of engineering polymers at strain rates of up to  $500 \text{ s}^{-1}$ , Int. J. Mech. 26 (11/12) 617-623.
- Lee E H (1960)** in Proceeding of the first symposium of naval structure mechanics, Pergamon Press, Oxford, pp456.
- Lee W M (1988)** Pressure measurements correlated with electrical explosion of metals in water. J. Appl. Phys. 64 (8) pp-3851
- Lindberg H E and Anderson D L (1968)** Dynamic pulse backing of cylindrical shells under transient lateral pressures. AIAA J. 6(4) 589-598.
- Lindberg H E (1970)** Dynamic pulse of cylindrical shells. TR 001-70, April 1970 Poulter Lab., Stanford Research Inst., Menlo Park, Calif. 36-38.
- Lindholm U S (1964)** Some experiments with the split Hopkinson pressure bar. J. Mech. Phys. Solids 12 317-335.
- Mehta P K and Davids N (1966)** A direct numerical analysis method for cylindrical and spherical elastic waves. AIAA J. 4(1) 112-117.
- Malatynski M and Klepaczko J (1980)** Experimental investigation of plastic properties of lead over a wide range of strain rates. Int. J. Mech. Sci. 22 173-183.
- Malvern L E, Tang T, Jenkins D and Gong J (1986)** Dynamic compressive strength of cementitious materials. Mat. Res. Soc. Symp. Proc. 64 119-138.
- Matsuoka S (1992)** Relaxation phenomena in Polymers. Hanser Pub. New York.
- Megson T H G (1987)** Strength of materials for civil engineers. 2nd ed. Edward Arnold, pp50.
- Morris D H and Riley W F (1972)** A photomechanical material for elastoplastic stress analysis. Exp. Mechanics 12 (10) 448-453.

## References

- Nakumura Y, Tsuno, Takao (1980)** High speed Schlieren system, as applied to measure high velocity flow. *Annu. Rep Eng. Res. Inst., Faculty of Eng., Univ. of Tokyo*, **39** 151-154.
- Nazarenko S, Bensason S, Hiltner A and Baer E (1994)** The effect of temperature and pressure on necking of polycarbonate. *Polymer* **35** (18) 3883-3892.
- Niordson F I (1965)** A unit for testing materials at high strain rates. *Exp. Mech.* **5** pp29.
- Parry D J, Dixon P R, Hodson S and Al-Maliky N (1994)** Stress equilibrium effects within Hopkinson bar specimens. *J. de Physique IV* **4** C8 107-112.
- Parry D J and Griffiths L J (1979)** A compact gas gun for materials testing. *J. Phys. E: Sci. Instrum.* **12** 56-79.
- Parry D J, Stewardson H R and Ahmad S (1988)** Measurement of high strain rates properties of materials using an exploding wire technique. *J. Physique* **49** 689-94.
- Parry D J, Stewardson H R, Ahmad S H and Al-Maliky N (1990)** The application of cylindrical blast waves to impact studies of materials. *19<sup>th</sup> Conf. High speed photography*, Cambridge.
- Parry D J and Walker A J (1988)** A microcomputer based split Hopkinson pressure bar system. *IOP short meetings ser. no. 16*, ed. Yettram A L V.
- Peapell P N and Belk J A (1985)** Basic materials studies. Butterworths & Co. (Publisher) Ltd.
- Rajendran A M and Fyfe I M (1982)** Inertia effects on the ductile failure of thin rings. *J. Appl. Mech.* **49** pp31.
- Ramberg W and Osgood W R (1943)** Description of stress-strain curves by three parameters. *NACATN* **192**.
- Rand J L (1967)** US naval ordnance laboratory report NOLTR67-156.
- Reiner M (1960)** Plastic Yielding anelasticity. *J. Mech. Phys. Solids* **8** 255-261.
- Richard R M and Blacklock J R (1969)** Finite element analysis of inelastic structures. *AIAA J.* **7**(3) 432-438.
- Rietsch F and Bouette B (1990)** The compression yield behaviour of PC over a wide range of strain rates and temperatures. *Eur. Polym. J.* **26** 1071-1075.
- Ritchie R D (1965)** *Physics of plastics*. ILife Book Ltd., London.
- Ron P H, Rahatgi V K and Rau R (1983)** Rise time of a vacuum gap triggered by an exploding wire. *IEEE trans. Plasma Sci.* **PS-11** (4) 274-278.
- Rosenberg Z and Partom Y (1983)** Measurement of residual strains and uniaxial tension states of shock-loaded polymethylmetacrylate with the longitudinal strain gauge technique. *J. Phys. D: Appl. Phys.* **16** 1195-1200.
- Saimoto S and Thomas D (1986)** A novel method to measure the elastic modulus of polymers as a function of tensile deformation. *J. Mat. Sci.* **21** 3686-3690.

## References

- Samanta S K (1971)** Dynamic deformation of aluminium and copper at elevated temperatures. *J. Mech. Phys. Solids* **19** 117-135.
- Schmit R M and Fyfe I M (1973)** An examination of dynamic fracture under biaxial strain conditions. *Exp. Mech.* **13** 163-167.
- Schöfer R Seydel V and Jäger (1977)** On the propagation of shock waves of wire explosions in water. Part 7, *Naturforsch. Z.*, **32 A Part 7** 736-745.
- Seguela R and Rietsch F (1990)** Double yield point in polyethylene under tensile loading. *J. Mat. Sci. Lett.* **9** 46-47.
- Sharpe Jr. W N and Hoge K (1972)** Specimen strain measurement in the split Hopkinson pressure bar experiment. *Exp. Mech.* **12** 570-574.
- Siebel E (1923)** *Stahl u. Eisen, Dusseldorf* **43** pp1295.
- So-Young S and Kim U (1984)** A physical interpretation of metal explosion phenomena. *J. Korean Phys. Soc.* **17**(1) pp63
- So-Young S and Kim U (1984)** Oscillographic and Schlieren - streak photographic investigation of an exploding wire discharge. *J. Korean Phys. Soc.* **17** (2) 167-169.
- Steer P, Rietsch F, Lataillade J L, Marchand A and El Bounia N (1985)** *J. de Physique* **46 C5** 415-423.
- Suhara K (1986)** V-I characteristics measurements of short gap arcs initiated by wire explosion. IC-CEMCA Conf., Nagoya Japan, 167-174.
- Swallowe G M, Field J E and Walley S M (1984)** Heat generation during impact on polymers. *Inst. Phys. Conf. Oxford, ser. no. 70* 443-444.
- Swallowe G M, Field J E and Horn L A (1986)** Measurements of transient high temperatures during the deformation of polymers. *J. Mat. Sci.* **21** 4089-4096.
- Swift R P and Fyfe I M (1970)** Elastic-viscoplastic theory examined using radial cylindrical stress waves. *J. Appl. Mech.* **37** (1) 1134-1140.
- Truss R W, Clarke P L, Duckett R A and Ward I M (1984)** *J. Polym. Sci.:polym. Phys. edition* **22** 191-209.
- Vincent P I (1960)** The tough-brittle transition in thermoplastics. *Polymer* **1** 424-444.
- Vlostos A E (1973)** Electrical explosion of tungsten wires in vacuum. *J. Appl. Phys.* **44** (1) 106-112.
- Walker A G (1987)** Mechanical behaviour of copper at high strain rates. Ph.D thesis, Department of Physics, Loughborough University.
- Walley S M, Field J E, and Safford N A (1991)** A comparison of the high strain rate behaviour in compression of polymers at 300 K and 100 K. *J. de Physique IV* **1** 185-190.
- Walley S M and Field J E (1994)** Strain rate sensitivity of polymers in compression from low to high rates. *DYMAT J.* **1** (3) 211-227.



## References

- Walley S M, Field J E, Pope P and Safford N (1989)** A study of the rapid deformation behaviour of a range of polymers. *Phil. Trans. R. Soc. Lond.A* **328** 1-33.
- Walley S M, Field J E, Pope P H and Safford N A (1991)** The rapid deformation behaviour of various polymers. *J. de Physique III* **1** 1889-1925.
- Walling H C, Forrestal M J and Tucker W K (1972)** An experimental method for impulsively loading ring structures. *Intl. J. Solids and Structures* **8** 825-831.
- Walling H C and Forestal M J (1973)** Elastic-plastic expansion of 6061-T6 aluminium ring. *AIAA J.* **11** (8) 1196-1197.
- Ward I M (1979)** Mechanical properties of solids polymers. John Wiley and sons.
- Warnes R H, Duffy T A, Karp R R and Carden A E (1981)** An improved technique for determining dynamic material properties using the expanding ring. In *Shock wave and high strain rate phenomena in metal.* ed. Meyer M A and Murr L E, Plenum Press, New York, 23-36.
- Warnes R H, Karp R R and Follansbee P (1985)** The freely expanding ring test- a test to determine material strength at high strain rates. *J. Physique* **46** C5-583-90.
- Watson Jr. H (1970)** Gage-length errors in the resolution of dispersive stress waves. *Exp. Mech.* **12** 352-358.
- Weiss R T, Goldsmith W and Chase K (1970)** Mechanical and optical properties of an anelastic polymer at intermediate strain rates and large strains. *J. Polymer Sci. A-2* **8** 1713-1722.
- Wiebusch K and Richter R (1986)** Impact strength of nylon 6 and 66 in the dry and moist states. *J. Mat. Sci.* **21** 3302-3316.
- Wulf G L (1974)** Dynamic stress-strain measurements at large strains. *IOP Conf. ser no. 21 "Mechanical properties at high rates of strain"* ed. Harding J, 48-52.
- Yakimura K (1987)** Shock wave energy of wire explosion in air. *Sci. and Eng. Rev. of Doshisha Univ.* **28** (2) 63-73.
- Young R J, Bowden P B (1974)** *J. Materials Sci.* **2** 2034-2051.
- Young R J and Lovell P A (1991)** *Introduction to polymers.* 2nd ed. chap. 5, Chapman and Hall, 310-393.

## APPENDIX HOPK-BAR PROGRAM

```
1 DECLARE SUB INTRO ()
2 DECLARE SUB EER ()
3 DECLARE SUB AVERAGE ()
4 DECLARE SUB SHB ()
5 DECLARE SUB MENU ()
6 DECLARE SUB INTR ()
7 DECLARE SUB INITIL ()
9 COMMON SHARED MK%, A, TP, ND, DE, EE, ES, F, FH(), I, J, K, JJ, SL, EL
10 COMMON SHARED DN, PN, NN, LP, SR, BR, FR, MR, PO, VS, T, BT, FT, PU, N1
11 COMMON SHARED FF, F1, G1, F2, K1, KK, K2, N3, CS, FY, VI, S1, S2, EB, DB
12 COMMON SHARED A$, C$, CC$, D$, DD$, F$, FF$, F1$, F2$, F3$, RF$, WF$, M$
13 COMMON SHARED AT$, DT$, PV$, Z$, T1$, CH$, IL$, PR$, TX$, PC, AN$, PX$
14 COMMON SHARED TIM$, MI, G2, HH, L, PP, MM$, PD, ET1(), ET2(), ST1(), ST2()
15 COMMON SHARED SS(), SS1(), SS2(), ST(), ET(), ES(), ES1(), ES2(), ER(), ER1()
16 COMMON SHARED ER2(), T(), T1(), T2()
18 ON ERROR GOTO 7510
19 CLS : SCREEN 12
20 INPUT "          INPUT YOUR NAME "; USenames$: PRINT
21 CALL SHB
30 COLOR 2
40 LOCATE 8, 1
50 PRINT TAB(16); "USER NAME : "; USenames$: PRINT
60 CALL INTR: COLOR 2: PRINT : PRINT TAB(35); "PLEASE"
70 PRINT TAB(10); "INPUT THE FIRST DIGIT OF DATA POINTS HAVE BEEN TRANSLATED"
80 PRINT TAB(26); "( "; : COLOR 4: PRINT "1"; : COLOR 2: PRINT "024, ";
81 COLOR 4: PRINT " 2"; : COLOR 2: PRINT "048, "; : COLOR 4: PRINT " 3"; : COLOR 2
82 PRINT "072, "; : COLOR 4: PRINT " 4"; : COLOR 2: PRINT "096) "
83 NT$ = INPUT$(1)
90 IF VAL(NT$) = 1 THEN NT = 1024
100 IF VAL(NT$) = 2 THEN NT = 2048
110 IF VAL(NT$) = 3 THEN NT = 3072
120 IF VAL(NT$) = 4 THEN NT = 4096
121 COLOR 4: PRINT TAB(35); NT: COLOR 2
130 IF NT <> 1024 AND NT <> 2048 AND NT <> 3072 AND NT <> 4096 THEN 60
140 N2 = NT / 1024
150 DIM A(1024 * N2), TIMDAT(1024 * N2), T(300), T2(300)
160 DIM SS(300), ES(300), ST(300), ET(300), TR(300), P(17), FH(2), P$(9)
162 DIM ST1(300), ET1(300), SS1(300), ES1(300), ER(300), ER1(300)
164 DIM ST2(300), ET2(300), SS2(300), ES2(300), ER2(300), T1(300)
190 Z% = 1: MK% = 4: N1 = 2
200 CALL INITIL
310 ON MK% GOTO 320, 200
320 PRINT TAB(20); "HOPKINSON BAR DATA CONTROL AND ANALYSIS"
330 PRINT TAB(33); "SOFTWARE"
340 PRINT TAB(6); "THIS PROGRAM CAN BE USED TO ANALYSE DATA FROM BOTH COMPRESSION AND"
350 PRINT TAB(31); "TENSILE TESTS"
360 PRINT TAB(6); "CHANNEL 1 DATA REFERS TO STRAIN DATA FROM BAR NEARER TO GAS GUN"
370 PRINT TAB(6); "COMPRESSION TESTS: CH1 FOR INCID & REFL PULSES - CH2 FOR TRANS PULSE"
380 PRINT TAB(6); "TENSILE TESTS: CH1 FOR TRANS PULSE - CH2 FOR INCID & REFL PULSES"
390 GOSUB 6260
400 INPUT "HOPK BAR(431 OR MARAGING(M))"; ASS$
401 IF ASS$ = "431" OR ASS$ = "M" THEN 420
410 IF ASS$ <> "431" AND ASS$ <> "M" THEN 400
420 IF ASS$ = "431" THEN 440
430 EB = 187: C0 = 4818: MI = 38.78 * 10 ^ 6: GOTO 450
440 EB = 212: C0 = 5240: MI = 40.87 * 10 ^ 6
450 CLOSE #1: CLOSE #2: CLOSE #3: CLOSE #4: CLOSE FH(1): CLOSE FH(2)
451 CLS : COLOR 7: CALL SHB: LOCATE 5, 1: COLOR 2
460 CALL MENU ' MAIN DIRECTORY
470 PRINT TAB(36); : N1$ = INPUT$(1): PRINT N1$
480 IF UCASE$(N1$) = "D" THEN GOSUB 7540: GOTO 450
490 IF VAL(N1$) < 1 OR VAL(N1$) > 9 THEN 470
500 ON VAL(N1$) GOSUB 520, 1950, 1340, 4320, 5010, 5440, 6710, 7080, 7490
510 GOTO 450
```

```

520 PRINT "TRANSFER OF SPECIMEN AND APPARATUS PARAMETERS TO DISK"
530 INPUT "MATERIAL TESTED "; MM$
540 INPUT "COMPRESSION OR TENSILE (C OR T)"; CC$
550 IF UCASE$(CC$) = "C" THEN TX$ = "COMPRESSION"
560 IF UCASE$(CC$) = "T" THEN TX$ = "TENSILE"
570 INPUT "TEST TEMP. IN C (E.G. 020)"; TM$
580 INPUT "ANNEALING TEMP. IN C (E.G. 310) "; AN$
590 INPUT "PROJECTILE TIME(1 TO 2) IN MSEC "; T1
600 INPUT "PROJECTILE TIME(2 TO 3) IN MSEC"; T2
610 S1 = 100 / T1: S2 = 100 / T2
620 VI = S2 - (S1 - S2) * .72
630 TP = INT(VI): IF (VI - INT(VI)) >= .5 THEN TP = INT(VI) + 1
640 PV$ = STR$(TP): PV$ = RIGHT$(PV$, 2): IF PV$ < "10" THEN PV$ = RIGHT$(PV$, 1)
650 INPUT "PROJECTILE LENGTH (CM) LP = "; LP
660 INPUT "STEEL OR ALUMINIUM PROJECTILE (S OR A) OR E FOR ELSE"; PR$
670 IF UCASE$(PR$) = "S" OR UCASE$(PR$) = "A" OR UCASE$(PR$) = "E" THEN 690
680 IF UCASE$(PR$) <> "S" AND UCASE$(PR$) <> "A" AND UCASE$(PR$) <> "E" THEN 660
690 IF UCASE$(PR$) = "S" THEN PX$ = "STEEL"
700 IF UCASE$(PR$) = "A" THEN PX$ = "ALUMINIUM"
710 IF UCASE$(PR$) = "E" THEN INPUT "ENTER COMPLETE NAME OF THE PROJECTILE"; PX$
720 INPUT "POISSON'S RATIO PO ="; PO
730 INPUT "IDENTITY LETTER (E.G. A)"; IL$
740 M$ = LEFT$(MM$, 4)
750 CC$ = LEFT$(CC$, 1)
760 F$ = M$ + PV$ + IL$
770 INPUT "PULSE SHAPER USED (Y OR N)"; A$
780 IF UCASE$(A$) = "Y" OR UCASE$(A$) = "N" THEN 790 ELSE GOTO 770
790 IF UCASE$(A$) = "N" THEN 810
800 INPUT "ANNEALING TEMP. (0 = UNANNEALED) "; AT$
810 AT$ = LEFT$(AT$, 1)
820 F$ = F$
830 Z% = 1: N1 = 2: MK% = 1
860 PRINT ""
870 INPUT "SAMPLING RATE ( PRESS <RETURN> FOR DEFUALT {1US} )"; SR$
880 IF SR$ = "" THEN SR = 1 ELSE SR = VAL(SR$)
881 PRINT "BAR TYPE IS = "; AS$
890 PRINT "WAVE VELOCITY IN THE BAR = "; C0; "M/S"
900 PRINT "ELASTIC MODULUS OF BARS = "; EB; "GPA"
910 PRINT "DIAMETER OF BAR = "; DB; "MM"
920 IF UCASE$(CC$) = "C" THEN TX$ = "COMPRESSION" ELSE TX$ = "TENSILE"
930 PRINT "PROJECTILE IS "; PX$
940 PRINT "PROJECTILE LENGTH = "; LP; "CM"
941 PN = 130: IF L = 30 THEN PN = 170
950 PRINT "SAMPLING RATE = "; SR; " /S"
960 INPUT "STRAIN GAUGE FACTOR <RETURN> FOR DEFUALT (F1=2.14) = "; F1$
961 F = VAL(F1$): IF F1$ = "" THEN F = 2.14
970 INPUT "STRAIN GAUGE FACTOR <RETURN> FOR DEFUALT (F2=2.14) "; F1F$
971 FF = VAL(F1F$): IF F1F$ = "" THEN FF = 2.14
980 INPUT "GAIN OF SG1 AMPLIFIER"; G1
990 INPUT "GAIN OF SG2 AMPLIFIER"; G2
1000 INPUT "DATE OF THE EXPERIMENT"; DT$
1010 INPUT "TIME OF EXPERIMENT"; TIM$
1020 INPUT "SAMPLE LENGTH (MM)"; LS
1030 INPUT "SAMPLE DIAMETER (MM)"; SD
1040 INPUT "POWER SUPPLY VOLTAGE (IN VOLTS)"; E
1050 INPUT "VOLTAGE ACROSS SG1 (VOLTS)"; VA
1060 INPUT "VOLTAGE ACROSS SG2 (VOLTS)"; VB
1070 INPUT "TIME DELAY BETWEEN TRANS & REFL PULSES (MICROSEC)"; DE
1080 INPUT "DISK DRIVE TO STORE THE FILE (A OR B)"; DD$
1090 PRINT : PRINT "THE PARAMETER WILL BE STORED IN FILE "; F$
1100 INPUT "ARE YOU SURE THE PARAMETERS WERE CORRECT, SAVE (S) OR REENTER(R)"; N$
1110 IF UCASE$(N$) = "R" OR UCASE$(N$) = "S" THEN 1120 ELSE GOTO 1100
1120 IF UCASE$(N$) = "R" THEN 530
1130 GOSUB 6260
1140 F3$ = DD$ + "." + F$ + CHR$(51)
1150 WF$ = F3$
1160 OPEN WF$ FOR OUTPUT AS FH(1)
1170 PRINT "TRANSFERRING PARAMETERS TO DISK ....."
1180 P(1) = SR: P(2) = LP

```

```

1190 P(3) = G1: P(4) = G2: P(5) = F: P(6) = LS: P(7) = SD: P(8) = E
1200 P(9) = VA: P(10) = VB: P(11) = DE: P(12) = FF: P(13) = VI: P(14) = PO
1210 P$(1) = DT$: P$(2) = TIM$: P$(3) = TX$: P$(4) = PX$: P$(5) = DATE$: P$(6) = TIME$
1220 P$(7) = TMS$: P$(8) = AN$
1230 CS = 0
1240 FOR J = 1 TO 14: CS = CS + P(J): NEXT
1250 PRINT #FH(1), CS
1260 FOR J = 1 TO 14
1270 PRINT #FH(1), P(J)
1280 NEXT
1290 FOR J = 1 TO 8
1300 PRINT #FH(1), P$(J)
1310 NEXT
1320 CLOSE FH(1)
1330 GOTO 450
1340 INPUT "NAME OF FILE HOLDING DATA "; F$
1350 PRINT "DISK DRIVE (A OR B)"; : DD$ = INPUT$(1): PRINT DD$
1360 IF UCASE$(DD$) = "A" OR UCASE$(DD$) = "B" THEN 1370 ELSE GOTO 1350
1370 INPUT "CH1 OR CH2 DATA (1 OR 2)"; C$
1380 IF C$ = "1" OR C$ = "2" THEN 1400
1390 GOTO 1370
1400 RF$ = DD$ + ":" + F$ + C$
1410 GOTO 1420
1420 A$ = RF$
1430 OPEN A$ FOR INPUT AS FH(1)
1440 INPUT #FH(1), NAMTXT$, DATTXT$, TIMTXT$
1450 INPUT #FH(1), ND
1460 CLOSE FH(1)
1470 PRINT : PRINT "THERE ARE "; ND; " DATA POINTS IN THIS FILE"
1480 PRINT "DATA POINT FROM (0 TO "; ND; " )"
1490 INPUT "      "; J
1500 PRINT " TO DATA POINT ("; J; " TO "; ND; " )"
1510 INPUT "      "; I
1520 PRINT "SELECT CODE (1 - 4) - "
1530 PRINT "1. LIST DATA ON SCREEN"
1540 PRINT "2. LIST DATA ON LINE PRINTER"
1550 PRINT "3. RETURN TO HOPK-BAR DIRECTORY"
1560 PRINT "4. RETURN TO CHANGE THE SELECTED DATA POINTS"
1570 PRINT ""
1580 PRINT "SELECT CODE "; : N3$ = INPUT$(1): PRINT N3$
1590 IF VAL(N3$) = 3 THEN N3 = 3: GOTO 450
1600 IF VAL(N3$) = 4 THEN N3 = 4: GOTO 1480
1610 IF VAL(N3$) < 1 OR VAL(N3$) > 4 THEN 1580
1620 N3 = VAL(N3$)
1630 DN = N3 + 2
1640 FH(2) = 3
1650 IF DN = 3 THEN 1660
1660 IF DN = 3 THEN OPEN "SCRN:" FOR OUTPUT AS FH(2)
1670 IF DN <> 3 THEN OPEN "LPT1:" FOR OUTPUT AS FH(2)
1680 IF C$ = "1" AND UCASE$(CC$) = "C" OR C$ = "2" AND UCASE$(CC$) = "T" THEN Z$ = "INCIDENT"
1690 IF C$ = "1" AND UCASE$(CC$) = "T" OR C$ = "2" AND UCASE$(CC$) = "C" THEN Z$ = "TRANSMITTER"
1700 IF CC$ <> "0" THEN 1760
1710 INPUT "COMPRESSION OR TENSILE DATA (C OR T)"; CC$
1720 IF UCASE$(CC$) = "C" THEN TX$ = "COMPRESSION"
1730 IF UCASE$(CC$) = "T" THEN TX$ = "TENSILE"
1740 IF UCASE$(CC$) = "C" OR UCASE$(CC$) = "T" THEN 1680
1750 GOTO 1710
1760 PRINT #FH(2), : PRINT #FH(2), TAB(12); "USER NAME : "; USenames$: PRINT #FH(2), : PRINT #FH(2), "      ";
Z$;
1770 PRINT #FH(2), " BAR DATA FROM "; J; " TO"; I;
1780 PRINT #FH(2), " "; F$; " "; "["; TX$; " TEST]"
1790 PRINT #FH(2), ""
1800 PRINT "PLEASE WAIT.....": PRINT : PRINT
1810 IF DN = 3 THEN PRINT : PRINT " TIME          DATA VALUES (MV)"; "          "; DATE$: ELSE GOTO 1850
1820 PRINT " (US)"; " 0 1 2 3 4 5 6 7 8 9"
1830 PRINT " ----"
1840 IF DN = 3 THEN 1880
1850 PRINT #FH(2), " TIME          DATA VALUES (MV)"; "          "; DATE$
1860 PRINT #FH(2), " (US)"; " 0 1 2 3 4 5 6 7 8 9"

```

```

1870 PRINT #FH(2), " -----"
1880 GOSUB 5940
1890 CLOSE FH(2)
1900 INPUT "DO YOU WANT TO LIST MORE DATA (Y OR N)"; X$
1910 IF UCASE$(X$) = "Y" THEN 1340
1920 IF UCASE$(X$) = "N" THEN 1940
1930 IF UCASE$(X$) <> "Y" AND UCASE$(X$) <> "N" THEN 1900
1940 RETURN
1950 REM DATA ANALYSIS SECTION
1960 DA% = 1
1970 GOSUB 1990
1980 GOTO 2110
1990 INPUT "NAME OF FILE HOLDING SPECIMEN AND APPARATUS PARAMETER DATA"; F$
2000 INPUT "DISK DRIVE (A OR B)"; DD$
2010 IF LCASE$(DD$) = "A" OR LCASE$(DD$) = "B" THEN 2020 ELSE GOTO 2000
2020 RF$ = DD$ + ":" + F$ + CHR$(51)
2030 A$ = RF$
2040 OPEN A$ FOR INPUT AS #FH(1)
2050 INPUT #FH(1), CS
2060 INPUT #FH(1), SR, LP, G1, G2, F, LS, SD, E, VA, VB, DE, FF, VI, PO
2070 INPUT #FH(1), DT$, TIM$, TX$, PX$, DATEE$, TIMEE$, TMS$, AN$
2080 CLOSE FH(1)
2090 PN = 130: IF LP = 30 THEN PN = 170
2100 RETURN
2110 DN = 3: GOSUB 5080
2120 A1 = 1: A2 = 1
2130 REM CALIBRATION FACTORS CALC -F1 &F2
2140 N1 = (E - VA) / VA
2150 F1 = ((N1 + 1) ^ 2) / (N1 * F * G1)
2160 N2 = (E - VB) / VB
2170 F2 = ((N2 + 1) ^ 2) / (N2 * FF * G2)
2180 K1 = (F1) / (E)
2190 K2 = (F2) / (E)
2200 IF TX$ = "COMPRESSION" THEN CC$ = "C": IF TX$ = "TENSILE" THEN CC$ = "T"
2210 IF CC$ = "C" OR CC$ = "T" THEN 2230
2220 IF CC$ <> "C" AND CC$ <> "T" THEN GOTO 2200
2230 Z$ = "2": IF UCASE$(CC$) = "T" THEN Z$ = "1"
2240 PRINT "NUMBER OF POINTS TO BE ANALYSED (PN= "; PN; " <ENTER> FOR DEFUALT": INPUT PNX$
2250 IF PNX$ = "" THEN PN = PN ELSE PN = VAL(PNX$)
2260 PRINT PN
2270 PRINT TAB(20); "ANALYSIS.....": PRINT : PRINT
2280 PRINT "CHANNEL "; Z$; " DATA - TRANSMITTED PULSE "
2290 PP = 1: IF UCASE$(CC$) = "T" THEN PP = -1
2300 IF A1 = -1 AND UCASE$(CC$) = "T" THEN PP = 1
2310 IF A2 = -1 AND UCASE$(CC$) = "C" THEN PP = -1
2320 RF$ = DD$ + ":" + F$ + Z$
2330 A$ = RF$
2340 OPEN A$ FOR INPUT AS FH(1)
2350 INPUT #FH(1), NAMTXT$, DATTXT$, TIMTXT$
2360 INPUT #FH(1), ND
2370 CLOSE FH(1)
2380 CH$ = "TRANS"
2390 PRINT "THERE ARE "; ND; " DATA POINTS IN "; F$ + Z$
2400 J = 1: J = ND
2410 GOSUB 6090
2420 PRINT "SEARCHING FOR START OF TRANSMITTED PULSE"
2430 B = 20
2440 GOSUB 6290
2450 BT = B: FT = BT + PN
2460 PRINT "DATA POINT "; BT; " TO "; FT + 40; " WILL BE ANALYSED"
2470 PRINT "AVERAGE OF 15 DATA POINTS BEFORE TRANSMITTED PULSE "
2480 PRINT "THIS WILL BE ZERO POINTS OF DATA"
2490 PRINT "FINDING BASELINE OF TRANSMITTED"
2500 TPL = 0
2510 FOR J = BT - 20 TO BT - 1
2520 TPL = TPL + A(J)
2530 NEXT
2540 TPL = TPL / 20: TPL = TPL * 1000
2550 IF TPL - INT(TPL) >= .5 THEN TPL = INT(TPL) + 1

```

```

2560 TPL = TPL
2570 PRINT "BASELINE FOR CHANNEL "; Z$; " DATA IS ";
2580 PRINT USING "####.#"; TPL;
2590 PRINT " MV"; " BETWEEN ("; BT - 20; " & "; BT; ")"
2600 INPUT "ALTER BASELINE (Y OR N)"; A$
2610 IF UCASE$(A$) = "N" THEN 2640
2620 IF UCASE$(A$) <> "Y" THEN 2600
2630 INPUT "NEW BASELINE VALUE (IN MV)"; TPL
2640 FOR J = BT - 20 TO FT + 20
2650 A(J) = A(J + 1) - (TPL / 1000)
2660 NEXT
2670 PRINT "ANALYSING TRANSMITTED PULSE DATA..... "
2680 KK = K2: IF CC$ = "T" OR CC$ = "R" THEN KK = K1
2690 TP = EB * 10 ^ 9 * DB ^ 2 / (SD ^ 2)
2700 FOR J = BT TO FT + 40
2710 JJ = J - BT
2720 A = A(J) * KK
2730 SS(JJ) = A * TP * PP
2740 NEXT J
2750 PRINT "ANALYSIS COMPLETED"
2760 GOSUB 6260
2770 Z$ = "1": IF UCASE$(CC$) = "T" THEN Z$ = "2"
2780 PRINT "CHANNEL "; Z$; " DATA INCIDENT & REFLECTED PULSES"
2790 RF$ = DD$ + ":" + F$ + Z$
2800 A$ = RF$
2810 OPEN A$ FOR INPUT AS FH(1)
2820 INPUT #FH(1), NAMTXT$, DATTXT$, TIMTXT$
2830 INPUT #FH(1), ND
2840 CLOSE FH(1)
2850 J = 1: I = ND
2860 PRINT "THERE ARE "; ND; " DATA POINTS IN "; F$ + Z$: PRINT
2870 GOSUB 6090
2880 PRINT "FINDING START OF INCIDENT PULSE....."
2890 CH$ = "INCID": PP = 1: B = 20
2900 IF UCASE$(CC$) = "T" THEN PP = -1
2910 IF A2 = -1 AND UCASE$(CC$) = "T" THEN PP = 1
2920 IF A1 = -1 AND UCASE$(CC$) = "C" THEN PP = -1
2930 GOSUB 6290
2940 CH$ = "REFL": PP = -1: B = B + 150
2950 IF UCASE$(CC$) = "T" THEN PP = 1
2960 IF A2 = -1 AND UCASE$(CC$) = "T" THEN PP = -1
2970 IF A1 = -1 AND UCASE$(CC$) = "C" THEN PP = 1
2980 PRINT "FINDING START OF REFLECTED PULSE....."
2990 GOSUB 6290
3000 BR = B: FR = BR + PN
3010 SA = 0
3020 REM FIND AVG OF 20 PTS AT END OF REFL PULSE
3030 FOR J = FR TO FR + 19
3040 SA = SA + A(J)
3050 NEXT
3060 SA = SA / 20: SA = SA * 1000
3070 IF SA - INT(SA) >= .5 THEN SA = INT(SA) + 1
3080 SA = SA
3090 PRINT "BASELINE OF CHANNEL "; Z$; " DATA IS ";
3100 PRINT USING "####.#"; SA; : PRINT " MV"; " BETWEEN ("; FR; " & "; FR + 20; ")"
3110 INPUT "ALTER BASELINE (Y OR N)"; A$
3120 IF UCASE$(A$) = "N" THEN 3150
3130 IF UCASE$(A$) <> "Y" THEN 3110
3140 INPUT "NEW BASELINE VALUE (IN MV) "; SA
3150 ED = BR - BT
3160 PRINT "REFLECTED PULSE STARTS "; ED; " MICROSECS AFTER TRANS PULSE"
3170 IF DE <= ED THEN 3510
3180 PRINT "THIS DELAY SHOULD BE "; DE; " MICROSECS"
3190 INPUT "DO YOU WANT TO MODIFY START OF REFLECTED PULSE (Y OR N)"; A$
3200 IF UCASE$(A$) = "N" THEN 3510
3210 IF UCASE$(A$) <> "Y" THEN 3190
3220 PRINT "MODIFYING START OF REFLECTED PULSE....."
3230 JJ = 0
3240 TP = DE - ED

```

```

3250 FOR J = BR TO FR
3260 IF A(J) > A(J + TP) THEN 3280
3270 J = FR: GOTO 3290
3280 JJ = JJ + 1
3290 NEXT
3300 FOR J = BR + JJ - 1 TO BR STEP -1
3310 A(J + TP) = A(J)
3320 NEXT
3330 BR = BR + TP: FR = FR + TP
3340 PRINT "REFLECTED PULSE NOW START AT "; BR
3350 PRINT "I.E."; DE; " MICROSECS AFTER TRANSMITTED PULSE"
3360 INPUT "DO YOU WANT TO SEE MODIFIED REFLECTED PULSE (Y OR N)"; A$
3370 IF UCASE$(A$) = "N" THEN 3510
3380 IF UCASE$(A$) <> "Y" THEN 3360
3390 RB = BR
3400 FOR J = BR TO FR
3410 PRINT J, A(J)
3420 JJ = J - RB
3430 IF JJ < 20 THEN 3500
3440 RB = J
3450 INPUT "MORE (Y OR N)"; A$
3460 IF UCASE$(A$) = "Y" THEN 3500
3470 IF UCASE$(A$) <> "N" THEN 3450
3480 J = FR
3490 GOTO 3510
3500 NEXT
3510 FOR J = BR - 20 TO FR + 20
3520 A(J) = A(J + 1) - (SA / 1000)
3530 NEXT
3540 PRINT "START CORRECTION OF REFLECTED PULSE = ";
3550 PRINT USING "####.#"; A(BR) * 1000; : PRINT " MV"
3560 PRINT "END CORRECTION OF REFLECTED PULSE = ";
3570 PRINT USING "####.#"; A(FR) * 1000; : PRINT " MV"; " CORRESPONDING TO B.L OF ";
3580 PRINT USING "####.#"; SA; : PRINT "MV"
3590 INPUT "DO YOU WANT TO CHANGE THESE VALUES (Y OR N)"; A$
3600 IF UCASE$(A$) = "N" THEN 3650
3610 IF UCASE$(A$) <> "Y" THEN 3590
3620 INPUT "START CORRECTION (IN MV)"; ES: ES = ES / 1000
3630 INPUT "END CORRECTION (IN MV)"; EE: EE = EE / 1000
3640 GOTO 3670
3650 ES = A(BR)
3660 EE = A(FR)
3670 PRINT "CORRECTING REFLECTED PULSE BASELINE ....."
3680 FOR JJ = BR TO FR
3690 J = JJ - BR
3700 A(J) = A(JJ) - (((ES - EE) * (PN + BR - JJ) / PN) + EE)
3710 NEXT
3720 PRINT "ANALYSING REFLECTED PULSE DATA....."
3730 REM CALCULATE STRAIN IN SAMPLE
3740 REM SS=ENG.STRESS ,ES=ENG. STRAIN
3750 REM ST=TRUE STRESS ,ET=TRUE STRAIN
3760 REM TR=STRAIN RATE
3770 TP = 0
3780 MR = SR * .000001
3790 J = 1: I = ND
3800 FY = 2 * C0 * 1000 / LS
3810 KK = K1: IF UCASE$(CC$) = "T" THEN KK = K2
3820 FOR JJ = BR TO FR + 40
3830 J = JJ - BR
3840 A = A(J) * KK
3850 TP = TP + A * MR
3860 ETR = A * FY * PP
3870 ES(J) = TP * FY * PP
3880 TR(J) = PP ^ 2 * ETR / (1 + PP * ES(J))
3890 NEXT JJ
3900 PRINT "ANALYSIS COMPLETED.. "
3910 GOSUB 6260
3920 REM CALC TRUE STRESS,STRAIN,STRAIN RATE
3930 PP = -1: IF UCASE$(CC$) = "T" THEN PP = 1

```

```

3940 PRINT "CALCULATING TRUE STRESSES & STRAINS....."
3950 FOR J = 1 TO PN: ET(J) = 0: ST(J) = 0: NEXT
3960 FOR J = 1 TO PN
3970 IF ES(J) > 1 THEN PP = ABS(PP) ' GUARD AGAINST RIDICULOUS ES VALS
3980 ET(J) = PP * LOG(1 + PP * ES(J))
3990 ST(J) = SS(J) * EXP(PP * 2 * PO * ET(J))
4000 NEXT
4010 PRINT : PRINT "CALCULATIONS COMPLETED"
4020 GOSUB 6260
4030 INPUT "DO YOU WANT TO STORE STRESS/STRAIN RESULTS ON DISK (Y OR N)"; A$
4040 IF UCASE$(A$) = "N" THEN 450
4050 IF UCASE$(A$) <> "Y" THEN 4030
4060 PRINT "ANY PREVIOUS RESULTS FROM DATA FILE "; F$; " WILL BE ERASED "
4070 INPUT "CONTINUE WITH TRANSFERRING TO DISK (Y OR N)"; A$
4080 IF UCASE$(A$) = "N" THEN 450
4090 IF UCASE$(A$) <> "Y" THEN 4070
4100 WF$ = DD$ + "." + F$ + CHR$(52)
4110 OPEN WF$ FOR OUTPUT AS FH(1)
4120 PRINT " TRANSFERRING RESULTS TO DISK"
4130 PRINT " PLEASE WAIT....."
4140 FOR J = 1 TO PN
4150 PRINT #FH(1), J;
4160 PRINT #FH(1), " "; ST(J);
4170 PRINT #FH(1), " "; ET(J);
4180 PRINT #FH(1), " "; TR(J);
4190 PRINT #FH(1), " "; SS(J);
4200 PRINT #FH(1), " "; ES(J)
4210 NEXT
4220 CLOSE FH(1)
4230 WF$ = WF$ + ".DAT": OPEN WF$ FOR OUTPUT AS FH(1)
4240 FOR J = 0 TO PN
4241 PRINT #FH(1), USING "#####"; J;
4250 PRINT #FH(1), CHR$(9); USING "###.#"; ST(J) / 10 ^ 6;
4260 PRINT #FH(1), CHR$(9); USING "###.###"; ET(J) * 100;
4261 PRINT #FH(1), CHR$(9); USING "###.###^"; TR(J);
4270 PRINT #FH(1), CHR$(9); USING "###.#"; SS(J) / 10 ^ 6;
4280 PRINT #FH(1), CHR$(9); USING "###.###"; ES(J) * 100: NEXT
4290 CLOSE FH(1)
4300 GOSUB 6260
4310 GOTO 450
4320 REM RESULTS
4321 N1 = 1
4330 IF N1 = 1 OR N1 = 2 THEN GOSUB 4800
4340 IF DA% = 1 THEN 4380
4350 PRINT
4360 GOSUB 6260
4370 RETURN
4380 PRINT "TRANSFER RESULTS TO :-"
4390 PRINT "1. SCREEN"
4400 PRINT "2. LINE PRINTER"
4410 PRINT "3. RETURN TO HOPK-BAR MENU"
4420 INPUT "SELECT CODE"; DN
4430 IF DN = 3 OR DN = 3 THEN RETURN
4440 IF DN < 1 OR DN > 3 THEN 4380
4450 DN = DN + 2
4460 IF DN = 3 THEN FH(2) = 2 ELSE FH(2) = 3
4470 L = 1: R$ = RIGHT$(F$, 2): R$ = LEFT$(R$, 1)
4480 REM IF R$ = "%" OR RIGHT$(F$, 1) = "5" OR RIGHT$(F$, 1) = "6" THEN 5120
4490 INPUT "ENTER MICROSEC INTERVAL FOR RESULTS TABLE "; L
4500 PRINT "ENTER MAXIMUM TIME (US) PNN = (0 - "; PN - 1; ") "; : INPUT PNN: PNN = PNN
4510 IF DN = 3 THEN OPEN "SCRN:" FOR OUTPUT AS FH(2) ELSE OPEN "LPT1:" FOR OUTPUT AS FH(2)
4520 FOR X = 1 TO 1: PRINT #FH(2), : NEXT X
4550 PRINT #FH(2), : IF N1 = 1 THEN T1$ = " STRESS/STRAIN RESULTS"
4560 PRINT #FH(2), TAB(12); "USER NAME : "; USNAME$, DATE$, TIME$: PRINT #FH(2), : PRINT #FH(2), T1$
4570 PRINT #FH(2), : PRINT #FH(2), " FILENAME HOLDING RESULTS = "; F$; " "; DATE$
4580 IF N1 = 1 THEN 4590
4590 PRINT #FH(2),
4600 PRINT #FH(2), " TIME(US) TRUE TRUE STRAIN RATE ENGINEERING ENGINEERING"
4610 PRINT #FH(2), " STRESS(MPA) STRAIN(%) (/SEC) STRESS(MPA) STRAIN(%)"

```



```

4620 PRINT #FH(2), " -----"
4630 T = 0
4640 FOR J = 0 TO PNN STEP L
4650 IF J > 0 AND ST(J) = 0 AND ET(J) = 0 THEN 4730
4660 IF N1 = 1 THEN 4670 ELSE GOTO 4730
4670 PRINT #FH(2), " "; USING "####"; J;
4680 PRINT #FH(2), " "; USING "#####.##"; ST(J) / 10 ^ 6;
4690 PRINT #FH(2), " "; USING "####.##"; ET(J) * 100;
4700 PRINT #FH(2), " "; USING "##.##^"; TR(J);
4710 PRINT #FH(2), " "; USING "#####.##"; SS(J) / 10 ^ 6;
4720 PRINT #FH(2), " "; USING "#####.##"; ES(J) * 100
4730 IF R$ = "%" THEN 4750
4740 T = T + L
4750 NEXT
4760 IF DN = 4 THEN 4780
4770 GOSUB 6260
4780 CLOSE FH(2)
4790 GOTO 4320
4800 INPUT "DO YOU WANT RESULTS FROM DISK FILE (Y OR N)"; AX$
4810 IF UCASE$(AX$) = "N" THEN RETURN
4820 IF UCASE$(AX$) <> "Y" THEN 4800
4830 DA% = 1
4840 INPUT "FILENAME "; F$
4850 INPUT "DISK DRIVE (A OR B)"; DD$
4860 IF DD$ = "A" OR DD$ = "B" THEN 4880
4870 IF DD$ <> "A" AND DD$ <> "B" THEN 4850
4880 FT$ = CHR$(52)
4890 INPUT "SMOOTHED RESULTS (Y OR N)"; A$
4900 IF UCASE$(A$) = "Y" THEN FT$ = CHR$(53)
4910 INPUT "AVERAGED RESULTS (Y OR N)"; A$
4920 IF UCASE$(A$) = "Y" THEN FT$ = CHR$(54)
4930 RF$ = DD$ + ":" + F$ + FT$
4940 OPEN RF$ FOR INPUT AS #FH(1)          ' READ RESULTS
4941 J = 1
4950 DO UNTIL EOF(FH(1))
4960 INPUT #FH(1), T, ST(J), ET(J), TR(J), SS(J), ES(J)
4970 J = J + 1: LOOP
4980 PN = J: CLOSE #FH(1)
4990 RETURN
5000 Z% = 1
5010 PRINT "PARAMETERS ENTERED FROM KEYBOARD "
5020 INPUT "LIST PARAMETERS ON SCREEN OR PRINTER (S OR P)"; AS$
5030 IF UCASE$(AS$) = "S" THEN DN = 3
5040 IF UCASE$(AS$) = "P" THEN DN = 4
5050 IF UCASE$(AS$) = "S" OR UCASE$(AS$) = "P" THEN 5070
5060 GOTO 5020
5070 GOSUB 1990
5080 IF DN = 3 THEN FH(2) = 3 ELSE FH(2) = 2
5090 IF DN = 3 THEN OPEN "SCRN:" FOR OUTPUT AS FH(2)
5100 IF DN <> 3 THEN OPEN "LPT1:" FOR OUTPUT AS FH(2)
5110 PRINT #FH(2), : PRINT #FH(2), TAB(15); "USER NAME : "; USENAME$, DATE$, TIME$
5120 PRINT #FH(2), : PRINT #FH(2),
5130 PRINT #FH(2), TAB(15); "-----"
5140 PRINT #FH(2), TAB(15); " * PARAMETERS ENTERED FROM KEYBOARD    **
5150 PRINT #FH(2), TAB(15); "-----"
5160 PRINT #FH(2), TAB(15); " * DATE OF THE EXPERIMENT = "; DT$
5170 PRINT #FH(2), TAB(15); " * TIME OF THE EXPERIMENT = "; TIM$
5180 PRINT #FH(2), TAB(15); " * DATE OF THE ANALYSIS = "; DATEE$
5190 PRINT #FH(2), TAB(15); " * TIME OF ANALYSIS = "; TIMEE$
5200 PRINT #FH(2), TAB(15); " * FILENAME = "; F$
5210 PRINT #FH(2), TAB(15); " * SAMPLING RATE = "; SR; " US"
5220 PRINT #FH(2), TAB(15); " * TEST TYPE = "; TX$
5230 PRINT #FH(2), TAB(15); " * PROJECTILE MATERIAL = "; PX$
5240 PRINT #FH(2), TAB(15); " * PROJECTILE LENGTH = "; LP; " CM"
5250 PRINT #FH(2), TAB(15); " * TEST TEMPERATURE = "; TM$; " C"
5260 PRINT #FH(2), TAB(15); " * ANNEALING TEMPERATURE = "; AN$; " C"
5270 PRINT #FH(2), TAB(15); " * GAIN OF SG1 AMPLIFIER = "; G1
5280 PRINT #FH(2), TAB(15); " * GAIN OF SG2 AMPLIFIER = "; G2
5290 PRINT #FH(2), TAB(15); " * STRAIN GAUGE FACTOR(F1)= "; F

```

```

5300 PRINT #FH(2), TAB(15); " * STRAIN GAUGE FACTOR(F2)= "; FF
5310 PRINT #FH(2), TAB(15); " * SAMPLE LENGTH      = "; LS; " MM"
5320 PRINT #FH(2), TAB(15); " * SAMPLE DIAMETER    = "; SD; " MM"
5330 PRINT #FH(2), TAB(15); " * POWER SUPPLY VOLTAGE = "; E; " VOLTS"
5340 PRINT #FH(2), TAB(15); " * VOLTAGE ACROSS SG1  = "; VA; " VOLTS"
5350 PRINT #FH(2), TAB(15); " * VOLTAGE ACROSS SG2  = "; VB; " VOLTS"
5360 PRINT #FH(2), TAB(15); " * POISSON'S RATIO    = "; USING "###.###"; PO
5370 PRINT #FH(2), TAB(15); " * DELAY BETWEEN PULSES = "; DE; " US"
5380 PRINT #FH(2), TAB(15); " * VELOCITY OF IMPACT ="; USING"###.###"; VI;PRINT #FH(2)," M/S"
5390 PRINT #FH(2), TAB(15); " * ....."
5400 CLOSE FH(2)11
5410 IF DN = 4 THEN RETURN
5420 GOSUB 6260: SCREEN 0: COLOR 2
5430 RETURN
5440 REM COMPARE SG & PROJ VEL READINGS
5450 PRINT ""
5460 PRINT "PLEASE INPUT THE FOLLOWING INFORMATION CORRECTLY"
5470 INPUT "1- POWER SUPPLY VOLTAGE (IN VOLT)"; E:
5480 INPUT "2- STRAIN GAUGE FACTOR"; F:
5490 INPUT "3- GAIN OF SG1 AMPLIFIER"; G1:
5500 INPUT "4- GAIN OF SG2 AMPLIFIER"; G2:
5510 INPUT "5- VOLTAGE ACROSS SG1 (IN VOLT)"; VA:
5520 INPUT "6- VOLTAGE ACROSS SG2 (IN VOLT)"; VB:
5530 INPUT "7- TEST TYPE (C OR T)"; CC$:
5540 INPUT "8- PROJECTILE DENSITY (KG/M^2)"; PD:
5550 INPUT "9- PROJECTILE WAVE VELOCITY (M/S)"; PC:
5560 INPUT "10- SIZE OF SG1 PULSE ( IN MV)"; PA: PA = PA / 1000:
5570 INPUT "11- SIZE OF SG2 PULSE (IN MV)"; PB: PB = PB / 1000:
5580 PRINT "FOR INCORRECT ENTRIES TO THE ABOVE QUESTIONS GOTO LINES SHOWN ABOVE"
5590 PRINT "AND RE-ENTER THE CORRECT VALUES, BY INPUTTING THE LINE NO."
5600 INPUT "DO YOU WANT TO CORRECT ANY VALUES (Y OR N)"; A$
5610 IF UCASE$(A$) = "N" THEN GOTO 5650
5620 IF UCASE$(A$) <> "Y" THEN 5600
5630 INPUT "PLEASE INPUT THE FIRST INCORRECT LINE NO."; HH
5640 ON HH GOTO 5470, 5480, 5490, 5500, 5510, 5520, 5530, 5540, 5550, 5560, 5570
5650 NA = (E - VA) / VA
5660 NB = (E - VB) / VB
5670 SA = (NA + 1) * (NA + 1) * PA / (NA * F * E * G1)
5680 SB = (NB + 1) * (NB + 1) * PB / (NB * F * E * G2)
5690 PRINT "STRAIN FROM STRAIN GAUGES 1 = "; : PRINT USING "###.###"; SA *100;
5700 PRINT " %"
5710 PRINT "STRAIN FROM STRAIN GAUGES 2 = "; : PRINT USING "###.###"; SB *100;
5720 PRINT " %"
5730 VS = SA * EB * 10 ^ 9 * (1 / MI + 1 / (PD * PC))
5740 PRINT "PROJECTILE VEL FROM STRAIN GAUGES 1 =";:PRINT USING"###.###"; VS;
5750 PRINT " M/S"
5760 VS = SB * EB * 10 ^ 9 * (1 / MI + 1 / (PD * PC))
5770 PRINT "PROJECTILE VEL FROM STRAIN GAUGES 2 =";:PRINT USING"###.###"; VS;
5780 PRINT " M/S"
5790 GOSUB 6260
5800 RETURN
5810 ND = K - J + 1
5820 PRINT "TRANSFERRING DATA FROM PC TO DISK....."
5830 CS = 0
5840 FOR J = J TO K: CS = CS + A(I): NEXT
5850 PRINT #FH(1), CS;
5860 PRINT #FH(1), " "; ND;
5870 FOR I = J TO K
5880 PRINT #FH(1), A(I); " ";
5890 NEXT
5900 CLOSE #FH(1)
5910 PRINT "TRANSFER IS COMPLETE."
5920 GOSUB 6260
5930 RETURN
5940 GOSUB 6090
5950 DN = 4
5960 NN = (DN - 2) * 5
5970 FOR K = J TO I STEP NN
5980 PRINT #FH(2), " "; USING "###.###"; K;

```

```

5990 PRINT #FH(2), "";
6000 FOR L = 1 TO NN - 1
6010 PRINT #FH(2), "", USING "####.#"; A(K + L) * 1000;
6020 NEXT L
6030 PRINT #FH(2), "", USING "####.#"; A(K + L) * 1000
6040 NEXT K
6050 IF DN = 4 THEN 6070
6060 GOSUB 6260
6070 PRINT #FH(2), : CLOSE FH(2)
6080 RETURN
6090 OPEN A$ FOR INPUT AS FH(1)
6100 IF N3 = 1 THEN 6130
6110 PRINT "TRANSFERRING DATA FROM DISK TO PC"
6120 PRINT "PLEASE WAIT....."
6130 INPUT #FH(1), NAMTXT$, DATTXT$, TIMTXT$
6140 TP = 0
6150 INPUT #FH(1), ND
6160 FOR K = 1 TO ND
6170 INPUT #FH(1), TIMDAT(K), A(K)
6180 TP = TP + A(K)
6190 NEXT
6200 CLOSE FH(1)
6210 IF CS = TP THEN 6230
6220 IF ND = K THEN 6230
6230 IF N3 = 1 THEN 6250
6240 PRINT "TRANSFER COMPLETED"
6250 RETURN
6260 COLOR 4: PRINT : PRINT TAB(26); "HIT <SPACE BAR> TO CONTINUE": COLOR 2
6270 C$ = INPUT$(1): IF C$ <> " " THEN 6270
6280 RETURN
6290 REM FIND START OF PULSE
6300 TP = 0: JJ = 0
6310 FOR J = B TO I STEP 10
6320 IF (A(J) - A(J - 1)) * PP < 1 THEN 6340
6330 B = J - 20: J = I
6340 NEXT
6350 TP = 0: JJ = 0
6360 FOR J = B TO I
6370 IF A(J) * PP > A(J + 1) * PP THEN 6470
6380 IF A(J) = A(J + 1) AND TP = 0 THEN 6470
6390 IF A(J) = A(J + 1) THEN 6440
6400 TP = TP + 1
6410 IF TP < 4 THEN 6480
6420 B = J - 4 - JJ
6430 J = I: GOTO 6480
6440 JJ = JJ + 1
6450 IF JJ > 3 THEN 6470
6460 GOTO 6480
6470 TP = 0: JJ = 0
6480 NEXT
6490 REM MANUAL CHECK OF START OF PULSE
6500 PRINT ""; CH$; " PULSE STARTS AT "; B
6510 INPUT "DO YOU WANT TO CHECK (Y OR N)"; A$
6520 IF UCASE$(A$) = "N" GOTO 6700
6530 IF UCASE$(A$) <> "Y" GOTO 6510
6540 J = B: IF J < 10 THEN 6580
6550 FOR J = B - 10 TO B + 10
6560 PRINT J, USING "####.#"; A(J + 1) * 1000
6570 NEXT J
6580 INPUT "DO YOU WANT TO CHANGE PREDICTED START VALUE (Y OR N)"; A$
6590 IF UCASE$(A$) = "N" GOTO 6700
6600 IF UCASE$(A$) <> "Y" GOTO 6580
6610 PRINT "APPROX. START OF "; CH$; " PULSE";
6620 INPUT B
6630 FOR J = B - 10 TO B + 10
6640 PRINT J, USING "####.#"; A(J + 1) * 1000
6650 NEXT J
6660 INPUT "DO YOU WANT TO ENTER APPROX. START AGAIN (Y OR N)"; A$
6670 IF UCASE$(A$) = "Y" THEN 6610

```

```

6680 IF UCASE$(A$) <> "N" THEN 6660
6690 INPUT "ENTER EXACT STARTING VALUE "; B
6700 RETURN
6710 PRINT "AVERAGED RESULTS"
6720 PRINT "THIS ROUTINE CAN BE USED TO AVERAGE 2 OR MORE RESULTS FILES "
6730 PRINT "ALTERNATIVELY THE AVG OF RESULTS FILES CAN BE INPUT FROM KEYBOARD"
6740 PRINT "TO BE STORED ON DISK"
6750 DA% = 1
6760 INPUT "FROM KEYBOARD (Y OR N)"; A$
6770 IF UCASE$(A$) = "Y" THEN 6830
6780 IF UCASE$(A$) <> "N" THEN 6760
6790 PRINT "AUTOMATIC RESULTS AVERAGING "
6800 IF UCASE$(A$) = "N" THEN CALL AVERAGE
6810 GOSUB 6260
6820 RETURN
6830 INPUT "RESULTS FILENAME "; F$
6840 INPUT "DISK DRIVE (A OR B)"; DD$
6850 IF UCASE$(DD$) <> "A" AND UCASE$(DD$) <> "B" THEN 6840
6860 WF$ = DD$ + "." + F$ + CHR$(54)
6870 INPUT "HOW MANY DATA POINTS (1-200)"; ND
6880 IF ND > 200 THEN 6870
6890 PRINT "ENTER COORDS OF STRESS(MPA) & STRAIN(%)"
6900 FOR J = 1 TO ND
6910 PRINT "COORDS OF POINT NO"; J;
6920 INPUT ST(J), ET(J)
6930 ST(J) = ST(J) * 10 ^ 6
6940 ET(J) = ET(J) / 100
6950 TR(J) = 0
6960 NEXT
6970 OPEN WF$ FOR OUTPUT AS FH(1)
6980 GOSUB 6260
6990 PRINT "TRANSFERRING RESULTS TO DISK..... "
7000 FOR J = 1 TO ND
7010 PRINT #FH(1), J;
7020 PRINT #FH(1), " "; ST(J);
7030 PRINT #FH(1), " "; ET(J);
7040 PRINT #FH(1), " "; TR(J)
7050 NEXT
7060 CLOSE FH(1)
7070 RETURN
7080 PRINT "THIS SUBROUTINE CUTS THE HIGH FREQUENCY OFF FROM THE RESULTS"
7090 GOSUB 4800
7100 INPUT " INPUT HOW MANY ITERATION (E.G 1=1ST ORDER, 2=2ND ORDER, ETC.)"; NOI
7110 IF ABS$(AX$) = "Y" THEN STP = 4 ELSE STP = 1
7120 PRINT "SMOOTHING RESULTS....."
7130 FOR F = 1 TO NOI: PRINT " "; " ";
7140 FOR J = 1 TO PN - STP
7150 IF ABS(ST(J)) <> ABS((ST(J - 1) + ST(J + 1)) / 2) THEN 7160 ELSE ST(J) = ST(J): GOTO 7170
7160 ST(J) = (ST(J - 1) + ST(J + 1)) / 2
7170 NEXT
7180 FOR J = 1 TO PN - STP
7190 IF ABS(ET(J)) <> ABS((ET(J - 1) + ET(J + 1)) / 2) THEN 7200 ELSE ET(J) = ET(J): GOTO 7210
7200 ET(J) = (ET(J - 1) + ET(J + 1)) / 2
7210 NEXT
7220 FOR J = 1 TO PN - STP
7230 IF ABS(TR(J)) <> ABS((TR(J - 1) + TR(J + 1))) / 2 THEN 7240 ELSE TR(J) = TR(J): GOTO 7250
7240 TR(J) = (TR(J - 1) + TR(J + 1)) / 2
7250 NEXT
7260 FOR J = 1 TO PN - STP
7270 IF ABS(SS(J)) <> ABS((SS(J - 1) + SS(J + 1)) / 2) THEN 7280 ELSE SS(J) = SS(J):GOTO 7290
7280 SS(J) = (SS(J - 1) + SS(J + 1)) / 2
7290 NEXT
7300 FOR J = 1 TO PN - STP
7310 IF ABS(ES(J)) <> ABS((ES(J - 1) + ES(J + 1)) / 2) THEN 7320 ELSE ES(J) = ES(J):GOTO 7330
7320 ES(J) = (ES(J - 1) + ES(J + 1)) / 2
7330 NEXT
7331 PRINT " "; F; : NEXT F
7340 PRINT : PRINT "SMOOTHING COMPLETED.": GOSUB 6260
7350 INPUT "DO YOU WANT TO SAVE THE SMOOTHED RESULTS (Y OR N)"; A$

```

```

7360 IF UCASE$(A$) = "N" THEN RETURN
7370 IF UCASE$(A$) <> "Y" THEN 7350
7380 WF$ = DD$ + ":" + F$ + CHR$(53)
7390 OPEN WF$ + ".DAT" FOR OUTPUT AS #FH(1)
7400 OPEN WF$ FOR OUTPUT AS #3
7410 PRINT " TRANSFERRING RESULTS TO DISK": PRINT " PLEASE WAIT....."
7420 FOR J = 0 TO PN - STP
7421 PRINT #3, J, " "; ST(J); " "; ET(J); " "; TR(J); " "; SS(J); " "; ES(J)
7430 PRINT #FH(1), USING "####"; J;
7440 PRINT #FH(1), CHR$(9); USING "####.#"; ST(J) / 10 ^ 6; : PRINT #FH(1), CHR$(9); USING "###.###"; ET(J) *
100;
7450 PRINT #FH(1), CHR$(9); USING "###.###^^"; TR(J); : PRINT #FH(1), CHR$(9); USING "####.#"; SS(J) / 10 ^ 6;
7451 PRINT #FH(1), CHR$(9); USING "###.###"; ES(J) * 100
7460 NEXT
7470 CLOSE FH(1); CLOSE #3: PRINT : PRINT "TRANSFER COMPLETED.": GOSUB 6260
7480 RETURN
7490 CLS : PRINT "END OF THE PROGRAM      GOOD BYE...."
7500 CLOSE : END
7510 CALL EER
7520 GOSUB 6260
7530 RESUME 450
7540 CLS : SCREEN 0: PRINT " TYPE EXIT TO RETURN "
7550 SHELL
7551 SCREEN 12: CLS
7560 RETURN

7570 SUB AVERAGE
7583 INPUT "INPUT FIRST FILE NAME (COMPLETE NAME)"; A$
7584 INPUT "INPUT SECOND FILE NAME (COMPLETE NAME)"; S$
7585 INPUT "DISK DRIVE (A OR B)"; DD$
7586 A$ = DD$ + ":" + A$
7587 S$ = DD$ + ":" + S$
7588 OPEN A$ FOR INPUT AS #1
7589 OPEN S$ FOR INPUT AS #2
7590 J = 1
7591 WHILE NOT EOF(1)
7592 INPUT #1, T, ST1(J), ET1(J), ER1(J), SS1(J), ES1(J)
7593 J = J + 1
7594 WEND
7595 J1 = J
7596 J = 1
7597 WHILE NOT EOF(2)
7598 INPUT #2, T, ST2(J), ET2(J), ER2(J), SS2(J), ES2(J)
7599 J = J + 1
7600 WEND
7601 J2 = J
7602 CLOSE #1: CLOSE #2
7603 IF J1 <= J2 THEN J12 = J1 - 1 ELSE J12 = J2 - 1
7604 INPUT "INPUT THE AVERAGED RESULTS FILE NAME"; R$
7605 INPUT "DISK DRIVE (A OR B)"; DD$
7606 R$ = DD$ + ":" + R$ + CHR$(54)
7607 OPEN R$ FOR OUTPUT AS #3
7608 OPEN R$ + ".DAT" FOR OUTPUT AS #4
7609 FOR J = 1 TO J12 '130
7610 ST(J) = (ST1(J) + ST2(J)) / 2
7611 ET(J) = (ET1(J) + ET2(J)) / 2
7612 ER(J) = (ER1(J) + ER2(J)) / 2
7613 SS(J) = (SS1(J) + SS2(J)) / 2
7614 ES(J) = (ES1(J) + ES2(J)) / 2
7615 PRINT #3, J;
7616 PRINT #3, " "; ST(J);
7617 PRINT #3, " "; ET(J);
7618 PRINT #3, " "; ER(J);
7619 PRINT #3, " "; SS(J);
7620 PRINT #3, " "; ES(J)
7621 PRINT #4, USING "####"; J;
7622 PRINT #4, CHR$(9); USING "####.#"; ST(J) / 10 ^ 6;
7623 PRINT #4, CHR$(9); USING "###.###"; ET(J) * 100;
7624 PRINT #4, CHR$(9); USING "###.###^^"; ER(J);

```

```
7625 PRINT #4, CHR$(9); USING "####.#"; SS(J) / 10 ^ 6;
7626 PRINT #4, CHR$(9); USING "####.###"; ES(J) * 100
7627 NEXT
7628 CLOSE #3: CLOSE #4
7630 END SUB
```

```
7640 SUB EER
```

```
7649 PRINT : COLOR 4
```

```
7650 PRINT "THIS SUBROUTINE FOR ERROR HANDLING          NOORI"
```

```
7651 BEEP
```

```
7652 IF ERR = 2 THEN PRINT "SYNTAX ERROR"
```

```
7653 IF ERR = 3 THEN PRINT "RETURN WITHOUT GOSUB"
```

```
7654 IF ERR = 4 THEN PRINT "OUT OF DATA"
```

```
7655 IF ERR = 5 THEN PRINT "ILLEGAL FUNCTION CALL"
```

```
7656 IF ERR = 6 THEN PRINT "OVERFLOW"
```

```
7657 IF ERR = 7 THEN PRINT "OUT OF MEMORY"
```

```
7658 IF ERR = 9 THEN PRINT "SUBSCRIPT OUT OF RANGE"
```

```
7659 IF ERR = 10 THEN PRINT "DUPLICATE DEFINITION"
```

```
7660 IF ERR = 11 THEN PRINT "DIVISION BY ZERO"
```

```
7661 IF ERR = 13 THEN PRINT "TYPE MISMATCH"
```

```
7662 IF ERR = 14 THEN PRINT "OUT OF STRING SPACE"
```

```
7663 IF ERR = 16 THEN PRINT "STRING FORMULA TOO COMPLEX"
```

```
7664 IF ERR = 18 THEN PRINT "UNDEFINED USER FUNCTION"
```

```
7665 IF ERR = 19 THEN PRINT "NO RESUME"
```

```
7666 IF ERR = 20 THEN PRINT "RESUME WITHOUT ERROR"
```

```
7667 IF ERR = 24 THEN PRINT "DEVICE TIME-OUT"
```

```
7668 IF ERR = 25 THEN PRINT "DEVICE FAULT"
```

```
7669 IF ERR = 27 THEN PRINT "PRINTER OUT OF PAPER"
```

```
7670 IF ERR = 39 THEN PRINT "CASE ELSE EXPECTED"
```

```
7671 IF ERR = 40 THEN PRINT "VARIABLE REQUIRED"
```

```
7672 IF ERR = 50 THEN PRINT "FIELD OVERFLOW"
```

```
7673 IF ERR = 51 THEN PRINT "INTERNAL ERROR"
```

```
7674 IF ERR = 52 THEN PRINT "BAD FILE NAME OR NUMBER"
```

```
7675 IF ERR = 53 THEN PRINT "FILE NOT FOUND"
```

```
7676 IF ERR = 54 THEN PRINT "BAD FILE MODE"
```

```
7677 IF ERR = 55 THEN PRINT "FILE ALREADY OPEN"
```

```
7678 IF ERR = 56 THEN PRINT "FIELD STATEMENT ACTIVE"
```

```
7679 IF ERR = 57 THEN PRINT "DEVICE I/O ERROR"
```

```
7680 IF ERR = 58 THEN PRINT "FILE ALREADY EXIST"
```

```
7681 IF ERR = 59 THEN PRINT "BAD RECORD LENGTH"
```

```
7682 IF ERR = 61 THEN PRINT "DISK FULL"
```

```
7683 IF ERR = 62 THEN PRINT "INPUT PAST END OF FILE"
```

```
7684 IF ERR = 63 THEN PRINT "BAD RECORD NUMBER"
```

```
7685 IF ERR = 64 THEN PRINT "BAD FILE NAME"
```

```
7686 IF ERR = 67 THEN PRINT "TOO MANY FILES"
```

```
7687 IF ERR = 68 THEN PRINT "DEVICE UNAVAILABLE"
```

```
7688 IF ERR = 69 THEN PRINT "COMMUNICATION-BUFFER OVERFLOW"
```

```
7689 IF ERR = 70 THEN PRINT "DISK WRITE PROTECTED"
```

```
7690 IF ERR = 71 THEN PRINT "DISK NOT READY"
```

```
7691 IF ERR = 72 THEN PRINT "DESK MEDIA ERROR"
```

```
7692 IF ERR = 73 THEN PRINT "ADVANCE FEATURE UNAVAILABLE"
```

```
7693 IF ERR = 74 THEN PRINT "RENAME ACROSS DISKS"
```

```
7694 IF ERR = 75 THEN PRINT "PATH / FILE ACCESS ERROR"
```

```
7695 IF ERR = 76 THEN PRINT "PATH NOT FOUND"
```

```
7696 PRINT "PROGRAM RESTARTED WITHOUT LOSS OF DATA"
```

```
7697 PRINT : COLOR 2
```

```
7700 END SUB
```

```
7710 SUB INITIL
```

```
7711 PRINT TAB(27); "INITIALISING VARIABLES"; PRINT
```

```
7712 MK% = 1: A = 0: TP = 0: ND = 0: DE = 0: EE = 0: ES = 0: F = 0: FH(1) = 1: FH(2) = 3
```

```
7713 I = 0: J = 0: K = 0: JJ = 0: G2 = 0: SL = 0: EL = 0: L = 0: HH = 0
```

```
7714 DN = 0: PN = 130: NN = 0: LP = 0: SR = 0: BR = 0: FR = 0: MR = 0: PO = 0
```

```
7715 VS = 0: T = 0: BT = 0: FT = 0: PU = 0: N1 = 0: G1 = 0: PX$ = "0": TX$ = "0"
```

```
7716 FF = 0: F1 = 0: G1 = 0: F2 = 0: K1 = 0: KK = 0: K2 = 0: N3 = 0: CS = 0: FY = 0
```

```
7717 VI = 0: S1 = 0: S2 = 0: EB = 0: DB = 12.7: PP = 0: C0 = 0: MI = 0: PD = 0: PC = 0
```

```
7718 A$ = "0": C$ = "0": CC$ = "0": D$ = "0": DD$ = "0": F$ = "0": FF$ = "0"
```

```
7719 F1$ = "0": F2$ = "0": F3$ = "0": RF$ = "0"
```

```
7720 WF$ = "0": M$ = "0": MM$ = "0": TIM$ = "0": AN$ = "0": PR$ = "0": AT$ = "0"
```

7721 DT\$ = "0": PV\$ = "0": Z\$ = "0": T1\$ = "0": CH\$ = "0": IL\$ = "0"  
7730 END SUB

7740 SUB INTR

7741 REM HOPK-BAR VERSION 11/JAN./94 10:00PM

7742 PRINT TAB(16); .....

7743 PRINT TAB(16); \*\* WELCOME \*\*

7744 PRINT TAB(16); \*\* TO \*\*

7745 PRINT TAB(16); \*\* HOPK-BAR ANALYSIS PROGRAM \*\*

7746 PRINT TAB(16); \*\* PLEASE MAKE SURE YOU HAVE TWO TRANSLATED \*\*

7747 PRINT TAB(16); \*\* DATA FILES TO BE ANALYSED, AND BE SURE \*\*

7748 PRINT TAB(16); \*\* THAT THE PARAMETERS YOU ENTER ARE CORRECT \*\*

7749 PRINT TAB(16); \*\* NOORI 11/JAN./1994 \*\*

7750 PRINT TAB(16); .....

7751 CALL INTRO

7760 END SUB

7770 SUB INTRO

7771 DEFINT A-Z

7772 'SPARKLEPAUSE:

7773 ' CREATES FLASHING BORDER FOR INTRO

7774 LOCATE 23, 25: PRINT 'PRESS ANY KEY TO CONTINUE'

7775 COLOR 4, 0

7776 A\$ = " \* \* \* \* \* "

7777 WHILE INKEY\$ <> "": WEND 'CLEAR KEYBOARD BUFFER

7778

7779 WHILE INKEY\$ = ""

7780 FOR A = 1 TO 5

7781 LOCATE 1, 1 'PRINT HORIZONTAL SPARKLES

7782 PRINT MID\$(A\$, A, 80);

7783 LOCATE 19, 1

7784 PRINT MID\$(A\$, 6 - A, 80);'

7785

7786 FOR B = 2 TO 18 'PRINT VERTICAL SPARKLES

7787 C = (A + B) MOD 5

7788 IF C = 1 THEN

7789 LOCATE B, 80

7790 PRINT " \*";

7791 LOCATE 20 - B, 1

7792 PRINT " \*";

7793 ELSE

7794 LOCATE B, 80

7795 PRINT " \*";

7796 LOCATE 20 - B, 1

7797 PRINT " \*";

7798 END IF

7799 NEXT B

7800 NEXT A

7801 WEND

7802 CLS

7810 END SUB

7820 SUB MENU

7821 PRINT : PRINT " HOPK-BAR DIRECTORY "; DATE\$

7822 PRINT " .....

7823 PRINT " \* 1. TRANSFER PARAMETERS TO DISK \*\*

7824 PRINT " \* 2. HOPK BAR DATA ANALYSIS \*\*

7825 PRINT " \* 3. LIST DATA \*\*

7826 PRINT " \* 4. LIST RESULTS \*\*

7827 PRINT " \* 5. PARAMETERS ENTERED FROM KEYBOARD \*\*

7828 PRINT " \* 6. BAR STRAIN & IMPACT VELOCITY \*\*

7830 PRINT " \* 7. AVERAGE OF RESULTS FILES \*\*

7831 PRINT " \* 8. SMOOTH THE RESULTS \*\*

7832 PRINT " \* 9. FINISH \*\*

7833 PRINT " \* D. DOS SHELL NOORI 11/01/1994 \*\*

7834 PRINT " .....

7835 PRINT " SELECT NUMBER (1 TO 9 OR D)."

7840 END SUB

7850 SUB SHB  
7851 CLS : SCREEN 12  
7852 LINE (52, 35)-(244, 54), 3, BF 'TRANSMITTER  
7853 LINE (245, 38)-(262, 52), 4, BF 'SAMPLE  
7854 LINE (257, 35)-(437, 54), 3, BF 'INCIDENT  
7855 LINE (190, 44)-(207, 47), 5, BF 'STRAIN GAUGE 2  
7856 LINE (288, 44)-(303, 47), 5, BF 'STRAIN GAUGE 1  
7857 LINE (477, 35)-(527, 55), 3, BF 'PROJECTILE  
7858 LOCATE 2, 29: PRINT "SAMPLE"  
7859 LOCATE 4, 56: PRINT " <--"  
7860 LOCATE 2, 7: PRINT "TRANSMITTER"  
7861 LOCATE 2, 47: PRINT "INCIDENT"  
7862 LOCATE 2, 60: PRINT "PROJECTILE"  
7870 END SUB





